DOCTOR OF MEDICINE

The Non-Wnt Functions of APC
Unravelling the Link between APC and Apoptosis

Cuddihy, Jane

Award date:
2016

The Non-Wnt Functions of APC: Unravelling the Link between APC and Apoptosis

Jane Cuddihy

Doctor of Philosophy

Supervisors: Kevin Hiom and Inke Näthke, April, 2016

Table of Contents

Chapter 2 - Materials and Methods

2.1 Materials

2.2 Cell Culture Methods

2.3 Protein Methods

2.4 DNA/RNA Methods

2.5 Bacterial Handling Techniques

2.6 Microscopy

2.7 Fluorescence activated cell sorting (FACS)

Chapter 5 – Increased Bcl-2 and altered mitochondria may be responsible for the reduced sensitivity of *Apc* deficient cells to cytotoxic agents

Chapter 6 – Discussion

Appendix

List of Figures

List of Tables

Acknowledgements

Firstly, I would like to thank professors Kevin Hiom and Inke Näthke. Initially for giving me the opportunity to take on this PhD project and subsequently for providing many hours of help, advice and encouragement. I would like to give them a special thank you for all the hours spent guiding me on my thesis and scientific writing. I would also like to express thanks to the University of Dundee for funding my PhD.

I owe many thanks to the very helpful staff in both laboratories for technical advice, help in carrying out experiments and making the lab environment a nice place to work (Conor, Maggy, Anne, Ian, Aliya and Alistair). Also, thanks to my peers in both labs for additional help, motivation and understanding (Aisling, Olesja, Craig and Thomas). Thank you also to all the support staff at the Jacqui Wood Cancer Centre and the College of Life Sciences.

Lastly, I would like to acknowledge all the support I received from my parents, extended family and friends over the last three years of lab work. Moreover, all the support I received during the writing of this thesis.

Declaration

I confirm that I am the author of this thesis, which is a record of my own work done in the laboratory. I declare that this work has not been previously submitted for a higher degree.

Signed: _____ Date: _____

PI 1: _____ Date: _____

P1 2: _____ Date: _____

Abstract:

The Non-Wnt related functions of APC: the link between APC and apoptosis.

Colorectal cancer (CRC) is the second most common cause of cancer-related death in the UK and Western world. More than 90% of sporadic CRCs harbour mutations in the multi-functional tumour suppressor gene Adenomatous polyposis coli (*Apc*). The most commonly studied function of APC is its role as a scaffold for the β-catenin destruction complex involved in Wnt signalling. However, APC binds many other proteins. For example, it directly binds to and stabilises microtubules and actin. These non-Wnt related functions of APC are poorly understood.

My PhD examines non-Wnt functions of APC. To this end, I created degron-tagged APC in DT40 cells that allowed for the rapid, conditional degradation of endogenous APC. The aim was to identify the immediate effects on cellular processes. Then, to identify the contribution of different APC domains by measuring the ability to rescue any defects when reintroducing fragments of APC. However, creation of these degron-tagged *Apc* knock-in cell lines resulted in hypomorphic phenotypes and auxin-associated off-target effects. Nonetheless, I compared the response of APC^{high}, APC^{low}, and $APC^{minimal}$ cells to DNA damaging agents and Taxol® but found no significant differences.

Subsequently, I focused on the relationship between APC and apoptosis. Previous observations suggested that deficiency in *Apc* rendered cells less sensitive to low doses of Taxol®. However, *Apc* deficient cells were more readily killed when Taxol® was combined with the Bcl-2 inhibitor, ABT-737. One possible explanation is the increase in Bcl-2 protein upon *Apc* depletion. However, I found that ABT-737, Taxol® and *Apc* depletion each cause activation of the unfolded protein response. This suggests that these treatments elicit a stress response that can stimulate apoptosis. Moreover, the same treatments also cause changes in mitochondria. Importantly, all of these effects do not require an increase in the β-catenin protein. Together, my data reveal novel links between APC and apoptosis that could be exploited clinically.

Abbreviations

ADF	Advanced Dulbecco modified eagle medium-F12
AID	Auxin-inducible degron
APAF-1	Apoptosis protease activating factor 1
APC	Adenomatous polyposis coli
ATF4	Activating transcription factor 4
ATF6	Activating transcription factor 6
ATF6f	Activating transcription factor 6 fragment
ATR	ATM-Rad3-related protein
Bad	Bcl-2 associated death protein
Bax	Bcl2-associated X protein
Bak	Bcl-2 antagonist killer 1
Bcl-2	B cell lymphoma-2
Bcl-XL	Bcl-2 extra-large (long splicing form of Bcl-x)
Bcl-XS	Bcl-2 extra-small (short splicing form of Bcl-x)
Bcl-w	Bcl-2-like protein 2/BclL2
BER	Base excision repair
BiP	immunoglobulin binding protein
BH	Bcl-2 homology
Bid	BH3 interacting domain
Bik	Bcl-2 interacting killer
Bim	Bcl-2-interacting mediator of cell death
BMF	Bcl-2 modifying factor
Bok	Bcl-2 related ovarian killer
BrdU	5-Bromo-2'-deoxyuridine
BSA	Bovine serum albumin
Bsr	Blasticidin resistance cassette

β-TrCP	Beta-Transducin repeat-containing protein
cDNA	Complementary deoxyribonucleic acid
CIN	Chromosome instability
CK1	Casein kinase 1
CRC	Colorectal cancer
Ctnnb1	β-catenin
Ctrl	Control
C-APC	C-terminus of APC
C-FLIP	cellular FLICE-inhibitory protein
DAPI	4', 6-diamidino-2-phenylindole
DC	Destruction complex
DD	Death domain
DDR	DNA damage response
DEPC	Diethylpyrocarbonate
dH_20	Deionized water
DIABLO	Direct IAP-binding protein with low PI
DLG1	Discs large homolog 1
DPBS	Dulbecco's PBS
DMEM	Dulbecco modified eagle medium
DMSO	Dimethyl sulphoxide
DTT	Dithiothreitol
dNTPs	Deoxynucleotide triphosphates
Dsh	Dishevelled
EDTA	Ethylenediaminetetraacetic acid
EGTA	Ethylene glycol tetra acetic acid
EMPAI	Exponentially modified protein abundance index
ER	Endoplasmic reticulum
ERAD	Endoplasmic reticulum associated degradation

ESI-Trap	Electrospray ion trap (mass spectrometry)
EtOH	Ethanol (absolute)
FACS	Fluorescence activated cell sorting
FBS	Foetal bovine serum
FCS	Foetal calf serum
FSC	Forward scatter
Fzd	Frizzled
GAPDH	Glyceraldehyde-3-phosphate dehydrogenase
GFP	Green fluorescent protein
gPCR	Genomic polymerase chain reaction
GSK3β	Glycogen synthase kinase 3 beta
Hif-1α	Hypoxia inducible factor 1 alpha
HRK	Harakiri
Hsp60	Heat shock protein 60kDa
HU	Hydroxyurea
IAA	Indole-3-acetic acid (auxin)
IAP	Inhibitor of apoptosis protein
IF	Immunofluorescence
$InsP_6$	Inositol hexakisphosphate
IP	Immunoprecipitation
IRE	Inositol requiring enzyme
ISC	Intestinal stem cell
kDa	kilo-Daltons
KI	Knock-in
LB	Luria Bertani
LEF	Lymphoid enhancer-binding factor
LC-MS-MS	Liquid chromatography – mass spectrometry and liquid chromatography – tandem mass spectrometry

LOH	Loss of heterozygozity
MCR	Mutation cluster region
Mcl1	Myeloid cell leukaemia 1
MEFs	Mouse embryonic fibroblasts
Min	Multiple intestinal neoplasms
MAM	Mitochondria associated membrane
MOM	Mitochondrial outer membrane
MMP	Mitochondrial membrane potential
MMR	Mismatch repair
mRNA	Messenger ribonucleic acid
MT(s)	Microtubules(s)
M-APC	Middle portion of APC
NCDD	Nomenclature committee on cell death
ND	Not determined
NEAA	Non-essential amino acids
NER	Nucleotide excision repair
NHEJ	Non-homologous end joining
NUMA	Nuclear mitotic apparatus protein
N-APC	N-terminal domain of APC
O/n	Overnight
PAGE	Polyacrylamide gel electrophoresis
PAI	Protein abundance index
Par-4	Prostate apoptosis response gene-4
PARPi	Poly(ADP-ribose) polymerase ADP ribosyltransferase inhibitor
PBS	Phosphate buffered saline
PERK	Protein kinase-like ER kinase
PFA	Paraformaldehyde
PH3	Phospho-histone H3

PI	Propidium iodide
PS	Penicillin-streptomycin
PUMA	p53 upregulated modulator of apoptosis
P-IRE	Phospho-inositol requiring enzyme
qRT-PCR	Quantitative reverse-transcription polymerase chain reaction
RACE	Rapid amplification of cDNA ends
RIDD	Regulated Ire1-dependent decay
RIPA	Radio immunoprecipitation
ROS	Reactive oxygen species
RPM	Rounds per minute
RPMI	Roswell Park Memorial Institute
RNA	Ribonucleic acid
RNAi	Ribonucleic acid interference
RT	Room temperature
SCF	Skp1, cullin1, F-box protein
SDS	Sodium dodecyl sulphate
siRNA	Small interfering ribonucleic acid
Skp1	S phase kinase-associated protein 1
Sp	Species
SSB	Single strand breaks
SSC	Side scatter
S1P	Site 1 protease
S2P	Site 2 protease
tAPC	Truncated Adenomatous polyposis coli
tBID	Truncated BH3 interacting domain
TBS	Tris buffered saline
TCF	T-cell factor
TIR	Transport inhibitor response protein

Tm	Melting temperature
TRAIL	TNF-related apoptosis inducing ligand
UPR	Unfolded protein response
Wnt	Wingless-type MMTV integration site
WT	Wild-type

Chapter 1 - Introduction

1.1 Background on colorectal cancer

Nearly ten percent of all cancer diagnoses in the world are colorectal cancers (CRC). This makes CRC the third most common cancer in the world (according to the World Cancer Research Fund, 2012). Colorectal cancer is also the second most common cause of cancer death cancer in the UK (CRUK data, 2012). Currently, bowel screening is available biennially to anyone over the age of fifty in Scotland and 60 years of age in England. This is by means of the faecal occult blood test (FOBS) to detect blood traces in a stool sample (Hardcastle *et al.,* 1980). However, more effective means of CRC testing is needed, ideally, a method(s) to detect bowel polyps (pre-cancerous growths). Over and above this, an understanding is needed of the genotypic and phenotypic initiating events that cause polyps and subsequent carcinomas, to develop. Prevention or destruction of a polyp may be able to circumvent the downstream accumulation of mutations and consequential physiological changes that lead to adenocarcinomas in the intestinal tract. Thus, decreasing the tumour burden and potentially alleviating the condition. Adenomatous polyposis coli (*Apc*) is the most mutated gene in human cancers (Polakis, 2012) and *Apc* mutations have been found in >90% of sporadic colorectal cancers (CRCs). This makes *Apc* an attractive target for cancer research, in understanding the first changes in normal intestinal tissues that leads to polyp development.

1.2 Development of colorectal Cancer

Mutation of *Apc* is the first step in the development of CRC (fig 1.1). It causes a change in intestinal epithelia leading to aberrant crypt foci. Further accumulation of mutations can lead to the development of polyps, which through the accumulation of subsequent mutations can progress into cancerous tissue (fig 1.1). The progression of CRC is clinically subdivided into stages (fig 1.2), referring to the size and metastasis of the tumour, that give an outlook

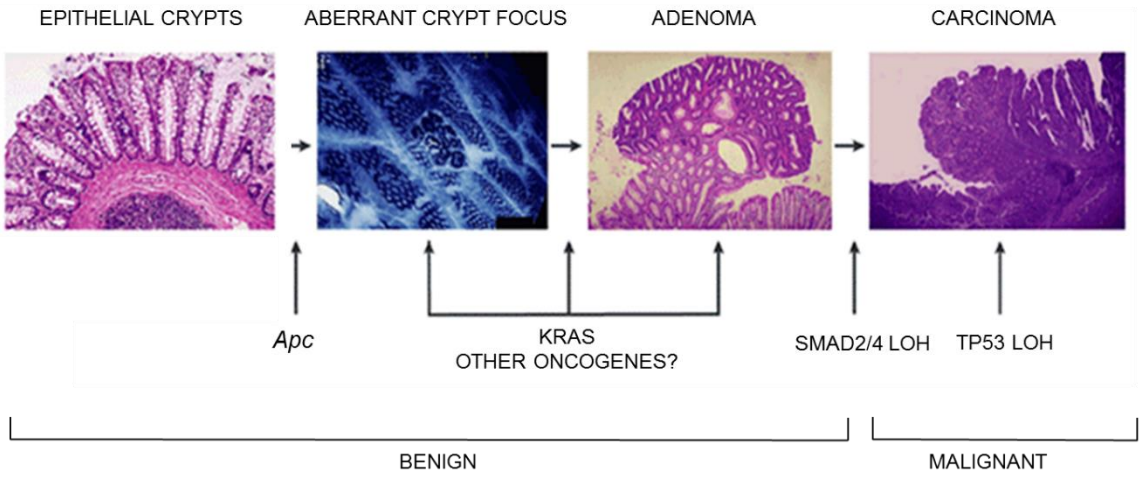

Fig 1.1 The development of colorectal cancer. The. Image edited from Fodde, Smits and Clevers (2001). In wild-type (normal) intestinal epithelia there is a clear boundary between crypts and crypts remain largely linear structures. Loss of Apc is the first step towards the decelopment of CRC and leads to aberrant crypt foci. The accumulation of other mutations such in genes such as Kras, or Apc LOH leads to adenoma/polyp development. Subsequent mutations in genes such as the tumour suppressos Tp53 lead to the cancerous development into a (malignant) carcinoma. Image edited from Fodde, Smits and Clevers (2001).

on the prognosis; TNM Stages (tumour, nodes, metastasis). Firsty, the T (tumour stage), T1 refers to a tumour still within the bowel epithelia. Stage T2 is a tumour that has grown into the muscle layer of the bowel. T3 means the tumour has grown into the outer lining of the bowel wall. T4 refers to a tumour that has grown through the outer wall of the bowel and as such much have grown into another part of the bowel, into other nearby structures or it may have broken through the peritoneum (fig 1.2). To classify the node(s) involvement of CRC progression, N0 means that there are no CRC cells contained within lymph nodes. Whereas, node stage N1 refers to up to 3 lymph nodes close to the bowel containing CRC cells. The last node stage N2 means there are CRC cells in more than 4 lymph nodes close to the bowel. Lastly the stages of metastasis can be classified in two groups. M0 means the cancer has not spread to other organs, whereas M1 means the cancer has spread to other parts of the body. All three results of the TNM stages are then put together, such as T2, N1, M0 to provide the clinical classification.

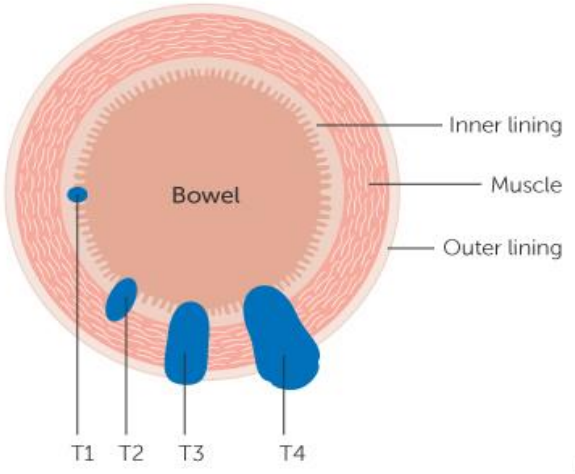

Fig 1.2 The TNM staging of colorectal cancer. The classification of a tumour depends on its TNM staging. T1 tumours remain within the inner lining of the bowel. T2 tumours have grown throught the inner lining. T3 means the tumour is growing through the muscle layer and T4 tumours have grown through the outer wall of the bowel. Imaged taken from CRUK.

Treatment for CRC is dependent on the stage and location of the cancer (information taken from CRUK, 2016). In those with early CRC surgery is usually the first option as up to all of the tumour can be removed. Radiotherapy is usually given in those with rectal tumours rather than those with bowel cancers. To treat T3 cancer, chemotherapy drugs such as Fluoracil are usually used after surgery. Combination therapy of two or more chemotherapeutic agents are currently in clnical trials. In advanced CRC (T4 cancer), the prognosis is poor with a terminal outlook and treatments are usually provided in an attempt to extend the life od the patient (rather than cure the disease).Surgery may be an option to remove blockages, slow the progression of the cancer, or remove a secondary cancer. Chemotherapy is the main course of treatment and if the first course was not successful, second and third courses – using different drugs can be administered. External beam radiotherapy may be used to shrink tumours, but is more likely to be used for a rectal tumour. An additional treatment for advanced bowel cancer is biological treatments – drugs that help to control the growth of the tumour(s). When used in combination with chemotherapy it can prolong life and importantly, improve the quality of life of the patient. Unfortunately, late stage CRC is very difficult to treat. The key in CRC treatment is in early detection.

1.3 Physiology of the human intestine

Maintaining the normal physiology of the intestine is key in preventing polyp and subsequent adenocarcinoma development. Therefore, an understanding of gut physiology is needed. The human intestine is the site of nutrient absorption and faecal matter creation in the body. The intestine is lined with an absorptive epithelial sheet, folded to form crypts of Lieberkühn that house the intestinal stem cells (fig 1.3). The intestinal stem cells are interspersed with anti-microbial secreting Paneth cells (Porter *et al.,* 2002), whom protect the crypt niche (reviewed by Clevers, 2013). These stem cells produce cells (Cheng and Leblond, 1974) that migrate upwards through the crypt and transit-amplifying compartment. These cells then terminally differentiate into the cell types found in that region of the intestinal tract (Bjerknes and Cheng, 1981). Once cells reach the villus tip (small intestine) or the surface of the colonic epithelium (colon) they are shed into the lumen.This migration takes three to five days (see a review by Barker, 2014), so cell numbers need to be frequently replenished. Due to this high rate of cell turnover, the only cells likely to harbour genetic changes for long enough to change gut physiology, are the intestinal stem cells (Potten and Loeffler, 1990). Mutation of *Apc* specifically in stem cells is thought to be the initiating event in intestinal tumorigenesis (Kinzler and Vogelstein, 1996; Rowan *et al.,* 2000; Radulescu *et al.,* 2010) – loss of APC in non-stem cells of the intestinal crypts does not result in tumorigenesis (Barker *et al.,* 2009). Loss of APC precedes changes in crypt biology indicated by the presence of polyps. This suggests that it APC is required for the correct maintenance of intestinal and colonic epithelia (Su *et al.,* 1992; Fodde *et al.,* 1994; Oshima *et al.,* 1995).

1.4 Adenomatous polyposis coli (APC)

The change from normal gut epithelium to a pre-cancerous polyp happens by mutation of the tumour suppressor gene Adenomatous polyposis coli (*Apc*) (Kinzler and Vogelstein, 1996; Rowan *et al.,* 2000; Radulescu *et al.,* 2010). Its gene product is a large (312kDa,

2843 amino acid), multi-domain tumour suppressor protein with many binding partners and interactors (fig 1.4). Known binding sites at the N-terminus (N-APC) consist of an

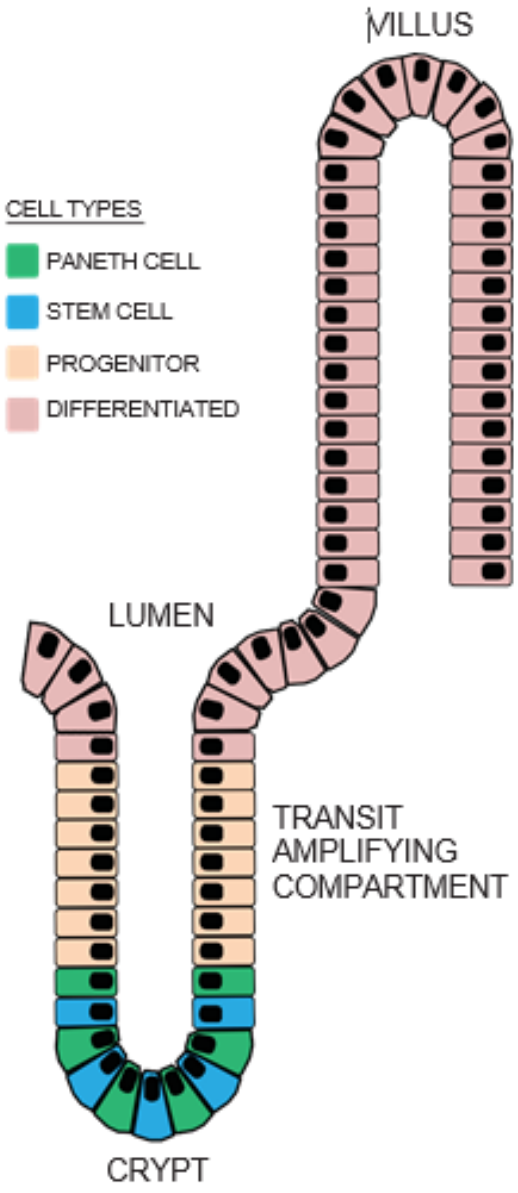

Fig 1.3 Crypt/Villus structure. The intestinal epithelium is invaginated. Folds create crypt structures that house the intestinal stem cells (SC) interspersed with anti-microbial secreting Paneth cells that protect the crypt niche. SCs produce progenitor cells that proliferate and migrate up through the transit amplifying region of the crypt where they will eventually terminally differentiate. In the small intestine these cells continue to migrate up through finger-like projections of the epithelium called villi. The villi protrude out into the lumen of the intestine. It takes 3-5 days for a cell to reach the villus tip before it is shed into the lumen.

oligodimerisation domain (Su *et al.,* 1993) and 7 Armadillo repeats that bind multiple partners (Hirschl, Bayer and Muller, 1996*)*. The middle portion of APC (M-APC) contains 3-15 amino acid (15R) and 7-20 amino (20R) repeats that bind axin and β-catenin, each with varying affinity - although when phosphorylated by axin, the 20mers have increased β-catenin affinity (Rubinfeld *et al.,* 1993; Rubinfeld, Tice and Polakis, 2001; Tickenbrock *et al.,* 2003; Liu *et al.,* 2006). These 15R and 20R regions (fig 1.4) are key for the function of APC in the Wnt pathway (see Xing *et al.,* 2004 for crystal structure detail of APC-β-catenin interaction). M-APC also has SAMP sites for axin binding, so-called after their consensus motif (serine, alanine, methionine, proline). The APC C-terminus (C-APC) has a basic domain for microtubule (MT) binding as well as a site for the MT binding protein EB1. The extreme C-terminus contains a PDZ.

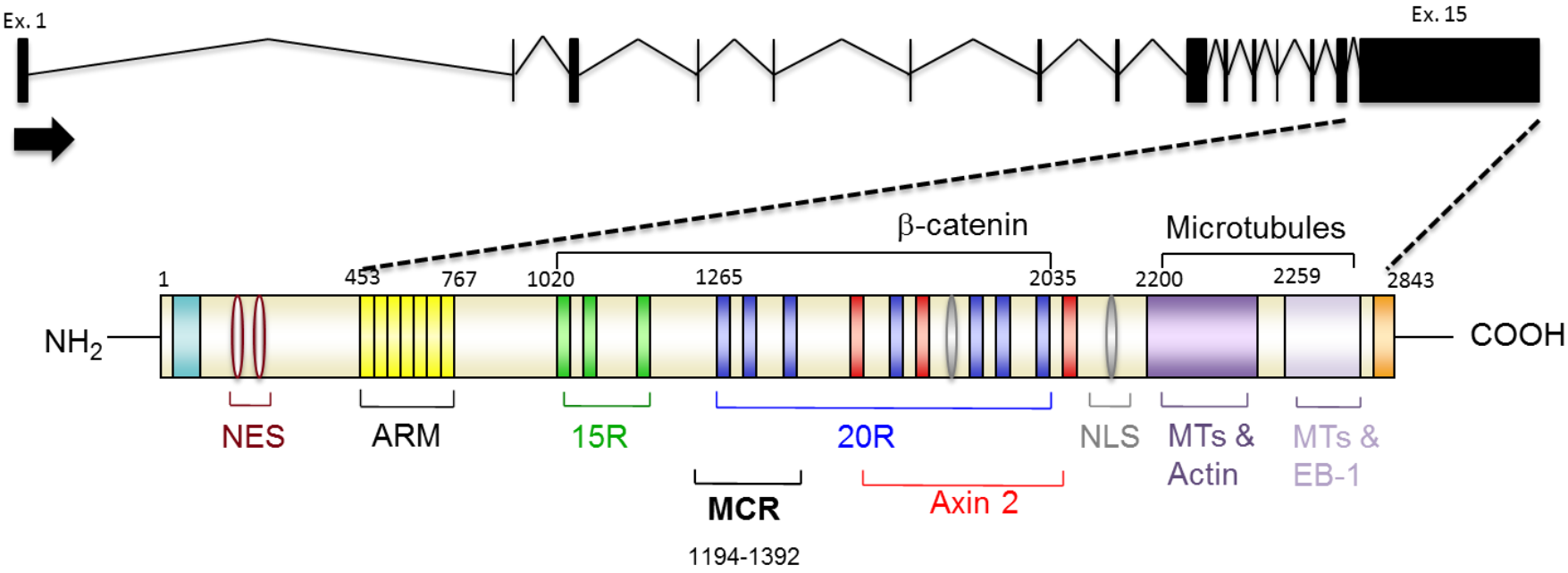

Fig 1.4 *Apc*. The top panel shows the intron/exon structure of the *Apc* gene found on 5q21-22 (Kinzler *et al.,* 1991). The black boxes represent exons and the arrow indicates the direction of transcription. The bottom panels shows the various binding domains within *Apc*. Exon 15 (top panel) contains the coding information for more than two thirds of *Apc*, as indicated by the dashed lines. Close to 75% of all *Apc* mutations occur in the mutation cluster region (MCR) resulting in an N-terminally truncated *Apc* (N-*Apc*) lacking most/all of the β-catenin, axin and microtubule binding domains.

domain (fig 1.4) allowing interaction with other PDZ-domain-containing proteins such as DLG1/SAP97 (Matsumine *et al.,* 1996). Importantly, APC binding to β-catenin and microtubules is mutually exclusive – APC can only bind one or the other (Penman, Leung and Näthke, 2005; Dikovskaya *et al.,* 2007).

Loss of *Apc* usually occurs through a nonsense mutation that falls within the mutation cluster region (MCR) (fig 1.4) (Mori *et al.,* 1992). This results in a truncated APC (N-APC) that lacks many binding sites including those for β-catenin, axin and microtubules (Su *et al.,* 1993). These N-terminal fragments cause dominant effects in the crypt. For instance, they induce aberrant cell migration (Nelson *et al.,* 2012). This results in the basal extrusion of epithelial cells instead of the apical extrusion seen in *Apc* WT cells (Marshall *et al.,* 2011). Thus heterozygous *Apc* is sufficient to create a dominant effect over the remaining wild type *Apc* allele and this is not correlated with large changes in the transcriptional activity of β-catenin. When both *Apc* alleles are lost, constitutive activation of proliferative pathways ensues through β-catenin, which accumulates in the nucleus and binds transcriptional coactivators TCF/LEF (Behrens *et al.,* 1996; van de Wetering *et al.,* 1997). This activates Wnt pathway gene transcription (for a list of Wnt target genes see appendix A). Understanding the entire spectrum of APC functions is key for understanding the changes that characterise *Apc* mutant cells and in treating CRC patients.

1.4.1 APC and Wnt signalling

Aberrant regulation of the Wnt signalling pathway due to mutant *Apc* is the best understood link between APC and cancer. This is because APC acts as a negative regulator of β-catenin as part of the Wnt signalling pathway (fig 1.5). Loss of function mutations in *Apc*, such as nonsense mutations found in CRC, abolish this function. APC is fundamental in the Wnt signalling pathway (fig 1.3) as it forms part of the β-catenin destruction complex (DC) along with the scaffold protein axin (Nakamura *et al.,* 1998) and kinases CK1 and GSK3β (Rubinfeld *et al.,* 1996; Behrens *et al.,* 1998; Ideka *et al.,* 1998). Axin may be the limiting step in DC formation as it is the least abundant member of the complex (Lee *et al.,* 2003).

.

In the absence of a Wnt signal (fig 1.5 - WNT OFF), the DC targets β-catenin for degradation by phosphorylation. CK1 phosphorylates β-catenin at serine 45 and this acts as a priming kinase for GSK3β (Liu *et al.,* 2002; Sakanaka, 2002), which subsequently phosphorylates serines 33, 37 and 41 (Winston *et al.,* 1999). Phospho-β-catenin is recognised by the F-box protein β-TrCP (Kitagawa *et al.,* 1999; Latres, Chjaur and Pagano, 1999; Winston *et al.,* 1999) and is subsequently degraded by the 26S proteasome (Hart *et al.,* 1999).

The 3-15R and 7-20R regions (fig 1.5) are key for the function of APC in the DC as they bind axin and β-catenin. This allows β–catenin to be phosphorylated at its N-terminus, targeting it for its ultimate destruction by the proteasome. Loss of this pathway plays an important role in tumorigenesis as an increase in β-catenin leads to its cytoplasmic accumulation and subsequent nuclear translocation. Here, it alters gene expression profiles upon binding the transcriptional coactivators TCF/LEF (Behrens *et al.,* 1996; Korinek *et al.,* 1997; van de Wetering *et al.,* 1997). (For a list of Wnt target genes see appendix A). This leads to an upregulation of oncogenes such as c-*Myc* (He *et al.,* 1998), *Cyclin D1* (Shtutman

et al., 1999; Tetsu and McCormick, 1999) and other genes thought to be involved in proliferation.

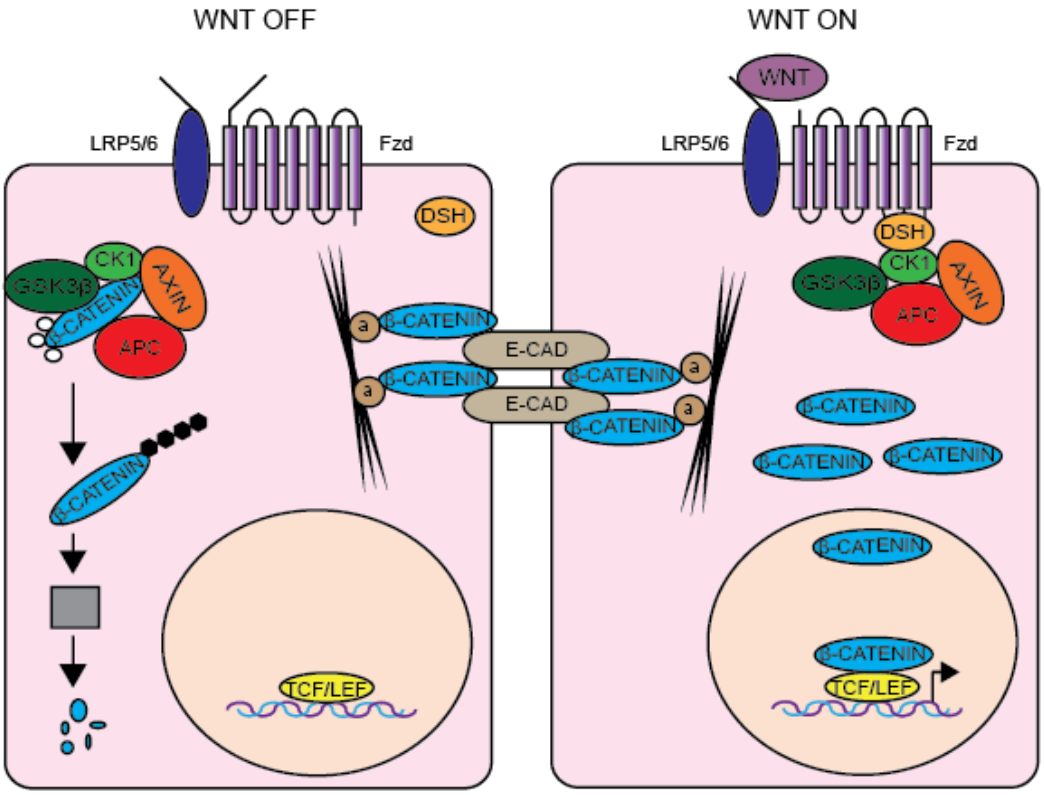

Fig 1.5. The β-catenin destruction complex in Wnt signalling. Beta-catenin is found at various locations within the cell; it binds E-cadherin at the membrane to form adherens junctions, it is found in the cytosol and in the nucleus. APC forms part of the β-catenin destruction complex (DC) with the scaffold protein Axin and kinases CK1 and GSK3β. In the absence of a Wnt ligand (WNT OFF) the DC binds cytosolic β-catenin through APC and Axin. CK1 phosphorylates β-catenin and is the priming kinase for subsequent GSK3β phosphorylation. Phosphorylated β-catenin is targeted for proteasomal degradation. However, upon a Wnt ligand binding (WNT ON) to the receptor LRP5/6 and its co-receptor Frizzled (Fzd), it is thought that the receptors recruit the adaptor protein Dishevelled (Dsh), which binds to the DC. This prevents the DC from phosphorylating β-catenin and targeting it for degradation. Subsequently, β-catenin accumulates in the cytosol, translocates to the nucleus and binds the transcriptional co-activators TCF/LEF. This induces transcription of Wnt target genes.

1.4.2 APC and microtubules

Other than Wnt signalling, APC has also emerged as a key regulator of microtubules (MTs). This is another link between APC and cancer as loss of *Apc* leads to chromosome instability (CIN) due to MT defects (Green and Kaplan, 2003). Microtubules are dynamic tubulin

polymers (consisting of α-β tubulin heterodimers) used by eukaryotes for cellular structure, a means of intracellular transport, mitotic spindles and together with actin and intermediate filaments they form the cytoskeleton. The APC C-terminus harbours a MT binding domain (Deka *et al.,* 1998) and a site to interact with the microtubule-binding protein EB1 (Berrueta *et al.,* 1998). Loss of *Apc* leads to chromosome instability (CIN). There are several reasons why this can occur.

APC binds to MT plus-ends, stabilising them (Mimori-Kiyosue, Shiina and Tsukita, 2000; Zumbrunn *et al.,* 2001; Mogensen *et al.,* 2002; Kroboth *et al.,* 2007). In *Apc* mutant cells MTs are less stable (Kita *et al.,* 2006; Kroboth *et al.,* 2007) meaning mitotic spindles may not form correctly, leaving unattached centrosomes. APC is also found at kinetochore-microtubule attachment sites during mitosis (Fodde *et al.,* 2001; Kaplan *et al.,* 2001), and *Apc* depleted cells show reduced kinetochore tension in mitosis (Dikovskaya *et al.,* 2007). Hence, *Apc* deficient cells may lack appropriate attachments required to pull apart sister chromatids appropriately. Indeed, *Apc* mutant cells are defective in chromosome segregation (Fodde *et al.,* 2001; Kaplan *et al.,* 2001; Dikovskaya, Newton and Näthke, 2004; Draviam *et al.,* 2006).

Fodde *et al.,* (2001) used FISH analysis on 2 ES cell lines, each containing differently truncated *Apc* (nonsense mutations). Both cell lines produced karyotypes with near-tetraploid genomes and more structural rearrangements than WT ES cells. This again indicates that a lack of WT *Apc* leads to problems with mitotic spindles. This results in a failure to maintain euploidy and chromosomal translocations (CIN).

1.4.2.1 Microtubule poisons

Microtubule poisons are commonly used chemotherapeutic agents used to disrupt MT dynamics. This results in altered spindle fibres in mitosis and functional changes in microtubules during interphase. The toxic effect of microtubule poisons is caused by

apoptosis due to a prolonged mitotic arrest (Ellis *et al.,* 1999). The MT poisons Nocodazole and Vinorelbine prevent MT polymerisation (Lobert, Vulevic and Correia, 1996). Taxol® stabilises MTs and prevents their depolymerisation (Schiff and Horwitz, 1980). APC-bound microtubules are stabilised and more resilient against depolymerising agents (Zumbrunn *et al.,* 2001). However, cells with mutant *Apc* arrest much less readily in mitosis in response to Taxol® (Radulescu *et al.,* 2010). Conversely, Vinorelbine kills *Apc* deficient cells more effectively than cells with WT *Apc* because it can kill cells in interphase, irrespective of a mitotic arrest (Klotz *et al.,* 2012). Investigating a means to kill *Apc* deficient cells using Taxol® means killing proliferating cells such as cancer cells. This would leave cells in interphase untouched, unlike Vinorelbine treatment.

1.4.2.2 Taxol® mechanism of action

Taxol® was the microtubule poison used for experiments in this thesis. Taxol® works as a microtubule poison because it binds the microtubule 'plus' ends, stabilising them, meaning they are resistant to depolymerisation induced by $Ca^{2+,}$ cold temperatures and dilution (Schiff, Fant and Horwitz , 1979). Specifically, Taxol® binds to the β-tubulin subunit of microtubules (Diaz, Menendez and Andreu, 1993; Rao *et al.,* 1994). Therefore, microtubules are unable to remain dynamic because they can no longer remodel themelves.

1.4.2.3 Microtubules and the spindle assembly checkpoint

One reason why *Apc* deficient cells do not arrest in response to Taxol® is a defective spindle assembly checkpoint (Fodde *et al*., 2001; Kaplan *et al*., 2001; Dikovskaya *et al.,* 2007). Disrupted mitotic spindles should activate the spindle assembly checkpoint during prometaphase in eukaryotic cells. This happens when chromosomes are misattached to cell poles by the mitotic spindle or through the use of MT poisons to disrupt MT dynamics. Checkpoint activation results in mitotic arrest (Hoyt Totis and Roberts, 1991). Activation of the spindle assembly checkpoint should therefore prevent CIN. Thus, *Apc* depleted cells

harbour CIN as a result of defective MTs and inactivation of the spindle assembly checkpoint that should detect spindle problems (Dikovskaya *et al.,* 2007). The lethality of MT poisons is due to apoptosis resulting from a prolonged mitotic arrest. However, *Apc* deficient cells do not efficiently undergo apoptosis in response to Taxol® treatment. Developing a means to kill *Apc* deficient cells is of great clinical benefit in treating CRC.

1.5 Cell death

Killing *Apc* deficient cells is important in treating CRC. Therefore, understanding the mechanisms that lead to cell death is key in activating these pathways. In 2005 the Nomenclature Committee on Cell Death (NCDD) proposed new criteria to define cell death. They stated that for a cell to die there must be irreversible loss of plasma membrane integrity (Kroemer *et al.,* 2005). There are many processes that lead to loss of membrane integrity (cell death). I will now introduce apoptotic cell death because that is what this thesis looked at.

1.5.1 Apoptosis

The best characterised and most studied form of programmed cell death is apoptosis, first described by Kerr, Wyllie and Currie, (1972). A more in depth understanding of its function came from later work done on the nematode worm *Caenorhabditis elegans.* Importantly, this showed that apoptosis is a key component during development and in maintaining healthy cells and tissues (Horvitz, 1999). According to the NCDD in 2009, the cellular changes leading to apoptotic cell death are: chromatin condensation, cell shrinkage (pyknosis), little to no modifications to organelles, nuclear fragmentation (karyorrhexis), membrane blebbing and the separation of these fragments into apoptotic bodies, with subsequent engulfment by phagocytes (Kroemer *et al.,* 2009). Additionally, a hallmark of apoptosis is caspase activation. There are two separate apoptotic pathways – the intrinsic mitochondrial pathway and extrinsic death receptor pathway. Both pathways converge on executioner caspase 3.

1.5.1.1 The extrinsic pathway

The extrinsic pathway of apoptotic cell death (fig 1.6) involves plasma membrane receptors relaying a death message to the cell. Death ligands such as CD95L, TRAIL or TNFα, bind to death receptors in the plasma membrane. The receptors have a cytoplasmic death domain (DD) that binds a cytosolic adaptor protein, which can transmit the death signal (Tartaglia *et al.,* 1993). This results in the activation of pro-caspase 8, which in turn activates the downstream effector caspase 3 (fig 1.6).

1.5.1.2 Bcl-2 family proteins

The Bcl-2 family of proteins (table 1.1) govern intrinsic apoptosis. The interaction of Bcl-2 proteins with each other controls the life/death fate of a cell (fig 1.7). Binding of proteins within the Bcl-2 family are well understood, but their regulation by signals out-with the family are poorly understood. The family is comprised of proteins that share between one and four BH (Bcl-2 homology) domains (fig 1.8) and is split into three subgroups (table 1.1).

TABLE 1.1

Bcl-2 Family Proteins

Pro-life "Guardians"	**Pro-death "Effectors"**	**BH3-only "Initiators"**	
Bcl-2	BAX	**Activators**	**Sensitizers**
Bcl-XL	BAK	PUMA	NOXA
Mcl-1	BOK	BIM	BAD
Bcl-w/Bcl2L2	Bcl-XS	tBID	BIK
A1			BMF
Bcl-B/Bcl2L10			HRK

Pro-life proteins, such as Bcl-2 contain all four BH domains and are the "guardians" of the cell against apoptosis (fig 1.8). They bind to pro-death proteins, neutralising their capacity to induce apoptosis (Zha *et al.,* 1996). Their pro-life function is evident as overexpression

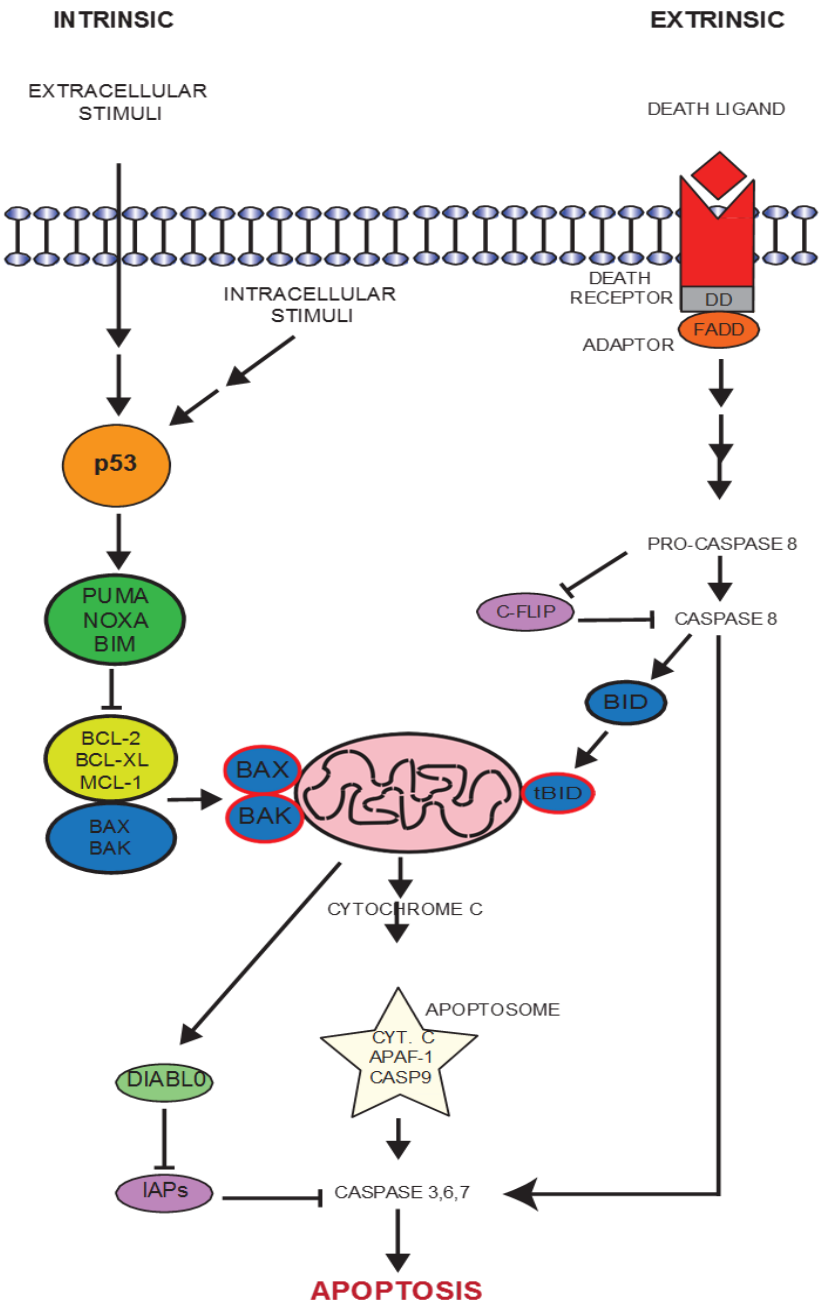

Fig 1.6. The extrinsic and intrinsic apoptotic pathways. Both pathways converge on the executioner caspases 3, 6 and 7. **The intrinsic pathway**. Extracellular apoptotic stimuli such as cytokine deprivation are passed across the plasma membrane. Intracellular stimuli such as increased ROS and intracellular Ca^{2+}, hypoxia or glucose deprivation transduce intracellular signals. Both intra and extracellular stimuli are thought to activate p53, which results in the transcription and post-translational modification of sensitizer BH3 proteins Pums, Noxa and Bim. These BH3 only proteins bind pro-life proteins Bcl-2, Bcl-XL and Mcl-1. This binding prevents them from heterodimerising with the pro-death proteins. This enables BAX and BAK to form a pore in the mitochondrial outer membrane from which cytochrome c can escape into the cytosol. Cytochrome c binds APAF-1 and caspase 9 to form the apoptosome, which can then activate the executioner caspases 3, 6 and 7. DIABLO is also released from the mitochondrial pore, inhibiting the executioner caspases inhibition by IAPS. **The extrinsic pathway**. A death ligand such as CD95L or TRAIL bind to its transmembrane death receptor such as CD95 or TRAIL-R1/2. This activates the death domain (DD) within the receptor, which then recruits an adaptor protein such as FADD, resulting in transduction of the apoptotic signal. Procaspase 8 is cleaved into the active caspase 8 (inhibiting the pro-survival C-FLIP). Caspase 8 then cleaves the executioner caspases 3, 6 and 7 and apoptosis ensues. **Pathway cross-talk**. The intrinsic and extrinsic pathways can cross-talk through the BH3-only protein BID, which is cleaved by caspase 8 in the extrinsic pathway. Activated Bid (tBid) then binds the mitochondrial outer membrane and forms a pore allowing the release of mitochondrial components such as cytochrome c.

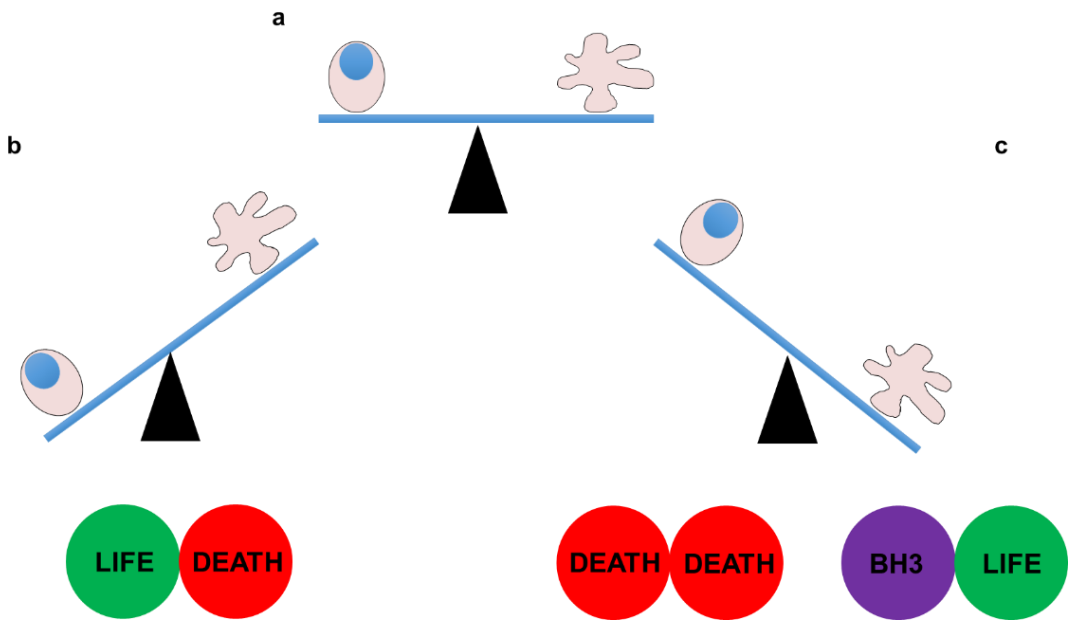

Fig 1.7. Bcl-2 family proteins life/death balance. (**a**) The relationship between the life and death of a cell relies on intricate partnerships between Bcl-2 proteins. The balance between life and death is shown schematically as a set of scales. (**b**) In order for a cell to live, the balance of the scales must tip in favour of the formation of pro-life protein interactions. The pro-life set of Bcl-2 proteins (green) must bind the pro-death proteins (red) to prevent them for executing apoptosis. (**c**) If the balance is to be tipped towards death, there needs to be more binding between protein partnerships that favour apoptosis. The BH3 proteins (purple) bind the pro-life proteins (green) and this frees up the pro-death proteins (red) to homo and heterodimerize, and illicit the apoptotic programme.

studies have shown that they confer resistance to apoptosis (McDonnell *et al.,* 1989; Strasser, Harris and Cory, 1991). Pro-death proteins such as Bax are the “effectors” of apoptosis and contain 3 BH domains (fig 1.8). They can both homodimerize and heterodimerize, which induces a conformational change from inert monomers to allow the exposure of the apoptotic BH3-domain (Czabotar *et al.,* 2013). Once bound to the mitochondrial outer membrane (MOM), the complex of pro-death proteins forms a pore in the membrane. This allows the release of cytochrome c (Jürgensmeier *et al.,* 1998) for subsequent assembly of the apoptosome and the execution of apoptosis (fig 1.6). However, the exact mechanism for BAX and BAK induced membrane permeabilisation is still unknown. BH3-only proteins are the “initiators” of apoptosis, conveying the message to start apoptosis. As the name suggests they contain just the BH3 domain (fig 1.8). They are

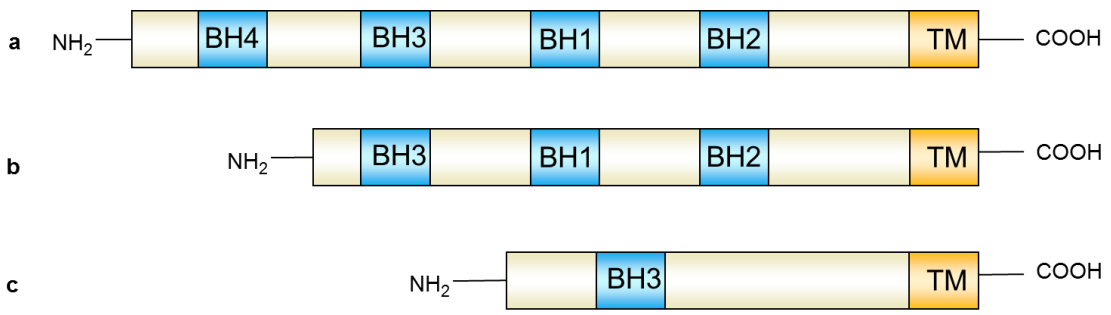

Fig 1.8. Structure of Bcl-2 family proteins. Representative examples of the BH domains in Bcl-2 family proteins. Different proteins within each group vary in size. (**a**) Pro-life proteins contain all 4 BH domains and a transmembrane domain TM. (**b**) Pro-death proteins express BH domains 1-3 and a TM domain. (**c**) BH3-only proteins lack BH 1, 2 and 4 but still possess a TM domain. Note that gene structures are not to scale.

induced either transcriptionally or post-translationally by cytotoxic stress signals (see review by Adams and Cory, 2007). BH3-only proteins can initiate apoptosis in two ways and as such are further classified into two subgroups (table 1.1). The “activators” directly bind pro-death proteins causing a conformational change that exposes their BH3 apoptotic domains (Letai *et al.,* 2002; Certo *et al.,* 2006). The “sensitizers” bind to pro-life proteins, preventing them from binding and neutralising pro-death proteins (Letai *et al.,* 2002; Chen *et al.,* 2005). Thus the BH3-only proteins both free-up and activate the pro-death proteins, to execute apoptosis.

1.5.1.3 The intrinsic pathway

The intrinsic/or mitochondrial pathway results in apoptosis induced by the release of cytochrome c from mitochondria (fig 1.6). It is carried out by Bcl-2 family proteins, stimulated by such factors as ER stress, UV-radiation, growth serum deprivation, increased ROS, increased intracellular Ca^{2+} and DNA damage (Galluzzi, Blomgren and Kroemer, 2009). Many factors of intrinsic pathway regulation are still unknown. However, cytotoxic stimuli are known to activate the tumour suppressor protein p53, which upregulates BH3-only proteins such as PUMA and NOXA (Villunger *et al.,* 2003) (fig 1.6). These BH3-only proteins bind to pro-life proteins such as Bcl-2, Bcl-XL and Mcl-1. This frees up pro-death

proteins BAX and BAK from their neutralising pro-life partners. In healthy cells BAK is constituently bound to the mitochondrial outer membrane (MOM) by its C-terminal transmembrane domain (Griffiths *et al.,* 1999). However, cytotoxic stimuli leads to the translocation of BAX from the cytosol to the MOM (Wolter *et al.,* 1997; Smaili *et al.,* 2001). BAK and BAX then homooligomerise via their BH3 domains (Dewson *et al.,* 2008). Subsequently, BAX and BAK are activated and form a pore in the MOM – the mechanism for which is unknown (see a detailed review by Czabotar *et al.,* 2014 discussing different models of BAX and BAK activation). This pore allows the release of cytochrome c, which binds with caspase 9 and APAF-1 to form the apoptosome (fig 1.6). The mitochondrial pore also allows the release of DIABLO (also known as SMAC), which binds and inhibits IAPs, preventing their inhibition of executioner caspases 3, 6 and 7 (fig 1,6) (Du *et al.,* 2000; Verhagen *et al.,* 2000). Together, the apoptosome and DIABLO allow the activation of procaspases 3, 6 and 7 and subsequent execution of apoptosis.

1.5.1.4 Crosstalk between the intrinsic and extrinsic pathways

Although the intrinsic and extrinsic apoptotic pathways are separate mechanisms that induce cell death, activation of caspase 8 as part of the extrinsic pathway can lead to mitochondrial damage and subsequent cytochrome c release (fig 1.6). After death receptor activation, caspase 8 can cleave the BH3-only protein Bid (Li *et al.,* 1998). The truncated and activated Bid (tBid) then translocates from the cytosol to mitochondria. This leads to cytochrome c release from the mitochondria (by an unknown mechanism) and apoptosis ensues (Luo *et al.,* 1998). Activation of Bid happens under specific circumstances such as non-steroidal anti-inflammatory (NSAID) drugs (Leibowitz *et al.,* 2014).

1.5.1.5 Small molecule inhibitors against pro-life proteins

Members of the pro-life Bcl-2 family of proteins are often over-expressed in cancer. This over-reliance of pro-life proteins makes it difficult to kill these cells and provides resistance to certain chemotherapeutics (Oltersdorf *et al.,* 2005). Inhibiting the pro-life proteins in these

cancer cells may enable them to be killed, paving the way for a new type of cancer therapy. Small molecule inhibitors are organic molecules of low molecular weight (usually below 750Da) meaning they are practical and cost-effective. Several small molecule inhibitors of pro-life Bcl-2 proteins have been produced, one of which, ABT-737, was used for the experiments in this thesis. Several next-generation Bcl-2 inhibtors based on the structure of ABT-737 are now in clinical trials (fig 1.9).

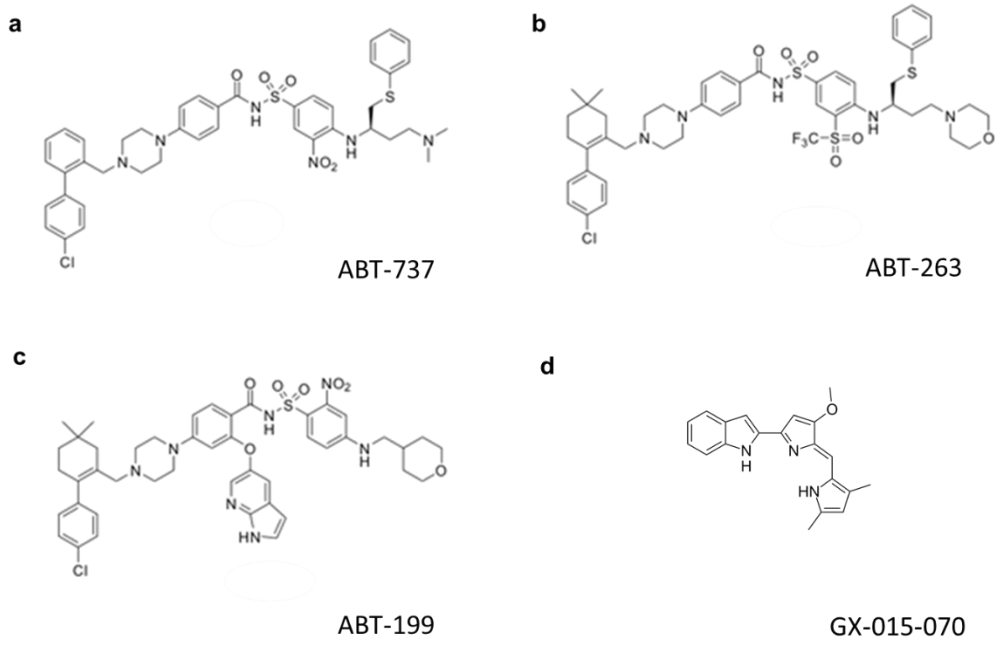

Fig 1.9. Chemical structures of Bcl-2 family protein inhibitors. (**a**) ABT-737. Structure taken from the Sussex Drug Discovery Centre. (**b**) ABT-263. Structure taken from the Sussex Drug Discovery Centre. (**c**) ABT-199. Structure taken from the Sussex Drug Discovery Centre. (**d**) GX-015-070 (Obatocloax). Image taken from Apexbio.

1.5.1.5.1 ABT-737

ABT-737 is a small molecule inhibitor of certain pro-life proteins, used for experiments in this thesis. Oltersdorf *et al.,* (2005) discovered ABT-737, a small molecule BH3 mimetic that binds Bcl-2, Bcl-XL and Bcl-w (fig 1.9a). ABT-737 does not directly activate pro-death proteins BAX or BAK. Instead, it mimics a BH3-domain and binds to the hydrophobic groove of its target pro-life proteins. This prevents their interaction with pro-death proteins. It is highly effective in perturbing Bim-Bcl-2 interactions, more so than Bim-Bcl-XL. Therefore

cells with high levels of Bcl-2 are especially susceptible to ABT-737 (Merino *et al.,* 2012). ABT-737 is currently in phase II clinical trials.

1.5.1.5.2 ABT-263 (Navitoclax)

Three key sites on the backbone of ABT-737 were identified, which affect its oral absorption, metabolism and charge. These sites were altered producing ABT-363, a second generation BH3 mimetic, structurally similar to ABT-737 but with the addition of being orally available (Fig 197b). It is selective against Bcl-2 and Bcl-XL and Bcl-w *in vitro* (Tse *et al.,* 2008). ABT-263 is currently in phase II clinical trials.

1.5.1.5.3 ABT-199

One side-effect from ABT-263 treatment was a reduction in platelets, specifically caused by Bcl-XL inhibition (which controls platelet lifespan) and ultimately meant that the drug is dose-limiting. The first small molecule inhibitor selective for Bcl-2 (alone) is ABT-199 (Souers *et al.,* 2013). Structurally similar to ABT-263 (fig 1.9c), it does not have an effect on platelets (Souers *et al.,* 2013; Vaillant *et al.,* 2013). The compound is currently in phase I clinical trials.

1.5.1.5.4 GX-015-070 (Obatoclax)

This compound (fig 1.9 d) works in two ways. It prevents Mcl-1 binding to Bak and it upregulates the BH3 only protein Bim (Trudel *et al.,* 2007). Konopleva et al., (2008) showed that this compound synergized with ABT-737 to induce apoptosis. Phosphorylated Bcl-2 was resistant to GX-015-070, but again compounding the treatment with ERK inhibitors sensitized cells with phosphor-Bcl-2 to apoptosis (Perez-Galan *et al.,* 2008). Therefore, GX-

O15-070 is emerging as a potent inducer of apoptosis when used in combination with another molecule to target Bcl-2 family proteins.

1.6 Cellular stress responses

This thesis examined the role of APC with two separate stress responses, which will now be introduced.

1.6.1 DNA damage response

There has long been a link between APC and DNA damage. This thesis aimed to discover a more robust link between the two. DNA damage is a normal consequence of DNA synthesis that needs to be corrected. DNA damage can also occur as the result of extracellular compounds and environmental agents such as chemical damage and UV-radiation. The DNA damage response (DDR) is the cooperation of cell cycle checkpoints, DDR signalling pathways and DNA damage repair in sensing, signalling and repairing DNA damage (see reviews by Rouse and Jackson, 2002; Ciccia and Elledge, 2009). DNA damage sensors ATM and ATR are recruited to damaged DNA where they act on cyclin-dependent kinases to arrest the cell cycle, allowing DNA repair to occur (Kastan *et al.,* 1992). There are multiple methods a cell can use to repair different types of damage, such as non-homologous end-joining (Thode, Schafer, Pfeiffer and Vielmetter, 1990), homologous recombination (Gerstel and Phillips, 1958; Stephens, 1961), single strand break (SSB) repair (Walker and Sridhar, 1976; Sheridan, R.B. and Huang, P.C. 1977), base-excision repair (BER) (Lindahl, 1974), nucleotide-excision repair (NER) (Grossman, Riazzudin, Haseltine and Lindan (1979) and mismatch repair (MMR) (Wildenberg and Meselson, 1975). This thesis will briefly introduce BER.

The base excision repair (BER) pathway typically removes incorrect or damaged bases that do not distort the helix structure, such as deamination, oxidation or alkylation. DNA glycosylases recognise and remove these bases from DNA by hydrolysing the glycosylic bond between the target base and deoxyribose sugar (Lindahl, 1974), creating AP site(s) (apurinic/apyrimidinic). An AP endonuclease then cleaves and removes the remaining DNA backbone at the 5' end. The endonuclease then recruits DNA polymerase β, which synthesises the correct base(s) and a ligase seals the single strand break (Bennett *et al.,* 1997). Short-patch BER is the correction of one base (Kubota *et al.,* 1996), whereas long-patch BER involves the processing of two or more bases (Klungland and Lindahl, 1997). Note that DNA damage resulting in helix distortion is often repaired by the related pathway, nucleotide excision repair.

1.6.2 The unfolded protein response

Over the course of this thesis a link was made between cell treatments ABT-737, Taxol® and siRNAs with ER stress, specifically, the unfolded protein response (UPR) (fig 1.7). The endoplasmic reticulum (ER) is a large tubular network that is a site of metabolic processes, the main store of intracellular calcium and the site of protein folding in the cell (Rao *et al.,* 2001). ER stress occurs when there is an accumulation of unfolded or misfolded proteins in the ER. To resolve the ER stress the cell activates the evolutionally conserved, pro-survival, unfolded protein response (UPR) (Hollien, 2013). This mechanism aims to resolve ER homeostasis by reducing the ER burden through signalling to both the nucleus and the cytosol (fig 1.7). This signalling acts to control gene transcription, protein translation and expansion of the ER to increase its protein folding capacity (Hetz, 2012). However, if the ER stress is irremediable then the UPR can initiate apoptosis (Nagawa *et al.,* 2000; Rao *et al.,* 2001; Marciniak *et al.,* 2004). If the ER stress continues without UPR activation, the toxic aggregation of unfolded proteins can lead to disorders such as Parkinson's disease, ischaemia and diabetes (Kaufman, 2002).

The UPR signals are transduced by three main stress sensors embedded in the ER (see an excellent review by Hetz, 2012). During unstressed conditions the ER chaperone BiP (also known as GRP78) binds to the luminal surface of the stress sensors. However, during ER stress (fig 1.7), BiP dissociation triggers sensor activation and the UPR (Bertolotti *et al.,* 2000).

The transmembrane kinase inositol requiring enzyme alpha (IREα) (Nikawa and Yawashita, 1992; Cox *et al.,* 1993) dimerises upon ER stress and autotransphosphorylates to activate its cytosolic RNase domain (Shamu and Walter, 1996; Liu, Schroder and Kaufman, 2000). The now active P-IRE (phosphorylated-IRE) has three main functions (fig 1.7). It recruits the adaptor protein TRAF2, which signals through JNK and interacts with NF-kB subunit IKK to alert the cell to ER stress (Hu *et al.,* 2006). P-IRE also degrades certain mRNAs through the RIDD protein, preventing de novo protein synthesis (Hollien *et al.,* 2009). P-IRE also induces gene-transcription of ER stress genes by inducing the mRNA processing of X-BP1. X-BP1 is a transcription factor of genes involved in protein folding, protein quality control and ER-associated degradation (ERAD) genes (Cox and Walter, 1996).

Another ER transmembrane stress sensor, protein kinase-like ER kinase (PERK) dimerises and autotransphosphorylates upon ER stress (Harding, Zhang and Ron, 1999; Liu, Schroder and Kaufman, 2000) (fig 1.7). Phosphorylated PERK (P-PERK) phosphorylates eukaryotic translation initiation factor two alpha (eIF2α) on serine 51 of the alpha subunit (Sudhakar *et al.,* 2000). Phosphorylated eIF2α halts most de novo protein synthesis by interfering with the translation-initiation complex (Srivastava, Davies and Kaufman, 1995). Lastly, peIF2α allows the translation of *ATF4* mRNA (fig 1.7), a transcription factor for genes involved in autophagy, apoptosis, amino acid metabolism and antioxidant responses (Harding *et al.,* 2000).

Thirdly, activating transcription factor 6 (ATF6) is another transmembrane stress sensor, which has a cytosolic basic leucine zipper (bZIP) transcription factor (Haze *et al.,* 1999) (fig 1.7). In stressed cells ATF6 is transported to the Golgi apparatus through interaction with the vesicular traffic protein COPII (Schindler and Schekman, 2009). At the Golgi, ATF6 is processed by proteases S1P and S2P to release the cytosolic bZIP fragment, ATF6f. ATF6f then translocates into the nucleus (Ye *et al.,* 2000). Here, it controls the transcription of *ERAD* genes and *X-BP1*, which is subsequently spliced by P-IRE (Yoshida *et al.,* 2001; Lee *et al.,* 2002; Yamamoto *et al.,* 2007).

1.7 Overall aims of the thesis

This thesis aims to examine the non-Wnt functions of APC. In order to achieve this I aimed to use a reverse-genetics approach to create a conditionally, degradable APC in DT40 cells using the auxin-inducible degron (AID) system. This meant that immediate consequences of APC depletion could then be studied. Once the cell-line had been produced I aimed to use it to deplete APC and then introduce fragments of *Apc* to determine if APC loss-induced phenotypes could be rescued. This would then link certain areas within APC with a specific cellular function. When the AID-system cell line produced off-target effects, a new approach of studying the non-Wnt functions of APC was required. My project moved on to examine the link between APC and (the non-Wnt function) apoptosis, previously eluded to in the literature, but which lacked molecular explanation. A previous student in the lab had discovered that the use of the Bcl-2 inhibitor ABT-737 overcame the resistance of *Apc* deficient cells to Taxol®. This then prompted a study into a link between APC and Bcl-2 family proteins (which govern the intrinsic apoptotic pathway). Once identified, I wanted to establish the link between APC and Bcl-2 and the effect(s) that *Apc* loss/mutant APC had on these proteins and their known functions. Furthermore, I wanted to be able to explain why Bcl-2 inhibitors sensitised *Apc* deficient cells to the microtubule poison Taxol®.

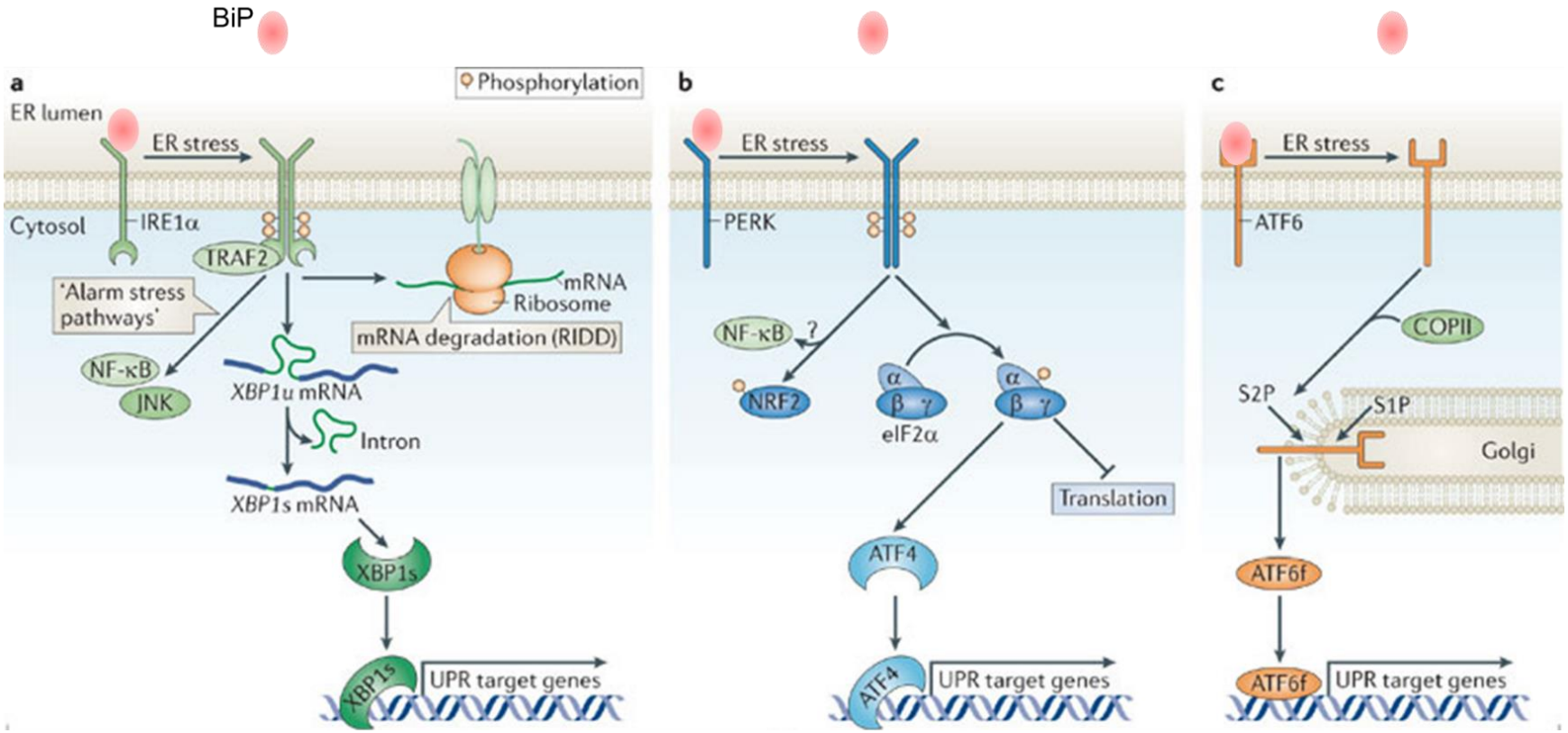

Fig 1.8. The unfolded protein response. In unstressed cells the ER chaperone BiP is bound to the luminal surface of all three ER transmembrane stress sensors, IRE, PERK and ATF6. (**a**) BiP dissociation upon ER stress leads to IRE dimerization and autotransphosphorylation. Phospho-IRE recruits the adaptor TRAF2 that signals to JNK and binds the NF-kB subunit IKK to alarm the cell to ER stress. P-IRE also causes mRNA degradation through the RIDD protein and induces XBP1 mRNA processing. The XBP1 protein is a transcription factor and activates transcription of UPR target genes. (**b**) After BiP dissociation, PERK dimerises and autotransphosphorylates. PERK then phosphorylates eIF2α which can inhibit de novo protein synthesis and activate ATF4, a transcription factor of UPR genes. (**c**) BiP dissociation leads to the binding of the vesicular transport protein COPII. ATF6 is transported to the Golgi where its cytosolic domain is cleaved by proteases S1P and S2P. The cleaved ATF6f is a transcription factor that activates transcription of UPR target genes. Figure adapted from Hetz (2012).

Chapter 2 - Materials and Methods

2.1 Materials

2.1.1 Antibiotics

2.1.1.1 Ampicillin

Ampicillin (Melford, 69-52-3) was stored at a stock concentration at 100µg/ml. Stored at -20°C.

2.1.1.2 Blasticidin

Blasticidin (Invivogen, ant-bl-5) was stored at a stock concentration at 10mg/ml. Stored at -20°C.

2.1.1.3 Kanamycin

Kanamycin (SIGMA, K1377-5G) was stored at a stock concentration at 50µg/ml. Stored at -20°C.

2.1.2 Drugs

2.1.2.1 ABT-737

A 1mM stock of ABT-737 (Selleck Chemicals, LLC S1002) was diluted in media and added to cells at a final concentration of 7µM for 24 hours before harvesting (unless otherwise stated).

2.1.2.2 Cisplatin

A 1mM stock of Cisplatin (Calbiochem, D00155099) was added to cells at a final concentration as indicated in the text, for 2 hours.

2.1.2.3 Hydroxyurea

A 100mM stock of Hydroxyurea (SIGMA, H8627-5G) was added to cells at a final concentration as indicated in the text, for 16 hours.

2.1.2.4 PARPi

A 10mM stock of PARPi (Olaparib, Axon Medchem, Axon 1463) was added to cells to a final concentration as indicated in the text, for 24hours

2.1.2.5 Taxol®

Taxol® (SIGMA T1912) was stored as a stock solution of 5.9mM. A dilution in media was made to create a working solution of 5.9µM and this was added to cells at a final concentration as stated in the text.

2.1.3 Buffers and Stains

2.1.3.1 Agarose-gel electrophoresis

2.1.3.1.1 50 X TAE

2M Tris Acetate, 50mM EDTA and 0.05% glacial acetic acid. A 1X solution was then used for agarose gel electrophoresis. Stored at RT.

2.1.3.2 Western blot

2.1.3.2.1 MEBC lysis buffer

50mM Tris-HCl pH 7.5, 100mM NaCl, 5mM EDTA-Na, 5mM EGTA-Na, 40mM β-glycerophosphate, 0.5% NP40. Inhibitors (10µg/ml) added right before use: LPC (leupeptin, pepstatin A and chemystatin), 1M NaF and 0.1M $NaVO_4$. Solution filter sterilised. Stored at 4°C.

2.1.3.2.2 RIPA lysis buffer

150mM sodium chloride, 1% NP-40/Triton-X-100, 0.5% sodium deoxycholate, 0.1% SDS and 50mM Tris, pH 8.0. Solution filter sterilised. Stored at 4°C.

2.1.3.2.3 PBS

80g NaCl, 2g KCl, 14.4g Na_2HPO_4, 2.4g KH_2PO_4 and H_20 up to 1L. Store at RT.

2.1.3.2.4.TBS

121.4g Tris, 81.9g NaCl and add H_20 up to 1L. Use HCl to pH to 7.4. Store at RT.

2.1.3.2.5 1X TBS-T/Wash buffer

1X TBS and 0.1% Triton-X. Stored at RT.

2.1.3.2.6 1X TBS-T Milk/blocking agent

10% 1X TBS, 5% non-fat milk, 1% donkey serum, 0.02% Triton X, 0.02% NaN_3. Stored at 4°C.

2.1.3.2.7 1XTBS-T – BSA

1X TBS, 0.02% Tween-20 and 5% BSA. Stored at 4°C.

2.1.3.2.8 Ponceau S

0.1% ponceau in 1% acetic acid. Stored at RT.

2.1.3.2.9 Nitrocellulose stripping buffer

NewBlot™ Nitrocellulose 5X stripping buffer (Li-cor® Biosciences 928-4030). Used neat for 15 mins.

2.1.3.2.10 Coomassie

2.1.3.2.10.1 Stain

0.1% Coomassie Brilliant blue, 50% EtOH and 10% acetic acid. Coomassie powder mixed in EtOH o/n and then other constituents were added. Solution filter sterilized. Stored at RT.

2.1.3.2.10.2 Destain 1

40% EtOH and 10% acetic acid. Stored at RT.

2.1.3.2.10.3 Destain 2

15% EtOH and 10% acetic acid. Stored at RT.

2.1.3.2.11 20x MOPS SDS-running buffer

MOPS 50mM, TRIS Base 50mM, SDS 3.47mM, EDTA 1mM. Sourced from FORMEDIUM™ (MOPS-SDS1000). Stored at RT.

2.1.3.2.12 Running buffer

1X MOPS and H_20 up to 500ml. To the central chamber of the gel tank, 0.25% NuPage antioxidant (Invitrogen NP0005) was added. Stored at RT.

2.1.3.2.13 Transfer buffer

2X Laemmli, 7.5% methanol and 0.02% of 20% SDS. Stored at 4°C.

2.1.3.2.14 10X Laemmli buffer (1L)

30g Tris Base, 144g glycine, 10g SDS and H_20 up to 1L. Store at RT.

2.1.3.2 Immunoprecipitation

2.1.3.2.1 IP wash buffer

20mM Tris-HCl pH 7.5, 150mM NaCl, 1mM EDTA 0,05% Triton-X-100, 5% glycerol and protease inhibitor cocktail (1 per 50ml/1:1000). Solution filter sterilized. Stored at 4°C.

2.1.3.3 Immunofluorescence in 2D (cell culture)

2.1.3.3.1 Permeabilisation buffer

1% NP40 in 1X PBS. Stored at RT.

2.1.3.3.2 Blocking Buffer

5% goat serum diluted in 1X PBS, 2% BSA, 0.02% NaN_3 and 0.1% TX-100. Stored at 4°C.

2.1.3.3.3 Incubation buffer

1X PBS, 2% BSA, 0.02% NaN_3 and 0.1% TX-100. Stored at 4°C.

2.1.3.3.4 Wash buffer

1X PBS, 0.02% NaN_3 and 0.2% BSA. Stored at 4°C.

2.1.3.3.5 Mounting medium

90% glycerol, 20mM Tris pH 8.8 and 0.5% p-phenylenediamine. Stored at RT.

2.1.3.4 FACs

2.1.3.4.1 Blocking buffer (100ml)

1X PBS, 0.1% Tween-20 and 1% Bovine Serum Albumin (Sigma-Aldrich).

Stored at 4°C.

2.1.4 Antibodies

2.1.4.1 Primary antibodies

TABLE 2.1

Primary Antibodies and IF Counterstains/Dyes

Name	Spec.	Application				Source	Antigen (aa)
		WB	IP	IF	FACS		
Ali (APC)	M mc	1/1000	1mg/ml	ND	ND	CRUK	-
Bcl-2 (E17)	R mc	1/1000	1/50	1/75	ND	Abcam ab32124	50-150
BrdU	M mc	ND	ND	ND	1/500	BD Pharmagen 555627	-
C-APC	R pc	1/1000	ND	ND	ND	Hybridoma	2815-2829
Calnexin (C5C9)*	R mc	1/1000	ND	ND	ND	CST 2679S	Full Length
CAIX	R pc	1/2000	ND	1/500	ND	Novus Biologicals NB100-417	400-500
DAPI	-	ND	ND	1/5000	ND	SIGMA D-9542	-
GAPDH	M mc	1/2000	ND	ND	ND	Millipore MAB374	Full
GFP	M mc	1/1000	ND	ND	ND	Roche 11814460001	-
HIF1-α	M mc	1/1000	ND	ND	ND	BD Bioscience 610958	610-727
Histone H3 (Phospho S10)	R pc	1/1000	ND	ND	1/300	Abcam ab5176	S10
Hoechst 33342	-	-	-	1/500	ND	Invitrogen Molecular Probes H1399	-
HSP60 (D85)*	R pc	1/500	ND	ND	ND	CST 4869S	D85 residue
IgG	M mc	ND	1mg/ml	ND	ND	SIGMA I-5381	-

IgG	R pc	ND	1mg/ml	ND	ND	SIGMA I-5006	-
IRE1 (14C10)*	R mc	1/1000	ND	ND	ND	CST3294	His963
IRE1 (Phospho S724) [EPR5253]	R mc	1/1000	ND	ND	ND	Abcam ab124945	S724
Keratin 18 (RCK 106)	M mc	Neat Hybridoma	ND	ND	ND	Ramaekers *et al.,* (1987)	-
MitoTracker® Deep Red FM	-	ND	ND	500nM	ND	Gibco™ 51985_026	-
Myc	M mc	1/1000	ND	ND	ND	Santa Cruz SC-9E10	408-439
Na/K ATPase*	R pc	1/1000	ND	ND	ND	CST 3010	Amino terminus
N-APC	R pc	1/1000	1mg/ml	ND	ND	Hybridoma	8-347
Par4*	R pc	1/500	ND	ND	ND	Abcam ab5787	324-342
PDI (C81H6)*	R mc	1/1000	ND	1/100	ND	CST 3501	Synthetic peptide
Phalloidin DyLight™ 550	-	-	-	1/500	ND	ThermoFisher 21835	F-actin binding
Topoisomerase II α (D10G9) XP®*	R mc	1/1000	ND	ND	ND	CST 12286	C-terminus
YL1/2 (tubulin)	Ra pc	1/25	ND	1/25	ND	Abcam ab6160	Full
β-catenin	M mc	1/1000	ND	1/500	ND	BD Biosciences 610154	571-781
β-catenin 74	R pc	1/1000	1mg/ml	ND	ND	Hinck, Nelson & Papkoff (1994)	-

Table 2.1. R=rabbit, Ra=rat, M=mouse, Mc=monoclonal, Nd=not determined, Pc=polyclonal, Spec=species.

2.1.4.2 Secondary antibodies

TABLE 2.2					
Secondary Antibodies					
Use	**Species**	**Excitation**	**Dilution**	**Incubation**	**Source**
WB	Rabbit	Alexa-Flour®680 800nm DyLight™	1/5000	1 hr RT	800nm – Rockland 680nm – Molecular Probes
WB	Mouse	Alexa-Flour®680 800nm DyLight™	1/5000	1 hr RT	
WB	Rat	Alexa-Flour®680 800nm DyLight™	1/5000	1 hr RT	
WB	Mouse anti-rabbit IgG Conformation Specific (no detection of denatured & reduced rabbit HC or LC)	-	1/2000	1hr RT	Cell Signalling 3678
WB	Goat anti-mouse IgG1 (LC specific)	800nm IRdye	1/15000	1hr RT	Li-cor Biosciences 926-32350
FACS	Goat anti-mouse	FITC	1/100	30min RT	BD Pharmagen 554001
FACS	Goat anti-rabbit	FITC	1/100	30min RT	BD Pharmagen 554020
IF	Rabbit	Alexa-Flour® 488	1/500	1 hr RT	Invitrogen Molecular Probes

2.1.5 Bacterial strains

Subcloning Efficiency™ DH5α™ competent cells (Invitrogen, 18265-017).

2.1.6 Plasmids

For available plasmid maps see supplementary figures 1 and 2.

2.1.6.1 pc.DNA3.1HisOsTlR9xMyc

A kind gift from Noel Lowndes (NUI, Galway), courtesy of Prof. Kanemaki of the Department of Biological Sciences, Graduate School of Science, Osaka University, Osaka, Japan.

2.1.6.2 pGK-Cre

See Lallemand *et al.,* (1998).

2.1.6.3 pGFP

A kind gift from MacKintosh lab, Cellular and Developmental Biology, University of Dundee (generated from pcDNA5.FRT).

2.1.6.4 pGFP-Bcl-2

Addgene plasmid #17999.

2.1.6.5 pEGFP-C1

Discontinued Clontech plasmid. See Addgene plasmid information 2487.

2.1.6.6 pCMV-NEO-BAM-APC

Generated in the lab. *Apc* cDNA with BamHI restriction sites.

2.1.6.7 pJET1.2/blunt

Obtained as part of the CloneJET PCR Cloning Kit, Thermo Scientific™, K1231.

2.1.6.8 pFLAG

A kind gift from MacKintosh lab, Cellular and Developmental Biology, University of Dundee (generated from pcDNA5.FRT).

2.1.6.9 pFLAG-Bcl-2

Addgene plasmid #18003.

2.1.6.10 pAID1.2N

A kind gift from Prof. Kanemaki of the Department of Biological Sciences, Graduate School of Science, Osaka University, Osaka, Japan.

2.1.6.11 Targeting vectors

Generated by CJ Baird, Hiom lab, Jacqui Wood Cancer Centre, University of Dundee.

2.1.6.11.1 pGFP-IAA17-APC-Bsd [+]

A GFP-degron (IAA17) tag targeted 5' of chicken *Ap*c exon 1 using 2 arms of homology. A floxed Bsr cassette is included in the same transcriptional orientation as the tags and *Apc*, driven by the β-actin promoter. 13,829bp.

2.1.6.11.2 pIAA17-APC-Bsd [+]

A degron (IAA17) tag targeted 5' of chicken *Ap*c exon 1 using 3 arms of homology. A floxed Bsr cassette is included in the same transcriptional orientation as the tags and *Apc*, driven by the β-actin promoter. 13,245bp.

2.1.7 Oligonucleotides

2.1.7.1 Oligonucleotides for gPCR

TABLE 2.3		
gPCR Primers EUROFINS MWG Operon 100μM Stock		
Name	**Sequence**	**Tm (°C)**
GFP F	CACATGAAGCAGCACGACTTCT	60.3
GFP R	AACTCCAGCAGGACCATGTGAT	60.3
Bsd F	ATGAAAACATTTAACATTTCTC	49.1
Bsd R	TAATTTCGGGTATATTTGAGVTGG	55.3
5'Arm-2R	GTGTGTTGGTGCAAGTTCAGG	59.3
5'Arm-3R	ACTGGTGATGTGGAATTTGC	59.3

5’Arm-4R	CAAGTGACAAGGTTTCAGA	59.3
5’Arm-5R	ACATTACTTCATCTCACCC	59.3
5’Arm-2 1F	CCTCTTAACTACCAACTCTACCA	58.9
IAA17 1R	AGCTCTGCTCTTGCACTTCTCC	58.9

2.1.7.2 siRNAs

TABLE 2.4		
siRNAs		
Name	**Source**	**Final Concentration**
Control siRNA	QIAGEN 1027281	10nM
CTNNB1	QIAGEN Flexitube 1027418; S102662478	10nM
APC	EUROFINS siAPC 5,6 & 7	10nM
Bcl-2_0	QIAGEN Flexitube SI00299397	20nM
Hif1α	5’-CUGAUGACCAGCAACUU-3’ (Eurofins)	20nM

2.1.7.3 qRT-PCR primers

TABLE 2.5		
qRT-PCR Primers EUROFINS MWG Operon 100μM Stock		
Name	**Sequence**	**Tm (°C)**
Actin F	CTGGGAGTGGGTGGAGGC	62.8
Actin R	TCAACTGGTCTCAAGTCAGTG	57.9
APC-1 F	GGAAGCATTATGGGACATGG	57.3
APC-1 R	TACTTCGCAGGCCTATTTGC	57.3
β-catenin-2 For	ATGGCTTGGAATGAGACTGC	57.3
β-catenin-2 Rev	TTCCATCATGGGGTCCATAC	57.3
Cyclin D F	GGCGGATTGGAAATGAACTT	55.3
Cyclin D R	TCCTCTCCAAAATGCCAGAG	57.3

2.1.8 Matrigel

Matrigel (basement membrane growth factor reduced), phenol red free (BD Bioscience 356231, batch 503306 11mg/ml).

2.2 Cell Culture Methods

2.2.1 Cell lines

See table 2.6.

TABLE 2.6							
Cell lines and organoids							
Name	**Type**	**Sp**	**Mutation(s)/Viruses / Morphology**	**Culture Media**	**Supplements**	**Culture Ad/S**	**Source**
341	MEFs	M	$APC^{+/+}$	DMEM [+]4.5g/L D-Glucose, L-Glutamine and Pyruvate (Gibco™ Life Technologies)	10% FBS, 1% NEAA, 1% P/S	Ad	Gift from R.A. Weinberg, Whitehead Institute, MA
335	MEFs	M	Unstable *Apc* mRNA	DMEM [+]4.5g/L D-Glucose, L-Glutamine and Pyruvate (Gibco™ Life Technologies)	10% FBS, 1% NEAA, 1% P/S	Ad	Gift from R.A. Weinberg, Whitehead Institute, MA
CaCo2	Colorectal adenocarcinoma	H	*Apc* 1367 C>T (nonsense mutation)	DMEM [+]4.5g/L D-Glucose, L-Glutamine and Pyruvate (Gibco™ Life Technologies)	10% FBS, 1% NEAA, 1% P/S	Ad	American Type Culture Collection®
DLD1	Colorectal adenocarcinoma	H	*Apc* nonsense mutation	DMEM [+]4.5g/L D-Glucose, L-Glutamine and Pyruvate (Gibco™ Life Technologies)	10% FBS, 1% NEAA, 1% P/S	Ad	American Type Culture Collection®
DT40	B cell lymphoma	Ck	1. *C-myc* activation (due to ALV integration) immortalizes cells	RPMI 1640 (1x) [+]L-glutamine (Gibco™, Life Technologies)	10% FBS, 3%CS, 1% P/S, 0.05% β-ME	S	American Type Culture Collection®
$DT40^{TIR}$	B cell lymphoma	Ck	1. *C-myc* activation (due to ALV integration) immortalizes cells 2. OsTIR1 random integration	RPMI 1640 (1x) [+]L-glutamine (Gibco™, Life Technologies)	10% FBS, 3%CS, 1% P/S, 0.05% β-ME	S	Created in lab
$DT40^{TIR}$-EGFP-	B cell lymphoma	Ck	1. *C-myc* activation (due to ALV integration)	RPMI 1640 (1x) [+]L-glutamine (Gibco™, Life Technologies)	10% FBS, 3%CS, 1% P/S, 0.05% β-ME	S	Created in lab

IAA17-APC-KI			2. GFP-IAA17 KI 5' to *Apc* exon 1				
$DT40^{TIR}$-IAA17-APC-KI	B cell lymphoma	Ck	1. *C-myc* activation (due to ALV integration) 2. IAA17 KI 5' to *Apc* exon 1	RPMI 1640 (1x) [+]L-glutamine (Gibco™, Life Technologies)	10% FBS, 3%CS, 1% P/S, 0.05% β-ME, 30ug/ml Blasticidin S	S	Created in lab
HCT116 (HD PAR 007)	Colorectal adenocarcinoma	H	1. β-catenin$^{Ser45\ del/+}$ 2. $KRAS^{G13D/+}$	RPMI 1640 L-Glutamine (Lonza, Biowhittaker® BE12-702F)	10% FBS, 1% P/S	Ad	Horizon Discovery
HeLa	Cervical adenocarcinoma	H	HPV insertion; degrades p53	DMEM [+]4.5g/L D-Glucose, L-Glutamine and Pyruvate (Gibco™ Life Technologies)	10% FBS, 1% NEAA, 1% P/S	Ad	American Type Culture Collection®
SW480	Colorectal adenocarcinoma	H	*Apc* 1330 C>T (nonsense mutation)	DMEM [+]4.5g/L D-Glucose, L-Glutamine and Pyruvate (Gibco™ Life Technologies)	10% FBS, 1% NEAA, 1% P/S	Ad	American Type Culture Collection®
U2OS	Osteosarcoma	H	(APC and β-catenin WT)	DMEM [+]4.5g/L D-Glucose, L-Glutamine and Pyruvate (Gibco™ Life Technologies)	10% FBS, 1% NEAA, 1% P/S	Ad	CRUK
WT Organoids	C57BL/6J	*Apc* WT mouse	Branched	Crypt Media: 500ml Advanced DMEM/F12 supplemented with 1% P/S, 1% HEPES, 1% 200mM Glutamax, 0.2% 500mM N-acetylcysteine, 1% 100X N2 and 2% 50X B27	Growth Factors, ENR diluted in crypt media: 5% 500ug/ml EGF, 2% 100ug/ml Noggin, 25% R-spondin conditioned media	-	Jackson Laboratory, CA USA

Min Organoids	C57BL/6J	*Apc* Min Mouse	1. $Apc^{Min/+}$ Codon 850 (nonsense) 2. $Apc^{Min/Min}$ 3. Branched until ~P5 - Then cysts	Crypt Media	1. ENR 2. None once cyst morphology	-	Jackson Laboratory, CA USA

Table 2.6. Ad=adherent, Ck=chicken, H=human, M=mouse, S=suspension, Sp=species

2.2.1.1 Suspension cells (DT40)

2.2.1.1.1 Passaging cells

DT40-KI transfected cells were grown with 30μg/ml Blasticidin S (selectable marker). The cells were incubated at 37°C/5% CO_2, grown to confluency (~1x10^6/ml), counted using the CASYcounter (Innovatis) and split every other day. Optimal cell culture was considered to have >90% viable cells. Cells were taken up from liquid nitrogen storage, cultured in a T-25 flask with 7ml pre-warmed media o/n at 37°C/5% CO_2 and split the next day (when confluent).

2.2.1.1.2 Freezing cells for long-term storage

3x10^6 cells were pelleted (~passage III-V) and resuspended in 500μl of freezing media (90% FBS: 10% DMSO). 500μl aliquots were frozen at -80°C for 24 hours and subsequently moved to liquid nitrogen for long-term storage.

2.2.1.2 Adherent cells

2.2.1.2.1 Passaging cells

To split the cells the media was aspirated, the cells washed in Dulbecco's PBS (DPBS), washed in trypsin (SIGMA T4174, diluted 1:100 in Dulbecco's PBS) and then incubated in trypsin at 37°C/5% CO_2 until the cells detached from the surface of the dish. Trypsin was then inactivated by adding fresh pre-warmed media to the dish (media was added at double the volume of trypsin). Depending on the desired dilution, a certain volume of the cell suspension was transferred into a new flask/dish (TPP) and the appropriate volume of media added. Cells were then incubated at 37°C/5% CO_2.

2.2.1.2.2 Freezing cells for long-term storage

Cells were washed in Dulbecco's PBS, trypsinized and resuspended in 50μl freezing media (90% FBS + 10% DMSO). Aliquots were then frozen at -80°C for 24 hours and subsequently moved to liquid nitrogen tanks for long-term storage.

2.2.2 Organoid culture

2.2.2.1 Intestinal crypt isolation

Crypt isolation was performed by Dr. Alistair Langlands (Näthke lab, University of Dundee) as per Sato.T *et al.,* (2009). Organoids were derived from *Apc* WT and *Apc*$^{Min/+}$ mice, see table 2.6.

2.2.2.2 Culturing and passaging

The protocol was adapted from Sato.T *et al.,* (2009) and carried out as follows. Media was aspirated from the wells of a 24 well plate without interfering with the Matrigel dot in the centre of the wells. 1ml of cold ADF added to each well. A pipette tip was used to scrape the bottom of the well to disrupt the Matrigel and resuspend the organoids. Then the solution was pipetted into a fresh falcon tube and mixed by pipetting. The tube was spun for 3mins at 600rpm to collect an organoid pellet. To wash the pellet it was resuspended in 3ml ADF and spun again for 3mins at 600rpm. The media was aspirated, but this time some media was left to leave a total volume of approximately twice the size of the pellet. The pellet was resuspended in the residual media. 100μl Matrigel was added and one drop of the Matrigel/media/organoid mixture was added to the centre of 6 wells in a 24-well plate. The plate was kept at 37°C/5% CO_2 incubator for >5mins to allow the Matrigel to set. Finally 500μL of pre-warmed crypt media (plus growth factors) (see table 2.6) was pipetted down the side of each well so as not to disturb the Matrigel dot. Plates were then put back into the incubator at 37°C/5% CO_2.

2.2.3 Transfection procedures

2.2.3.1 Transient transfection in suspension cells by electroporation

DT40 cells were set up one day prior to transfection at $2x10^5$/ml. On the day of transection, using the Amaxa® Cell Line Nucleofector® Kit T (Lonzabio): 82μL of room temperature Nucleofector® Solution added to 18μl of supplement, per transfection. $3x10^6$ cells were pelleted per transfection, the supernatant removed and the pellet resuspended in the 100μl Nucleofector® solution. 7-10μg of pDNA was typically added to the cell suspension, transferred to an Amaxa certified cuvette, inserted into the Nucleofector® cuvette holder and run under the appropriate program (B-0023). To electroporate the cells the cuvettes were incubated for 10mins at RT. Then 500μl of pre-warmed, pre-equilibrated RPMI 1640 + L-glutamine was added to the cuvette and gently transferred to a 6cm culture dish containing 5ml of pre-warmed media. Dishes were then incubated at 37°C/5% CO_2 for 48 hours.

2.2.3.2 Stable transfection for targeted insertion in DT40 Cells

Cells were set up one day prior to transfection at $2x10^5$/ml. On the day of transfection, $6x10^6$ cells were pelleted per transfection and 30μg of EtOH–purified, linearized targeting vector added. Cells/DNA/PBS mixture was electroporated using the Biorad Gene Pulser at 550V, 25μF and ∞ resistance. The time constant was usually in the region of 0.8ms. Cells were incubated on ice for 10 minutes, added to 20ml pre-warmed media and then left to recover o/n in 37°C/5% CO_2 incubator. Subsequently, the volume of the media was brought up to 60ml, 30μg/ml of the selective drug (Blasticidin S) added and the cells seeded onto 96 well plates using a multi-channel pipette. Colonies were expanded after 7-10 days into 24 well plates with 1ml of pre-warmed media and subsequently into 6 well plates with 4ml pre-

warmed media. Scaled up clones were cultured in T-75s and screened for targeted insertion of the targeting vector by genomic PCR (gPCR).

2.2.3.3 Transient transfection in adherent cells by chemical methods

Cells were set up one day prior to transfection at 25-30% confluency in a T25 flask (TPP). Fugene 6® transfection reagent (Promega E2691) was allowed to warm to room temperature and then 8μL was added to 50μl pre-warmed media, mixed and incubated at room temperature for 5 mins. 2μg of pDNA was then added to the Fugene/media and allowed to incubate at room temperature for >15mins (<45mins). The solution was added drop-wise onto the cells. The transfection procedure was repeated again after 24 hours and left for a further 24 hours (unless indicated) before the cells were harvested.

2.2.3.4 Excision of Floxed Sequences by Transient Expression of Cre

DT40$^{TIR\text{-}(GFP)\ IAA17\text{-}APC}$ cells were set up one day prior to transfection at 2x10^5/ml. On the day of transfection the bacteriophage P1 site-specific recombinase Cre was transiently transfected into 3x10^6 cells by adding 4μg of pPGK-Cre (Lallemand *et al.,* 1998). To transfect the cells they were electroporated with the Amaxa Nucleofector System (Lonzabio). The transfected cells were then grown in 6cm dishes with 5ml of RPMI and left to recover o/n in 37°C/5% CO_2 incubator. Subsequently subcloning by limiting dilutions was set up (see 2.2.4).

2.2.4 Subcloning by limiting dilution to derive clonally related cells from a heterogeneous population (DT40)

To generate a 96-well plate containing single cells per well, 3x50ml falcon tubes were prepared with 30, 100 and 300 cells in 20ml media respectively. 200μl of each dilution was plated out onto 96 well plates. Plates were then incubated for 7 days at 37°C/5% CO_2

without a change of medium. 24 subclones from each plate were then picked, replica-plated and grown both in the presence and absence of Blasticidin S. Clones that did not grow in the presence of the selective antibiotic were chosen indicating successful Cre recombination and Bsr excision. Loss of the Bsr cassette was then confirmed by PCR.

2.2.5 MTS cell proliferation assay

The MTS assay is a colorimetric viability assay. A tetrazolium compound is added to cells, and in viable, metabolically active cells the compound is bioreduced by NADPH/NADH into a soluble, formazan product. The absorbance (nm) of the formazan product is then measured to produce a measure of viability. The PROMEGA CellTiter 96® Aq_{ueous} One Solution Cell Proliferation Assay (G3580) was used as per the manufacturer's instructions. DT40 cells were cells cultured in T-25 flasks (15,000cells/100μl in a total volume of 5ml) with varying concentrations of: PARPi for 24 hours; Cisplatin for 2 hours; or Hydroxyurea for 16 hours. Cells were then pelleted, media aspirated off and the cells resuspended in the same volume of fresh media (no drug). 100μl of the cell suspension was pipetted into each well of a 96 well plate and left to equilibrate for 1hr at 37°C/5% CO_2. 24/48/72h after the drug was washed-off, 20μl of CellTiter 96® Aq_{ueous} One Solution Reagent added to each well and pipetted up and down to mix. Plates were incubated for 4 hours at 37°C/5% CO_2 and then the absorbance measured at 490nm using a plate reader (Biotek ELx808 Absorbance Microplate Reader).

2.2.6 Organoid cell viability assay

Organoids grown in Matrigel (see 217 and 2.2.2.2) were passaged and left for 2 days to allow adequate growth (cysts) and branching time (WT) before the assay. Organoids were then treated with varying concentrations of Taxol® for 24 hours and subsequently their viability was measured using the CellTiter-Glo® Luminescent Cell Viability Assay (Promega G7570). First, 250μl of media was removed from the wells, replaced with 250μL of CellTiter-

Glo® Reagent. Plates were then left at RT on an orbital shaker for 2 mins before sitting on the bench at RT for 10mins. Then the organoids were transferred into a luminometer-compatable 5ml tube (Sarstedt 55.476.005). The luminescence was then recorded using a luminometer (Lumat LB 9507, Berthold Technologies). A media only sample was used as a control for background luminescence, which was subtracted from the values of the sample readings.

2.2.7 Hypoxia treatment

HCT116 cells were set up 2 days prior to treatment at 10% confluency, in 15cm dishes (TPP). The dishes were put into a hypoxia chamber (1% O_2) for 24 hours. Subsequently, cells were lysed in MEBC lysis buffer (see Western blot) in the chamber to prevent reoxygenation.

2.2.8 Mitochondrial staining

Cells were set up in 3cm dishes (TPP) and treated as required. Media was aspirated and 500nM of MitoTracker® Deep Red FM (Invitrogen™ Molecular Probes™, M22426) diluted in Opti-MEM® reduced-serum medium (Gibco™, 51985_026) was added to the cells and incubated at 37°C/5% CO_2 for 45 mins. The media was aspirated, the cells washed once in Dulbecco's PBS (DPBS) and 2ml of fresh media was added. Cells were fixed and stained as detailed in 2.6.2 or they were imaged live. MitoTracker® has an emission wavelength of 665nm and was detected with a fluorescence microscope.

2.2.9 JC-1 Mitochondrial potential sensor

Cells were set up in 3cm dishes (TPP® cell culture plastics) and treated as required. Then JC-1 mitochondrial membrane potential probe (Invitrogen™ Molecular Probes™, T-3168) was added to the cells at a final concentration of 250nM, diluted in Opti-MEM® reduced-serum medium (Gibco™, 51985_026). Cells were incubated with JC-1 for 30mins at

37°C/5% CO_2. Then the media was aspirated off, the cells washed once in DPBS and 2ml fresh media was added. Cells were imaged live to detect JC-1 with a fluorescence microscope. JC-1 monomers emit at 520nm, whereas aggregates alone emit at 590nm.

2.3 Methods for Protein analysis

2.3.1 Cell lysis

Flasks/dishes of cells were cooled for 5 mins on ice and then washed twice in cold-PBS. Cells were lysed in 1X MEBC and incubated on ice for a further 5mins. The cells were then harvested using a cell scraper, transferred to Eppendorf tubes and centrifuged at 18,213xg for 20mins at 4°C. The protein concentration of the lysate was measured using the Bradford Assay (Bio-Rad Protein Assay Dye Reagent Concentrate 500-0006), according to the manufacturer's instructions, to ensure equal loading on an SDS-PAGE gel. Lysates were snap-frozen and stored long term at -80°C.

2.3.2 Bradford assay

2μl of lysate + 798μl H_20 + 200μl Coomassie Protein Assay solution (Thermo Scientific) was added to a 1ml protein UV-cuvette (VWR). The protein concentration was read at a wavelength of OD595nm using a spectrophotometer (Pharmacia Biotech Ultraspec 2000 UV/Visible spectrophotometer). Controls were measured using BSA standards (0, 0.25, 0.5, 1.0, 1.5 and 2.0mg/ml) to generate a standard curve. Then, samples were measured in triplicate, an average taken and the concentration in mg/ml calculated from the average. 50μg of protein lysate was used for a Western blot unless otherwise stated.

2.3.3 Western blot

2.3.3.1 SDS-Polyacrylamide electrophoresis (SDS-PAGE)

SDS-PAGE was carried out to separate proteins by size and for further analysis by Western blot. The sample lysates were prepared for loading onto a Novex 4-12% Bis-Tris gel by combining: 50μg of protein, 4x loading dye (NuPage) + Xμl H_20. Lysates were then boiled for 10mins and 1/20th 1M DTT added. A Novex tank was then prepared for SDS-PAGE by adding 200ml running buffer containing 1:400 NuPage® Antioxidant (Invitrogen NP0005) into the central chamber, with a further 300ml running buffer added to the outer chamber of the tank. The samples were then loaded into the wells of the gel using gel loading tips (STARLAB, I1022-0600). The tank was connected to a power pack and run at 90V for roughly 3 1/2 hours at RT, until the sample buffer dye had just run off the bottom of the gel.

2.3.3.2 Wet-transfer method

To transfer the gel onto a 0.1μm pore nitrocellulose membrane a transfer cassette was stacked from bottom to top in reagents pre-soaked in transfer buffer, as follows: sponge, 2x3mm filter paper, gel, membrane, 2x3mm filter paper, sponge. The transfer cassette was then put in a Bio-Rad transfer tank with an ice block placed at the back and the transfer chamber filled with the remaining transfer buffer. The tank was transferred o/n (≥16hrs) at 4°C.

2.3.3.3 Ponceau S stain for transferred proteins

The nitrocellulose membrane was stained with Ponceau S to confirm adequate transfer of proteins from the gel onto the membrane. The membrane was placed into a small container and covered with Ponceau. The container was put on a RT shaking plate for 10 mins. The Ponceau was then poured off and the membrane rinsed gently in cold water so the proteins were visible.

2.3.3.4 Blocking, antibody incubations and protein detection

Once transferred, the nitrocellulose membrane was blocked by adding TBS-T Milk and shaking at RT for 1 hour. Primary antibodies were then added, dilutions and incubations can be found in table 2.1. The membrane was then incubated with wash buffer for 3x10minute washes. Li-Cor specific secondary antibodies were then added and incubated at RT with shaking for 1 hour (for dilutions see table 2.2). The wash step was then repeated. Blots were imaged using the Li-Cor Odyssey chemiluminescent system.

2.3.3.5 Quantification of bands

Using the Li-Cor Odyssey software; boxes were drawn around the bands of interest to generate a numerical value based on the intensity of the band. The value for the untransfected sample/untreated control equals 100% band intensity. Subsequently, the value for each band was normalised by dividing it by the value of the equivalent loading control to generate a correction factor. Each band was then multiplied by the correction factor to compensate for loading. This number is then divided by the value for the untransfected sample/control and multiplied by 100 to report an increase or decrease relative to the untransfected/untreated control.

2.3.4 Co-immunoprecipitation (CoIP)

1.5ml screw-cap Eppendorf tubes were prepared on ice with 100μL protein A/G beads (SIGMA-ALRDRICH), washed twice in 750μl 1X MEBC and resuspended in 200μl 1X MEBC plus 5μg antibody (see table 2.1). IPs were carried out with specific antibodies in parallel to an IgG control. Tubes were then placed on a rotator at 4°C o/n to conjugate the antibody to the beads. The next day, cells lysed in 1X MEBC (as for WB), the protein concentration was measured by Bradford Assay and 50μg of the lysate kept for pre/input-controls. Xmg lysate (see figure legends) added to the washed and conjugated beads.

Tubes were then placed on rotator at 4°C for >2 hours. Tubes then centrifuged and the supernatant removed (saving 50μg for post-IP controls). The beads were then washed 5x in 750μl cold IP wash-buffer + protease inhibitors (same as WB) at 1:1000 - each wash requiring a 5 second pulse-spin to pellet the cells. To elute and run samples on Western blot, 20μl of 1.3x loading buffer (NuPage) was added, samples boiled, 1/20th 1M DTT added and then samples were loaded on a 4-12% Bis-Tris gel as for WB.

2.3.5 Proteasome inhibition

10μM MG132 (Sigma-Aldrich) was added to media. Cells were harvested after 2 hours at 37ºC/5%CO_2.

2.3.6 The auxin-inducible degron (AID) system

2.3.6.1 Inducing APC degradation

Cells were set up one day prior to AID test at 2x10^5/ml. To trigger degradation of degron-fused proteins 50mM auxin/indole-3-acetic-acid (IAA) (SIGMA) was added to the cultures (diluted in RPMI) to a final concentration of 500μM (unless otherwise stated). Cells were then harvested at certain time points after IAA addition and then pelleted for Western blot analysis.

2.3.7 Mass spectrometry

2.3.7.1 Sample preparation

U2OS cells were grown in T75 flasks (TPP) +/- 7μM ABT-737 for 24 hours. Cells were then harvested, lysed and a Bradford assay performed to determine the protein concentration of the lysate (as in 2.3.1 and 2.3.2). 100μg of each sample lysate was run on a 4-12% Bis-Tris gel (Novex). Once run, the gel was put into a 15cm dish (TPP) and stained with Coomassie (2.1.1.2.8) for 30-60mins. The gel was then destained for at least 1 hour in destain 1 and destain 2 until the background

was removed sufficiently to reveal protein bands. Finally, the gel was rinsed with dH_20. Bands of interest were excised from the gel using a scalpel and placed into an autoclaved 1.5ml Eppendorf tube. The mass-spectrometry facility at the University of Dundee performed in-gel digestion (de-staining, reductive alkylation and tryptic digestion) before running the samples on an ESI-Trap mass-spectrometer (Pharmacia Biotech Ultraspec 2000 UV/Visible spectrophotometer).

2.3.7.2 Data analysis

ESI-Trap tandem mass-spectrometry (MS) results were entered into MASCOT™ (Matrix Science) - a search engine that identifies proteins from MS data by matching identified peptides against the human NCBI protein database. Each peptide from the MS data was matched to a protein and given an ion score that represented the probability of the peptide match occurring at random. The sum of ion scores for each peptide comprising a given protein made up the protein score, which was arranged to provide a logical list of results. To examine whether a protein was enriched in ABT-737 treated U2OS cells versus untreated U2OS cells, an EMPAI analysis was done. This provided label-free quantitation of peptides within the given mixture from the data already generated. MASCOT™ calculated the EMPAI using the algorithm (10^{PAI}-1) on the top 20 proteins as given by the protein scores. This generated a list of proteins arranged by the most abundant.

2.3.8 Subcellular fractionation

Cells were set up, treated in T25 flasks and subsequently fractionated using the ProteoExtract® Subcellular Proteome Extraction Kit (Calbiochem 539790). Every step was performed on ice. To harvest cells they were washed 2x in cold PBS, 1ml of Wash Buffer added, and cells scraped and collected into a 1.5ml Eppendorf tube. The cells were centrifuged at 300xg for 10 minutes at 4°C, the supernatant aspirated and the wash step

repeated. To obtain fraction 1 (cytosol), 500μl Extraction Buffer I + 5μl inhibitor cocktail was used to resuspend the pellet. The cell solution was then incubated for 10 mins at 4°C with gentle agitation followed by centrifuging for 10mins at 1000xg. The supernatant collected was fraction 1. Next, 500μl of Extraction Buffer II + 5μl inhibitor cocktail was added to the pellet, incubated for 30 mins at 4°C with gentle agitation and centrifuged for 10 mins at 6000xg. The supernatant collected was fraction 2 (membrane). The residual material was gently resuspended in 250μl Extraction Buffer III + 5μl inhibitor cocktail + 1.5μl Benzonase® and incubated for 10 mins at 4°C with gentle agitation, then centrifuged for 10mins at 10,000xg. The supernatant collected was fraction 3 (nucleus). The pellet was then resuspended in 250μl Extraction Buffer IV +5μl inhibitor cocktail to provide fraction 4 (cytoskeleton). Fractions were snap-frozen and stored long term at -80 C. Fractions were then prepared for SDS-PAGE as explained in 2.3.3. The following proteins were used as fraction markers: GAPDH for cytosol, Hsp60 or Na/K ATPase for membrane, topoisomerase IIα for nucleus and keratin 18 for cytoskeleton (see table 2.1).

2.3.9 Mitochondrial fractionation

Cells were set up and/or treated one day prior to fractionation in T25 flasks and subsequently fractionated using the Mitochondrial/Cytosol Fractionation Kit (Abcam® ab65320). Every step was performed on ice. Cells were washed 2x in cold PBS and 500μl 1x Cytosol Extraction Buffer Mix (+1/500 protease inhibitors plus 1/1000 DTT) added and incubated on ice for 10 mins. Using a cell scraper the cells were then scraped from the plastic ware and transferred into a 1.5ml Eppendorf tube. To homogenise the cells, the lysate was passed 60 times with a Dounce tissue grinder (pre-chilled on ice) and the homogenate then transferred into a fresh 1.5ml Eppendorf tube and centrifuged at 700xg for 10mins at 4°C. The supernatant was then transferred into a new Eppendorf tube and centrifuged at 10000xg for 30mins at 4°C, the supernatant was the cytosolic fraction. The pellet left was the intact mitochondria, which was resuspended in 60μl cold PBS to form the

mitochondrial fraction. Fractions were snap-frozen and stored long term at -80°C. Hsp60/Na^+&K^+ ATP-ase was used as a mitochondrial fraction marker and GAPDH as the cytosolic marker (see table 2.1).

2.3.10 Endoplasmic reticulum isolation

Cells were set up at 15% confluency, two days prior to ER isolation, in T75 flasks. 7μM ABT-737 was added 24 hours prior to isolation (plus an untreated control). Every step was carried out on ice. The total ER (rough and smooth) was subsequently isolated using an edited protocol from the Endoplasmic Reticulum Enrichment Kit (Novus Biologicals NBP2-29482). Flasks were put on ice for 5 mins before the isolation started; cells were washed 2x in 1X PBS, then 1ml 1X Isosmotic Homogenization Buffer added plus 20μl 100X PIC. The cells were harvested using a cell scraper and the solution then transferred into a pre-chilled Dounce tissue grinder. The solution was homogenized by 60 passes with the tissue grinder and the homogenate transferred into a 1.5ml Eppendorf tube. The tube was centrifuged at 1,000xg for 10mins at 4°C. Then the floating lipid layer (if present) was removed and the supernatant transferred into a Beckman Polyallomer 3.5ml 13x51mm ultracentrifuge tube (Beckman 349623). The tubes were centrifuged at 12,000xg for 15mins at 4°C using a swinging bucket rotor (Beckman Coulter® SW 55 Ti) in an ultracentrifuge (Beckman Optima™ L-90K). The floating lipid layer (if present) was then removed and the remaining supernatant was centrifuged at 90,000xg for 60mins at 4°C in the same swinging bucket rotor in the ultracentrifuge. The supernatant was discarded and the pellet resuspended in 100μl 1X suspension buffer and 10μL 100X PIC. Samples were then subject to a Bradford assay to determine the protein concentration, snap frozen and stored at -80°C.

2.3.11 Bcl-2 chemical inhibition using ABT-737

ABT-737 (Selleck Chemicals LLC S1002) a BH3 mimetic, was diluted in media to create a working solution of 1mM. It was then added to the cells media at a final concentration of 7μM. Untreated cells were grown in parallel as controls. Cells were incubated at 37°C/5% CO_2 for 24 hours before harvesting.

2.4 DNA/RNA Methods

2.4.1 Genomic DNA extraction from DT40 cells

The E.Z.N.A. SQ Blood Kit (OMEGA Bio-tek) DNA purification protocol (edited) for cultured cells 0.5-1x10^6 was used. Cells were pelleted, resuspended in 25μl PBS and vortexed. 150μl WTL buffer was added and mixed resulting in a viscous solution. 1μl RNase A was added to the lysate, incubated at 37°C for 10mins and cooled to RT. 50μl of PCP Buffer was added, vortexed for 30secs and incubated on ice for 5mins. The lysate was centrifuged at max speed for 3mins at RT to pellet cells. The supernatant was transferred to a fresh 2ml Eppendorf tube containing 150μl 100% isopropanol, inverted 30-40x and centrifuged at ≥13,000xg for 1min at RT to pellet the DNA. Supernatant was decanted, the pellet blotted briefly on a paper towel, 150μl ice-cold 70% EtOH was added, inverted and centrifuged at ≥13,000xg for 2mins at RT. Then the EtOH was poured out carefully, excess blotted off and the pellet air-dried for 10mins. The DNA was rehydrated in 40-200μl 8mM NaOH (depending on the size of the pellet), incubated at 65°C for 1hr and the NaOH was neutralised with 1:100 1M Tris, pH 7. 5. The DNA was left at RT o/n with occasional mixing. A spectrophotometer was then used to measure the concentration and purity of the DNA, which was diluted 1μl in 70μl H_20. The DNA was stored long-term at -20°C.

2.4.2 Screening for targeted insertion by gPCR

10ng/μl of genomic DNA was used per PCR reaction in conjunction with the Takara LA Taq™ (TAKARA BIO INC) 'cool start method'. Samples were run on a 0.7% agarose gel

and agarose-gel electrophoresis used to size-separate amplified fragments. The gel was run at 90V for >45mins and images taken using a UV transilluminator. PCR reactions and associated programs used for PCR screening with two targeting vectors are shown below.

pEGFP-IAA17-APC KI					
PCR Reaction		**Cycles**			
dH_20	12.6μl	Initial Denaturation	94°C	1m	
PI (20μM) 5'Arm-2R	0.5μl	Denaturation	98°C	10s	X34
P2 (20μM) GFP R	0.5μl	Annealing	66°C	30s	
Template gDNA (10ng/μL)	1μl	Extension	72°C	6m	
dNTPs (2.5mM)	3.2μl	Final Extension	72°C	10m	
10x LA Buffer II (Mg^{2+}plus)	2μl	Hold	4°C	∞	
LA-Taq polymerase	0.2μl				
Total Volume	*20μl*				

pIAA17-APC KI					
PCR Reaction		**Cycles**			
dH_20	12.6μl	Initial Denaturation	94°C	1m	
PI (20μM) 5'Arm-2R	0.5μl	Denaturation	98°C	10s	X34
P2 (20μM) IAA17 R	0.5μl	Annealing	63.5°C	30s	
Template gDNA (10ng/μL)	1μl	Extension	72°C	6m	
dNTPs (2.5mM)	3.2μl	Final Extension	72°C	10m	
10x LA Buffer II (Mg^{2+}plus)	2μl	Hold	4°C	∞	
LA-Taq polymerase	0.2μl				
Total Volume	*20μl*				

2.4.3 PCR product Blunt-end ligation and subsequent PCR product sequencing

Following gPCR, the PCR product was ligated into a T4 cloning vector (RBC RC001 RC013) using the reaction mixture shown below. Both a dilute and a concentrated reaction for each sample plus a positive and negative control were made. Reactions were incubated o/n at 4°C. Reactions (4 per sample) were then plated out onto ampicillin containing agar plates and put into a 37°C incubator o/n. Isolated colonies from sample plates were then used to inoculate a starter culture of 3ml LB + ampicillin (1/1000). Starter cultures were grown at 37°C with shaking for 8-10 hours. 400μl was then used to make a mini-prep culture with 40ml LB + ampicillin (1/1000), cultured with shaking o/n at 37°C. The following day a

Mini-prep of each culture was carried out and the concentration of the resulting plasmid DNA was measured with a spectrophotometer. 500ng of the pDNA was then digested using ECORI to establish plasmids containing PCR inserts; correctly sized inserts were then sent for Sanger sequencing using M13F and M13 R primers.

Blunt-end ligation using the T&A cloning vector			
	Sample	**Positive Control**	**Negative Control**
Ligation buffer A	1μl	1μl	1μl
Ligation buffer B	1μl	1μl	1μl
T&A cloning vector	2μl	2μl	2μl
PCR product	2/5μl	-	-
T4 DNA ligase	1μl	1μl	1μl
Control DNA	-	3μl	-
dH_20	3/0μl	2μl	5μl
Total Volume	*10 μl*	*10μl*	*10μl*

2.4.4 Restriction digest to linearize targeting vectors

Per digestion, 50μg of pDNA was set up in a 300μl digest with 10x fast digest buffer (Fermentas), SalI (Invitrogen) at 1:60 and χμl d H_20 and incubated o/n at 37°C. Agarose gel electrophoresis at 90V was subsequently carried out with 500ng of the digest alongside undigested targeting vector (control) to establish if digestion had occurred.

2.4.5 Ethanol precipitation of targeting vectors

30μl of 3M NaAc pH 5.2 was added to a 300μl restriction digest (after o/n digestion) in a 1.5ml Eppendorf tube. 660μl ice-cold EtOH was added to the tube, inverted to form a white precipitate and incubated at 4°C >30mins or -20°C o/n. The tube was then centrifuged at 4°C for 30mins at maximum speed and supernatant decanted to leave a DNA pellet. 1.5ml ice-cold 70% EtOH added, the tube was inverted several times, centrifuged at RT for 5 mins at max speed and the wash step repeated. The supernatant was decanted, the excess blotted, the pellet air-dried for ~10mins and resuspended in 30μl PBS. Samples were stored at -20°C.

2.4.6 DNA gel electrophoresis

0.7% agarose was dissolved in 50ml 1x TAE together in a conical flask by heating in a microwave. One drop of Ethidium bromide using a dropper (Invitrogen, 15585-011) was then added to the cooled agarose solution before it was poured into a gel tank containing a comb and left to set. (Note that for cloning purposes, GelRed (Biotium, 41005) was added to the cooled agarose rather than the mutagen Ethidium bromide). The tank was then filled with 1x TAE. Samples were prepared by adding DNA (50ng per band is sufficient to detect on a gel) to 6X loading dye (Thermo Fisher, R0611) and water to make up a volume of approximately 10μl per sample. Samples were then loaded into the wells of the gel and run alongside 5μl of a 1kb DNA ladder (New England Biolabs N3232L). The gel was then run at 110V/400mA until the ladder had sufficiently migrated through the gel (30-90 minutes). The gel was then imaged using a UV transilluminator.

2.4.7 Reverse-Transcription PCR (RT-PCR) in DT40 cells

2.4.7.1 RNA isolation

Cells were pelleted, lysed in 0.2ml of RNA-Bee RNA isolation agent (Amsbio, CS-501B) per $6x10^6$ cells and mixed by repeated pipetting. 0.2ml of chloroform was added per 1ml of RNA-Bee, the tube shaken vigorously for 15-30 secs and incubated on ice for 5mins. The homogenate was then centrifuged at 4°C, 12,000xg for 5mins. The aqueous phase was transferred into a fresh tube, 500μl of 100% isopropanol added and incubated for 5-10mins at RT. The solution was centrifuged at 12,000xg for a further 5mins at 4°C to form an RNA precipitate at the bottom of the tube. The supernatant was removed and the pellet washed in 75% EtOH (at least 1ml per 1ml of RNA-Bee), shaking the tube to dislodge the pellet from the side of the tube. Centrifuged for 5mins at 7500g and 4°C and the wash repeated. The pellet was air-dried for up to 10mins and dissolved in 100μl DEPC H_2O.

2.4.7.2 cDNA synthesis

cDNA synthesis was done using the Thermo Scientific Maxima First Strand cDNA Synthesis kit utilising both random hexamers and oligo (dTs) as shown below.

First Strand cDNA synthesis		Cycles		
Template RNA	10ng/χμl	Hexamer Primer Incubation	25°C	10m
Oligo (d)Ts (100pmol)	1μl	Oligo dT Incubation	50°C	30m
Random Hexamers (100pmol)	1μl	Termination	85°C	5m
10mM dNTPs	1μl	Hold	4°C	∞
Nuclease-free H20 (DEPC)	χμl			
5x RT buffer	4μl			
Maxima H Minus Enzyme Mix	1μl			
Total Volume	*20μl*			

2.4.7.3 RT-PCR

PCR with the generated cDNA was carried out using GFP F and GFP R primers (table 2.3) with DreamTaq™ polymerase (ThermoFisher, EPO711). Reaction components and cycle programs are outlined below.

2.4.8 Quantitative Reverse-Transcription PCR (qPCR)

DreamTaq™ PCR		Cycles		
dH_20	12.5μl	Initial Denaturation	95°C 5s	
PI (20μM)	0.5μl	Denaturation	95°C 40s	x35
P2 (20μM)	0.5μl	Annealing	60°C 40s	
Template cDNA	2μl	Extension	72°C 6m	
dNTPs	2μl	Final Extension	72°C 5m	
Buffer	2μl	Hold	4°C ∞	
DreamTaq™ polymerase	0.5μl			
Total Volume	*20μl*			

2.4.8.1 RNA extraction from cultured adherent cells

RNA was extracted using the NucleoSpin RNA kit according to manufacturer's instructions (Macherey-Nagel 740955.250). Cells were set up prior to harvest in a T75 flask so as to be confluent on the day of harvesting. The media was aspirated

and the cells washed 1x in cold PBS, then 700μl of Buffer RA1 and 7μl β-mercaptoethanol were added in drops around the flask. The cell solution was then collected with a cell scraper, transferred into a violet NucleoSpin filter within a 2ml collection tube and centrifuged for 1min at 11,000xg. The filter was then discarded and 350μl of cold EtOH added to the lysate and pipetted up and down 5 times to mix. Then the solution was transferred into a NucleoSpin RNA column within a new 2ml collection tube, centrifuged for 30s at 11,000xg and the column was placed in a fresh 2ml collection tube. Next, 350μl of MDB was added to the column to de-salt the membrane, centrifuged again for 1min at 11,000 and 95μl DNase reaction mixture was added onto the centre of the column and incubated for 15mins at RT. (DNase reaction mixture: 10μl reconstituted rDNase + 90μl reaction buffer for rDNase, per RNA isolation, made in a 1.5ml Eppendorf tube.) 200μl Buffer RAW2 was added to wash the column and centrifuged for 30s at 11,000xg. The column was added to a new 2ml collection tube, 600μl Buffer RA3 added to the column and centrifuged at 11,000xg for 30s. The flow-through was discarded and 250μl Buffer RA3 was added and centrifuged at 11,000xg for 2mins to dry the membrane in the column. To elute the RNA, the column was placed into a 1.5ml nuclease-free collection tube, 60μl RNase-free H_20 added and then centrifuged for 1min at 11,000xg. The RNA concentration was then measured using a spectrophotometer and subsequently diluted to a concentration of 200ng/μl. RNA was kept on ice at all times and stored at -20°C.

2.4.8.2 cDNA synthesis

cDNA was synthesized using the qSCRIPT™ cDNA synthesis kit (Quanta Biosciences 95047-500). Multiple reactions were set up each containing 1μg RNA (5μl of RNA at 200μng/μl). A 15μl master-mix was made (minus the RNA) and

reactions were added to 0.2ml thin-walled clear PCR tubes (AXYGEN 321-10-05). The RNA was added (1μg) and the tubes put into a PCR machine (Eppendorf Mastercycler Gradient) and the program set as below. A no-reverse transcriptase (NRT) control sample was also made.

First strand cDNA Synthesis			
Components	**1 Rxn**	**Programme**	
Template RNA	5μl (1μg)	22°C	5m
Nuclease-free H_20	5μl	42°C	30m
qSCRIPT reaction mix (5X)	4μl	85°C	5m
qSCRIPT RT	1μl	4°C	∞
Total Volume	*20μl*		

2.4.8.3 Primer optimization: melt curve and melt peak setup and analysis

The annealing temperature and efficiency for each primer needed to be optimised before use. Both of these were simultaneously tested by preparing a 96 well plate with 2 replicates of each condition as follows:

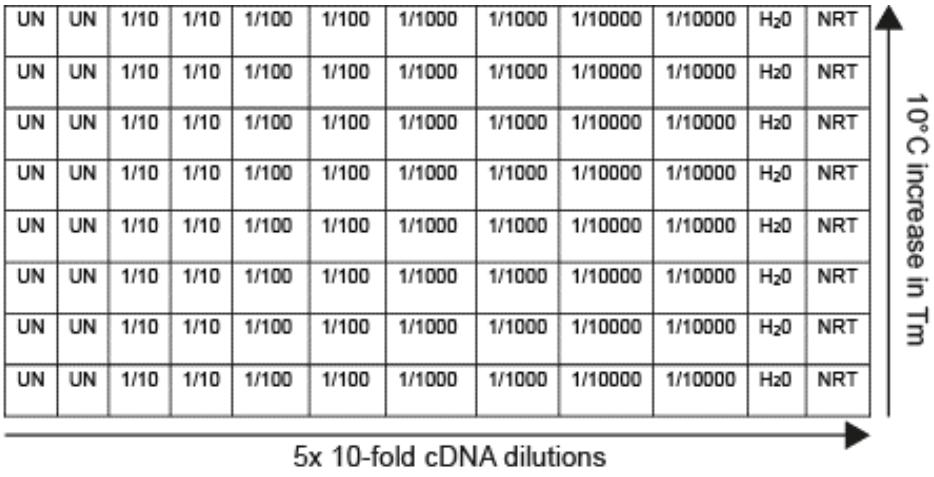

A temperature was chosen with the lowest Ct value (best amplification) and the lowest amount of unspecific product, which is the best compromise between target gene primers and the reference gene primers. The cDNA concentration was chosen based on the primer efficiency generated by the software, with the best giving between 90-110% efficiency.

2.4.8.4 qRT-PCR sample preparation

Samples were prepared using the Perfecta® SYBR® Green FastMix® (Quanta Biosciences 95072-012) as outlined below. Target genes were examined as well as a comparison to the reference gene actin.

qRT-PCR Sample Preparation	
Components	**1 Rxn**
SYBR 2X	10μl
Primers F+R (10μM)	0.6μl
Nuclease-free H_20	4.4μl
Template (100pg/μl)	5μl
Total Volume	*20μl*

2.4.8.5 Cycle programming

cDNA samples were run on the Bio-Rad CFX Connect™ Real-Time PCR Detection System using a 3-step cycle program as shown below.

qRT-PCR 3-Step Cycle Program Conditions				
Cycle Program	95°C	30s		
	95°C	5s	x39	
	X°C	15s		
	72°C	10s		PLATE READ
Melt Curve Analysis	95°C	1m		
	55°C	1m		
	55°C -> 95°C (0.5°C increments)	5s		PLATE READ

2.4.8.6 Analysis

qRT-PCR analysis was done using CFX Manager™ Software.

2.4.9 RNAi

Cells were plated out one day prior to transfections in T-25s (TPP) so that cells were are 40% confluent on the day of siRNA transfection. For each knock-down, 10μl of siRNA

duplex was incubated with 400μl of pre-warmed Opti-MEM® reduced-serum medium (Gibco™, 51985_026) in a 1.5ml Eppendorf tube and flicked to mix. 14μl of INTERFERin® (PolyPlus Transfection™ 409-50) transfection reagent was added and the tube vortexed for 10 seconds to homogenise the solution. Tubes were then incubated at RT for 10 minutes. Meanwhile, the media was aspirated off the cells and replaced with 6ml of pre-warmed media. Then 400μl of the transfection mix was dropped onto the cells and the flask was swirled to mix. Flasks were then put in a 37°C/5% CO_2 incubator and left for 48 hours. If a second siRNA transfection was required to increase the efficiency of the knock-down, the same procedure was repeated 24 hours after the initial transfection.

For *Apc* mutant cells (CACO2 and SW480), knockdowns were performed using Lipofectamine® 3000 transfection reagent (Life Technologies, L3000001). 14μl of Lipofectamine® 3000 was added to 400μl of Opti-MEM® (reduced-serum medium (Gibco™, 51985_026) and mixed well by vortexing. 10μl of siRNA was then added, mixed by pipetting and incubated at RT for 5 mins. The siRNA-lipid complexes were then added to the cells drop-wise and incubated at 37°C/5% CO_2. A further transfection was carried out 24 hours later, with cells harvested a further 24 hours after, totalling 48 hours post first transfection.

2.5 Bacterial Handling Techniques

2.5.1 Transformation

50μl of Subcloning Efficiency™ DH5α™ (Invitrogen, 18265-017) competent cells (per transformation) were thawed on ice in a 14ml round-bottomed tube. 3ng of pDNA/targeting vector or 5μl of a ligation was added to the cells, incubated on ice for 30mins, heat shocked at 42°C for 45 seconds and returned to the ice for 2 minutes. 250μl of pre-warmed SOC

medium was added and incubated with shaking at 37°C for 1 hour at 225rpm. 75μl of each transformation was spread onto pre-warmed antibiotic plates and incubated at 37°C o/n.

2.5.2 Plating out bacteria

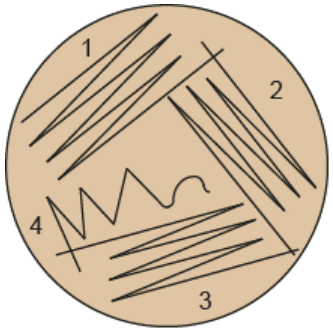

Transformed bacteria were pipetted drop-wise onto the applicable antibiotic agar plate and the solution was spread around the plate using a sterile plastic spreader. Colonies from pre-existing plates could also be transferred to a fresh plate in order to maintain the stock. A sterile loop was used to pick a single colony from a plate and then streaked onto the appropriate plate to form streak 1. A new loop was and passed through streak 1 to create streak 2 and so on until there are 4 streaks. The fourth was streaked into the centre of the plate and contained single colonies.

2.5.3 Bacterial Cultures

For a starter culture/miniprep culture; 5ml LB + 1:1000 antibiotic was inoculated with a single isolated colony and incubated all day (>8hrs) at 37°C with shaking. For a midi-prep, 40ml LB + 1:100 starter culture + 1:1000 antibiotic was cultured in a 250-500ml conical flask o/n with shaking at 37°C.

2.5.4 Minipreps

To isolate DNA, the E.Z.N.A. Fastfilter Plasmid Mini Kit (OMEGA Bio-tek D6905-03), and the vacuum protocol was used. A miniprep culture was pelleted by centrifugation, the supernatant decanted, the pellet resuspended in 250μl Solution I and then transferred into a fresh 1.5ml Eppendorf tube. 250μl Solution II was added, incubated at RT for 2mins and the tube inverted gently several times to obtain a clear lysate. 350μl Solution III was then added and the tube immediately inverted several times to form a white precipitate. Tubes

were then centrifuged at max speed for 10mins. The vacuum manifold was then prepared and 100μl of Equilibration Buffer was added to the columns first, followed by the cell lysate. When all the lysate had passed through the column 500μl HB buffer was added and then 2 washes of 700μl DNA Wash Buffer. The columns were then air-dried; put into collection tubes and centrifuged at 13,000 rpm for 2 mins. 30μl of pre-warmed (55°C) Elution Buffer was added to the centre of the column, incubated at RT for 1min, then spun at 10,000 rpm for 1 min. The eluted material was passed over the column again and spun for a further 1min to elute any residual DNA. The DNA content of the sample was then measured. Similar protocols were followed for Midi/Maxipreps.

2.5.5 Long-term storage of transformants

To store transformed bacteria long-term; 700μl of a starter culture was added to 300μl glycerol, snap-frozen on dry ice and stored at -80°C. When needed, the stock was taken up on dry ice (so as not to thaw) and a small amount was scraped from the vial and spread onto the applicable antibiotic plate, which was then put into a 37°C incubator o/n. The glycerol stock was returned to -80°C.

2.6 Microscopy

2.6.1 Preparing collagen coated coverslips

In the tissue-culture fume hood: 22x22mm, 1.5 thickness coverslips (VWR 631-0125) were put into a 15cm sterile dish with enough 70% EtOH to cover the slides. Then using sterile forceps the coverslips were taken out of the 70% EtOH, put into individual wells of a 6 well dish (TPP) and washed 2x in DPBS. Collagen VII (SIGMA C8897, from rats' tails) was added, enough to cover the slide and the bottom of the dish/well. Slides were then left in the tissue culture hood all day to allow the collagen to coat the coverslip. The collagen was

then aspirated off, the lids were removed and the uncovered dishes/plates left in the fume hood o/n in UV light to sterilise.

2.6.2 Preparing cells for immunofluorescent staining

Cells were seeded onto collagen-covered coverslips and left to recover o/n at 37°C/5% CO_2. Cells were fixed by aspirating the media and gently pipetting 200μl of pre-warmed 4% PFA onto the edge of the plate/dish and left at RT for 10 mins. The PFA was aspirated off, the coverslips were transferred into a dark and humid box and 200μl of IF wash buffer was added to the corner of the coverslip. The cells were left for 10 mins at RT, then 200μl permeabilisation buffer was added to the coverslip and left for 10 mins. The wash step was repeated and then 200μl of blocking buffer was added and the cells left at RT for 30 mins. Primary antibody(s) (table 2.1) was added (diluted in incubation buffer) and incubated for 1hr at RT. Then the cells were washed 3x5mins in wash buffer, which was then aspirated off. Secondary antibody(s) (table 2.2) was then added (dilution in incubation buffer) for 1 hr at RT and washed 3x5mins in wash buffer. Cells were then counterstained with 1/5000 DAPI (SIGMA D-9542) in 200μl PBS, and phalloidin at 1/500 for 1 hr at RT (table 2.1). PBS/counterstain(s) was then aspirated and the slides washed 1x in cold PBS. Coverslips were then mounted onto slides.

2.6.3 Mounting the coverslips

To mount the slides, 10μL of mounting medium was added to the centre of a microscope slide, the PBS (from 2.6.2) was aspirated from the slide and using sterile forceps, the coverslip was carefully placed face-down onto the drop of mounting medium. Once the mounting medium had spread across the slide it was sealed with nail-polish. When dry (>15mins in the dark) the back of the coverslip was washed in MilliQ water to remove salt crystals before viewing under a microscope. Slides were stored at -20°C.

2.6.4 Microscopes

IF imaging of fixed/live cells was performed with a Zeiss 700 microscope using Zen 2011 software. Time-lapse brightfield videos of organoids were recorded using a Leica DMIRB inverted microscope and OpenLab software. Images were taken every 30 mins for 48 hours. Tisse culture fluorescence microscopy was carried out using the Invitrogen™ EVOS Floid™ cell imaging system.

2.6.5 Image analysis

Images from the Zeiss 700 were saved as LSM files and opened in Volocity 6.4 (Perkin Elmer). MitoTracker® images were analysed using Imaris (Bit Plane). Organoid movies were assembled using FIJI by Image J (Schindelin *et al.,* 2012).

2.7 Fluorescence activated cell sorting (FACS)

2.7.1 Preparing suspension cells for FACS (with fixation)

DT40 cells were pelleted in a 15ml falcon tube and washed 2x in 1ml cold PBS. The cells were resuspended in 250μl cold PBS and then 2ml cold-70% EtOH was added while vortexing to fix the cells. The cells were then kept at -20°C for ≥5hrs. Once the cells were treated with antibodies (see below and table 2.1), they were pelleted and resuspended in PBS 500μl/RNase A 1:1,000/PI 20μg/μl in 5ml round-bottomed FACS tubes. FACS was done using the Becton Dickinson LSRFortessa™ flow-cytometer and 10,000 events were measured per sample.

2.7.2 Measuring the quantity of cells in G2/M by treatment with BrdU

$DT40^{TIR}$ and $DT40^{TIR;(GFP)IAA17\text{-}APC}$ cells were incubated at 37°C/5% CO_2 with 20μM BrdU for 20mins, then fixed and kept at -20°C for ≥5hrs as in 2.7.1. The fixed cells were then pelleted and washed once in 2ml cold-PBS. The cells were pelleted again and resuspended in 1ml

2M HCl/0.5% Triton-X-100 (to relax the DNA for BrdU antibody access) while vortexing and incubated at RT for 30mins. The cells were pelleted and washed in 1ml PBS and then pelleted and resuspended in 1ml PBS/0.1% Tween 20/1% BSA (blocking agent). Again the cells were pelleted (centrifuged at 300rcf for 5mins at RT), resuspended in 100μl blocking agent + Anti-BrdU antibody (1:500) and incubated at RT for 1 hour. The cells were washed again in blocking agent, then resuspended in blocking agent + secondary antibody (1:100) and incubated at RT for >30mins. Cells were then prepared for FACS as outlined in 2.7.1.

2.7.3 Measuring the quantity of cells in mitosis by treatment with anti-PH3

DT40^{TIR} and DT40$^{TIR;\ (GFP)IAA17\text{-}APC}$ cells were fixed and kept at -20°C for ≥5hrs as detailed in 2.7.1. The fixed cells were pelleted and washed once in 2ml cold-PBS. The cells were pelleted and resuspended in 1ml 2M HCl/0.5% Triton-X-100 while vortexing and incubated at RT for 30mins. The cells were pelleted and washed in 1ml PBS, pelleted and resuspended in 1ml PBS/0.1% Tween 20/1% BSA (blocking agent). Again the cells were pelleted (centrifuged at 300rcf for 5mins at RT), resuspended in 100μl blocking agent + Phospho-Histone H3 antibody (1:300) and incubated at RT for 1-2hrs. The cells were washed again in blocking agent, resuspended in blocking agent plus secondary antibody (1:100) and incubated at RT for >30mins. The cells were then prepared for FACS as outlined in 2.7.1.

2.7.4 Preparing adherent cells for FACS (live cells) to measure mitochondrial membrane potential (MMP)

U2OS cells were grown in T25s (TPP) and treated as required. Then, the media was aspirated and the cells were washed once in DPBS. 2ml of pre-warmed Opti-MEM® reduced serum media (Gibco™, 51985_026) was added to the flask containing 500nM MitoTracker® Green (Invitrogen Molecular Probes M-7514), which is MMP independent and 250nM MitoTracker Red CMXRos (CST 9082), which is MMP dependent. The cells

were put back into the incubator at 37°C/5% CO_2 for 45 minutes. The cells were then harvested for FACS (see 2.7.1).

2.7.4.1 Measuring MMP and quantifying mitochondria

To measure the MMP cells were prepared for FACS without fixation. The media was aspirated from the flasks, washed 1x in DPBS, 1.5ml trypsin added and the flasks were put back into the incubator at 37°C/5% CO_2. Once the cells had detached from the flask, 3ml of pre-warmed media (DMEM) was added to inactivate the trypsin. The cell solution was transferred into a 50ml falcon tube and the cells were spun down. Then, the falcon tubes were put on ice to prevent changes in MMP, the media was poured off the pellet and the tube was flicked to redistribute the cells into a single cell suspension within the small volume of residual liquid remaining. 500µl PBS-BSA (2%) containing 5µg/ml DAPI was added to the single cell suspension and the solution was transferred into a FACS tube and kept on ice. FACS was performed after gating of cells (selected by DAPI) to exclude the G0-subG1 population. Cells were then examined by size (FSC and SSC) and their MitoTracker® Green and CMXRos content.

2.7.5 Statistical Analysis

The gating of cells was achieved with BD FACSDiva™ software while carrying out the experiment. Further analysis was performed using FlowJo single cell analysis software for FACS data.

Chapter 3

Generating cells expressing APC that can be conditionally and reversibly degraded.

Background

Adenomatous polyposis coli (APC) is a multi-functional tumour suppressor protein. It is key in governing several cellular processes in epithelial cells. Its best defined role is in canonical Wnt signalling as part of the β-catenin destruction complex. APC is also involved in regulating the cytoskeleton as it binds microtubules and actin (Mogensen *et al.,* 2002; Kita *et al.,* 2006; Kroboth *et al.,* 2007; Moseley *et al.,* 2007). This binding action stabilises microtubules (Zumbrunn *et al.,* 2001). Consequently, APC has an indirect but important role in microtubule dynamics, mitotic spindle assembly, cell division and cell migration. In addition to these roles there are links between APC and cellular metabolism, apoptosis, cellular proliferation, trafficking, cell polarity, cell adhesion and DNA damage. Moreover, human APC has been found to interact with more than 100 other proteins that contribute to at least 24 different cellular functions (Nelson and Näthke, 2013). How APC contributes to or regulates the functions of the proteins it binds, or how they are coordinated, is not known.

Aim

The aim of this PhD was to use a reverse genetics approach to study the non-Wnt-related functions of APC. To this end I needed to generate a cell line expressing APC that could be rapidly and conditionally degraded (fig 3.1). This would permit the study of APC loss prior to its impact on the transcriptional repertoire of the cell. Such a cell line would also enable rescue of observed phenotypes by re-introducing full length APC (by relieving the inhibition) or fragments of *Apc*.

Model System

The model system used to carry out genetic manipulation in order to create a degradable APC, was DT40. These white-leghorn chicken (*Gallus gallus*) cells are ALV (Avian-leukosis

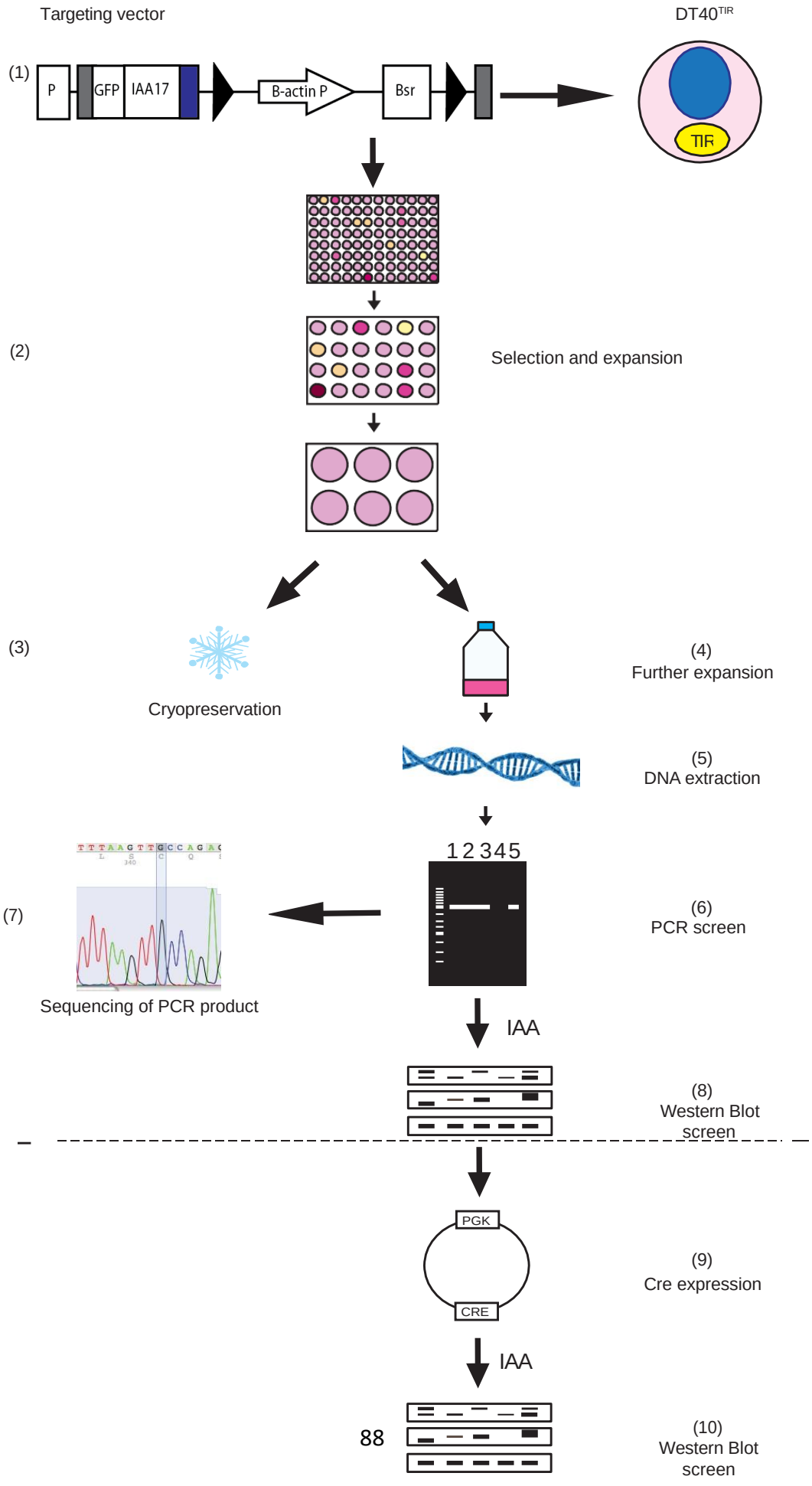
Targeting vector
DT40TIR
(1)
P
GFP
IAA17
B-actin P
Bsr
TIR
(2)
Selection and expansion
(3)
Cryopreservation
(4)
Further expansion
(5)
DNA extraction
12345
(6)
PCR screen
(7)
Sequencing of PCR product
IAA
(8)
Western Blot
screen
PGK
CRE
(9)
Cre expression
IAA
(10)
Western Blot
screen

Figure 3.1. Workflow to create a degron knock-in at the *Apc* N-terminus. (**1**) Ethanol precipitated and linearized targeting vector was stably transfected into DT40 cells harbouring a transgene expressing the TIR protein ($DT40^{TIR}$). **(2)** Transfected clones were selected in media containing Blasticidin and expanded. Clones were frozen **(3)** and expanded **(4)** prior to extraction of genomic DNA **(5)**. Successful targeting of the degron was determined by PCR **(6)**. PCR products were then sequenced **(7)**. Western blot screening of targeted clones determined auxin (IAA) sensitivity **(8)**. Where indicated, the Blasticidin resistance cassette contained within intron 1 was removed after transient expression of Cre recombinase **(9)** and screened by Western blot **(10)**.

virus) induced B-cell lymphoma cells. The ALV virus integrated upstream of *c-myc* and this lead to their immortalisation. These chicken B cells were chosen for several reasons. Firstly, they are very efficient at homologous recombination, making them genetically tractable and a good model to study cell autonomous functions. Secondly, *Apc* is conserved in DT40 and has 84% protein homology with human APC (see appendix B). In addition, these cells have a fast doubling time of 11-12 hours when cultured at 37°C. Lastly, *Apc* is on the Z chromosome in chicken and therefore present in only one copy.

The reasoning for creating an EGFP-(degron)-tagged APC was because there is currently no cell line containing robust GFP-APC, available as a reagent. Possessing EGFP-APC would allow for GFP-pull down experiments to examine APC-interacting proteins. In addition, the EGFP-tag would allow for the visualisation of the APC fusion protein using IF, and the production of quantitative APC experiments using such methods as FACS analysis.

Generation of Constructs

To degrade endogenous APC, the Auxin-Inducible Degron (AID) system was used (Nishimura *et al.,* 2009). In cells expressing a TIR protein, which forms a specific SCF^{TIR} E3 ubiquitin ligase, the AID system depletes endogenous proteins tagged with a short degron motif, in the presence of auxin. Auxin binds the degron-fusion protein and the SCF^{TIR} ubiquitin ligase, bringing them closer together. This results in the ubiquitination and subsequent degradation of the protein (fig 3.2). This protein degradation is conditional, only

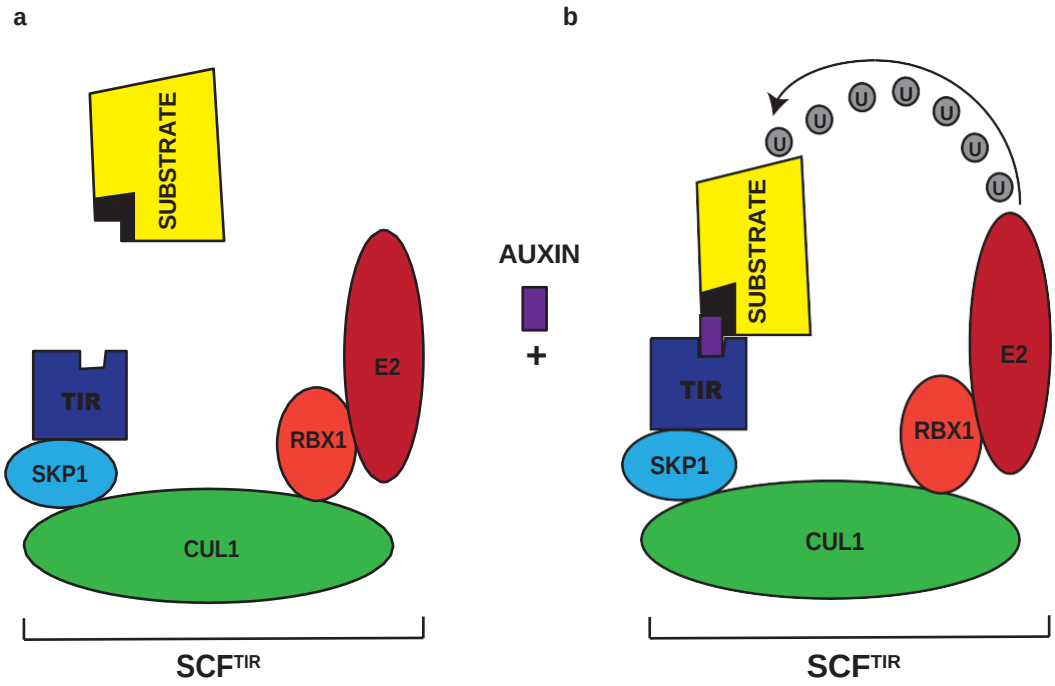

Figure 3.2. The AID system. (**a**) When the exogenous F-box protein TIR protein is expressed, it joins up with Cul1 and Skp1 to form the SCF^{TIR} E3 ubiquitin ligase. The ligase degrades proteins containing a degron motif (represented by the black area within the substrate) in the presence of auxin. (**b**) Once auxin is added it binds to both the degron and the F-box TIR protein, bringing the substrate into contact with the SCF^{TIR}. This allows the poly-ubiquitination of the substrate, targeting it for proteasomal degradation.

happening in the presence of auxin and the protein depletion is reversible upon auxin withdrawal.

As the C terminus of *Apc* contains important PDZ and microtubule binding domains, the degron motif was fused to the N terminus of *Apc*. A knock-in of (EGFP)-degron protein-coding cDNA was targeted 5' of *Apc* by homologous recombination (fig 3.3). In order to produce a contiguous mRNA the (EGFP)-degron coding sequence was inserted upstream of *Apc* exon 1. The ATG start codon of *Apc* was deleted and reintroduced at the start of both the EGFP and degron cDNA sequences. Both additionally contained Kozak sequences to enhance translational initiation by the ribosome. Expression of heterologous reporter proteins such as EGFP can sometimes alter protein expression, often due to codon bias in the host cell/organism (Baca and Hol, 2000; Yilmaz and Arslanyolu, 2015).

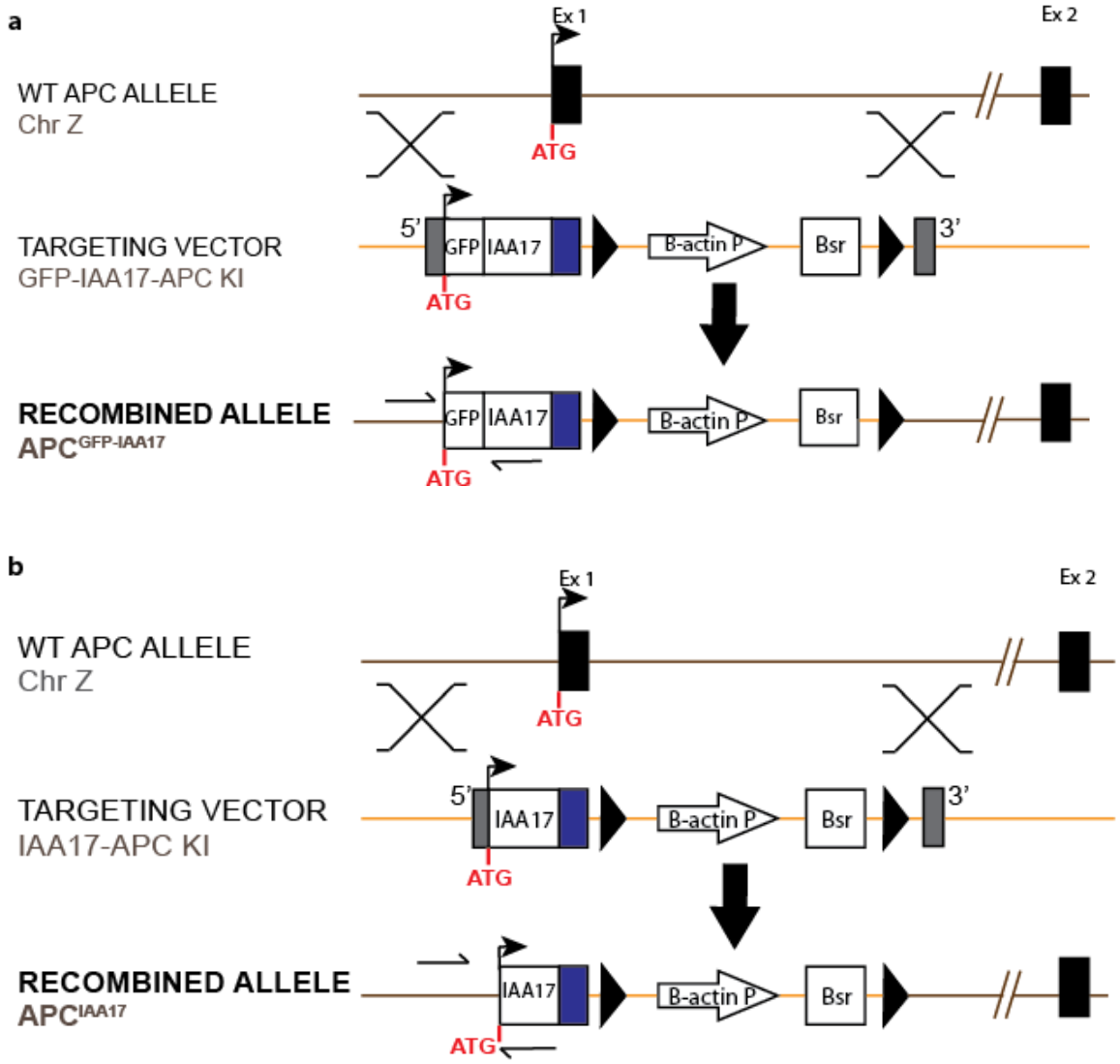

Figure 3.3. Targeting strategy to create a degron-*Apc* knock-in by homologous recombination. The targeting vectors were designed to introduce a short (EGFP)-degron sequence immediately 5' of the endogenous *Apc* start codon to produce a contiguous mRNA. Regions of homology within the targeting vector are shown in grey. Recombinant exon 1 (with a deleted start codon) is shown in blue. The start codon was reintroduced at the start of both the EGFP and degron sequences. A floxed Blasticidin selectable marker was introduced in intron 1 under control of a β–actin promoter. Lox P sites are represented by black triangles. Position of PCR primers are shown on the recombined allele. **(a)** Targeting strategy to knock-in EGFP-degron cDNA using pEGFP-IAA17-APC. **(b)** The same strategy was employed as in (a) to knock-in degron cDNA (without GFP) 5' of *Apc*. In this case, a degron motif was targeted 5' to exon 1 using the targeting vector pIAA17-APC.

Therefore, the degron cDNA also contained a kozak sequence in case the EGFP was not expressed. Note that the (EGFP)-degron-*Apc* allele remained under the control of the endogenous *Apc* promoter. To target the (EGFP)-degron cDNA 5' of the *Apc* start codon,

a targeting vector was produced by amplifying 3 specific genomic regions at the *Apc* locus, by PCR. These regions were termed 'arms of homology'. The homologous regions were designed to flank exon 1; a 5' region upstream of exon 1 and a 3' region in intron 1. A floxed Blasticidin S (Bsr) resistance cassette, driven by the β-actin promoter, was also inserted into intron 1 in the same transcriptional orientation as *Apc*. A map of the targeting vector(s) is shown in supplementary figure 1.

Results Summary

- Generation of a conditionally, degradable APC in DT40^{TIR} cells using the Auxin-Inducible Degron system (AID).
- The degron-A*pc* allele was hypomorphic.
- Off-target effects associated with the use of auxin reduced the usefulness of these cells to study the non-Wnt functions of APC.

Results

3.1 Establishing a control cell population; DT40^{TIR}

In order to make degradable APC, the AID system and its three main components were used (fig 3.2). Firstly, a thermostable F-box TIR protein isolated from the rice plant *Oryza sativa* was needed to form SCF^{TIR} complexes in DT40 cells. Secondly, a degron motif (IAA17) taken from *Arabidopsis thaliana* was tagged onto the N-terminus of *Apc* in cells stably expressing the TIR protein. Lastly, indole-3-acetic acid (auxin) was used to bind both the degron motif within the substrate and the SCF^{TIR} complex, bringing them together to allow APC ubiquitination and degradation (fig 3.2).

First, varying concentrations of auxin (from 0-2μM) were added for 24 hours to ensure the viability of DT40 cells was not altered, which it was not, at any auxin concentration used (supplementary figure 3). In order to use this system to degrade endogenous APC, the AID

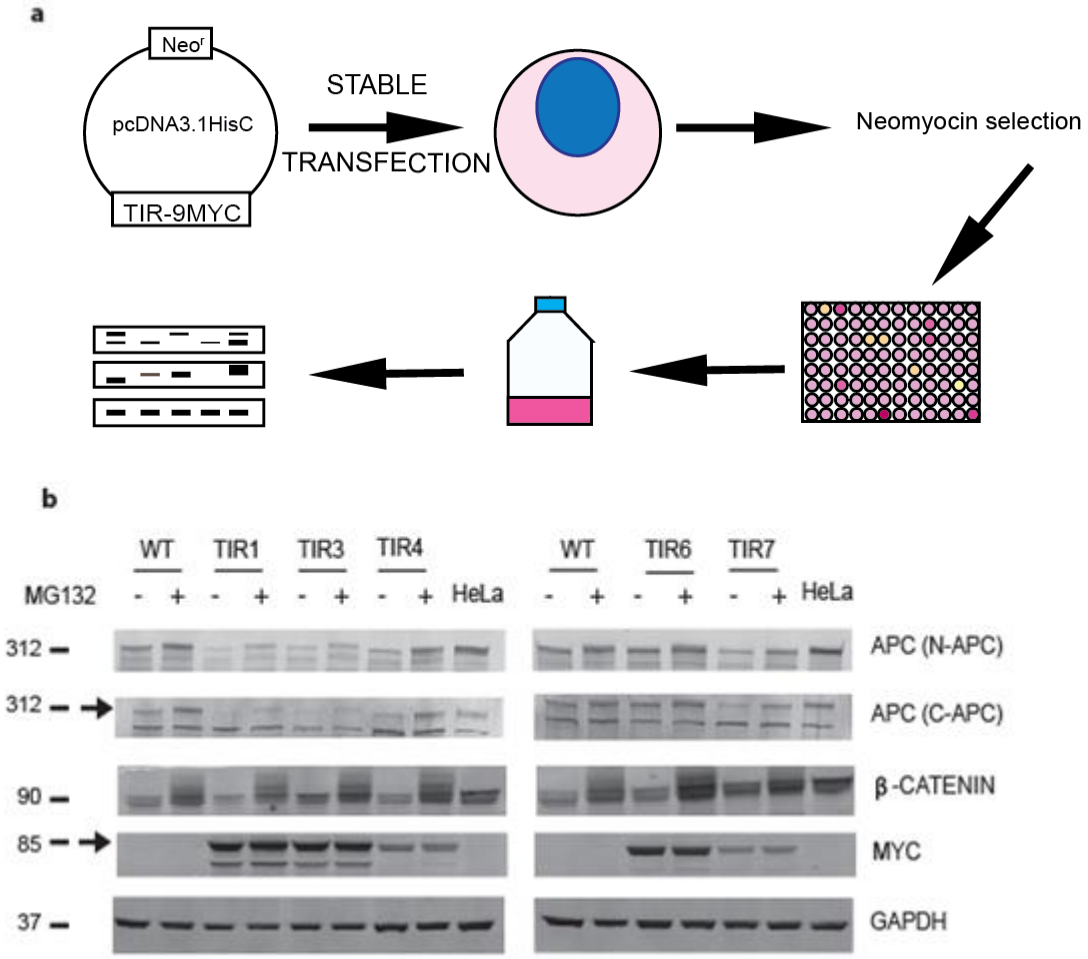

Figure 3.4. Creation and selection of a control cell population. (a) DT40^{TIR} cells were created by stable transfection of WT DT40 cells with a mammalian expression vector containing the TIR protein with a 9xMyc tag (pcDNA3.1HIS OsTIR9xMyc). Cells were cultured under G418 selection. (Carried out by C.J Baird). Clones were analysed by Western blot to confirm expression of the TIR protein using an anti-Myc antibody. **(b)** Individual clones were cultured +/- 10μM MG132 for 2 hours (to determine if APC is still poroteasomally degraded in DT40^{TIR} cells) and subject to Western blot with antibodies against APC, β-catenin, Myc and loading control GAPDH. Protein expression in the clones was compared to untransfected WT DT40 cells. Data is representative of 3 technical replicates.

system required DT40 cells that stably expressed the TIR protein. This allows the SCF^{TIR} E3 ubiquitin ligase complex to spontaneously form. A DT40 cell line stably expressing OsTIR9xMyc, had been generated previously. Several different clones were examined for TIR expression (using the Myc tag for detection) and APC and β-catenin levels (fig 3.4). Clone 4 was chosen as it had levels of APC and β-catenin most similar to WT cells. This clone then formed the control cell population DT40^{TIR}.

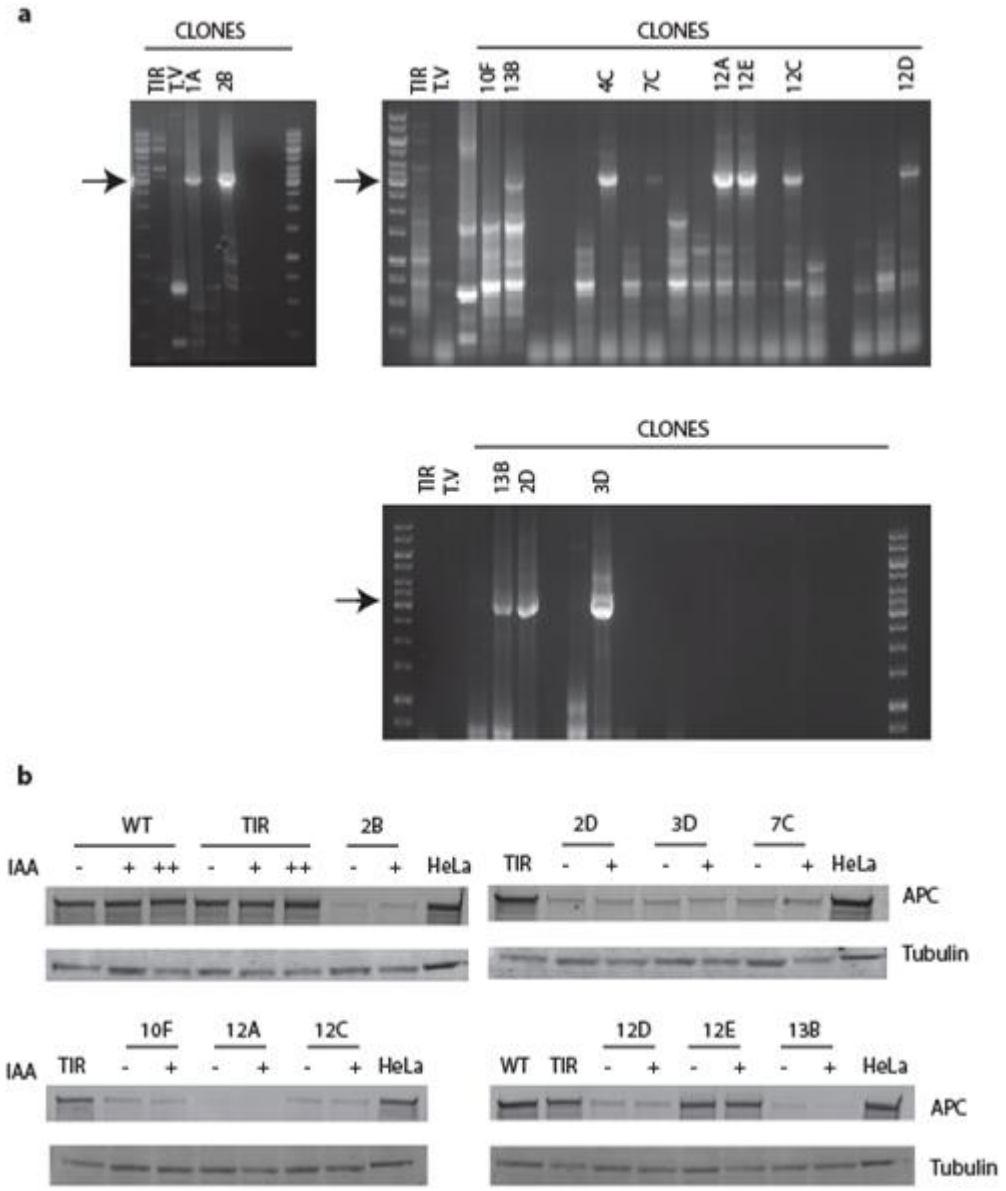

Figure 3.5. Screening EGFP-IAA17-APC clones for the presence of targeted insertions and auxin sensitivity. (a) Genomic PCR was carried out using one primer within the targeting vector (GFP R) and one upstream (5'Arm-2R), as shown in figure 3.2. DNA from DT40^{TIR} cells and the targeting vector (T.V) were used as negative controls. The PCR product of ~4,000bp is indicated by the arrow. **(b)** 10 clones picked from (a) (9 contained targeted insertions and 1 (10F) was negative) were cultured in 500μM IAA for 1 hour and subject to Western blot analysis to measure levels of APC. HeLa cell lysate was used as a positive control for APC protein expression. {+} represents 500μM IAA (auxin) and {++} reprents 1mM IAA. Data is representative of 3 technical replicates.

3.2 Creating EGFP-IAA17-APC in DT40^{TIR} cells

A targeting vector, pEGFP-IAA17-APC (see supplementary figure 1) was stably transfected into DT40^{TIR} cells by electroporation. Transfectants were selected using Blasticidin and

Blasticidin resistant clones identified and expanded. Cells harbouring insertions of pEGFP-IAA17-APC were identified by PCR using one primer within the targeting vector (GFP R) and one primer upstream of the insertion (5'arm-2R) (fig 3.5). The optimisation of the PCR screen is shown in supplementary figure 4. Nine positive clones and one negative clone (10F) were chosen to test for auxin-induced degradation of APC. Each clone was cultured with 500µM auxin for one hour, harvested and analysed by Western blot for the presence of APC. None of the clones exhibited decreased APC protein after auxin treatment. One clone, (12A) had little detectable APC, one clone (12E) had near WT levels of APC and the other 8 clones had markedly decreased APC protein (APC^{low}). This indicated that the EGFP-degron-*Apc* was hypomorphic. Unexpectedly, no expression of GFP was detectable (fig 3.5 and data not shown). It has previously been shown that gene expression can be affected by the close proximity of a cassette expressing antibiotic resistance, to gene regulatory elements (Chen *et al.,* 1993). Therefore, in an attempt to rescue APC expression in APC^{low} clones, the floxed Blasticidin resistance (Bsr) cassette in intron one was removed by transient expression of a plasmid encoding the bacteriophage P1 Cre recombinase (fig 3.6a). Successful Cre recombination resulted in Bsr excision as confirmed by PCR (data not shown). Excision of the Bsr partly rescued APC expression and additionally, induced auxin sensitivity (auxin-induced APC degradation) in 2of 5 Bsr^{-} clones (fig 3.6b, c). Note that the Western blot (fig3.6b) result is different in the Western blot quantitation in fig 3.6c, after protein bands were normalised to the loading control (tubulin) in TIR cells. This then provised a true, quantitative result.

3.3 Creating IAA17-APC in $DT40^{TIR}$ cells

A knock-in of the *Apc* allele in $DT40^{TIR}$ cells had been achieved that directed EGFP-degron cDNA upstream of *Apc*. However, the GFP was not translated: the GFP was not detectable by Western blot using an anti-GFP antibody (chicken or mouse species), nor did the anti-APC antibody(s) detect a larger protein attributable to the EGFP tag; no EGFP was detected using a tissue culture fluorescence microscope; no EGFP was picked up using FACS

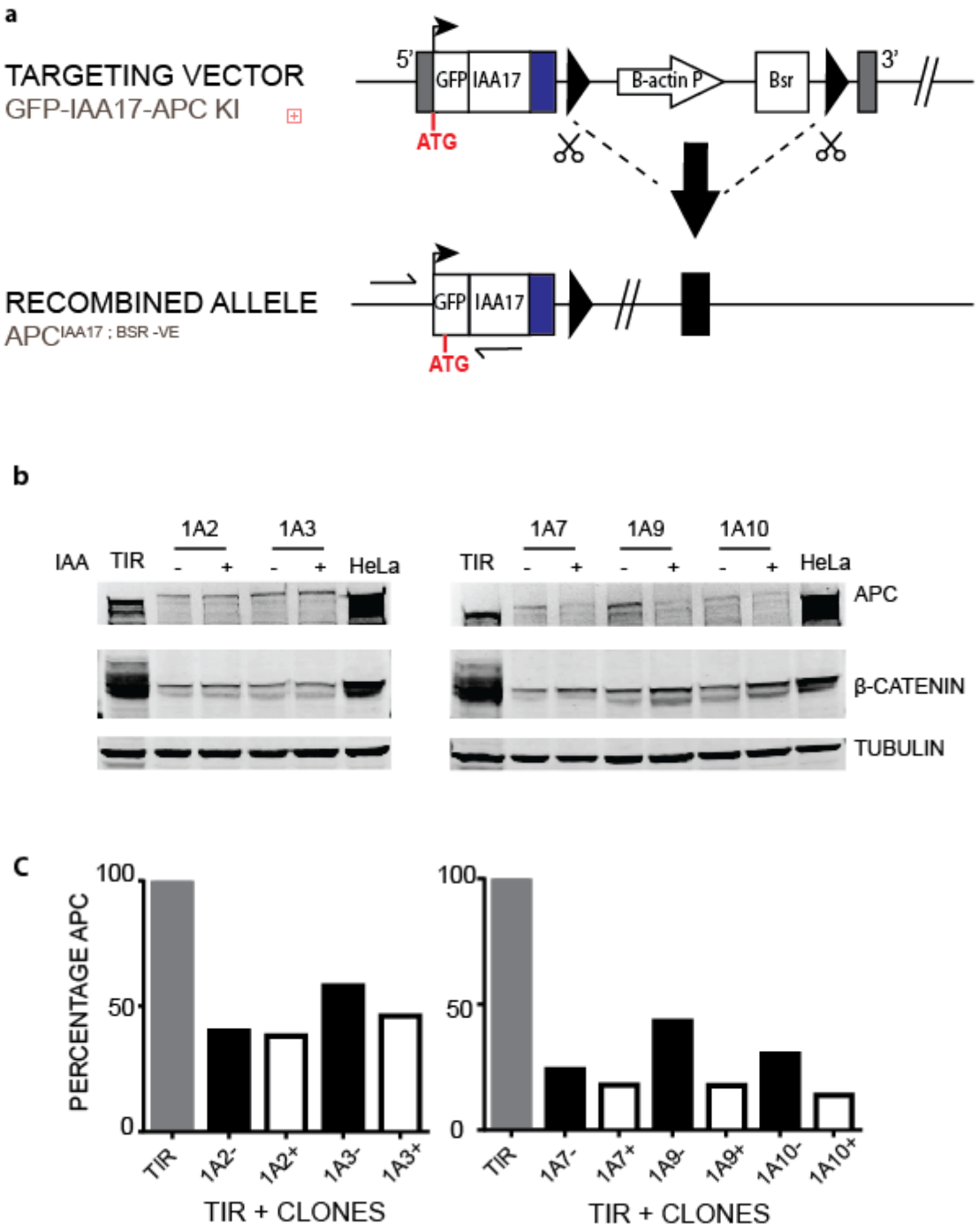

Figure 3.6. Removal of the resistance cassette induces auxin sensitivity. (a) Schematic detailing the structure of the N-terminal degron-*Apc* allele before and after transient expression of Cre, which removes the resistance cassette. Lox P sites are represented by black triangles. **(b)** Western blot of proteins in 5 clones after Cre expression and subsequently cultured +/- 500μM IAA for 1 hour. **(c)** Quantification of APC expression in each clone (b) compared to DT40^{TIR} cells. Data is representative of 3 technical replicates.

analysis; nor was APC picked up following a GFP-trap pull-down experiment (lall experiments were compared to EGFP positive controls – data not shown). Therefore, production of a degron-*Apc* was required, i.e. an *Apc* locus containing no EGFP cDNA. DT40^{TIR} cells were transfected with pIAA17-APC (see supplementary figure 1), transfected cells selected with Blasticidin and positive clones expanded. As before, targeted insertions were selected using a PCR screen with primers - IAA17 R and 5'Arm-2R (fig 3.7a). PCR optimisation is shown in supplementary figure 5. Three PCR positive clones and one PCR negative clone were selected and the Bsr cassette in intron 1 removed after expression of Cre. Bsr excision was again verified by PCR (data not shown). AuXin mediated APC depletion was then measured (fig 3.7b) in four original (O1, X4, O2, V5) and five daughter (O1E, X4A, X4H, O2E, V5G) clones (Bsr^{-}).

APC expression was partly rescued in all five Bsr^{-} daughter clones and auxin sensitivity was also detected in all five, i.e. APC was depleted upon auxin treatment (fig 3.7b). Two clones were then chosen representing varying APC levels in comparison to DT40^{TIR}: V5 (APC^{minimal}) had very little APC concomitant with high levels of β-catenin, as expected based on the role of APC in the β-catenin DC. X4A (APC^{low}) expressed an intermediate level of APC between that of DT40^{TIR} (APC^{high}) and clone V5 (APC^{minimal}). These clones were subject to a timecourse of 500μM auxin treatment to determine if APC levels fluctuated at different rates in cells with more/or less APC. However, increasing the incubation time did not affect APC depletion as protein levels remained largely consistent throughout the timecourse (fig 3.7c). Therefore, the amount of APC present in a cell did not appear to affect the rate of APC depletion. Three of five degron-APC clones (fig 3.7b) with the Bsr removed (X4A, X4H and V5G) showed APC depletion after a one hour incubation with 500μM auxin. However, APC expression was decreased in all clones, even before the addition of auxin. This again suggested that knocking-in the degron motif produced a hypomorphic allele with reduced APC expression. While the addition of auxin to these hypomorphic cell lines did reduce the APC protein (in clone X4A), degradation of APC was not complete.

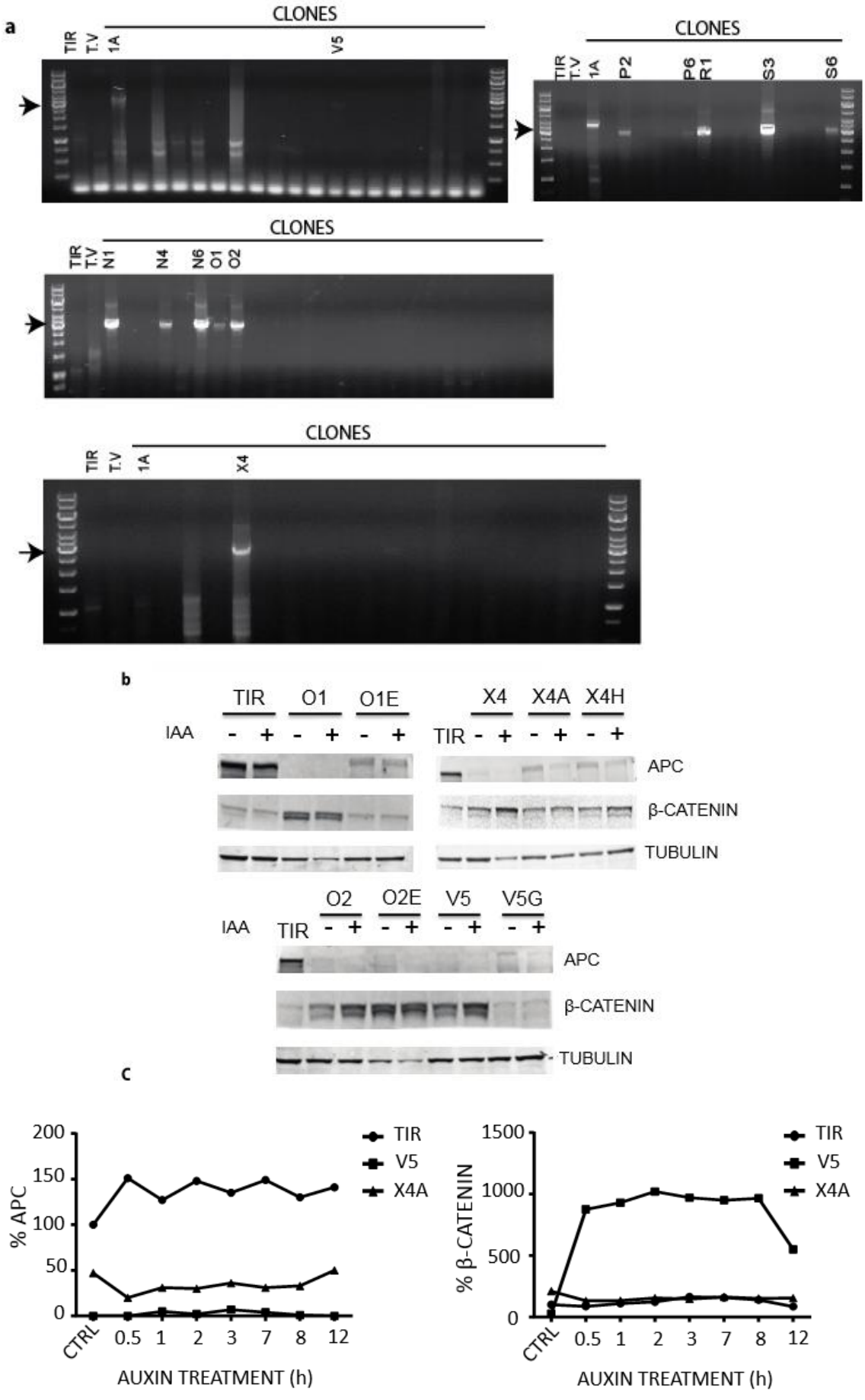
a
CLONES
TIR
T.V
1A
V5
CLONES
TIR
T.V
1A
P2
P6
R1
S3
S6
CLONES
TIR
T.V
N1
N4
N6
O1
O2
CLONES
TIR
T.V
1A
X4
b
TIR
O1
O1E
X4
X4A
X4H
IAA
- + - + - +
TIR - + - + - +
APC
β-CATENIN
TUBULIN
O2
O2E
V5
V5G
IAA
TIR - + - + - + - +
APC
β-CATENIN
TUBULIN
c
% APC
200
150
100
50
0
TIR
V5
X4A
CTRL 0.5 1 2 3 7 8 12
AUXIN TREATMENT (h)
% β-CATENIN
1500
1000
500
0
TIR
V5
X4A
CTRL 0.5 1 2 3 7 8 12
AUXIN TREATMENT (h)

Figure 3.7. Screening of IAA17-APC clones for targeted insertion and auxin sensitivity. (a) Genomic DNA PCR was performed using one primer within the targeting vector and one upstream, as in figure 3.2. DNA from DT40^{TIR} cells and the targeting vector were used as negative controls. Clone 1A from the previous transfection (EGFP-IAA17 positive) was used as a positive control. The PCR product of 3358bp is indicated by the arrow. **(b)** Clones containing the targeted insertion (a) were subject to transient expression of Cre to recombine out the resistance cassette. Parental clones (Bsd+) and daughter clones (Bsd-) were cultured +/- 500μM IAA for 1 hour. Western blots show APC and β-catenin levels in each clone. **(c)** 2 clones were chosen from (b) representing different APC expression levels and subjected to a time course of 500μM IAA treatment. Graph shows quantification of APC and β-catenin protein expression levels. Data is representative of 3 technical replicates, except (b), which is representative of 3 biological replicates.

3.4 Attempting to further deplete APC by increasing the auxin incubation time

Next, a more complete reduction of APC was attempted. Nishimura *et al.,* (2009) added 500μM auxin for 15 minutes to degrade GFP in *S. cerevisiae* expressing a degon-GFP protein and a TIR protein. In the experiments above a one hour auxin (500 μM) incubation was used. To determine whether APC depletion might require a longer exposure to auxin three clones with different levels of APC expression (DT40^{TIR}, X4A and V5) were incubated in 500μM auxin for 24 hours. However, increased degradation of APC was not detected even after this prolonged treatment. Moreover, an off-target effect of auxin addition was detected. Specifically, APC depletion with a concomitant increase in β-catenin was observed in DT40^{TIR} cells when exposed to auxin (fig 3.8a). This suggested that the AID system may be malfunctioning in DT40^{TIR} cells. This means that SCF^{TIR} complexes in these cells were able to degrade APC without a degron, in the presence of auxin – in opposition to the theory (fig 3.2). Thus, the control cell population was not reliable.

3.5 Attempting to increase APC depletion by increasing the amount of SCF^{TIR} E3 ubiquitin ligases

Even though auxin caused degradation of APC in control cells (DT40^{TIR}) it was important to try to increase APC depletion in targeted clones. The rate limiting step in APC degradation may be the availability of the TIR protein to form the SCF^{TIR} complex. APC might only be fully degraded if there is sufficient specific E3 ubiquitin ligases available to ubiquitylate the

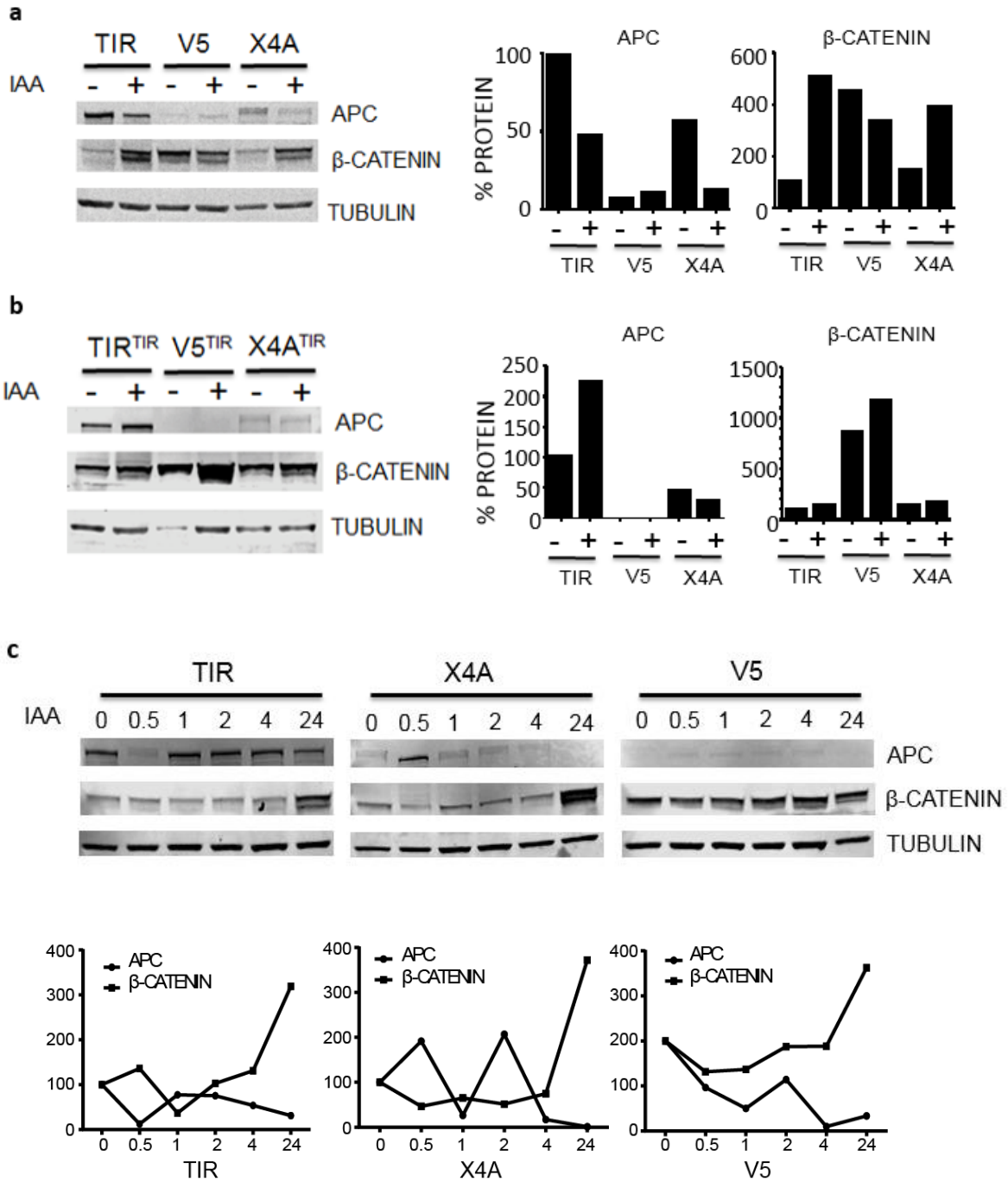

Figure 3.8. Variable response of degron-APC to auxin. (a) Clones were cultured in 500μM IAA for 24hours. Western blot shows APC and β-catenin levels, with quantitations in the right-hand panels. **(b)** Clones were transiently transfected with pcDNA3.1HisC-TIR9Myc and 24 hours later were cultured in 500μM IAA for a further 24 hours. Protein levels were quantified, shown in the right-hand panels. **(c)** Clones were treated with 1mM IAA for 24 hours. Upper panels show Western blot and quantifications are in the lower panels. Data is representative of 3 technical replicates.

degron motif. Hence a plasmid carrying TIR cDNA was transiently transfected into $DT40^{TIR}$, X4A and V5 cells to increase the available ligase. Cells were then incubated with 500μM auxin for 24 hours. This resulted in no detectable APC in clone V5 and a corresponding, large increase in the amount of β-catenin (~4x). There was no effect on the degradation of APC in clone X4A, but again there was an effect in $DT40^{TIR}$ cells (fig 3.8b); TIR transient transfection plus auxin in $DT40^{TIR}$ cells led to a 2 fold increase in APC. This showed that unmodified APC in the control cells was also affected by auxin. This further confirms the unreliability of these cells for my studies.

3.6 Attempting to increase APC depletion by increasing the auxin concentration

Finally, I determined whether a more specific decrease in degron-APC could be achieved using a different concentration of auxin. Nishimura *et al.,* (2009) used up to 500μM to degrade their proteins of interest, the largest of which was 100kDa (MCM4). I hypothesised that as APC is more than three times larger than MCM4, it may require a higher concentration of auxin to target APC effectively and rapidly. $DT40^{TIR}$, X4A and V5 cells were cultured in 1mM auxin over 24 hours to determine whether a higher auxin concentration could more efficiently deplete APC. This proved successful in the APC^{low} clone X4A, which had no detectable APC after treatment with 1mM auxin for 24 hours (fig 3.8c), concomitant for an increase in β-catenin. Increasing the auxin concentration had no visible effect on the APC in V5, although the β-catenin levels did increase with time. This suggested that there was some reduction of APC that could not be detected by Western blot. (Note the APC quantification of V5 is somewhat unreliable because there is so little APC to begin with). Unsurprisingly, once again there was an off-target effect; a decrease in APC and associated increase in β-catenin after 24 hours 1mM auxin in control $DT40^{TIR}$ cells.

3.7 An Alternative approach to the AID system

Due to the problems resulting from targeting the degron motif 5' of *Apc* in DT40^{TIR} cells, I attempted to degrade APC using the original AID system method (Nishimura *et al.,* 2009). This involved expressing both the TIR and EGFP-degron-*Apc* cDNAs in one plasmid. Once transfected into cells this would produce the TIR protein and separate EGFP-degron-APC fusion protein, with the aim of degrading APC upon the addition of auxin. I.e. exogenous APC would be targeted for degradation.

Firstly, EGFP (from pEGFP-C1) was cloned into a plasmid containing both TIR and degron cDNA (pAID1.2N, see supplemental figure 2) using the restriction site BstXI. This targeted EGFP to the N-terminus of the degron motif (for EGFP-degron expression). This then enabled *Apc* cDNA to be cloned (from pCMV-Neo-Bam-APC) into the plasmid's multiple cloning site (PvuI and MluI restriction sites) to produce a GFP-degron-APC fusion protein. Transformation of competent bacteria with pAID1.2N-EGFP-APC resulted in no colonies (data not shown). Therefore, the whole process was repeated, but the EGFP and *Apc* cDNAs were firstly inserted into separate pJET1.2 cloning vectors. This ensured that cloning produced complete cDNA sequences when the cDNAs were further cloned from pJET1.2 into pAID1.2N using BstX1 (EGFP) or PvuI and MluI (*Apc*). Cloning of *Apc* cDNA (into pAID1.2-EGFP) and subsequent transformation of bacteria with pAID1.2-EGFP-APC resulted in one bacterial colony. Mini-preps were then carried out using the transformed bacteria. To check if ligation of the vector (pAID1.2-EGFP) and insert (*Apc* cDNA) was successful, a restriction digest was carried out using PvuI and MluI restriction enzymes, followed by agarose-gel electrophoresis. This showed that the insert was present, but it ran at the wrong molecular weight (data not shown). This suggested that the *Apc* cDNA had undergone some sort of structural rearrangement, possibly forming a quadraplex. This meant that the pAID1.2-EGFP-APC plasmid I had generated could not be used for AID

system experiments. Due to time pressure at this stage in my PhD, I had to move on with the project and so moved away from the generation of AID system cell lines.

3.8 Conclusions

To conclude, a conditionally, degradable, endogenous APC was created in DT40^{TIR} cells. APC was depleted after a one hour incubation with 500μM auxin. Nonetheless, we concluded that this system was not the best option for studying the non-Wnt functions of APC for a number of reasons. The degron-*Apc* is a hypomorphic allele and results in cells with 50-100% less APC than control DT40^{TIR} cells. Whereas, a one hour incubation with 500μM auxin had minimal affect in DT40^{TIR} cells, increased concentrations of auxin or longer incubation times caused an off-target effect. Specifically, it led to decreased WT APC (and produced a concomitant increase in β-catenin) when cells were treated with 500μM auxin for 24 hours. The cumulative effect of increased TIR expression plus 500μM auxin resulted in the opposite effect – an increase in APC. For these reasons the degron-*Apc* generated in the lab was not used to examine non-Wnt functions of APC.

Chapter 4

Response of degron-APC cells to Taxol® and DNA damaging agents.

Background

Most *Apc* mutant cells, found in the majority of CRCs, possess truncated *Apc* expressing the N-terminal third of the gene. This usually includes the oligomerisation and armadillo domains and some/no β-catenin binding domains. These cells do not arrest as well as WT APC cells at the spindle assembly checkpoint (SAC) during mitosis, in response to arresting agents such as Taxol®. Taxol® suppresses microtubule dynamics by binding to tubulin. Cells with different expression levels of full-length APC provided an opportunity to study the involvement of APC in mitotic arrest, i.e. it whether there is a threshold concentration of APC required for cells to adequately arrest in response to Taxol®.

Evidence in the literature linking APC and DNA damage further suggests examining a functional link between APC and cell cycle progression, which can be affected by DNA damage (Narayan and Jaiswal, 1997; Steffensen *et al.,* 1997; Jaiswal *et al.,* 2006; Balusu *et al.,* 2007). There are several ways a cell can respond to DNA damage, employing various repair pathways to fix the damage. For example: single strand break repair (SSB), nucleotide excision repair (NER), base excision repair (BER), mismatch repair (MMR), non-homologous end joining (NHEJ) and homologous recombination (HR). These can all be executed in response to upstream signals that recognise DNA damage. The degron-APC cells provided an opportunity to study the relationship between APC levels and DNA damage response in DT40 cells, a standard system for studying DNA damage.

Aim

I aimed to determine if decreased APC protein caused changes in cell cycle or DNA damage response using cells with varying levels of APC.

Model System

The overall aim of my PhD was to study the non-Wnt functions of APC using a reverse genetics approach. I generated a degron-*Apc* cell line $DT40^{TIR;\ (GFP)\ IAA17\text{-}APC}$ that allowed for the controlled degradation of endogenous APC upon addition of auxin. The degron-*Apc* allele was hypomorphic and it generated clones with varying full-length APC expression. Certain clones were chosen to study cell cycle and DNA damage response; X4A (APC^{low}) and V5 ($APC^{minimal}$) in comparison to the control cell population $DT40^{TIR}$ (APC^{high}).

Method

To study changes in the cell cycle in $DT40^{TIR}$, X4A and V5 cells, FACS analysis was used to separate cells into G1, S and G2/M phases. Cells were incubated for 20 minutes with 20μM of the synthetic nucleoside Bromodeoxyuridine (BrdU), which is taken up by cycling cells. The cells were then washed, harvested, fixed and stained with an anti-BrdU antibody to asses cells' proliferation, and PI to demonstrate the cells' DNA content. To examine cells in mitosis, cells were harvested, fixed and stained with an anti-PH3 antibody and PI. Cells were treated with varying concentrations and time periods of Taxol® and then stained with anti-BrdU or PH3 antibodies. The selection of live, single cells used for this FACS analysis and subsequent experiments is shown in supplementary figure 6.

To examine how cells with diminished APC responded to DNA damage, the colorimetric MTS cell viability assay was used to measure the percentage of viable cells in a sample. After incubating cells in different concentrations of PARPi, Cisplatin or HU the drugs were washed off and cells resuspended in drug-free media. After 24, 48 or 72 hours the MTS assay was used to measure the viability of the cells.

Results Summary

Cells with reduced APC levels:

- Arrested in mitosis less well in response to low doses of Taxol®.
- Exhibited no changes in DNA damage response after treatment with PARPi.
- Recovered better from Cisplatin-induced DNA damage.
- Recovered less well from HU-induced DNA damage.

Results

4.1 Establishing the cell cycle profile of WT APC cells

In order to determine if a decrease in APC resulted in cell cycle changes, the cell cycle profile of APC WT cells was established. $DT40^{TIR}$ cells were incubated with BrdU and washed, harvested, fixed and stained with an anti-BrdU antibody (fig 4.1 top panel) and PI (fig. 4.1 bottom panel). The cells were gated using FACS to exclude G0 and sub-G1 cells (using PI-supplementary figure 6) and the remaining cells were analysed for cell cycle distribution. Next, $DT40^{TIR}$ cells were treated with varying concentrations of Taxol® for 24 hours, then fixed and stained with PI. FACs analysis then determined the percentage of cells at each phase of the cell cycle (fig 4.1b). The untreated (control) $DT40^{TIR}$ cells had almost 60% of cells in S phase, with 20% in S and G2/M phases. This distribution changed dramatically upon the addition of 10nM Taxol®. The proportion of G2/M cells increased to 70% after treatment with at least 10nM Taxol®. The number of cells in S phase decreased to as low as 0% (1µM). This shows that the Taxol® was effective in arresting the cells.

4.2 Comparing G2/M arrest using BrdU

In order to examine how lowered APC expression may affect the cell cycle, the 3 varying APC expressers (APC^{high}, APC^{low} and $APC^{minimal}$) were treated with 100nM Taxol® for 6 hours, as well as growing untreated cells as control samples.

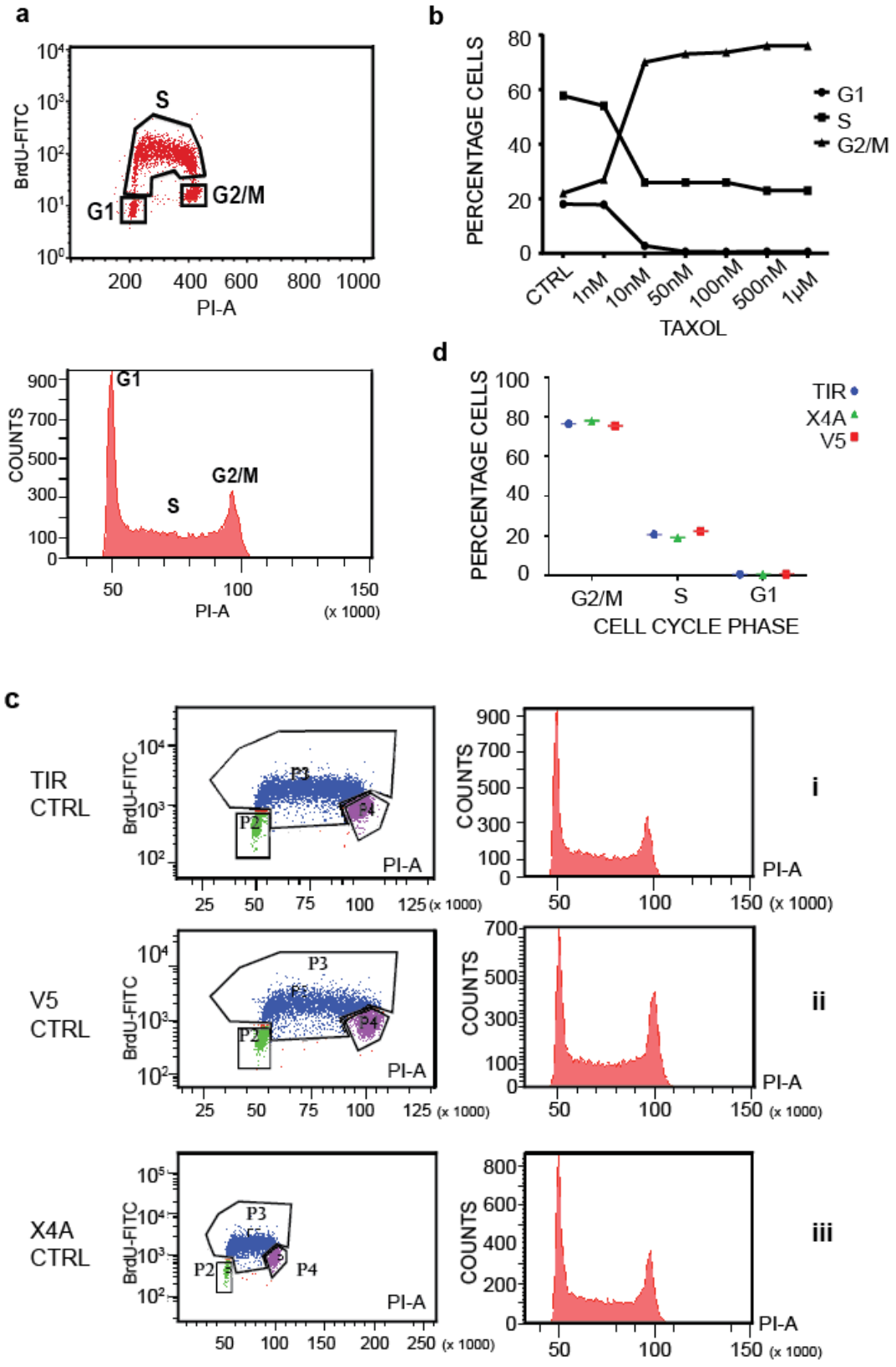
a
BrdU-FITC
S
G1
G2/M
PI-A
COUNTS
G1
S
G2/M
PI-A
(x 1000)
b
PERCENTAGE CELLS
G1
S
G2/M
CTRL
1nM
10nM
50nM
100nM
500nM
1μM
TAXOL
d
PERCENTAGE CELLS
TIR
X4A
V5
G2/M
S
G1
CELL CYCLE PHASE
c
TIR CTRL
V5 CTRL
X4A CTRL
BrdU-FITC
PI-A
P2
P3
P4
COUNTS
i
ii
iii

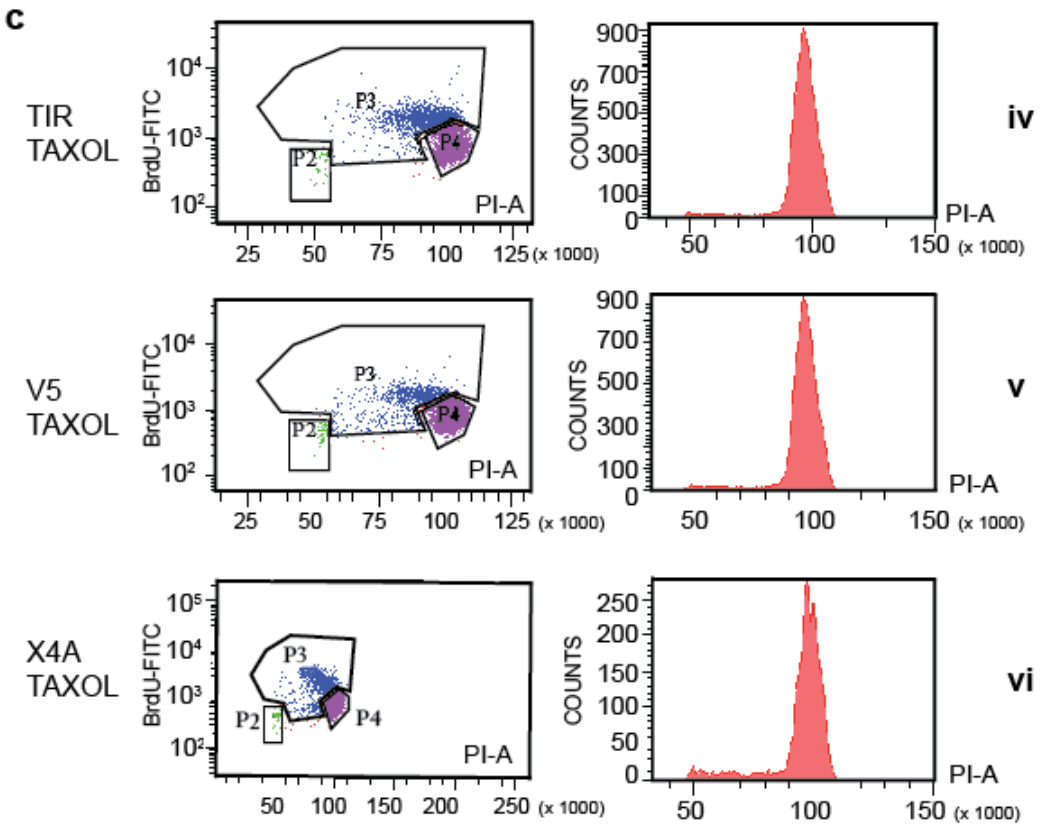

Figure 4.1. Lowering APC expression has no effect on G2/M arrest induced by Taxol®. (a) DT40^{TIR} cells were incubated with 20 μM BrdU for 20 mins, fixed and stained with an anti-BrdU antibody (top panel) and PI to look at the distribution of cells within the cell cycle (bottom panel). **(b)** DT40^{TIR} cells treated with varying concentrations of Taxol® for 24 hours. **(c)** Clones (IAA17-APC cells) and control DT40^{TIR} cells were treated with 500μM Taxol® for 6 hours and subsequently incubated with 20 μM BrdU for 20 mins. Cells were then fixed and stained with anti-BrdU and PI and analysed by FACS. The left hand panel for each cell line represents the BrdU plot, with gating to show how cells were selected for each cell cycle stage. The right hand panel represents the PI plot, showing the number of cells in G1 versus G2/M. **(d)** Quantification of the percentage of cells in G2/M, S and G1 based on the BrdU and PI FACS analysis in Taxol® treated cells (c).

A concentration of 100nM Taxol® was chosen for further experiments, as this concentration achieved 0% of cells in S phase (fig 4.1b). The incubation period was decreased from 24 to 6 hours-due to the higher concentration. Subsequently, the cells were incubated with BrdU before harvesting, fixing and staining with an anti-BrdU antibody and PI (fig 4.1c). Both the BrdU plot (left panel) and the PI plot (right panel) show the distribution of cells within the cell cycle and reveal the effect of the arresting agent Taxol®. In all 3 cell lines the proportion of cells in G2/M versus S or G1 phase was unchanged in the presence of Taxol®

(fig 4.1d) – 76.6% of APC^{high}, 78% of APC^{low} and 75.6% of $APC^{minimal}$ cells were in G2/M phase. This suggested that Taxol® (100nM) had the same effect in all 3 cell lines.

4.3 Evaluating mitotic arrest using Phospho-Histone H3

BrdU treatment did not reveal if cells were arrested at the G2/M checkpoint, or whether they had progressed into mitosis and subsequently arrested. Cells in mitosis contain phosphorylated N-terminal histone tails on histone H3 (PH3) to allow for chromatin relaxation around the nucleosome. Aurora B phosphorylates serine 10 of histone H3 to produce phosphohistone 3, during mitosis (Hsu *et al.,* 2000). This enables chromosome pairing and assembly in mitosis (Hans and Dimitrov, 2001).The proportion of cells in mitosis was not significantly different in Taxol® treated cells with less APC (fig 4.2b). However, it was possible that the concentration of Taxol® was too high to detect subtle changes in mitotic arrest. Therefore, a Taxol® titration was performed (6 hour incubation) and the cells stained with anti-PH3 for FACS analysis (fig 4.3a). The titration showed that at low doses of Taxol®, there were more mitotically arrested cells in cells containing less APC. These cells were more sensitive to Taxol® than cells with WT APC levels. However, this could also mean that cells with less APC proliferated faster and thus more cells arrested in mitosis. (Due to a faster cell cycle, more cells were generated, so there were more cells available to go through mitosis - higher PH3).

4.4 Cells with reduced APC arrest less well in mitosis in response to low doses of Taxol®

To determine if there was a temporal response to Taxol®, a time-course of low-dose Taxol® treatment at 5nM (fig 4.3b), 10nM (fig 4.3c) and 20nM (fig 4.3d) was performed. The number of cells in mitosis was determined by FACS using PH3. No difference can be seen in the distribution of APC-varying cells when treated with 5nm or 10nM Taxol®. Although changes seem to occur at 9+ hours Taxol® treatment, there were more dying cells at these time-points and so these are not accurate reflections of cell cycle distribution.

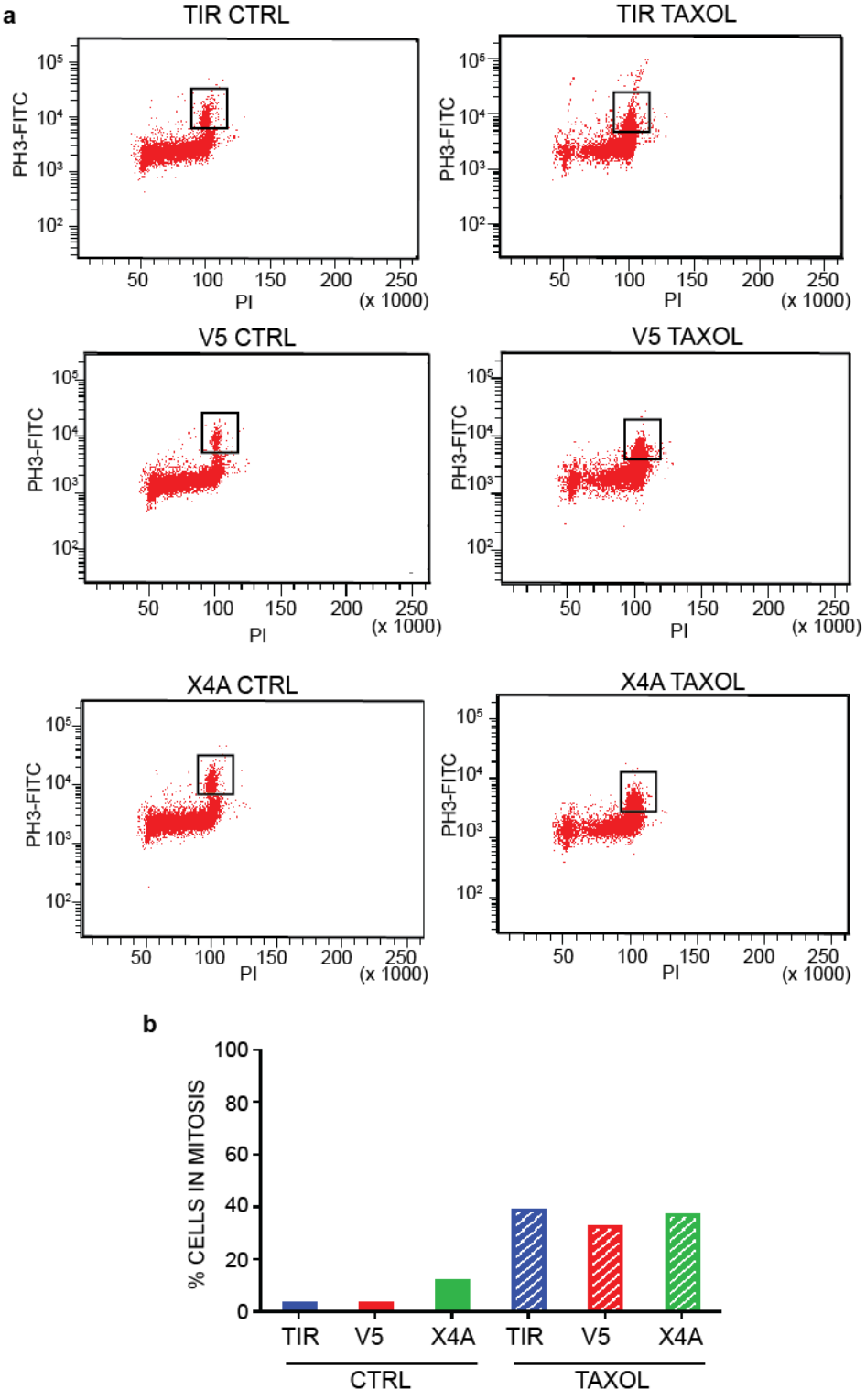

Figure 4.2. Lowering APC expression has no effect on mitotic arrest in response to 100nM Taxol®. (a) APC^{high} (DT40^{TIR}), APC^{low} (X4A) and APC^{minimal} (V5**)** cells were treated with 100nM Taxol® for 6 hours or left untreated (ctrl). Cells were fixed and stained with an anti-PH3 antibody and PI and analysed by FACS. The black box represents the mitotic cells. **(b)** Quantification of the varying APC cells in mitosis when untreated (ctrl) or Taxol® treated, taken from (a).

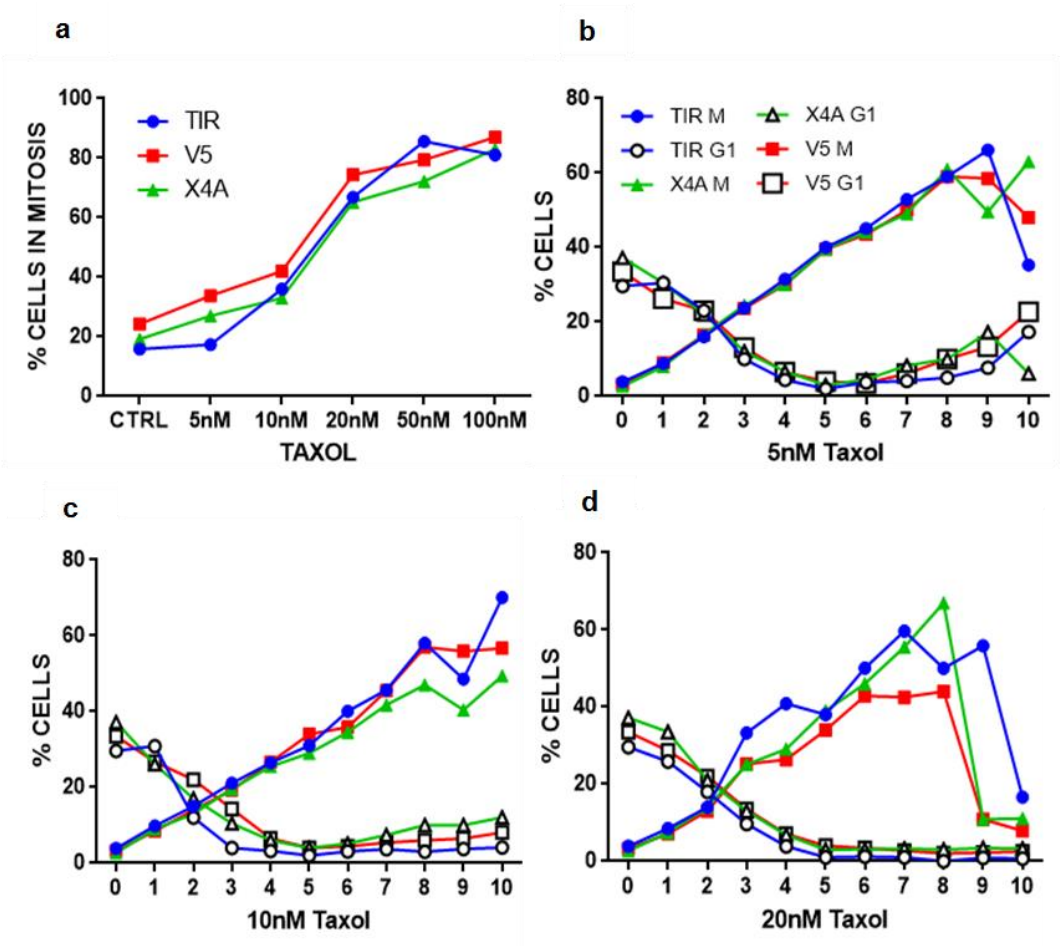

Figure 4.3. Cells with lowered APC expression arrest less well in mitosis in response to low doses of Taxol®. (a) Cells with varying APC expression; APC^{high} ($DT40^{TIR}$), APC^{low} (X4A) and $APC^{minimal}$ (V5) were treated with 100nM Taxol® for 6 hours. Cells were then fixed, stained with an anti-PH3 antibody and PI and analysed by FACS. **(b)** Cells were treated with 5nM Taxol®, harvested every hour for 10 hours, stained with an anti-PH3 antibody and PI and analysed by FACS (**c**) as in (b) treated with 10nM Taxol® (**d**) as in (b) treated with 20nM Taxol®.

However, slight changes seemed to occur when cells with varying APC levels were treated with 20nM Taxol®; APC^{low} and $APC^{minimal}$ cells (with <50% less APC than APC^{high} cells) arrested less well than APC WT cells ($DT40^{TIR}$). $APC^{minimal}$ cells arrested the least and APC^{low} cells arrested less than APC^{high} and more than $APC^{minimal}$. Hence the cells with an intermediary amount of APC arrested at an intermediate level. This result is in opposition to what was observed at low doses of Taxol® in fig 4.3a, where there were more reduced-APC cells arrested in mitosis after 6 hours 20nM Taxol® treatment. However, the data in fig 4.3d is consistent over several hours (hours 3, 4, 6 and 7). Due to these experiments only being carried out once, it is therefore difficult to make any robust conclusions from the data. The experiments need to be repeated to determine whether the data in fig 4.3a or 4.3d is correct.

4.5 Cells with less APC respond differently to DNA cross-linkers and stalled replication forks

Next, to examine the DNA damage response (DDR), $DT40^{TIR}$, X4A and V5 cells were treated with three different DNA damaging agents. The response of APC^{high}, APC^{low} and $APC^{minimal}$ cells were measured to drugs that affect DNA in three different ways: PARPi inhibits the PARP protein required to repair SSBs in DNA; Cisplatin cross-links DNA and cells require mechanisms to excise the lesion(s) from one or both DNA strands, such as topoisomerase proteins; and Hydroxyurea (HU) is thought to deplete the nucleotide pool, causing replication fork crashes that must be resolved. I hypothesized either: an initial decrease in cell viability after drug treatment (due to cell death induced by the DNA damage); or stasis in cell numbers - as the cell cycle was paused in order for the DNA damage to be repaired. Subsequent survival rates then depended on how effectively cells repaired the DNA damage.

$DT40^{TIR}$, V5 and X4A cells were incubated with PARPi, Cisplatin or HU. The drug was then washed off and cells were resuspended in drug-free media. 24, 48 and 72 hours later, cell viability was measured using an MTS assay (fig 4.4). Different incubations of each drug

were used so that the MTS assay measured the viability after DNA damage was incurred as a result from each DNA damaging agent – the same incubation of each drug may have resulted in measuring cell death rather than DNA damage, due to the different potencies of each drug used. The most potent agent (Cisplatin) had a direct affect on DNA, whereas HU and PARPi affect DNA damage response pathways and (as they are less potent) require a longer incubation time.

There was no difference between the responses of the different cells to PARPi (fig 4.4a). However, at 72 hours post-Cisplatin (fig 4.4b), there were more APC^{low} and $APC^{minimal}$ cells, with $APC^{minimal}$ cells showing the highest survival. Perhaps cells with less APC can repair DNA cross links faster and consequently proceed through the cell cycle sooner. Whereas, APC^{high} cells ($DT40^{TIR}$) may still be repairing DNA and cannot continue through the cell cycle. Conversely, cells with less APC may not notice and/or repair cross-links. Instead these cells may continue through the cell cycle without repairing the damage.

After HU treatment, cells with less APC recovered less well. $APC^{minimal}$ cells recovered the least and APC^{low} cells demonstrated that an intermediate level of APC produced an intermediary response to HU between APC^{high} and $APC^{minimal}$. This is the opposite response to Cisplatin.

4.6 Conclusions

With regards to the cell cycle, APC depleted cells seemed to arrest less well to low doses of Taxol®, although the difference is slight. There appears to be a positive correlation between the level of APC and mitotic arrest; the more APC available to the cell, the more cells arrest in mitosis in response to Taxol®. This is evident as cells with the least amount of APC ($APC^{minimal}$) arrested the least in response to Taxol® and cells with an intermediary level of APC (APC^{low}) arrested less than APC^{high}, but more than APC^{low}. However, this was not measured statistically due to the changes being small. Thus, only a trend can be

reported at this time. Results from the viability assay suggested that APC-reduced cells coped with SSB as readily as APC WT cells. They coped with replication fork crashes less well, and either repaired cross-links more efficiently than APC WT cells ($DT40^{TIR}$), or did not respond to them. Why this is the case is unclear. However, as each repair pathway comprises many different proteins and upstream signals, it is possible that APC^{low} and $APC^{minimal}$ cells have different proportions of these repair proteins and thus cope differently when various DNA damage occurs. It is also plausible that APC may bind to certain DNA damage proteins, either acting to activate or inactivate them (Narayan *et al.,* 2005; Balusu *et al.,* 2007; Jaiswal *et al.,* 2013), or causing steric hindrance. Nevertheless, it is important to remember that changes observed in APC viability were small. Importantly, it is possible that APC deficient cells may not die very well, regardless of drug treatment. Therefore, looking at apoptosis in these cells is important to determine how to kill them specifically.

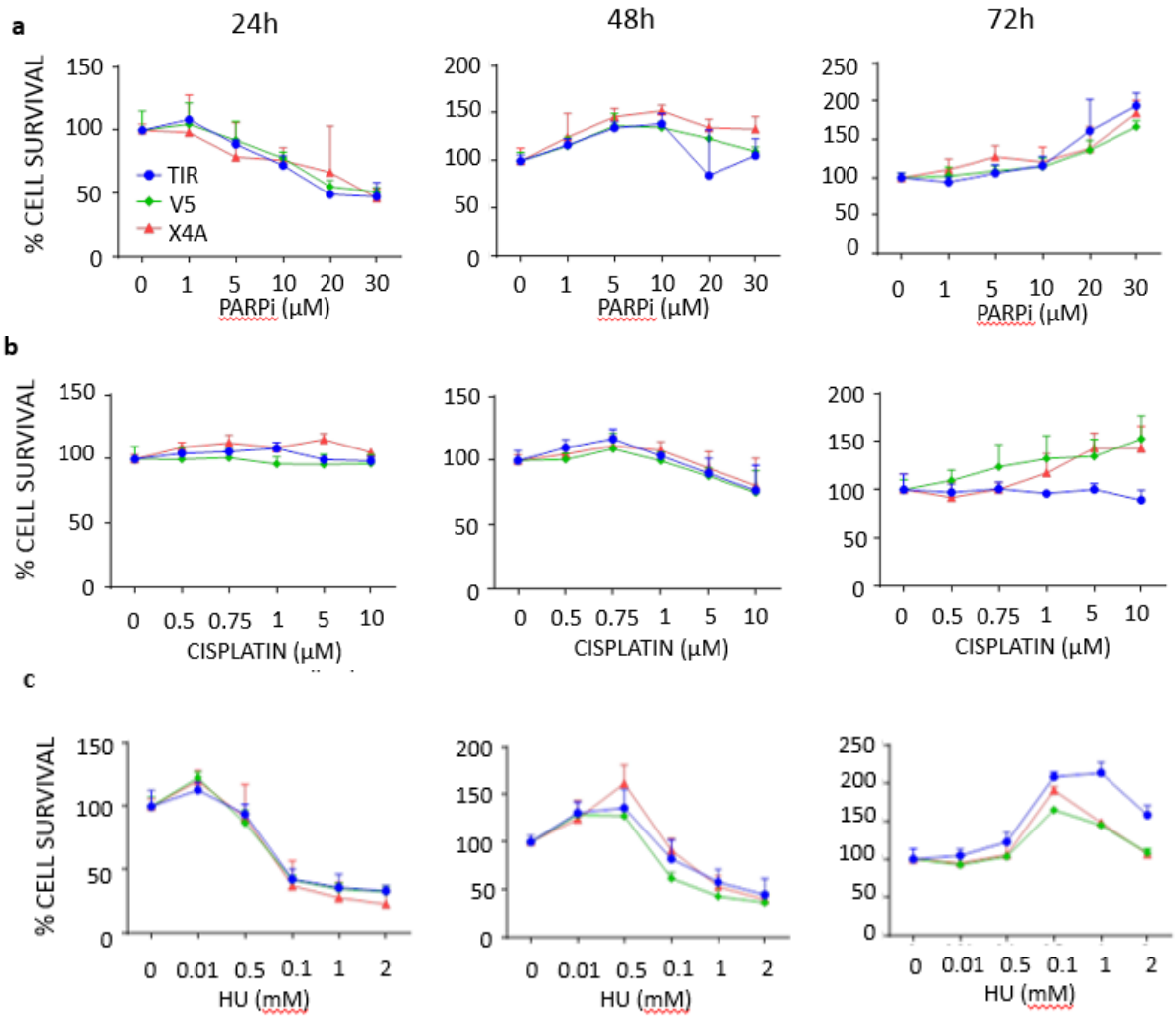

Figure 4.4. Having less APC may alter cells' response to some DNA damaging agents. MTS assays were performed on DT40^{TIR} cells and IAA17-APC clones after exposure to DNA damaging agents, which affect different DNA repair pathways. After PARPi, Cisplatin or HU drug treatments, cells were washed and re-suspended with drug-free media. Cells were seeded into 96 well plates, 12,000 per well and cell survival was measured 24, 48 and 72 hours post drug treatment. **(a)** PARPi treatment for 24 hours. **(b)** Cisplatin treatment for 2 hours. **(c)** Hydroxyurea treatment for 16 hours.

Chapter 5

Increased Bcl-2 and altered mitochondria may be responsible for the reduced sensitivity of *Apc* deficient cells to cytotoxic agents.

Background

Apc mutant cells like those found in more than 90% of sporadic CRCs have a compromised spindle assembly checkpoint. This is partly due to the loss of C-terminal microtubule binding domains of *Apc* (Munemitsu *et al.,* 1994; Smith *et al.,* 1994; Muhua *et al.,* 1998; Kaplan *et al.,* 2001; Dikovskaya *et al.,* 2007). This means that *Apc* mutant cells treated with microtubule poisons such as Taxol®, do not arrest in G2/M as readily as *Apc* WT cells. Consequently, these mutant cells also do not undergo apoptosis induced by a prolonged mitotic arrest (Radulescu *et al.,* 2010). However, exactly how a mitotic arrest induces apoptosis or how APC is linked with apoptosis in unknown. Understanding the latter connection is important to identify a means to selectively kill *Apc* mutant cells.

For over twenty years a link between APC and apoptosis has been investigated (Browne *et al.,* 1994; Dikovskaya *et al.,* 2007; Cristofaro *et al.,* 2015). Previous observations in the Näthke lab showed that *Apc* deficient cells were less sensitive to low doses of Taxol®, but were more readily killed by the combination of Taxol® and the Bcl-2 inhibitor ABT-737 (unpublished data). This functional link between APC and apoptosis still lacked a molecular explanation. The aim of this thesis was to investigate the link between APC and apoptosis and establish how it was related to functions of APC in Wnt signalling.

Aim

The aim of this study was to investigate why *Apc* deficient cells are less sensitive to low doses of Taxol® and how the Bcl-2 inhibitor ABT-737 induces Taxol® sensitivity. Then to determine a mechanism for this resistance that might be clinically exploitable to specifically kill these cells.

Model System

2D cell culture models of human epithelial cancer cell lines were used: *Apc*$^{+/+}$ U2OS and HeLa cells, *APC*$^{+/+}$; *β-catenin*$^{\Delta Ser45/+}$ HCT116 CRC cells, *Apc*$^{1367/1367}$ CaCo2 CRC cells and *Apc*$^{1308/1308}$ SW480 CRC cells. Some findings were then validated in a 3D model system; *Apc*$^{+/+}$ and *Apc*$^{Min/Min}$ intestinal organoids derived from A*pc* WT and A*pc*^{Min} mice, on a C57BL/6J background (see table 2.6). *Apc*$^{Min/+}$ was the first mouse model for polyposis and is the most frequently used model of *Apc* mutation-induced CRC. It has a nonsense mutation in *Apc* at codon 850 that produces a short, truncated *Apc* (N-*Apc*). This N-*Apc* fragment lacks the β–catenin and microtubule binding domains (Su *et al.,* 1992). These heterozygous mice develop numerous intestinal polyps analogous to the human condition Familial Adenomatous Polyposis (FAP). Patients with FAP develop numerous (10's to 1,000's) benign colonic polyps. This is a fully penetrant condition due to an inherited autosomal dominant, nonsense mutation in *Apc.* When left untreated, these polyps can accrue further mutations and develop into adenocarcinomas (CRC).

Method

To identify changes in the apoptotic machinery in *Apc* mutant cells, I focused on Bcl-2 (B cell lymphoma-2) family proteins as they are a key component of the intrinsic apoptosis machinery. RNAi was used to knock-down *Apc*, *CTNNB1 (β-catenin*) and a candidate gene *Par-4* (prostate apoptosis response gene-4) in human epithelial cancer cell lines. The effects on the pro-life protein Bcl-2 were then examined. Different fractionation techniques were used to establish changes in protein levels in various cellular compartments. Most procedures were carried out in the presence and absence of the Bcl-2 inhibitor (a BH3 mimetic) ABT-737 (Oltersdorf *et al.,* 2005). Changes in the unfolded protein response (UPR) were studied by examining phospho-IRE protein levels and changes in mitochondria were investigated using the mitochondria-selective probes MitoTracker® (Calarco, 1995) and JC-1 (Smiley *et al.,* 1991). Once changes in these proteins in cell culture experiments

were identified, the effects of Taxol® and ABT-737 on intestinal organoids, a 3D tissue-mimetic model, were investigated.

Results Summary

- *Apc* depletion caused a β-catenin-independent increase in Bcl-2.
- ABT-737 treatment caused an increase in Bcl-2 in the membrane fraction, but not mitochondrial or ER membranes.
- Taxol®, ABT-737 and *Apc* depletion activated the unfolded protein response, and caused a change in the localisation and/or structure of mitochondria – a read out for cellular stress.
- *Apc* depleted cells are smaller (μm^2 and FSC).

Results

5.1 *Apc* depletion causes an increase in Bcl-2 in certain cell-lines

To establish whether there is a link between APC and apoptotic proteins, RNAi was used to knock-down *Apc* and *Apc*/*β-catenin* in U2OS and HeLa cells. Then, levels of the pro-life protein Bcl-2, which is involved in protecting cells from apoptosis, were examined. A Western blot showed that upon *Apc* depletion there was a variable increase in Bcl-2 in U2OS cells that was not affected by *β-catenin* depletion (fig 5.1a). This suggested that the increase in Bcl-2 caused by *Apc* knock-down may be β-catenin (Wnt pathway) independent. This is consistent with the data that Bcl-2 also increased when the RNAi experiment was repeated in CRC cells expressing a truncated *Apc* (N-*Apc*), which is inactive in Wnt signalling (fig 5.1b). However, this increase was variable and less strong in HeLa cells and not robust. Knocking down *β-catenin* alone did not cause a change in Bcl-2 consistent with the conclusion that Bcl-2 changes are independent of β-catenin status (fig 5.1c). However, to fully exclude a relationship between *β*-catenin and Bcl-2 changes, experiments overexpressing β-catenin are required.

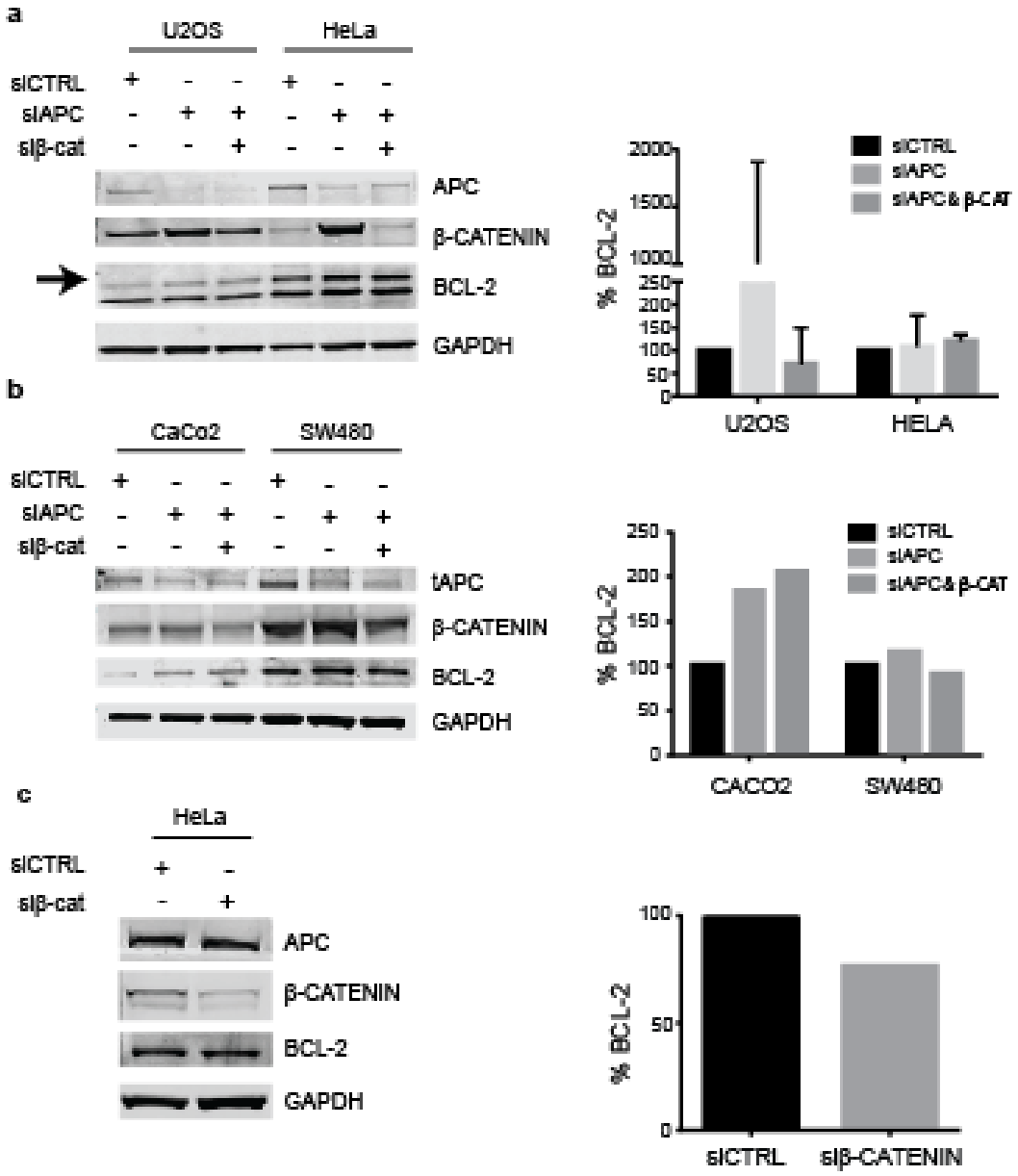

Figure 5.1. *Apc* depletion causes an increase in Bcl-2 in certain cell-lines. **(a)** U2OS and HeLa cells were treated with *ctrl, Apc and β-catenin* siRNAs. Western blot (left panel) and quantification (right panel) shows a variable increase in Bcl-2 in U2Os cells, but not HeLa cells. N=3, error bars represent the standard deviation. **(b)** *Apc* mutant CaCo2 and SW480 cells were treated as in (a). Western blot (left panel) and quantification (right panel) shows an increase in Bcl-2 in CaCo2 cells, but not SW480 cells. (**c**) HeLa cells were treated with *β-catenin* siRNA alone to determine if the Bcl-2 increase upon *Apc* knock-down was β-catenin dependent.

5.2 Par-4 protein levels cannot explain the increase in Bcl-2 upon *Apc* depletion

Next, experiments were needed to establish if the effect of APC on Bcl-2 was direct or indirect. Specifically, experiments aimed to determine if APC binds Bcl-2 directly or whether another protein is involved that links APC and Bcl-2. A potential candidate for such an indirect link to Bcl-2 was revealed in mass-spectrometry datasets from the lab, which identified binding partners of endogenous APC. Specifically, we found that APC co-immunoprecipitated with Par-4 (unpublished data). Par-4 transcriptionally inhibits *Bcl-2* through a WT1 (Wilms' tumour 1) binding site in the *Bcl-2* promoter (Cheema *et al.,* 2003). I hypothesized that APC could bind to Par-4, sequestering it and preventing its degradation. This in turn would maintain low/reduced levels of Bcl-2 by Par-4-mediated transcriptional inhibition (fig 5.2a). In this model, *Apc* depletion would lead to release and degradation of Par-4 causing an increase in Bcl-2, as observed upon *Apc* knock-down (fig 5.2b). A potential flaw with this theory is that sequestration by APC might also prevent Par-4 from reaching its target sites in the nucleus. However, APC is present in the nucleus (Henderson, 2000; Neufeld *et al.,* 2000) and thus could bind Par-4 where it is active, i.e. the nucleus. To test this idea, *Apc* or *β-catenin* were knocked down using RNAi in U2OS and HeLa cells (data from fig 5.1) and levels of Par-4 were compared (fig 5.2d). In addition to the increase in Bcl-2 there was also an increase in Par-4, the opposite of the expected change. The same was observed when *Apc* and *β-catenin* were knocked-down in CRC cell lines with mutant, truncated *Apc* (fig 5.2e). Thus, the increase in Bcl-2 resulting from *Apc* depletion could not be explained by a reduction in Par-4 protein (fig 5.2c). An alternative possibility that could explain the observations is that when Par-4 is bound to APC it is active and represses Bcl-2; but when *Apc* is depleted and Par-4 is released it is inactive and can no longer inhibit Bcl-2. Based on the finding that, neither WT nor mutant (truncated) APC could be co-immunoprecipitated with Par-4 (data not shown), it is unlikely that Par-4 acts as a link between APC and Bcl-2.

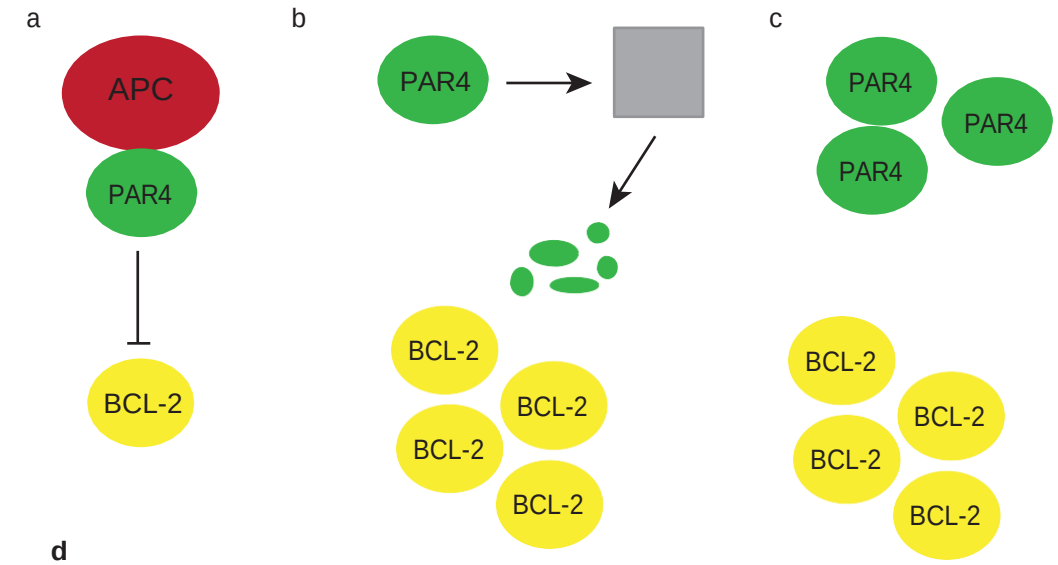
a
APC
PAR4
BCL-2
b
PAR4
BCL-2
BCL-2
BCL-2
BCL-2
c
PAR4
PAR4
PAR4
BCL-2
BCL-2
BCL-2
BCL-2

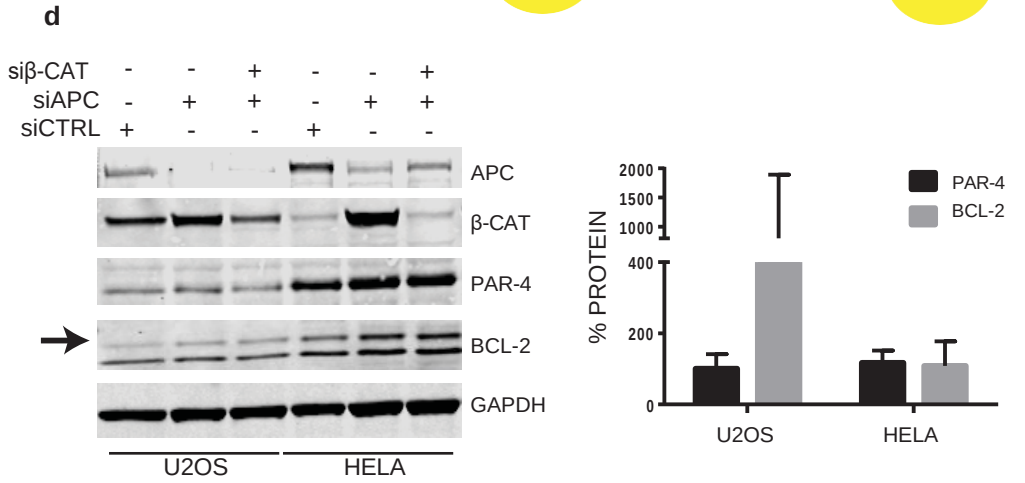
d
siβ-CAT - - + - - +
siAPC - + + - + +
siCTRL + - - + - -
APC
β-CAT
PAR-4
BCL-2
GAPDH
U2OS
HELA
% PROTEIN
2000
1500
1000
400
200
0
PAR-4
BCL-2
U2OS
HELA

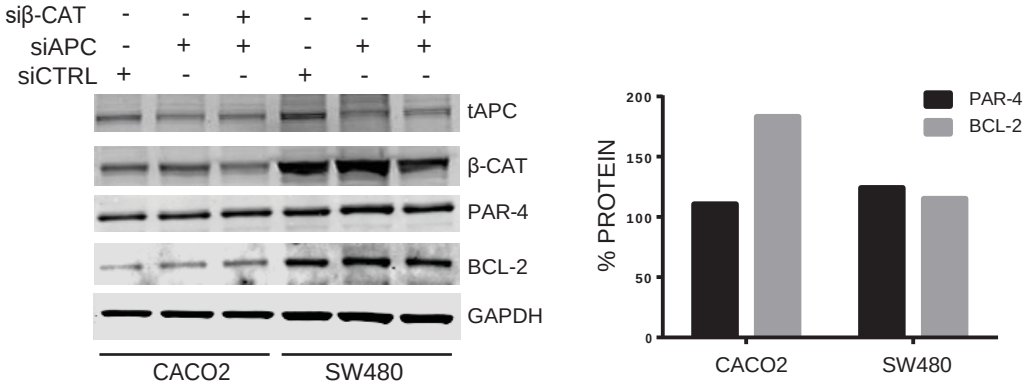
e
siβ-CAT - - + - - +
siAPC - + + - + +
siCTRL + - - + - -
tAPC
β-CAT
PAR-4
BCL-2
GAPDH
CACO2
SW480
% PROTEIN
200
150
100
50
0
PAR-4
BCL-2
CACO2
SW480

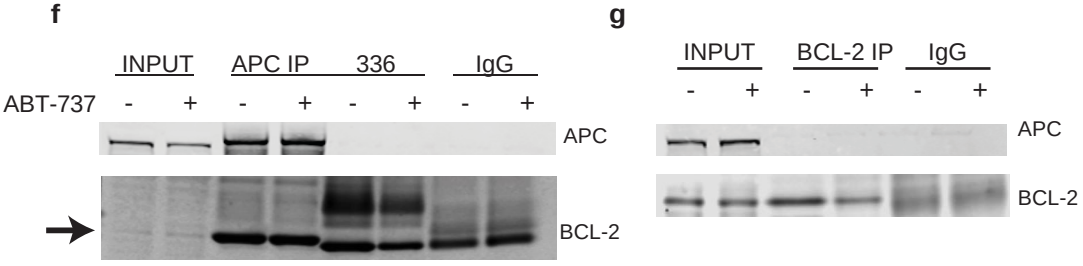
f
INPUT
APC IP
336
IgG
ABT-737 - + - + - + - +
APC
BCL-2
g
INPUT
BCL-2 IP
IgG
- + - + - +
APC
BCL-2

Figure 5.2. Par-4 protein levels cannot explain the increase in Bcl-2 upon *Apc* knock-down. Model showing how Par-4 and APC could be linked: (**a**) APC protects Par-4 from degradation, resulting in Par-4-mediated Bcl-2 inhibition; (**b**) APC loss leads to Par-4 degradation and subsequent Bcl-2 increase. (**c**) Experimental results show that APC loss leads to an increase in Par-4 as well as Bcl-2. (**d**) *Apc* and *β-catenin* were knocked down in U2OS and HeLa cells. Western blots show levels of Par-4 and Bcl-2. The right-hand panel shows the quantification of the Western blot, with relative amounts of Par-4 and Bcl-2 compared to control siRNA (100%). **(e)** *Apc* and *β-catenin* were knocked down in CaCo2 and SW480 cells. Western blots show levels of Par-4 and Bcl-2. The right-hand panel shows the quantification of the Western blot, with relative amounts of Par-4 and Bcl-2 compared to control siRNA (100% protein intensity). (**f**) APC IP (2mg lysate) in U2OS cells shows an inconclusive CoIP with Bcl-2. 336 is a negative control for the Ali APC antibody used (see table 2.1). For uncut blots, see supplementary figure 7. (**g**) Bcl-2 IP (2mg lysate) in U2OS cells is negative for a Bcl-2-APC CoIP.

To look for a direct link between APC and Bcl-2, Co-IPs were used. Bcl-2 did not co-immunoprecipitate (IP) with APC (fig 5.2f and supplementary figure 7). Furthermore, IPs for Bcl-2 did not reveal APC (fig 5.2g). This was despite the fact that, full-length and mutant APC were previously shown to associate with Bcl-2 in HCT116, SW480 and HEK293^{APC1309} cells when using Co-IP (Brocardo *et al.,* 2007); However, in this case, Co-IPs were performed with ectopically expressed proteins. In the absence of further data, an interaction between APC and Bcl-2 could not be confirmed. More experiments are needed to unravel the relationship between APC and Bcl-2.

5.3 ABT-737 causes a Bcl-2 increase in the membrane fraction

The elevated Bcl-2 levels that occurred in response to *Apc* depletion (fig 5.1) may provide some explanation as to why *Apc* deficient cells do not die in response to Taxol® as readily as *Apc* WT cells. Previously, we found that a combination of the Bcl-2 inhibitor ABT-737 with Taxol® killed *Apc* deficient cells more effectively than wild type cells, or than either drug individually (unpublished data). To establish if this increased sensitivity could be explained by changes in Bcl-2, HCT116 CRC cells (*Apc*$^{+/+}$) and U2OS cells were treated with 7μM ABT-737 for 24 hours (fig 5.3a). This caused an increase in Bcl-2 in both cell lines. To determine where this Bcl-2 increase occurred, HCT116 cells were again treated with ABT-737 and fractionated to separate cytosol, membrane, nucleus and cytoskeletal compartments. Western blots showed an increase in Bcl-2 in the membrane fraction upon

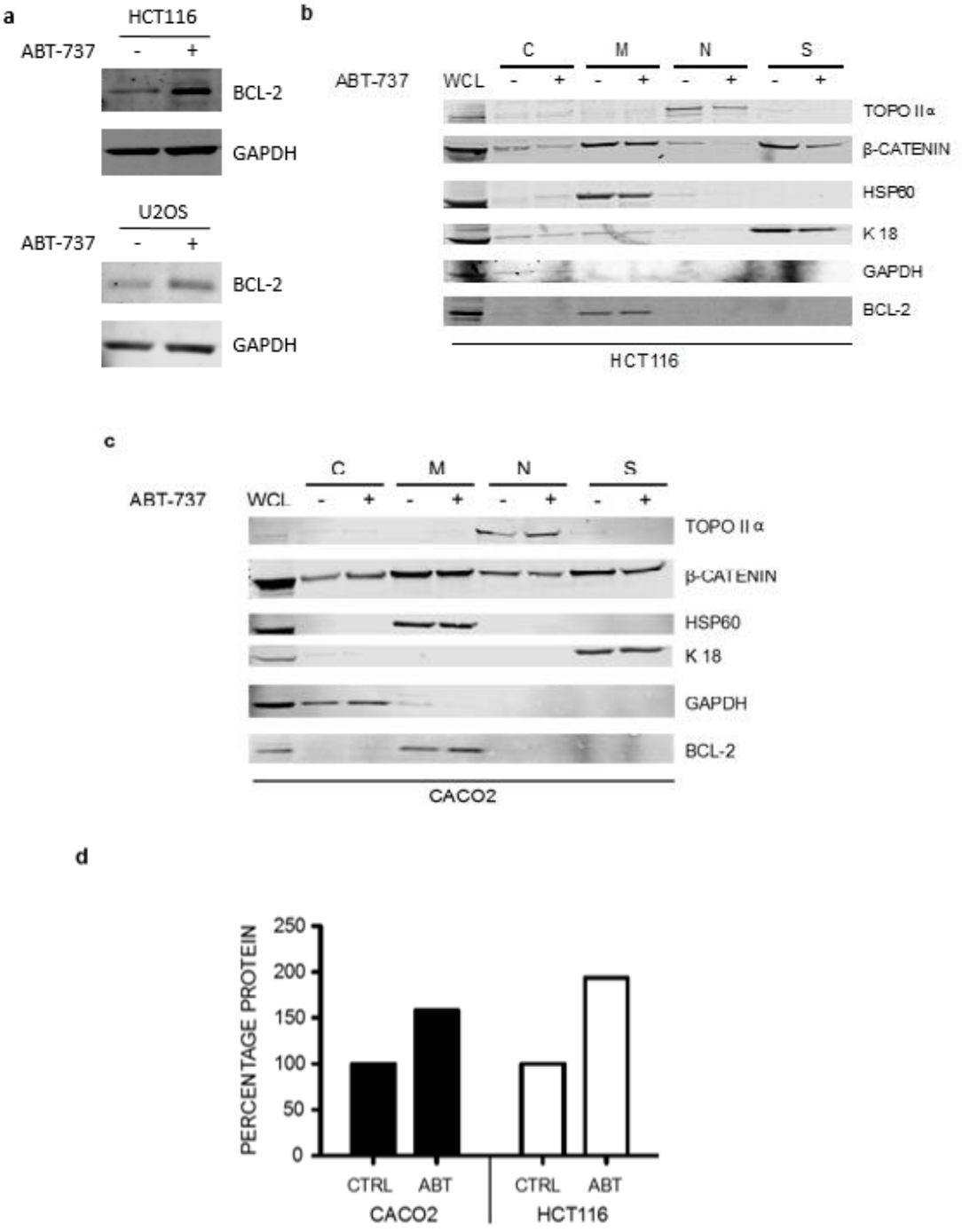

Figure 5.3. ABT-737 causes a Bcl-2 increase in the membrane fraction. (a) Western blot of whole cell lysate showing an increase in Bcl-2 after 7μM ABT-737 treatment (24h) in HCT116 cells (top panel) and U2OS cells (bottom panel). (**b**) HCT116 cells were treated plus/or minus 7μM ABT-737 for 24 hours. The proteins were then separated into cytosol (C), membrane (M), nucleus (N) and cytoskeletal (S) fractions. Fractions were subject to Western blot alongside a whole cell lysate (WCL) control to look at Bcl-2 protein levels. TopoIIα is a nuclear marker, HSP60 is a membrane marker, Keratin 18 is a cytoskeletal marker and GAPDH is a cytosolic marker. B-catenin demonstrates a good fractionation as it is present in every fraction. (**c**) CaCo2 cells were subject to Western blot after being treated and fractionated as in (b). For uncut membranes and molecular weights (a-b) see supplementary figure 8. (**d**) Quantification of Bcl-2 present in the membrane fraction of HCT116 (a) and CaCo2 (b) cells, plus/or minus ABT-737.

ABT-737 treatment (fig 5.3a). The same was true in CaCo2 (*Apc*$^{-/-}$) (fig 5.3b) and U2OS cells (supplementary figure 8). The quantification also showed that membrane-associated Bcl-2 (fig 5.3c) increased by more than 50% in CaCo2 cells and nearly doubled in HCT116 cells, upon ABT-737 treatment versus no treatment.

5.4 The ABT-737-induced Bcl-2 increase does not accumulate at mitochondria or the ER

Knowing that ABT-737 caused an increase in membrane-associated Bcl-2 prompted an investigation as to which specific membrane compartment this protein accumulated. One approach was to identify the relative abundance of Bcl-2 in the different compartments where Bcl-2 is found.

Bcl-2 is a membrane protein and uses its C-terminal transmembrane domain to insert into cellular membranes (Hockenbery *et al.,* 1990; Krajewski *et al.,* 1993; Nguyen *et al.,* 1993; Akao *et al.,* 1994). Bcl-2 is best known for its association with the mitochondrial outer membrane (MOM) (Krajewski *et al.,* 1993; Nguyen *et al.,* 1993; de Jong *et al.,* 1994). There, its function is to maintain mitochondrial membrane integrity (Vander Heiden *et al.,* 2000) and help maintain the mitochondrial membrane potential (Δψm). Therefore, it was possible that the increase in membrane-associated Bcl-2 in response to ABT-737 occurred at the mitochondrial membrane. To test this idea, protein lysates of U2OS cells treated with ABT-737 were separated into cytosolic and mitochondrial fractions. Western blots revealed that Bcl-2 in the mitochondrial fraction did not change in response to ABT-737 treatment (fig 5.4a).

Bcl-2 does not only bind to the MOM, but also to the endoplasmic reticulum (ER) at contact sites between the ER and mitochondria (Franke and Kartenbeck, 1971). These sites are now termed mitochondria associated membranes (MAM) and form bridges to join

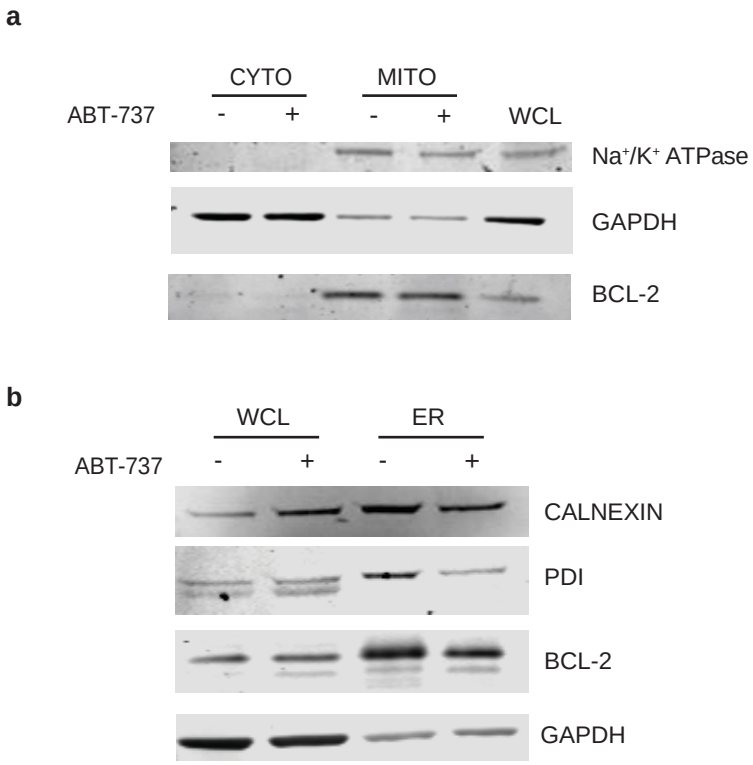

Figure 5.4. The ABT-737-induced Bcl-2 increase does not occur at mitochondrion or ER. (**a**) U2OS cells were treated plus/or minus 7μM ABT-737 for 24 hours and subsequently separated into cytosolic and mitochondrial fractions. Western blot shows Bcl-2 levels as well as the mitochondrial marker Na^+/K^+ ATPase and the cytosolic marker GAPDH. N=3, experiments are representative of biological replicates. (**b**) U2OS cells were treated as in (a). The endoplasmic reticulum was then isolated and subject to Western blot alongside a whole cell lysate (WCL) control. ER markers are Calnexin and protein disulphide isomerase (PDI). N=3, experiments are representative of 3 technical replicates.

mitochondria and the ER (Lithgow *et al.,* 1994). To test if the increase in membrane-associated Bcl-2 upon ABT-737 treatment occurred at the ER, the ER was isolated from U2OS cells after treatment with ABT-737. Then, the ER associated proteins were examined by Western blot. However, there was no increase in Bcl-2 in the ER fraction after ABT-737 treatment (fig 5.4b). Thus the membrane where Bcl-2 is enriched remained unidentified.

5.5 ABT-737 causes a stress response that mimics the effect of hypoxia on APC

One observation made throughout experiments using ABT-737 was that it caused a reduction in APC in $APC^{+/+}$ U2OS cells (fig 5.5a) and HCT116 cells (fig 5.5b), by up to 50%

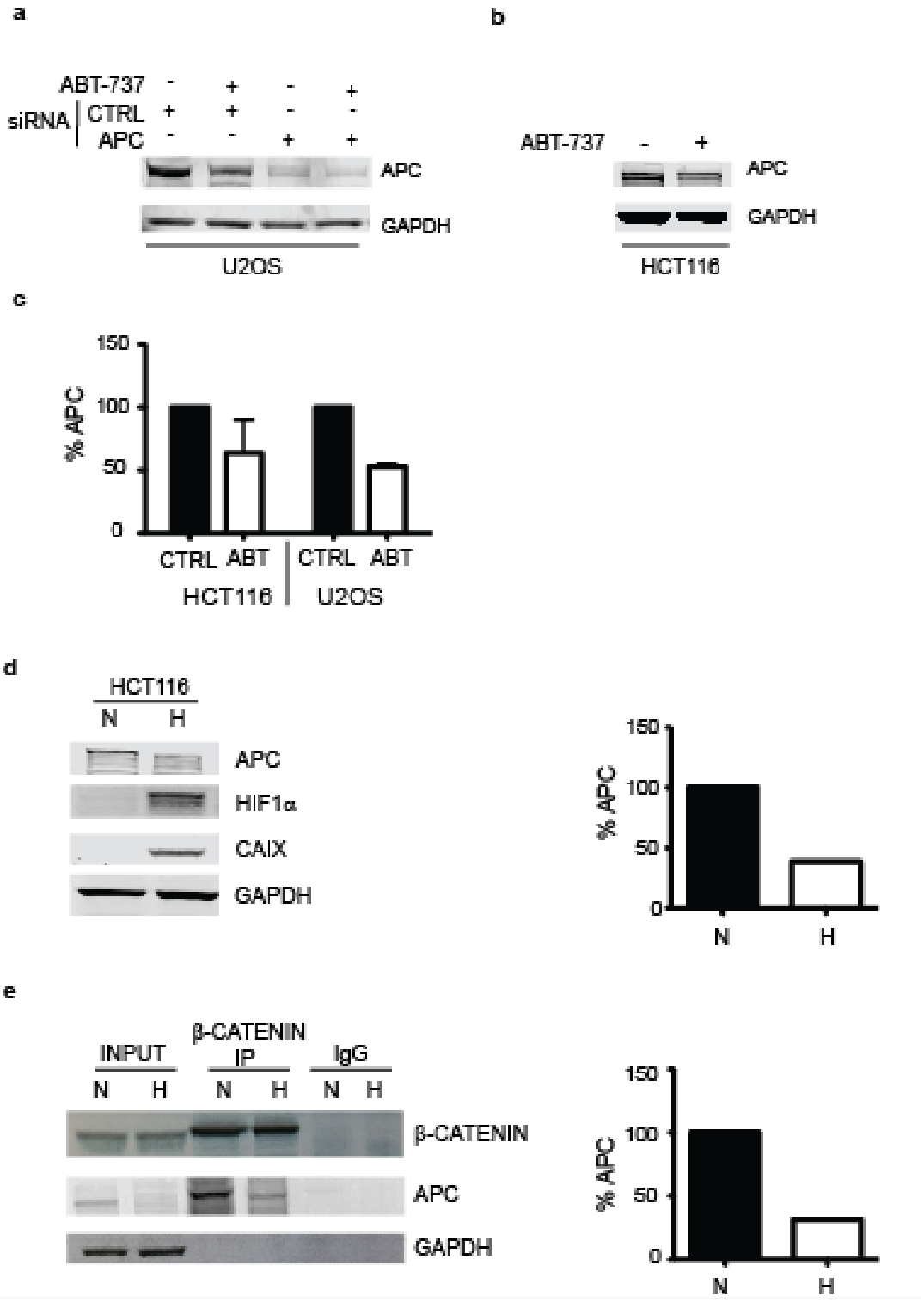

Figure 5.5. ABT-737 causes a stress response on APC similar to hypoxia. (**a**) U2OS cells were treated with ctrl or *Apc* siRNA, plus/or minus 7μM ABT-737 for 24 hours. Western blot shows a decrease in APC upon ABT-737 treatment. (**b**) HCT116 cells as treated in (a). (**c**) Quantification of APC from (a-b). (**d**) HCT116 cells were cultured in normoxia (N) or hypoxia at 1% O_2 (H) for 24 hours. Cells were lysed and subject to a Western blot (left panel) to look for APC. The hypoxia marker Hif-1α and its target gene CAIX were used as markers of hypoxia. The right panel shows the quantification of APC. (**e**) HCT116 cells were cultured as in (d). 1mg of the lysate was used to IP β-catenin and look for a β-catenin-APC CoIP (left panel). The quantification of the amount of APC bound to β-catenin (CoIP) is shown in the right panel.

(fig 5.5c). This was similar to the effect of hypoxia (Newton *et al.,* 2010). Exposing HCT116 cells to hypoxia (1% O_2) resulted in a decrease in APC (fig 5.5d left panel) by up to 50% (fig 5.5d right panel). This reduction in APC led to fewer APC-β-catenin complexes (fig 5.5e) relative to the amount of the APC (fig 5.5e right panel). This reduction in the amount of APC bound to β-catenin is predicted to result in an increase in β-catenin available for binding TCF/LEF and activation of Wnt target genes (see appendix A). Similarly, it is likely that an ABT-737-induced APC reduction could result in an increase in Wnt-target genes also. However, ABT-737 did not lead to an increase in one target gene (*Cyclin D*) looked at by qRT-PCR, in both U2OS and HCT116 cells (supplementary figure 9). More replicates and other target gene analysis is needed to conclude anything about the impact of ABT-737 on Wnt signalling. Nevertheless, treatment with ABT-737 (up to 10μM for 24 hours – analogous to my method) has been reported to alter the transcription of 430 genes by at least two-fold in PV-10 renal carcinoma cells (Song *et al.,* 2011). Unfortunately, a list of these affected genes is not available so I could not determine whether *Apc* was affected by ABT-737 in PV-10 cells.

5.6 ABT-737, Taxol® and siRNA treatment activate the unfolded protein response

When using the anti-Bcl-2 antibody for Western blot, I noticed it recognised an extra band that correlated with APC status and ABT-737 treatment (increasing). Mass spectrometry (MS) showed that this band did not represent Bcl-2 family proteins. However, it revealed many stress response proteins in that area of the gel (supplementary figure 10).

The idea that ABT-737 was a stressor because it decreased APC like hypoxia, was consistent with my finding that the ER chaperone Calnexin increased after ABT-737 treatment (fig 5.4b). This indicates ER stress, specifically activation of the unfolded protein response (UPR), a mechanism conserved across eukaryotes (see a review by Hollien, 2013). This data prompted an investigation into stress responses.

When cells experience stress, induced by extrinsic or intrinsic cues, this can lead to an accumulation of unfolded or misfolded proteins in the ER causing proteotoxicity (see a detailed review of UPR activation by Tameire *et al.,* 2015). In response to the increase in unfolded proteins cells activate the UPR to relieve the ER stress and restore proteostasis. Signal transduction during the UPR is facilitated by three main stress sensors IRE, PERK and ATF6 and leads to: pausing of the cell cycle, expansion of the ER and reduction in most *de novo* protein synthesis, except for some ER-resident proteins (e.g. Calnexin). This allows cells to cope with the ER burden (see a detailed review by Hetz, Chevet and Oakes, 2015). If a cell can resolve the ER stress it resumes the cell cycle. If the stress is irremediable then the UPR will elicit apoptosis (Zinszner *et al.,* 1998).

To determine if ABT-737 caused ER stress and activation of the UPR, levels of phospho-IRE (P-IRE), a marker of UPR activation, were measured in isolated ER fractions - taken from data in fig 5.4. In both WCL and ER samples there was a significant increase in P-IRE after ABT-737 treatment (fig 5.6a). This indicated activation of the UPR and confirmed previous data. Wroblewski *et al.,* (2013) showed activation of the UPR by ABT-737 in human melanoma cells by examining p-eIF2α levels. Next, I wanted to determine if UPR activation in response to ABT-737 was robust in other cell types and whether other treatments elicited the same response. HeLa cells were treated with an *Apc* or control siRNA together with ABT-737 and Taxol® (fig 5.6b). Then P-IRE levels were measured by Western blot. *Apc* knock-down resulted in an almost 30% increase in P-IRE relative to total IRE. Both ABT-737 and Taxol® treatment (in conjunction with mutant APC) also caused an increase. ABT-737 caused the largest increase (72%, in conjunction with control siRNA). A similar pattern of UPR activation was observed in CaCo2 CRC cells (fig 5.6c).

This data suggests that ABT-737, *Apc* loss and importantly control siRNA, all activate the UPR. Moreover, it suggests they are all stressors on the cell. However, as the control siRNA treatment elicited the same response as the *Apc* siRNA (UPR activation),

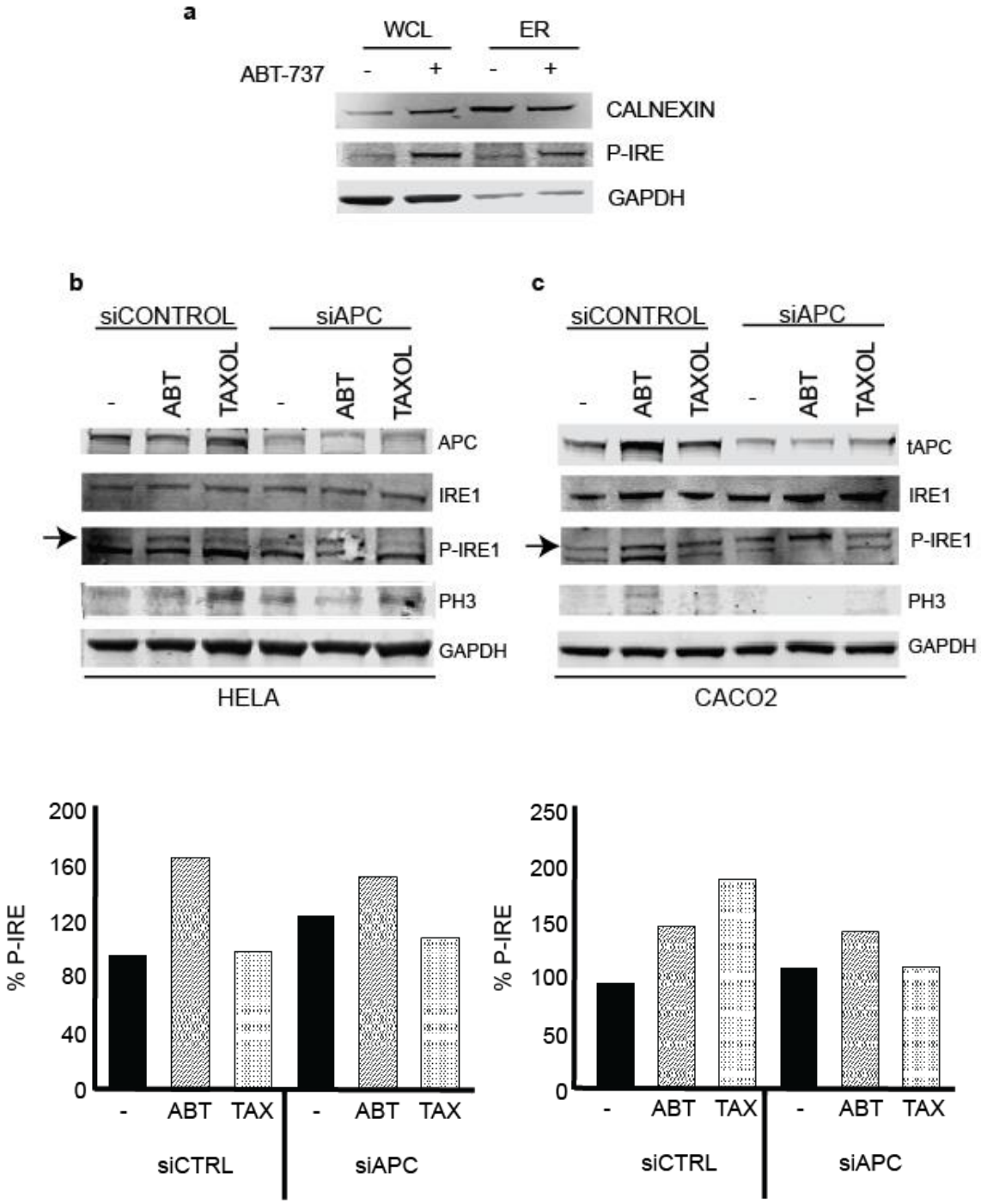

Figure 5.6. ABT-737, Taxol® and siRNA treatment activate the unfolded protein response. (**a**) The Western blot from the ER isolation (same as fig 5.4) was re-blotted with an anti-P-IRE antibody. (**b**) HeLa cells were treated with either ctrl or *Apc* siRNA in conjunction with 7μM ABT-737 or 250nM Taxol®. A Western blot then identified total and phospho-IRE levels and phospho-histone H3 (PH3) to determine if the Taxol® had efficiently arrested the cells. The bottom panel shows the quantification of P-IRE relative to total IRE levels. (**c**) CaCo2 cells treated as in (b). The bottom panel shows the P-IRE quantification relative to total IRE levels.

it is impossible to tell whether *Apc* loss activated the UPR or if it was the siRNA treatment itself. Therefore, no conclusions can be drawn about the *Apc* siRNA treatment.

5.7 *Apc* loss may activate the UPR via Hif-1α

APC has previously been linked to hypoxia, another stress-induced pathway (see 5.5 and Newton *et al.,* 2010). Specifically, APC and the hypoxia-inducible transcription factor Hif-1α have an antagonistic connection. Hypoxia represses *Apc* via a Hif-responsive element (HRE) in the *Apc* promoter. Conversely, Hif-1α depletion leads to an increase in *Apc* mRNA and protein (Newton *et al.,* 2010). The hypoxia-induced decrease in APC is likely a survival mechanism that cancer cells can exploit to promote proliferation. Important for the experiments in this thesis, Hif-1α also induces the UPR to facilitate the survival of hypoxic tumours (Bi *et al.,* 2005; Rouschop *et al.,* 2009).

Based on these links between APC and HIF-1α, it was important to establish whether activation of the UPR upon *Apc* loss was Hif-1α dependent. Therefore, P-IRE levels were measured by Western blot (fig 5.7) in U2OS cells knocked down for *Apc*, *Hif-1α* or both using siRNA. The effect of the proteasome inhibitor MG132 was also investigated to permit sufficient accumulation of the highly labile Hif-1α protein (in normoxia). Strikingly, the control siRNA again caused upregulation of phospho-IRE by 71%. This is more evidence that suggested the transfection process itself caused the cells to become stressed and activate the UPR. Therefore, any UPR effect seen in *Apc* and *Hif-1α* depleted cells may be due to the siRNA transfection procedure. Thus, no robust conclusions can be drawn from the experiment. Moreover, every cell treatment used to far has stressed the cells, resulting in UPR activation.

5.8 ABT-737, Taxol® and *Apc* loss cause no obvious change to Bcl-2 localisation

Experiments in this thesis revealed that *Apc* depletion leads to an increase in Bcl-2 (fig 5.1) and that ABT-737 caused an increase in membrane-associated Bcl-2 (fig 5.3). To

characterise these changes in more detail and identify the membrane compartment where the Bcl-2 protein accumulated, immunofluorescence (IF) was used. I specifically focused on mitochondria using MitoTracker® because: Bcl-2 binds the MOM; and ABT-737 activates the intrinsic/mitochondrial apoptotic pathway by inhibiting the formation of Bcl-2-Bax dimers. Therefore, any morphological changes of mitochondria in response to *Apc* depletion or ABT-737 treatment was investigated.

None of the anti-Bcl-2 antibodies allowed detection of endogenous Bcl-2 by IF, so cells were transfected with pGFP-Bcl-2 and its distribution examined by IF. Mitochondria were revealed well and GFP-Bcl-2 also appeared to localise to the ER (fig 5.8a). To confirm that GFP-Bcl-2 was indeed localised to the ER, cells were co-stained with an antibody against the ER marker Calnexin. The distribution of GFP-Bcl-2 and Calnexin overlapped (fig 5.8b), which suggested that Bcl-2 was mostly associated with the ER/mitochondria associated membranes/mitochondria. A vehicle control produced no obvious change to its localisation or mitochondria (fig 5.8b bottom panels). Treatment with *Apc* siRNA, Taxol® or ABT-737 resulted in no obvious change in the intensity or localisation of GFP-Bcl-2 (data not shown). However, these treatments produced a change in mitochondria.

5.9 ABT-737, Taxol® and *Apc* loss cause a change in mitochondria indicative of cellular stress

From the IF experiments in fig 5.8 and fig 5.9, changes in mitochondrial location were observed. ABT-737, Taxol® and both control and *Apc* siRNA treatments caused a pronounced retraction of mitochondria from the cell periphery. Instead mitochondria were concentrated around nuclei (fig 5.8c) and this peri-nuclear clustering was often asymmetric. The changes in mitochondria in control siRNA treated cells (fig 5.8) together with previous data (fig 5.6) provide further evidence to the idea that the transfection procedure itself

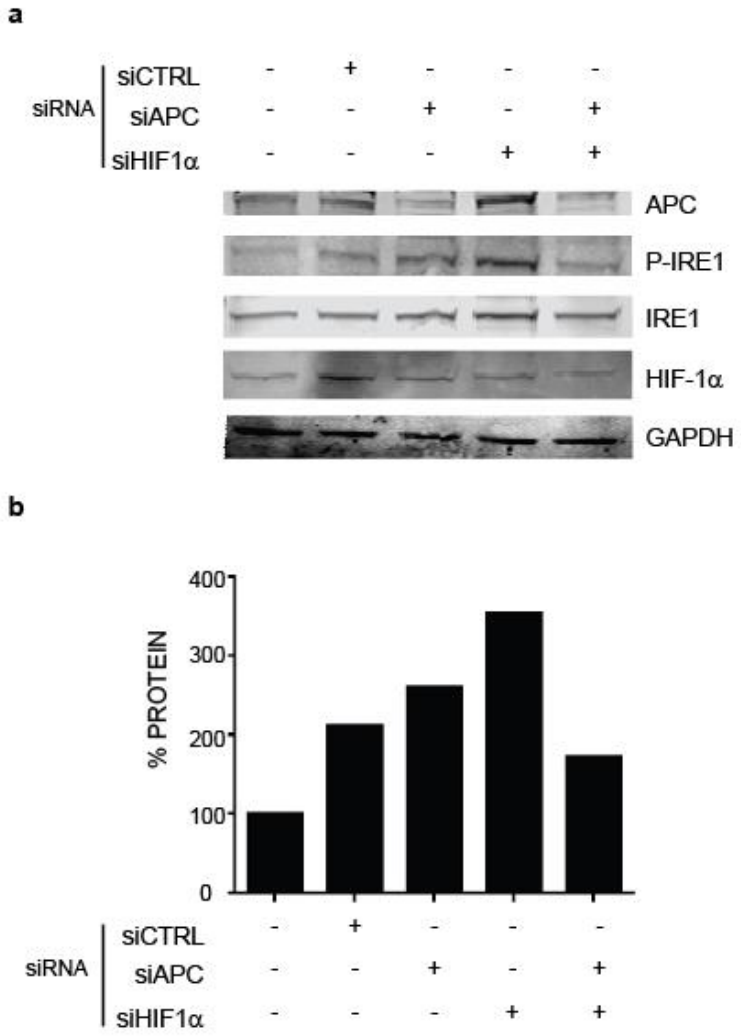

Figure 5.7. *Apc* loss may activate the UPR via stress-activated Hif-1α. (**a**) U2OS cells were treated with 10μM MG132 and either ctrl, *Apc* and/or *Hif-1α* siRNA. A Western blot then shows APC, Hif-1α and P-IRE protein levels. (**b**) Quantification of P-IRE from (a) relative to total-IRE.

causes cellular stress. It is therefore difficult to deduce anything about specific effects on the localisation of mitochondria in response to siAPC, as the phenotype may be a result of stress from the transfection procedure. However, all cellular treatments used caused activation of the UPR (stressors) and subsequently all change the distribution of mitochondria. The stress could result in a change in the distribution of mitochondria, so mitochondrial location could be a read out for ER stress. In fact, two known stressors, oxidative stress and hypoxia, have previously been reported to cause peri-nuclear

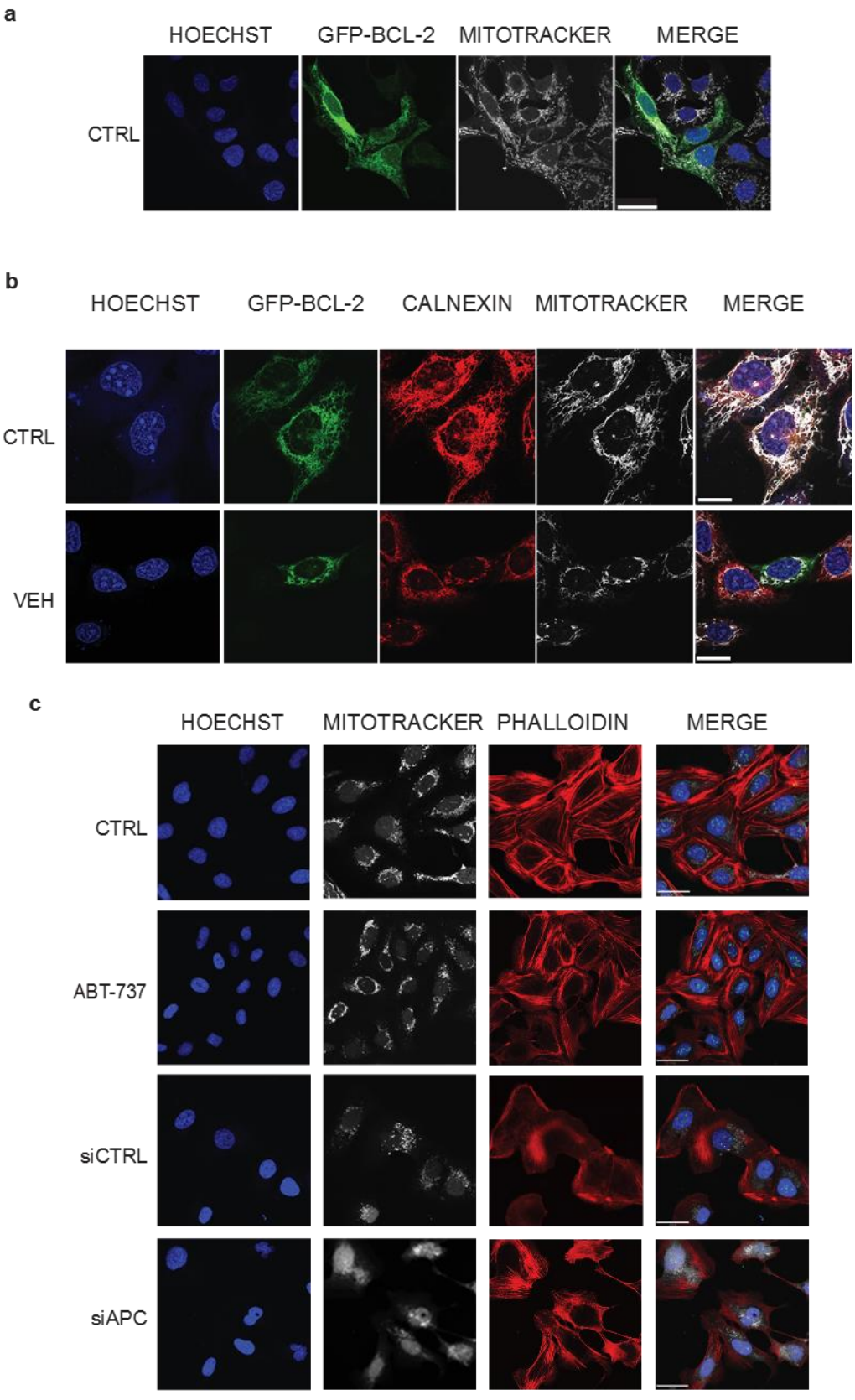
a
HOECHST
GFP-BCL-2
MITOTRACKER
MERGE
CTRL
b
HOECHST
GFP-BCL-2
CALNEXIN
MITOTRACKER
MERGE
CTRL
VEH
c
HOECHST
MITOTRACKER
PHALLOIDIN
MERGE
CTRL
ABT-737
siCTRL
siAPC

Figure 5.8. ABT-737, Taxol® and *Apc* loss cause no obvious changes to Bcl-2 localisation by IF. (**a**) U2OS cells were transfected with pGFP-Bcl-2. 48 hours post-transfected the cells were incubated with MitoTracker® for 45 minutes before being fixed and counterstained with Hoechst. GFP-Bcl-2 and MitoTracker® were detected using fluorescence microscopy. The scale bar represents 37µm. (**b**) Untreated (ctrl) and vehicle treated U2OS cells were transfected and treated as in (a). The cells were fixed and stained with an anti-Calnexin antibody and then counterstained with Hoechst. The scale bar represents 9 (ctrl) and 37µm (veh). (**c**) Untreated (ctrl) U2OS cells, or cells treated with 7µM ABT-737 (24 hours), 250nM Taxol® (6 hours) or *Apc* siRNA (48 hours) were cultured with MitoTracker® as in (a). Cells were then fixed and counterstained with Hoechst and phalloidin. The scale bar represents 37µm except siCTRL, which is 34µm.

clustering (Hallmann *et al.,* 2004; Swiger *et al.,* 2008; Al-Mehdi *et al.,* 2012). Hence, drug-induced and transfection-induced stress affecting mitochondria is plausible.

Further experiments focused on mitochondrial morphology as this can indicate their state. There are three main observable mitochondrial shapes. Normally, mitochondria appear as either individual organelles or extended filamentous structures, closely associated with the ER and they extend outwards from a perinuclear region (Johnson *et al.,* 1980). Mitochondria can also appear globular, when swollen. Interestingly, ABT-737 treated and *Apc* depleted cells, showed a lack of filamentous mitochondria. Importantly, only *Apc* depleted cells had mitochondria resembling large, globular structures akin to swollen mitochondria. This suggests that something in *Apc* depleted cells is different from other stressors (control siRNA, Taxol® and ABT-737), resulting in mitochondrial swelling - which warranted further investigation.

To further explore the effect of *Apc* loss on mitochondria, live imaging was performed on U2OS cells treated with MitoTracker®. Cells with and without *Apc* were compared (fig 5.9). As before, in untreated (ctrl) cells, filamentous mitochondria are clearly visible (fig 5.9a). Again *Apc* depleted cells contained swollen mitochondria, concentrated in a peri-nuclear region.

Swollen mitochondria as a result of *Apc* loss may be a direct consequence of the Bcl-2 increase seen upon *Apc* knock-down (fig 5.1). Bcl-2 binds the mitochondrial outer membrane (MOM), where it has been shown to have *in vitro* channel activity (Schendel *et al.,* 1997). Bcl-2 may act specifically as a weak K^+ ion channel (Schlesinger *et al.,* 1997). Based on these findings, an increase in Bcl-2 could lead to an increase in mitochondrial ion channels on the MOM causing an influx of ions and water. This causes swelling of the inner mitochondrial matrix and distention of the inner and outer mitochondrial membranes. The result would be the swollen mitochondria seen by IF upon *Apc* knock-down. However, this theory is unlikely as ABT-737 treated cells also have increased Bcl-2 but show no swollen mitochondria. Alternatively, the swollen mitochondria may be unrelated to Bcl-2 levels and caused by some other consequence of *Apc* loss.

To summarise the mitochondrial data so far, all cell treatments (control and *Apc* siRNA. Taxol® and ABT-737) caused peri-nuclear clustering of mitochondria, which was often asymmetric. Additionally, all cell treatments were stressors on the cell resulting in UPR activation. Therefore, mitochondrial translocation may be a read out for cellular stress. However, only *Apc* siRNA caused a morphological change from filamentous to swollen mitochondria,

5.10 ABT-737, Taxol® and *Apc* loss do not affect mitochondrial functionality

Next, to establish if mitochondria in ABT-737 treated cells (retracted to a perinuclear region) were still functional, the cationic dye JC-1 was used. The monomeric form is taken up by all mitochondria, but it aggregates only in mitochondria with an active membrane potential ($\Delta\psi m$). Therefore, mitochondria with depolarised membranes (i.e. compromised function) show fewer aggregates. As JC-1 cannot be visualised in fixed cells, cells were treated plus/or minus ABT-737 and live cell microscopy performed. As before (figs 5.8 and 5.9a) ABT-737 treatment resulted in mitochondria accumulating in a peri-nuclear region, usually

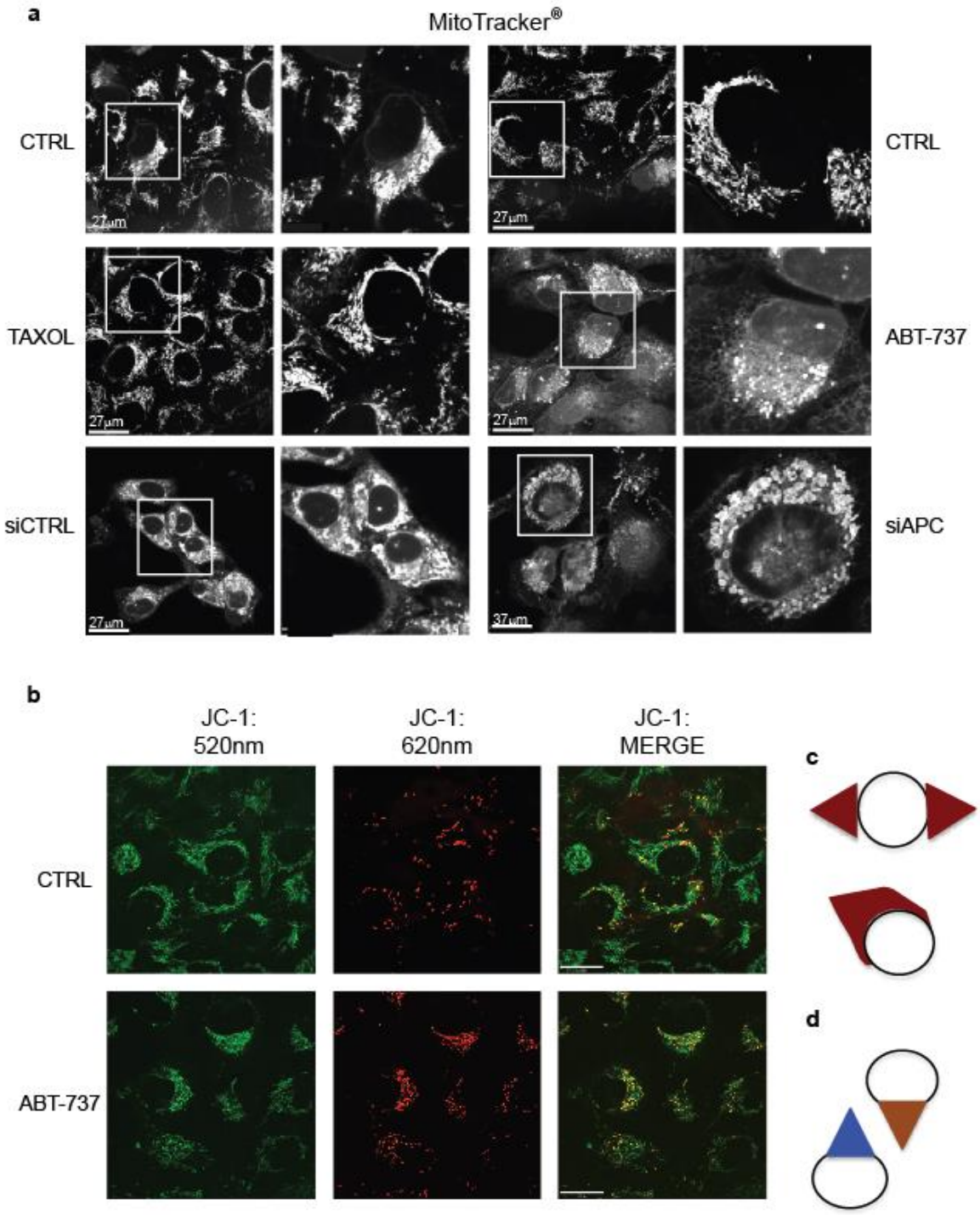

Figure 5.9. ABT-737, Taxol® and *Apc* loss cause a change in mitochondria indicative of cellular stress. (**a**) U2OS cells were treated with either control or *Apc* siRNAs for 48 hours, 250nM Taxol® for 6 hours, 7µM ABT-737 for 24 hours or untreated. Cells were then incubated with MitoTracker® for 45 minutes before live imaging was performed to identify mitochondria. The white box in the left hand panel represents the area magnified in the right hand panel. The scale bar represents 27µm, except siAPC whose scale bar represents 22µm. (**b**) U2OS cells were treated plus/or minus 7µM ABT-737 for 24 hours and then incubated with JC-1. JC-1 monomers are shown in the green channel and aggregates in the red channel. The scale bar represents 27µm. (**c**) Schematic representing the spread of mitochondria in untreated U2OS cells. (**d**) Schematic representing the altered distribution of mitochondria in ABT-737 treated U2OS cells.

asymmetric. This is shown schematically in fig 5.9c-d. Surprisingly, the JC-1 was still aggregating in mitochondria of ABT-737 treated cells. This suggested that they maintained a 'normal' membrane potential and were functioning normally. This suggested that ABT-737 induced a change in the localisation of mitochondria, but not the functionality; mitochondria still had active membrane potentials. ABT-737 also affected mitochondrial morphology as there are far fewer filamentous mitochondria after treatment. Due to the non-uniform uptake of JC-1, quantitative data could not be produced. This lead to the use of other experimental techniques to achieve quantitative results.

5.11 *Apc* loss and ABT-737 treatment have opposing effects on mitochondria

The IF data suggested a change in mitochondrial morphology from filamentous to globular structures in *Apc* depleted cells. It also showed less filamentous mitochondria in ABT-737 treated cells. To establish whether these structural changes reflected mitochondrial fusion or lack of fission, Imaris (Bitplane) was used to measure the number of mitochondria present in cells. Cell size was also measured to establish whether it was affected by either treatment, to compare the number of mitochondria per cell. There was a positive correlation between cell size and mitochondrial number (fig 5.10a) as previously observed in budding yeast (Rafelski *et al.,* 2012). Cells treated with either ABT-737 or *Apc* siRNA were smaller and had fewer mitochondria. The same was true for cells transfected with pGFP-Bcl-2 (supplementary figure 11). These transfected cells were smaller in area (μm^2) and had fewer mitochondria, in comparison to untreated cells. Therefore, all three treatments caused a decrease in cell size and a corresponding (proportional) reduction in mitochondria. This could be another function of stress in the cell; to reduce cell size.

Calculating the ratio of mitochondria per unit space revealed that the number of mitochondria per μm^2 was similar in all cases (fig 5.10b). This is consistent with the idea that the concentration of mitochondria in cells is relatively constant but does not reveal any effect of APC or ABT-737 on this parameter. A reduction in mitochondria is often due to

mitophagy, the destruction of mitochondria by autophagy (Kim, Rodriguez-Enriquez and Lemasters, 2007). This usually happens when mitochondria are defective, damaged or stressed (Gilkerson *et al.,* 2012). An increase in mitochondrial number can de due to increased mtDNA production in response to oxidative stress, but this is poorly understood (Lee *et al.,* 2000). Therefore, the lack of a change in mitochondrial number indicates that the mitochondria themselves are not stressed or defective when treated with *Apc* siRNA, ABT-737 or pGFP-Bcl-2. Thus, although the position of mitochondria in the cell moved away from the cell periphery, the number remains largely unchanged. Together with the JC-1 staining (fig 5.9) this suggests, that mitochondria are not stressed and functioned normally.

To measure more subtle changes in mitochondrial function in *Apc* depleted, ABT-737 and Taxol® treated cells, flow activated cell sorting (FACS) was used. CMXRos was used to measure changes in mitochondrial membrane potential (MMP), which relates to the MMP-independent dye MitoTracker® Green (to measure differences in the number of mitochondria). In cells lacking *Apc*, the mitochondria:MMP ratio shifted to the right (fig 5.10c). This suggested that mitochondria have a decreased MMP. This was in opposition to what was expected based on biochemical data showing that siAPC cells have more Bcl-2 - which maintains MMP (fig 5.1). Conversely, the mitochondria:MMP ratio decreased in ABT-737 treated cells and suggested a slight increase in MMP. This indicates that the mitochondria were 'healthier' than siAPC cells. However, these changes are minor and only trends can be reported at this time.

To summarise the data, control siRNA, Taxol®, ABT-737 and *Apc* depletion all caused activation of the UPR, as measured by P-IRE (fig 5.6). Equally, all cell treatments caused a translocation of mitochondria to a peri-nuclear region, which did not affect mitochondrial function (figs 5.8 and 5.9). Together, this data suggested that stressed cells cluster their mitochondria around the nucleus. However, only *Apc* loss had a measurable effect on

mitochondria, causing mitochondrial swelling (fig 5.8 and 5.9) and decreased mitochondrial function (fig 5.10c).

5.12 Combining Taxol® and ABT-737 treatment kills *Apc*$^{Min/Min}$ organoids more efficiently

Next, I wanted to confirm previous data from 2D cell culture in intestinal organoids (a 3D system representative of *Apc* depleted CRC cells). Comparing the response of these organoids to Taxol® and ABT-737 treatment could show whether lack of full length APC rendered three dimensional epithelial structures (resembling intestinal) tissue, more sensitive to these agents.

Intestinal organoids with wild-type *Apc* (*Apc*$^{+/+}$, APC WT) or mutant Apc (*Apc*$^{Min/Min}$ cysts) mimicking *Apc* loss (see table 8) were used. Firstly, the viability of organoids was measured 24 hours after treatment with increasing concentrations of Taxol® (fig 5.11a). *Apc* deficient cells do not arrest efficiently in response to Taxol® (Dikovskaya *et al.,* 2007; Radulescu *et al.,* 2010). Therefore, I expected cells in *Apc* WT organoids to arrest in mitosis and eventually apoptose. Whereas, I expected cells in the *Apc*$^{Min/Min}$ cysts not to arrest and to die less readily, similar to *Apc* deficient cells. Indeed, *Apc* mutant cysts were largely unaffected by Taxol®, even at doses up to 1µM. Whereas, the viability of *Apc* WT organoids decreased to 63% upon treatment with 500nM Taxol®. Previous data in the lab had already shown that ABT-737 reduced the viability of *Apc* WT organoids at a dose of 1µM, but 10µM ABT-737 was required to affect *Apc*$^{Min/Min}$ cysts (data not shown). Therefore, the *Apc*–deficient cysts required higher doses of ABT-737 to reduce viability, but were largely unaffected by high doses of Taxol®. Previous data in the lab also suggested that treating *Apc* depleted cultured cells with ABT-737 increased their sensitivity to Taxol®. Therefore, it was important to test whether the same is true for organoids, which represent a more physiological situation than cultured cells. I also aimed to investigate the effects of these compounds on the morphology of these 3D structures.

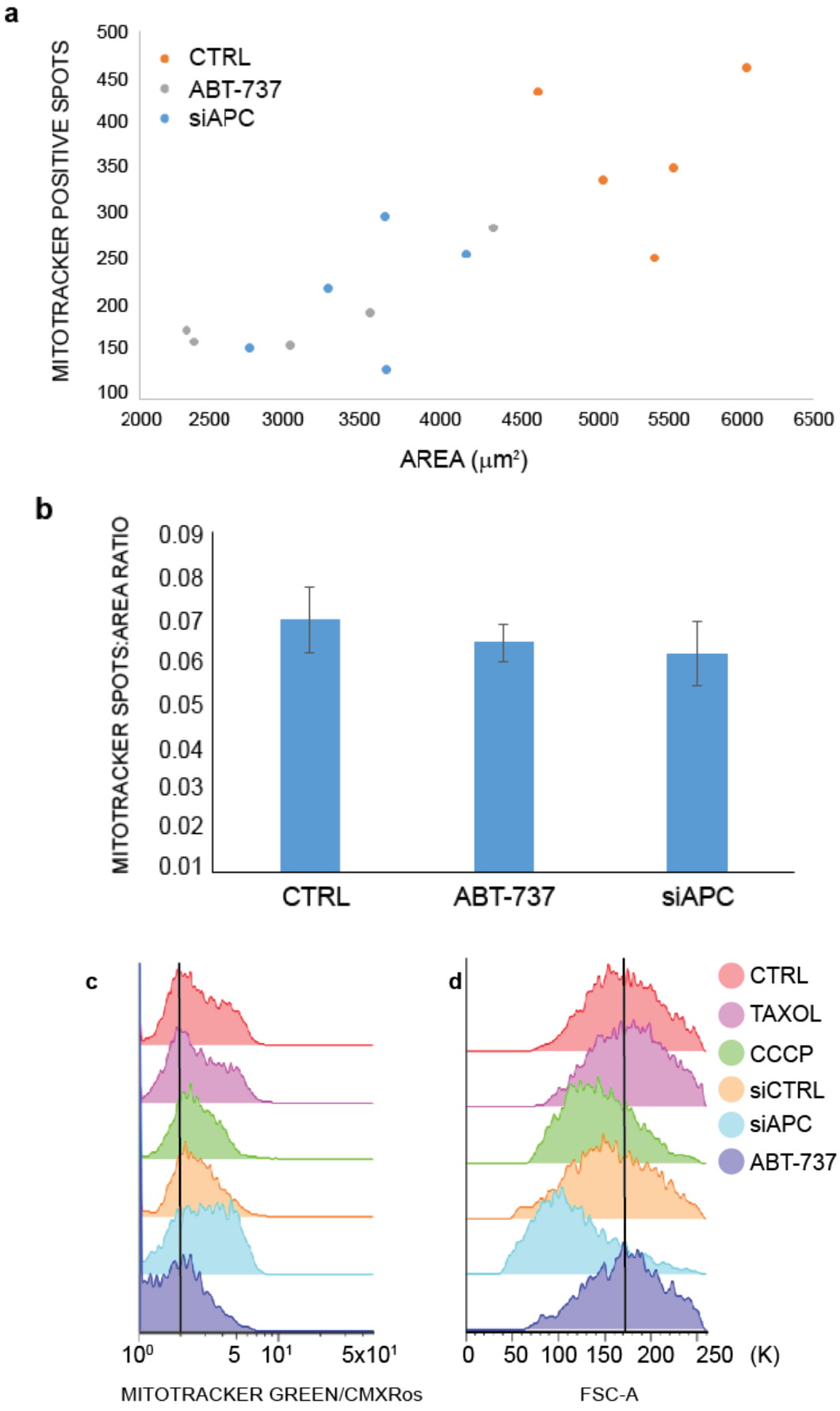
a
MITOTRACKER POSITIVE SPOTS
500
450
400
350
300
250
200
150
100
CTRL
ABT-737
siAPC
2000
2500
3000
3500
4000
4500
5000
5500
6000
6500
AREA (μm²)
b
MITOTRACKER SPOTS:AREA RATIO
0.09
0.08
0.07
0.06
0.05
0.04
0.03
0.02
0.01
CTRL
ABT-737
siAPC
c
10⁰
5
10¹
5x10¹
MITOTRACKER GREEN/CMXRos
d
0
50
100
150
200
250
(K)
FSC-A
CTRL
TAXOL
CCCP
siCTRL
siAPC
ABT-737

Figure 5.10. *Apc* loss and ABT-737 treatment have opposing effects on mitochondria. (**a**) U2OS cells were treated with 7μM ABT-737 for 24 hours, *Apc* siRNA for 48 hours, or untreated (ctrl). The cells were then cultured with MitoTracker® for 45 minutes. Mitochondria were visualised using fluorescent microscopy. Images were then imported into the microscopy software Imaris. Using fluorescence detection the number of MitoTracker®-positive spots was counted and the area of the cells were measured. 5 cells were analysed per treatment. There is a positive correlation between cell size and mitochondrial number. (**b**) The number of mitochondria were divided by the area of the cell to give a ratio of MitoTracker® positive spots: area. The bar graph shows that there is no difference in number of mitochondria per area between treatments. Error bars represent the standard error, n=5 cells. (**c**) U2OS cells were treated as indicated, incubated with MitoTracker® Green and CMXRos, prepared for FACS and counterstained with DAPI. *Apc*–depleted cells have a higher ratio of mitochondria: MMP meaning that there are less mitochondria with active MMPs. (**d**) U2OS cells treated as in (c). *Apc*–depleted cells are smaller in size based on FSC.

Organoids were cultured in Taxol®, ABT-737 or both (ABTTAX) for 48 hours and images recorded every 30 minutes. As expected, Taxol® arrested cells in organoids with WT *Apc*, but not those with Apc^{Min}. This arrest was established visually by a halt in organoid growth and the rounding-up of cells. ABT-737 had no visible effect on the growth of WT organoids, although it appeared to retard the growth of Apc^{Min} cysts. Combining both drugs (ABTTAX) killed cysts, indicated by the appearance of many dead cells within one-two hours, no further growth, and partial shrinking of the organoid. The effect of ABTTAX on *Apc* WT organoids was less severe. The organoids appeared to be arrested as indicated by a halt in growth, with partial cell death. These observations suggest that although there was no visible effect of ABT-737 alone, it rendered $Apc^{Min/Min}$ cells more sensitive to Taxol®, just as it did in 2D cell culture models (data not shown). Note that in fig 5.11b the 0h time point should read 45mins – the time taken to treat all organoids and set up plate on the microscope. This accounts for the cell death at the first timepoint in ABTTAX treated organoids.

Based on UPR data (fig 5.6), I hypothesised that $Apc^{Min/Min}$ intestinal organoids have increased P-IRE, similar to *Apc* mutant CaCo2 cells due to UPR activation. This could make $Apc^{Min/Min}$ organoids more sensitive to the combination of Taxol® and ABT-737, similar to *Apc* mutant CRC cells (fig 5.6 and unpublished data). Unfortunately, due to time constraints P-IRE in the organoids was not measured.

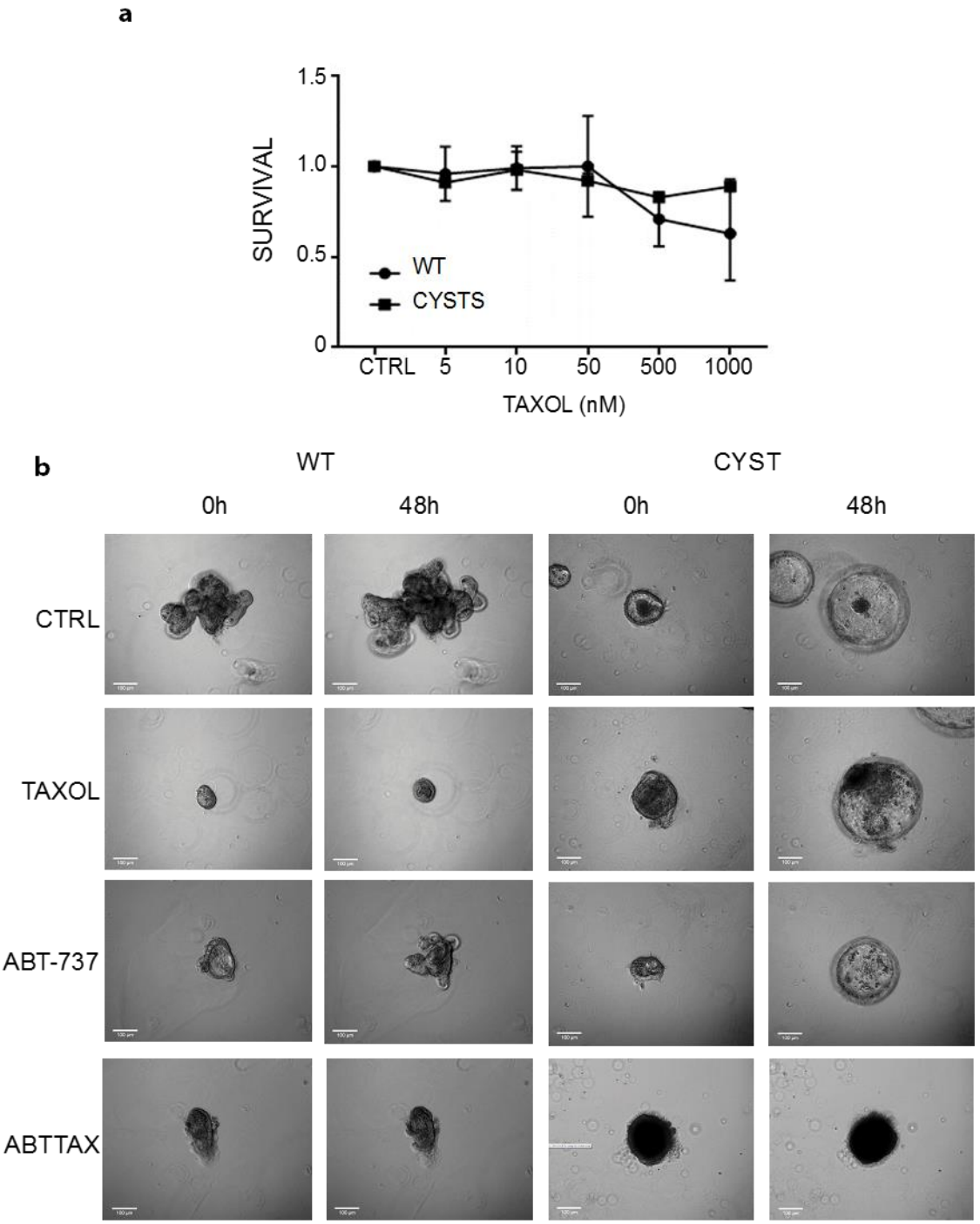

Figure 5.11. ABT-737 and Taxol® affect *Apc* WT and *Apc*^{Min} intestinal organoids differently. (**a**) Viability of *Apc* WT organoids and cysts (*Apc*$^{Min/Min}$) after treatments with varying doses of Taxol® for 24 hours. N=3, experiments representative of biological replicates, error bars represent the standard error. (**b**) *Apc* WT organoids and *Apc* mutant cysts were treated with 250nM Taxol®, 7µM ABT-737 or both (ABTTAX) as indicated. Organoids were cultured for 48 hours. Images taken from 48 hour videos are shown before filming commenced, immediately after drug addition (0h) and after 48 hours.

5.13 Conclusions

In summary, *Apc* deficient cells are not as readily killed by Taxol® as *Apc* WT cells, likely because their cell cycle arrest checkpoint is compromised (Dikovskaya *et al.,* 2007). In addition, they may be protected from death by an increase in Bcl-2. This protection can be overcome by combined treatment with the Bcl-2 inhibitor ABT-737. A possible mechanism is the activation of the unfolded protein response by control and *Apc* siRNA, Taxol® and ABT-737. This stress is reflected by a change in mitochondrial distribution. However, only *Apc* deficient cells had swollen mitochondria. Based on these findings, in $Apc^{Min/Min}$ cysts the UPR is expected to be activated, the mitochondria distributed closer to the nucleus, with a swollen appearance. In addition, cells in $Apc^{Min/Min}$ cysts are expected to contain higher amounts of Bcl-2 than those in wild type organoids. These changes could explain the increased sensitivity of cysts to the combination of Taxol® and ABT-737. These results warrant further examination to find mechanisms behind mitochondrial changes as well as a link to the UPR. Moreover, further work would determine if this combined therapy of ABT-737 and Taxol® is clinically useful in treating CRC.

Chapter 6 - Discussion

6.1 Off-target effects associated with the AID system

The AID system was able to partially degrade APC in 1 hour using 500μM auxin. However, when attempting to increase the effectiveness of the system (i.e. obtaining a greater/total APC depletion) off-target effects were observed in the control cell population DT40^{TIR}. The control DT40^{TIR} cells contain only the F-box protein TIR and do not have a degron motif. This suggests that the AID system has off-target effects in these cells. There are a number of possible explanations for these observations.

Ubiquitin-mediated protein degradation is irreversible and consequently is used in cellular processes that must proceed uni-directionally, such as the cell cycle and circadian rhythm. In fact, more than 80% of proteins are degraded by ubiquitin–mediated, 26S proteasomal degradation (Yen *et al.,* 2008) making substrate specificity crucial. The purpose of F-box proteins is to provide substrate specificity to E3 ligases by recognising short degradation motifs in substrates, termed degrons. SCF complexes are assembled by Cullin scaffold proteins. The Cullin carboxy terminus binds to the RING protein RBX1 that recruits the E2 ligase (fig 6.1). The amino terminal of the Cullin binds Skp1 and an F-box protein (see a detailed review by Skaar, Pagan and Pagano, 2013).

It is possible that in the AID system, the TIR protein from *Oryza sativa* (OsTIR1) may recognise a sequence in APC that acts as a degron and thus targets APC to the SCF^{TIR}, in the presence of auxin. Such a putative sequence would likely be hydrophobic, as the TIR binds IAA17 through hydrophobic interactions (Tan *et al.,* 2007). There are 69 known F-box proteins in humans. Most of these can recognise multiple substrates, usually through canonical phosphodegrons.

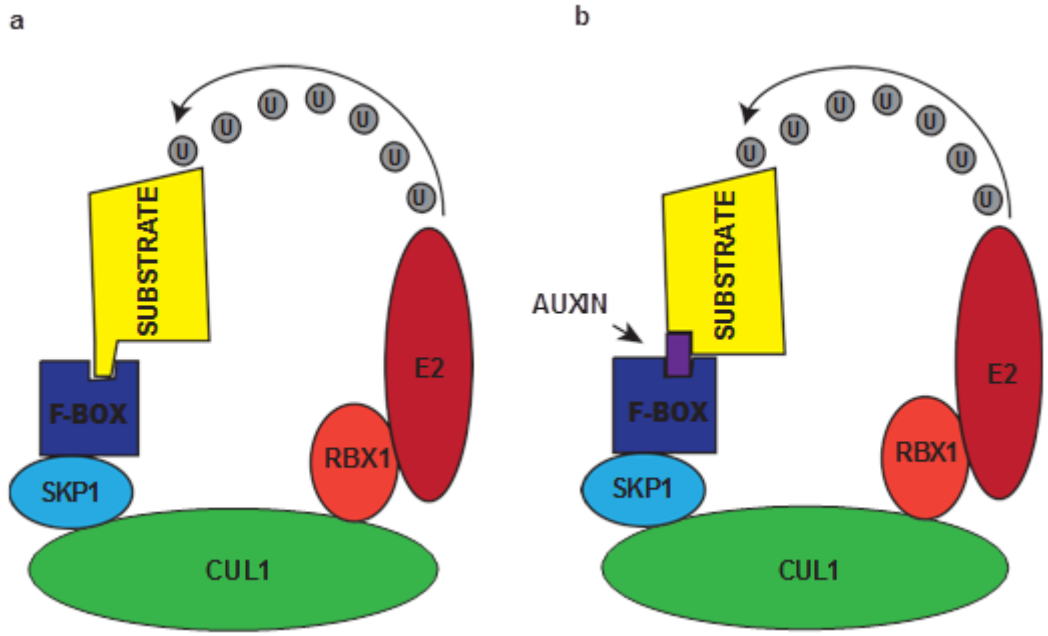

Fig 6.1. SCF complexes with and without the requirement of a cofactor. (**a**) Typical F-box-substrate recognition by a canonical degron that has been post-translationally modified, i.e. a phosphodegron. The scaffold protein Cullin1 (CUL1) binds RBX1 at its carboxy terminus, which in turn binds an E2 ubiquitin ligase. The amino terminal of CUL1 binds to the adapter protein SKP1, linking the Cullin to the F-box protein. SKP1 binds the F-box protein, which also binds to a substrate that is specific to that F-box protein, typically by recognizing a phosphodegron motif within the substrate. The E2 ligase then polyubiquitinates the substrate, targeting it for proteasomal degradation. (**b**) Inducible degron recognition by an F-box protein. CUL1 binds the same set of proteins as in (a). The F-box protein, in this case TIR, can only bind the substrate in the presence of auxin. Auxin binds to both the TIR F-box protein and the substrates' degron motif, bringing the substrate into the SCF^{TIR} complex in order to be polyubiquitinated.

For example, the F-box protein β-TrCP (encoded by both *FBXW1* and *FBWX11*) recognises the phosphorylated consensus motif DSGXXS (Hart *et al.,* 1999), with both Serine residues phosphorylated (i.e. a phosphodegron). However there are several post-translational modifications F-box proteins use to detect a degron, other than phosphorylation: glycosylation (Yoshida *et al.,* 2002) and methylation (Lee *at al.,* 2012). Even some unmodified degron motifs can act as substrates (D'Angiodella *et al.,* 2010).

These alternative degron motifs could explain why APC is degraded in cells containing SCF^{TIR} E3 ubiquitin ligase complexes even when it does not have a degron (IAA17) motif.

However, I could not find any canonical phosphodegron motifs in the *Gallus gallus* APC protein sequence. Nonetheless, an exact match to a consensus degron motif is not always necessary for substrate recognition by an F-box protein (Nash *et al.,* 2001). In summary, although only one degron motif (IAA17) has been identified thus far, it is possible that the TIR protein can recognise multiple degron motifs and that APC contains one of these, as yet unrecognised, motifs.

The LRR (leucine-rich-repeat) domain of the TIR protein is responsible for auxin binding (Tan *et al.,* 2007). It provides a structural framework for protein-protein interactions (Kobe and Kajave, 2001). APC contains many phosphorylation sites as well as sites for acetylation and methylation (fig 6.2). It is possible that certain post-translational modifications of APC act as non-canonical degron motifs and are recognised by auxin, bound to the TIR-LRR. This could lead to the degradation of APC in DT40^{TIR} cells (treated with auxin). A bioinformatics approach could identify potential non-canonical degrons in APC. This would involve comparing the APC protein sequence (plus/minus post-translational modifications) against all known degron motifs and post-translational modifications. However, there are other possible explanations for the degradation of APC in DT40^{TIR} cells in the presence of auxin, discussed below.

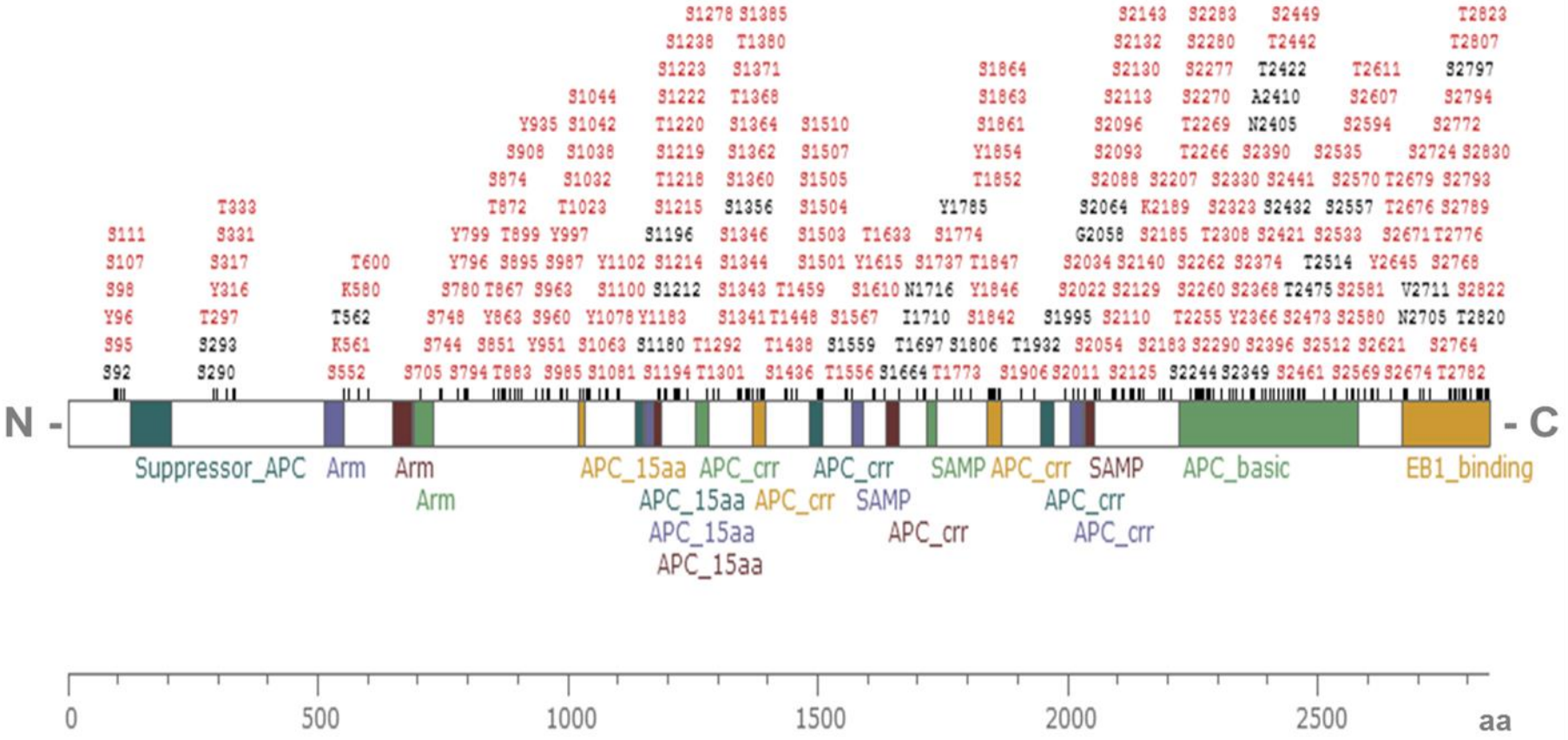

Fig 6.2. Sites of APC post-translational modification. Image taken from a search in www.phosphositeplus.org and modified. The scale represents amino acids 1-2843 of APC.

The AID system utilises an inducible degron mechanism and relies on the phytohormone auxin to stabilise a link between the TIR F-box protein and IAA17 (Tan *et al.,* 2007). TIR and IAA17 have low binding affinity in the absence of auxin, but nonetheless a low level of interaction can occur without auxin (Tan *et al.,* 2007). This may explain a very slight reduction in APC in control cells treated with auxin. However, the AID system may also require a co-factor other than auxin to function fully; the TIR protein incorporates the small molecule inositol hexakisphosphate ($InsP_6$, also known as phytate). Phytate acts as a structural cofactor supporting a key arginine residue (arg403) in the TIR, maintaining the integrity of the auxin-binding pocket (Tan *et al.,* 2007). DT40 cells possess phytate and are in fact used as a model system for studying inositol trisphostate receptor (IP_3R) signalling (Vazquez *et al.,* 2002). Perhaps, DT40 cells possess a high level of phytate or a different structural isoform, which can enhance the SCF^{TIR}-mediated degradation of proteins such as APC, in the absence of a degron (fig 6.3a-b). Additionally, Phytate has already been identified as an allosteric regulator of the Vibrio cholerae RTX toxin in eukaryotic cells (Lupardus *et al.,* 2008). Therefore, it is possible that phytate acts as an allosteric regulator of other proteins, such as TIR. This would explain my data - the degradation of a substrate lacking a degron motif (fig 6.3c). Alternatively, phytate is highly charged and a high concentration of phytate may change the charge of the TIR binding pocket. This could bring it into closer proximity with certain residues within APC, enabling APC to be targeted for degradation by the SCF^{TIR} - in the presence of auxin and without a degron motif. Structural modelling of the TIR binding pocket plus/minus phytate and plus/minus auxin could reveal such a possible conformational change/change in the charge of the binding pocket. This could show if the SCF^{TIR} can degrade APC in the absence of an IAA17 degron motif.

6.2 Modifying 5' regions of *Apc* affects APC protein expression

After transfecting DT40^{TIR} with both, pGFP-IAA17-APC or pIAA17-APC (for maps see supplementary figure 1), all resulting targeted clones (except clone 12E) produced 50-100% less APC than either WT DT40 or DT40^{TIR} cells (figs 3.4 and 3.6). Thus, the degron-*Apc* allele was hypomorphic. There are a number of reasons for these effects that are discussed below.

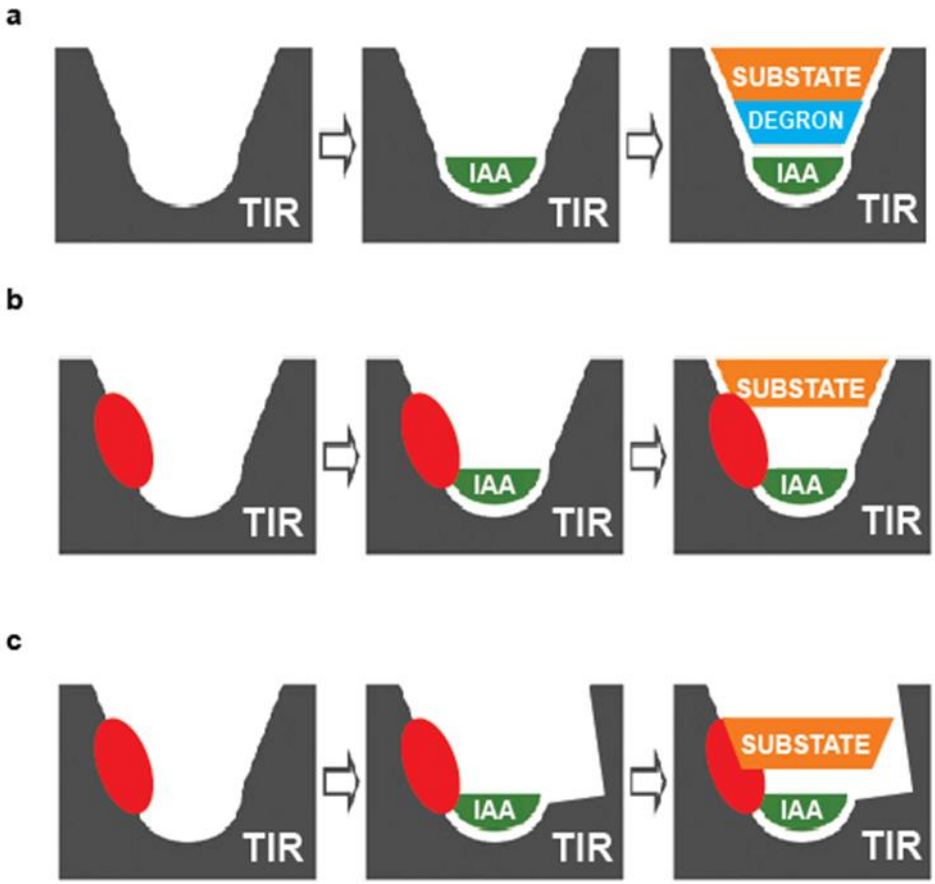

Fig 6.3. TIR-substrate binding with auxin and co-factor $InsP_6$. Alternative binding theories. (**a**) The TIR binding pocket (shown in grey) binds to IAA (auxin), which acts as a glue, binding to the degron motif found within the target substrate, in this case APC. (**b**) Knowing that the molecule $InsP_6$ (shown in red) binds to the auxin binding pocket within the TIR protein to maintain its structure, and knowing that in DT40^{TIR} cells there is APC (substrate) degradation in the absence of a degron motif, it is possible that the cofactor $InsP_6$ is able to link the substrate with the F-box protein TIR, without a degron. (**c**) $InsP_6$ binding may cause a conformational change in the TIR protein binding pocket. This creates a much wider binding pocket and provides entry for the substrate, which when bound to the $InsP_6$ molecule is joined to the TIR and so can be phosphorylated. Image modified from Tan *et al.,* (2007).

The intron/exon structure of the regulatory region of *Apc* (upstream from exon 1) is complex. Published works aiming to elucidate the functional significance of this structure is limited. *Apc* contains three alternative promoters, PN, P1A and P1B (fig 6.4a). P1B has not been extensively studied. PN drives a unique *Apc* transcript found in totipotent ES cells and mouse colon tissue, detected by 5' RACE (Karagianni *et al.,* 2005). P1A is the major promoter of multiple *Apc* transcripts and is present in most tissues (Rohlin *et al,* 2011). There are also three non-coding exons (fig 6.4) upstream of canonical exon 1 (as well as three alternative exon ones). Exon 1 contains a transcriptional start site (TSS) and Kozak sequence as do two of the three non-translated exons (0.3 and 0.1). This means that when alternative splicing creates transcripts lacking exon 1, the TSS and Kozak sequences are retained in the transcript (Santoro *et al.,* 1997). 5' *Apc* transcripts created by alternative splicing can generate up to six different mRNAs, based on the first few exons alone (Thliveris *et al.,* 1994) (fig 6.4b).

Taken together, the complex nature of the regulatory regions and start sites of *Apc* mean that genetic manipulation in this area is challenging. The GFP-degron and degron (alone) cDNA sequences were targeted immediately 5' of canonical exon 1. The multiple combinations of untranslated exons with both exons 1 and 2, make it likely that the presence of either GFP-degron or degron cDNA affected the alternative splicing of exons 0.3, 0.1 and 0.2. This may have produced less stable transcripts (resulting in less APC protein). Alternatively, transcripts may have lacked regulatory elements of untranslated exons that are involved in the transcription or translation of *Apc*. 5'RACE followed by DNA sequencing in targeted clones would determine which alternative exons are retained in the transcript. It would also help to identify the splicing of the mature mRNA and whether key regulatory regions of 5'*Apc* remain in the mRNA.

In summary, the degradation of APC in DT40^{TIR} cells incubated with auxin could result from several different mechanisms (fig 6.2-6.5). APC may contain a previously unidentified F-

box target sequence. The structure of the TIR-auxin complex may be altered due to post-translational modification of the TIR or the presence of altered/increased concentration of the co-factor phytate. Alternatively, post-translational modifications of the APC amino terminal may be recognised by auxin to promote recognition of APC by the SCF^{TIR}. Perhaps, several of these scenarios operate simultaneously resulting in APC degradation in $DT40^{TIR}$ cells.

6.3 Potential effects of low APC levels on DNA damage repair

In creating the degron-APC cell line ($DT40^{TIR;\ IAA17\text{-}APC}$), clones with lowered APC expression were unintentionally created. These clones, specifically V5 ($APC^{minimal}$) and X4A (APC^{low}) were treated with three DNA damaging agents and subsequent cell viability was measured using the MTS viability assay (fig 4.4). Possible explanations for these results will now be discussed. However, given the relatively small difference in DNA damage response in the APC–lowered cells, this discussion is mostly speculation. More work is needed to determine whether there is a true and significant link between APC and DNA damage response.

Both clones with lowered APC recovered better from the cross-linking agent Cisplatin. Cisplatin (*cis*-diammine-dichloro-$platinum^{II}$/DDP) causes DNA adducts of both inter- and intrastrand crosslinks. It is a neutral complex that reacts with water molecules *in vivo* to form a reactive aquated complex that can interact with DNA (see a review by Siddik, 2003). Upon cisplatin-induced DNA damage, the damage sensor and kinase ATR is activated (Damia *et al.,* 2001). ATR phosphorylates p53 (Tibbetts *et al.,* 1999), resulting in its activation to transduce a program of DNA damage response. An increase in DNA damage repair is associated with inhibition of drug-induced cytotoxicity. The repair of DNA crosslinks caused by Cisplatin requires Topoisomerase II (Topo II), which is reported to be overexpressed in certain cancers. Consequently, this causes platinum drug resistance (Ali-Osman *et al.,* 1993; Hengstler *et al.,* 1999). Therefore, it is reasonable to assume that DT40 cells (B-cell lymphoma cells) with low levels of APC overexpress Topoisomerase II to more

efficiently repair Cisplatin-induced damage. This theory would require an interaction between APC and Topoisomerase II, such as APC helping to degrade Topo II under normal conditions. This means that when APC levels are low/depleted, there is an increase in Topo II. In fact, Topo IIα can bind to the 15R and 20R repeats in the middle of APC (M-APC). Therefore, a link between APC and DNA damage response through topoisomerase II is possible (Wang *et al.,* 2008; Wang *et al.,* 2010). This theory would explain why APC^{low} and $APC^{minimal}$ cells recover quicker from Cisplatin than APC^{high} $DT40^{TIR}$ cells. Furthermore, loss of *Apc* causes an upregulation of p53 (Méniel *et al.,* 2015). In the APC^{low} and $APC^{minimal}$ cells, a predicted elevation in p53 levels could explain the increased survival of these cells compared to APC WT cells (with lower p53) exposed to Cisplatin – more p53 enables the faster/more efficient signalling in response to the presence of DNA adducts.

Apc has previously been linked to base excision repair, a mechanism used to repair abasic sites in DNA. A PCNA-like box was found in APC (Narayan *et al.,* 2005) that can bind DNA polymerase β. This prevents the polymerase from carrying out long-patch base excision repair (BER). Specifically, APC bound DNA polymerase β prevents polymerase β-directed strand displacement. Therefore, APC-bound polymerase β dictates the DNA repair pathway a cell can use, i.e. short nucleotide BER over long-patch BER (Narayan *et al.,* 2005; Balusu et al., 2007). The main repair pathway for DNA adduct removal (such as those caused by Cisplatin) is a BER-related mechanism called nucleotide excision repair (NER). Upregulation of only several of the 17 proteins required for NER results in an increased excision repair capacity in platinum-resistant cells (see a review by Reed, 1998). Again using the idea that APC could form complexes that regulated destruction of proteins other than β-catenin, APC may act to degrade one, or several of the NER proteins. Consequently upon APC loss, these NER

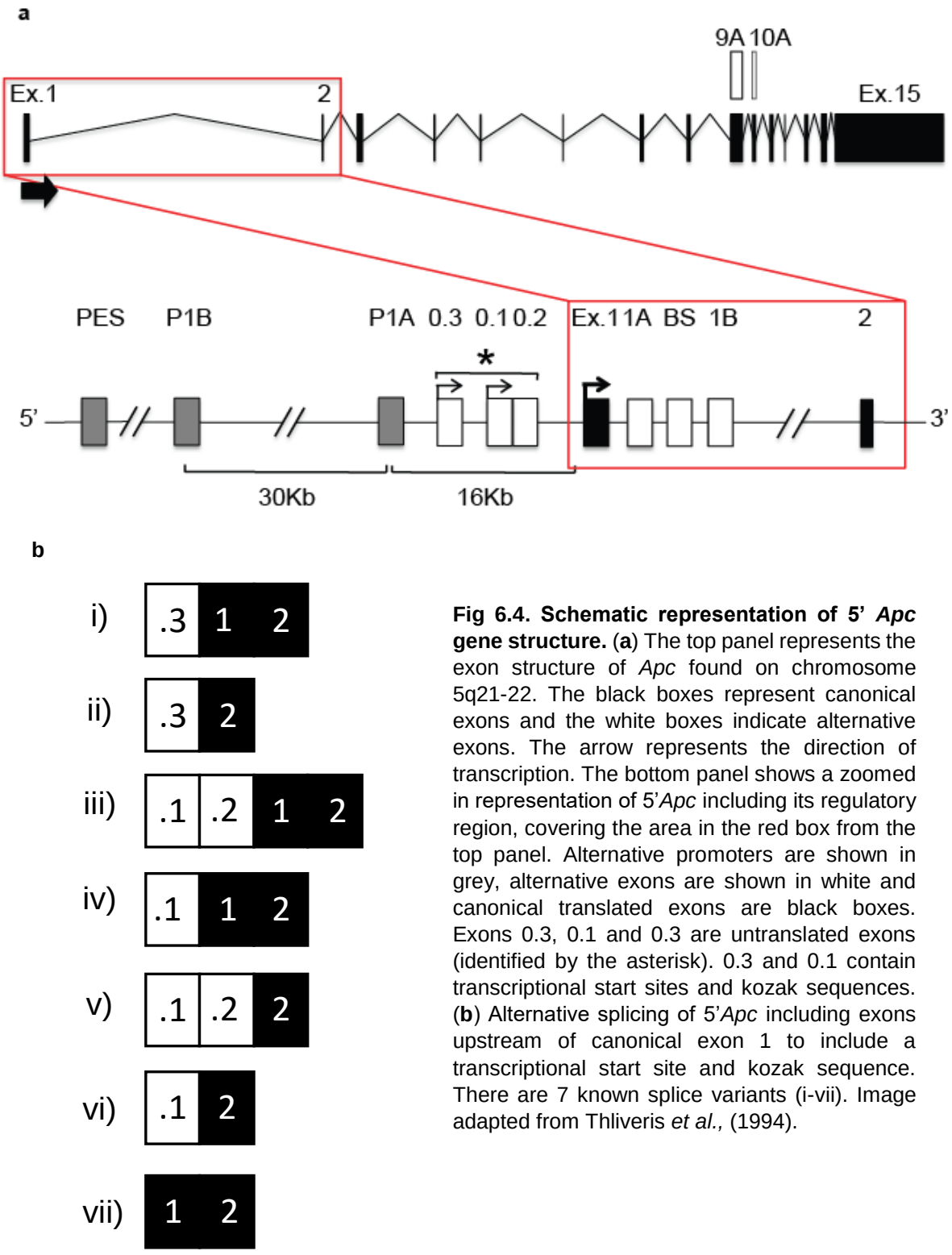

Fig 6.4. Schematic representation of 5' *Apc* gene structure. (**a**) The top panel represents the exon structure of *Apc* found on chromosome 5q21-22. The black boxes represent canonical exons and the white boxes indicate alternative exons. The arrow represents the direction of transcription. The bottom panel shows a zoomed in representation of 5'*Apc* including its regulatory region, covering the area in the red box from the top panel. Alternative promoters are shown in grey, alternative exons are shown in white and canonical translated exons are black boxes. Exons 0.3, 0.1 and 0.3 are untranslated exons (identified by the asterisk). 0.3 and 0.1 contain transcriptional start sites and kozak sequences. (**b**) Alternative splicing of 5'*Apc* including exons upstream of canonical exon 1 to include a transcriptional start site and kozak sequence. There are 7 known splice variants (i-vii). Image adapted from Thliveris *et al.,* (1994).

proteins are no longer degraded. APC^{low} and $APC^{minimal}$ cells would then contain more NER proteins than APC WT cells such as $DT40^{TIR}$. This would lead to more efficient NER in response to Cisplatin treatment, and increased viability in the MTS assay as seen in fig 4.4. To test this idea, using RNAi, *Apc* knock-down experiments could be performed on $Apc^{+/+}$ CRC cells such as HCT116. Subsequent Western blots would identify if certain NER proteins are increased in *Apc* depleted cells. Then, Co-IP experiments on any 'hits' from the Western blots would determine if APC and the NER proteins interacted directly. Proteasomal inhibitors such as MG132 would demonstrate whether any of the NER proteins investigated were in fact proteasomally regulated; as is expected for alternative APC destruction complexes. An alternative approach would be to over-express *Apc* and determine if NER proteins were depleted. However, this would be difficult in practice because over-expressing *Apc* leads to apoptosis-induced cell death in human CRC cells (Morin, Vogelstein and Kinzler, 1996). *Apc* overexpression also prevents cell cycle progression from G0/G1-S phase (Baeg *et al.,* 1995), which can lead to cell death. Additionally, over-expressing the C-terminal two thirds of *Apc* in *Xenopus* by only four fold compromises the mitotic spindle (Dikovskaya *et al.,* 2007). Therefore, Apc *overexpression* experiments may not provide useful experimental data.

However, It is important to consider that cells with reduced APC may not repair Cisplatin-induced DNA adducts better than cells with WT APC. In fact, these cells may simply not respond to this DNA damage because they do not recognize the damage, or simply fail to respond to it. In this case, these cells would not arrest in order to repair the DNA damage. Instead, they would continue through the cell cycle and as a result would exhibit chromosome instability and/ or genomic instability due to unrepaired DNA damage. This scenario provides another potential explanation for the increased survival of APC depleted cells in response to Cisplatin. To test this idea, the amount of the DNA damage sensors ATR and ATM and their phosphorylation should be measured in *Apc* depleted cells to determine if these proteins are activated in response to Cisplatin. If *Apc* depleted cells either

cannot sense DNA damage, or relay the damage signal through ATM/ATR, then the cells would not arrest in order to repair the damage.

Conversely, cells with reduced APC (APC^{low} and $APC^{minimal}$) recovered less well from HU-induced DNA damage than $DT40^{TIR}$ cells with WT APC (APC^{high}). There are currently no documented links between *Apc* and either replication forks or hydroxyurea. However, HU has a more potent effect in APC^{low} and $APC^{minimal}$ cells (fig 4.4), suggesting that they are less able to repair paused replication forks. Hydroxyurea (HU) stalls replication forks by depleting the nucleotide pool through ribonucleotide reductase inhibition (Elford, 1968). The mechanisms involved in rescuing these stalled forks are not clear. Sirbu *et al.,* (2013) found 139 proteins enriched at stalled replication forks in comparison to collapsed and active forks, using iPOND-mass-spectrometry. One group of proteins enriched at the site of the stalled forks are polymerases, required to synthesise DNA. APC has previously been shown to reside in the nucleus (Neufeld and White, 1997; Henderson, 2000; Sena *et al.,* 2006). Existing data in our lab (unpublished data) and data in the literature suggests that APC can bind to polymerases, specifically: polymerase β/beta (Narayan, Jaiswal and Balusu, 2005), which is required for BER (Bennett *et al.,* 1997); and polymerase σ/sigma (unpublished data), which is involved in mis-match repair (MMR) (Longely, Pierce and Modrich, 1997). Sirbu *et al.,* (2013) found Polymerase-δ/delta enriched at stalled replication forks. Together this suggests that loss of APC could cause a reduction in this polymerase, so that the replication fork cannot restart after damage/stalling. However at this time, these ideas are speculative. They imply that APC either: acts in a protective/stabilising role over polymerase δ under normal cellular conditions; or APC somehow modifies the function of the polymerase so it is unable to synthesize DNA at stalled replication forks. To determine if *Apc* depleted cells cannot restart stalled replication forks through a lack of certain polymerases, RNAi experiments followed by Western blots would determine if polymerase levels decreased after *Apc* knock-down. Additionally, immunoprecipitating APC and

determining if polymerases were bound to APC would show whether APC binds polymerases (Sirbu *et al.,* 2013).

To summarise the effect of APC on DDR, differences in the viability in response to DNA damaging agents were small and only slightly different than in control cells. It is possible that APC^{low} and $APC^{minimal}$ cells recovered better from Cisplatin due to higher levels of p53 and/or Topoisomerase II, enabling a faster/more efficient DNA repair. Alternatively, a more efficient nucleotide excision repair mechanism may be in effect in cells with reduced APC. Moreover, it is important to consider that cells with less APC may in fact not repair Cisplatin-induced DNA adducts at all, instead continuing through the cell cycle. On the other hand, APC^{low} and $APC^{minimal}$ cells recovered less well from Hydroxyurea than cells with WT APC levels. Recovery from HU-induced DNA damage requires the restarting of stalled replication forks. APC-reduced cells may lack or have reduced activity in some of the proteins required for the restart, such as a polymerase(s). Overall, much more work is needed to identify a more robust link between APC and DNA damage repair.

6.4 *Apc* depleted cells are more sensitive to the combination of Taxol® and a Bcl-2 inhibitor

Apc deficient cells such as those found in CRC cannot be killed efficiently by Taxol® (Radulescu *et al.,* 2010). They do not undergo apoptosis normally induced by a prolonged mitotic arrest. This is partly due to a compromised SAC in APC deficient cells leading to reduced mitotic arrest (Dikovskaya *et al.,* 2007; Radulescu *et al.,* 2010). Sensitising *Apc* depleted cells to Taxol® would allow these CRC cells to be killed and potentially alleviate the cancer.

6.4.1 *Apc* deficient cells and ABT-737 treated cells have increased Bcl-2

Experiments in this thesis identified another explanation as to why *Apc* deficient cells do not die in response to Taxol®. Human epithelial cancer cells depleted of *Apc* and CRC cells

with mutant *Apc* (N-*Apc*) all showed an increase in the pro-life protein Bcl-2 (fig 5.1). Bcl-2 -protects cells from apoptosis by several mechanisms. It binds the mitochondrial outer membrane (MOM) (Krajewski *et al.,* 1993; Nguyen *et al.,* 1993; de Jong *et al.,* 1994) where it maintains membrane integrity, maintaining the mitochondrial membrane potential Δψm (Vander Heiden *et al.,* 2000). Bcl-2 also binds to pro-apoptotic proteins, such as Bax, neutralising the apoptotic BH3 domain (Otlvai *et al.,* 1993; Yin *et al.,* 1994; Zha *et al.,* 1996; Petros *et al.,* 2001). An increase in Bcl-2 is expected to increase these functions.

We were unable to establish a direct interaction between APC and Bcl-2. Ongoing mass-spectrometry experiments in the lab also did not find an interaction between these two proteins. However, it is possible that the increased Bcl-2 in cells lacking *Apc*, is an indirect effect of *Apc* loss and is facilitated by intermediary protein(s). A role of Par-4 protein was ruled out as a means of increasing Bcl-2 after *Apc* depletion. More work is required to identify if protein(s) act as regulatory links between APC and Bcl-2.

The question remains, what the function of increased Bcl-2 is? Bcl-2 maintains mitochondrial outer membrane integrity, maintaining the mitochondrial membrane potential (MMP). An increase in Bcl-2 is thus expected to either further protect the MMP or increase it. However, FACS data (fig. 5.10), showed that cells depleted of *Apc* (and thus expressing increased Bcl-2) showed a slight decrease in the membrane potential of mitochondria as shown by an increase in the mitochondria:MMP ratio. This MMP change is very small and likely not significant. Thus although the result is opposite to what is expected (based on an increase in Bcl-2) it is likely not a reflection on the function of increased Bcl-2. Further repetition of this FACS experiment, is needed to confirm this result as robust.

Bcl-2 overexpression prevents the release of cytochrome c by maintaining the integrity of the mitochondrial membrane (Yang *et al.,* 1997). When cytochrome c is released, it triggers formation of the apoptosome (fig 1.4) (Kluck *et al.,* 1997; Yang *et al.,* 1997). Cells with

increased Bcl-2 are expected to have even less cytochrome c within the cytosol than wild type cells (Yang *et al.,* 1997). Moreover, a reduction in cytochrome c release may provide a mechanistic explanation as to why *Apc* deficient cells are not killed as readily by Taxol® – cytochrome c cannot be released due to increased Bcl-2 and a stronger mitochondrial membrane integrity. Therefore, apoptosis cannot be executed. Cytosolic cytochrome c detection by Western blot, IF or FACS in cells depleted of *Apc* and treated with Taxol® would show whether these cells have less cytochrome c in their cytoplasms. This could be a functional read out for increased Bcl-2 in *Apc* depleted cells.

The observation that *Apc* loss leads to increased Bcl-2 ties in with a recent paper stating that *Apc* loss primes cells for apoptosis and that Bcl-2 is required for intestinal tumorigenesis (van der Heijden *et al.,* 2016). Interestingly, they state that Bcl-2 increases at the mRNA and protein level, allowing transformation in cells with *Apc* loss. Inhibiting Bcl-2 in these *Apc* depleted cells (even by just heterozygous mutation) impaired adenoma formation and tumorigenesis, even in established adenomas.

In addition to *Apc* depletion, ABT-737 treatment also caused an increase in Bcl-2 (fig 5.3 and S8). Fractionation experiments showed that this increase occurred in the membrane fraction. However, there was no Bcl-2 increase at the mitochondria or ER of U2OS cells treated with ABT-737 (fig 5.4). Therefore, the location(s) of this Bcl-2 increase remains elusive. Bcl-2 is also known to bind to the nuclear outer membrane (Akao *et al.,* 1994) and the endoplasmic reticulum (Franke and Kartenbeck, 1971; Lithgow *et al.,* 1994). So, Bcl-2 has functions in multiple membrane compartment within the cell. In fact, these membranes all produce ROS (Freeman and Crapo, 1982) and it is possible that Bcl-2 is involved in an antioxidant pathway. An ABT-737 induced increase in membrane-associated Bcl-2 may be an attempt by cells to react to and minimize the damage that can result from ROS. Thus, examining Bcl-2 levels at the nuclear outer membrane after ABT-737 is important to

establish if this is where the increase occurs. An increase at the nuclear membrane may indeed show the cell trying to combat increased intracellular ROS levels.

Alternatively, the increase in membrane-associated Bcl-2 may be attributable to Bcl-2 within membrane bound vesicles. Such vesicles have multiple functions including protection from proteolysis and transport. Transport vesicles move molecules around the cell, between membrane-bound compartments, for example between the rough endoplasmic reticulum and the Golgi apparatus. Perhaps, ABT-737 causes the transport of Bcl-2 between cellular compartments. Alternatively, vesicles may act to protect Bcl-2 from ABT-737, or from proteolytic degradation. For instance all Gram negative bacteria use such vesicles to protect protein cargo from a host (Bonnington and Kuehn, 2014). To test these hypotheses, measuring the amount of Bcl-2 in the nuclear outer membrane and membrane-bound vesicles, using cell fractionation and Western blots could identify the location increased Bcl-2 induced by ABT-737. Identification of where the increased Bcl-2 localised could shed light on how it protects APC-deficient cells.

6.4.2 Taxol®, ABT-737 and siRNA treatment activate the unfolded protein response

Up to 30% of all eukaryotic proteins pass through the ER for folding, modification and assembly before being transported to other parts of the cell (Mendez *et al.,* 2015). To ensure ER homeostasis is controlled, the cell has developed a mechanism to recognise and rectify problems in the ER and restore proteostasis, called the unfolded protein response (UPR). Experiments in this thesis showed that control siRNA treatment, *Apc* depletion, Taxol® and the BH3 mimetic ABT-737 activated the UPR (fig 5.6). The unfolded protein response is a conserved mechanism (Hollien, 2013) to alleviate ER stress caused by the accumulation of misfolded and/or unfolded proteins. Activation of the UPR can happen through intrinsic (ROS, disturbed Ca^{2+} homeostasis, ATP depletion, inflammation, oncogenic mutations) or extrinsic (hypoxia, glucose deprivation, carcinogens) stressors (see a review by Senft and Ronai, 2015). The UPR is activated by three sensors embedded

in the ER that become activated in response to ER stress (fig 1.7): IRE1α/β (Nikawa and Yawashita, 1992; Cox *et al.,* 1993), PERK (Harding, Zhang and Ron, 1999) and ATF6 (Haze *et al.,* 1999). These sensors potentiate several signalling cascades that allow the ER to cope with stress and restore ER homeostasis. If the stress cannot be overcome, these sensors induce apoptosis.

Elevated P-IRE was found in both ER fractions and whole cell lysates of U2OS cells treated with ABT-737 (fig 5.6a). However, ABT-737 also caused an increase in Bcl-2 in the membrane fraction of HCT116, CaCo2 and U2OS cells (figure 5.3 and supplemental figure 8). It is not clear from my experiments whether ABT-737 activated the UPR directly, or indirectly through an increase in Bcl-2 protein levels. However, very recently, Bcl-2 over-expression was shown to enhance the splicing of XBP-1, an IRE1 target of UPR activation (Chonghaile *et al.,* 2015). This suggests that Bcl-2 can play a role in the UPR and that ABT-737-induced UPR activation is indirect, and can involve an increase in Bcl-2. Therefore, both *Apc* depletion and ABT-737 treatment may activate the UPR via increased Bcl-2, although more experiments are required to establish the details. For example, using RNAi to knock-down *Bcl-2* in *Apc* depleted and ABT-737 treated cells and measuring the relative amount of P-IRE. This would show whether UPR activation requires elevated Bcl-2.

Treatment with ABT-737 also elicited a UPR response in other cells types. ABT-737 caused a 78% increase in P-IRE in HeLa cells treated with a control siRNA (fig 5.6b) and 53% in CaCo2 CRC cells expressing mutant *Apc* (N-*Apc*) (fig 5.6c). Therefore ABT-737 is a robust activator of the UPR across cell types and regardless of *Apc* status.

6.4.3 Taxol®, ABT-737 and siRNA treatment affect mitochondrial localisation

When using IF to examine localisation of pGFP-Bcl-2 in U2OS cells, a change in the subcellular localisation of mitochondria was detected in *Apc* depleted, Taxol®, ABT-737 and control siRNA treated cells (fig 5.8-5.9). Normally, mitochondria are spread out widely

through the cytoplasm of a cell, often extending to the cellular periphery. Using the dye MitoTracker® to visualize mitochondria revealed mitochondria retracting to a peri-nuclear region, clustered around the nucleus, often skewed to one side of the cell and absent from the cell periphery. Consistently, biochemical experiments (fig 5.7) showed that control siRNA treated cells also show increased P-IRE levels indicative of UPR activation. Thus the siRNA procedure itself appeared to be causing cellular stress activating the UPR. This means that the change in mitochondrial localization in *Apc* knock-down cells may be due to the knock-down procedure, rather than *Apc* depletion. Moreover, the change in localization may be a mitochondrial response to cellular stress. Nonetheless, the clustering was most severe in ABT-737 treated cells.

A change in the distribution of mitochondria in the cell may indicate a change in cellular homeostasis. The change in localization was to a more peri-nuclear position that was often asymmetric. This mitochondrial distribution has previously been observed during oocyte fertilization, Herpes simplex virus infection, and embryonic development (Al-Mehdi *et al.,* 2012). Other mitochondrial redistribution patterns are also known to occur (fig 6.5). The peri-nuclear clustering of the mitochondria did not affect mitochondrial number, (fig 5.10a) indicating no change in mitochondrial fission or fusion associated with the mitochondrial translocation. However, measuring cell area (μm^2) in cells with control and *Apc* siRNA and ABT-737 showed that each treatment caused a reduction in both cell area and mitochondrial number. Thus, there is a positive correlation between cell size and mitochondria. It is possible that the shrinking in size of a cell is a stress response. The mTOR pathway has been shown to control cell size in response to energy stress (Sofer *et al.,* 2005). Hence, the mTOR pathway may also control cell size in response to ER stress. Additionally, the ER chaperone GRP78 (BiP) localises to mitochondria under ER stress and may help to relay the UPR signal to the mitochondria (Sun *et al.,* 2006). Therefore, GRP78 may be involved in the redistribution of mitochondria in response to ER stress.

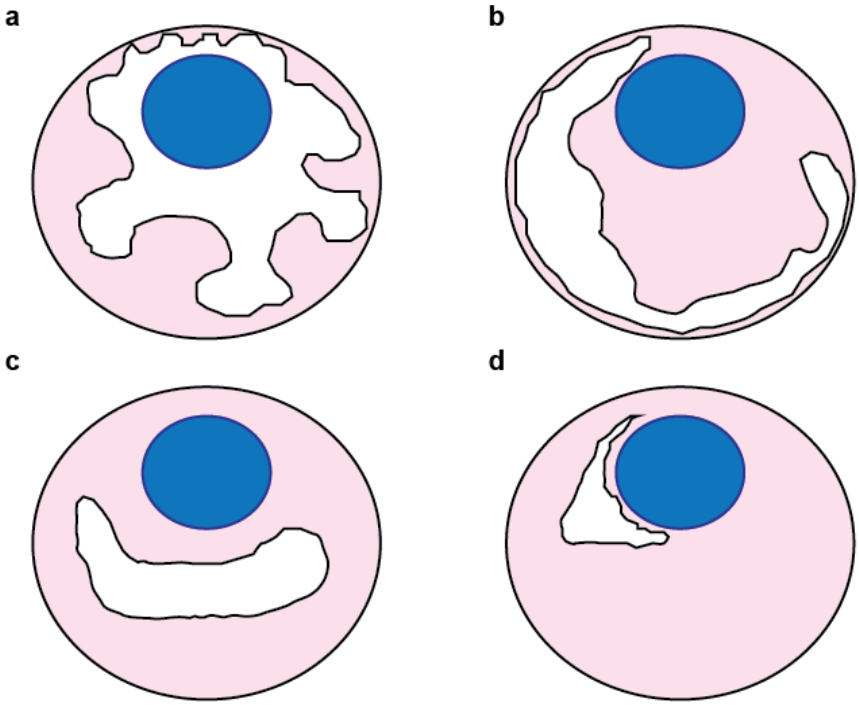

Fig 6.5. Different mitochondrial distributions. (**a**) The normal spread of mitochondria (shown in white) is throughout the cell and often extends to the cell periphery. (**b**) Subplasmalemmal redistribution orders the mitochondria to the plasma membrane, leaving much of the cytoplasm unoccupied with mitochondria. (**c**) Pan-cytoplasmic localization moves the mitochondria in close contact with the endoplasmic reticulum. (**d**) Asymmetrical peri-nuclear clustering takes the mitochondria away from the cell periphery and concentrates mitochondria around the nucleus, often asymmetrically.

6.4.4 ABT-737 does not affect mitochondrial function

To determine whether the severe peri-nuclear clustering of mitochondria in ABT-737 treated cells affected mitochondrial function, the mitochondria dye JC-1 was used to monitor MMP. Monomeric JC-1 accumulates in all mitochondria, but only aggregates in mitochondria with an active MMP. Therefore, mitochondria with depolymerized membranes, such as those undergoing apoptosis have no MMP, and contain no JC-1 aggregates. The data (fig 5.9) showed that in mitochondria of ABT-737 treated cells, the MMP is still active and resembles that in untreated cells. Therefore, although the mitochondria have redistributed within the cell, the functionality as judged by MMP is unchanged. This is consistent with Frieden *et*

al., (2004) who showed that there was no change in mitochondrial function despite mitochondrial relocalisation.

6.4.5 ABT-737 and *Apc* loss affect mitochondrial structure

Mitochondria can exist as individual organelles, filamentous structures or large spheres representing swollen mitochondria (Johnson *et al.,* 1980). Untreated U2OS cells had filamentous mitochondria (fig 5.8 and 5.9). Cells treated with either control siRNA or Taxol® retained filamentous mitochondria. However, ABT-737 treated cells contained either far fewer, or no filamentous mitochondria. Moreover, only in *Apc* depleted cells did the mitochondria appear swollen, appearing as very large, globular structures. Based on the fact that *Apc* depleted cells have increased Bcl-2 (fig 5.1), which binds to the mitochondrial outer membrane to maintain its integrity, Bcl-2 seems the most likely explanation for the change in mitochondrial structure. However, ABT-737 treated cells also show an increase in Bcl-2, but do not have swollen or filamentous mitochondria. It is possible that in ABT-737 cells, mitochondria exhibit an intermediary phenotype between filamentous structures (in untreated and Taxol® treated cells) and the swollen structures that result from *Apc* depletion – the filaments are broken up into smaller chains of mitochondria, or individual organelles (fig 6.6). Therefore, based upon the idea that an increase in Bcl-2 influences the structure of the mitochondria, there must be additional changes in *Apc* depleted cells that cause mitochondria to swell.

6.4.6 Mitochondria as a read-out for ER stress

Experiments in this thesis showed that Taxol®, control and *Apc* siRNA and ABT-737 activated the UPR (fig 5.6 and 5.7). Additionally, these treatments all caused asymmetric peri-nuclear mitochondrial clustering (fig 5.8 and fig 5.9). Hypoxia, a known activator of the UPR, also causes mitochondrial peri-nuclear clustering (Al-Mehdi *et al.,* 2012). Taken together this suggested that the change in localisation of mitochondria to a more peri-nuclear region may be a result of ER stress and UPR activation (as mitochondrial peri-nuclear clustering is already associated with the UPR activator hypoxia). A more robust link between UPR activation and fusion protein Mfn-2 controls the UPR and lies upstream or PERK, which controls mitochondrial morphology and can execute mitochondrial swelling. Therefore, swelling of mitochondria may be a signal for ER stress and UPR activation.

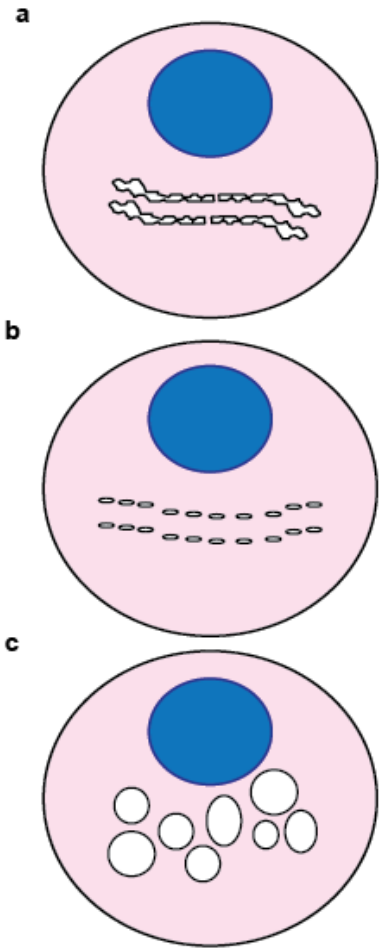

Fig 6.6. Different mitochondrial structures associated with ABT-737 and siAPC. (**a**) Filamentous mitochondria (shown in white) in untreated cells, forms chains of mitochondria. (**b**) Mitochondria in ABT-737 treated cells are neither filamentous nor swollen, they are more like individual organelles or small chains of mitochondria. (**c**) The mitochondria in Apc depleted cells are large, globular mitochondria and appear swollen.

6.4.7 Combining Taxol® and ABT-737 kills intestinal organoids with mutant *Apc*

Intestinal organoids were used as a more physiological, 3D system to test the effect of Taxol® and ABT-737 on WT or mutant *Apc* cells *(*cysts*)*. Organoids were treated with either Taxol®, ABT-737 or both (ABTTAX) and the effects followed over 48 hours. As expected based on 2D cell culture data (Dikovskaya *et al.,* 2007; Radulescu *et al.,* 2010), Taxol® caused organoids with WT *Apc* to arrest in mitosis, whereas, organoids with mutant *Apc*

continued to grow. ABT-737 had no visible effect on WT organoids although it appeared to slow the growth of *Apc* mutant cysts. ABTTAX had a severe impact on cysts, causing death within several hours of treatment. It had less impact on the organoids with WT *Apc*. This may be because the cysts are already stressed due to the presence of mutant *Apc* and the addition of two more stressors (Taxol® and ABT-737) could cause cell death by an additive effect. Moreover, this data ties in with work done by van der Heijden *et al.,* (2016), whom showed that intestinal stem cells that had lost *Apc* could be primed for apoptosis by inhibiting Bcl-2 – impairing tumorigenesis (fig 6.7).

Although a conclusion cannot be drawn from my experiments as whether *Apc* loss causes ER stress - due to the control siRNA also eliciting UPR activation, a recent publications showed that *Apc* is a cellular stressor (van der Heijden *et al.,* 2016). Here, organoids were assessed on their readiness to undergo apoptosis as analysed by a mitochondrial priming assay (Ryan, Brunelle and Letai, 2010; van der Heijden *et al.,* 2016). This showed that in *Apc* deficient organoids, cells showed a much higher rate of membrane depolarisation attributable to intrinsic pathway cell death when treated with the BH3-only Bcl-2 family protein BID.

In summary of the Bcl-2 data (fig 6.8), *Apc* depleted cells cannot be killed by Taxol® as readily as *Apc* WT cells and are more sensitive to the combination of Taxol® and the Bcl-2 inhibitor ABT-737. Experiments in this thesis discovered that *Ap*c depleted cells had increased Bcl-2, a pro-life protein. This may in part explain why these cells do not die as readily - Bcl-2 counteracts the cells being primed for apoptosis when *Apc* is lost (fig 6.7) (van der Heijden *et al.,* 2016). Moreover, these cells were more sensitive to the Bcl-2 inhibitor ABT-737 (as seen by van der Heijden *et al.,* 2016), which also increased Bcl-2 levels. ABT-737 also depleted APC by around 50%. This APC depletion effect was similar to that caused by hypoxia, a known stressor on the cell (fig 6.8). This link to cell stress led to the discovery that *Apc* loss, Taxol® and ABT-737 treatment all caused ER stress and

activated the unfolded protein response (UPR), similar to hypoxia. Consistently, these cellular treatments also resulted in the redistribution of mitochondria to a peri-nuclear region, suggesting that the translocation of mitochondria is a consequence of ER stress. However, these treatments did not affect the functionality of the mitochondria, as measured by the mitochondrial membrane potential (MMP) probe JC-1. Only *Apc* loss caused a significant change in the mitochondrial structure from filamentous to swollen, globular structures. However, ABT-737 treated cells had mitochondria akin to an

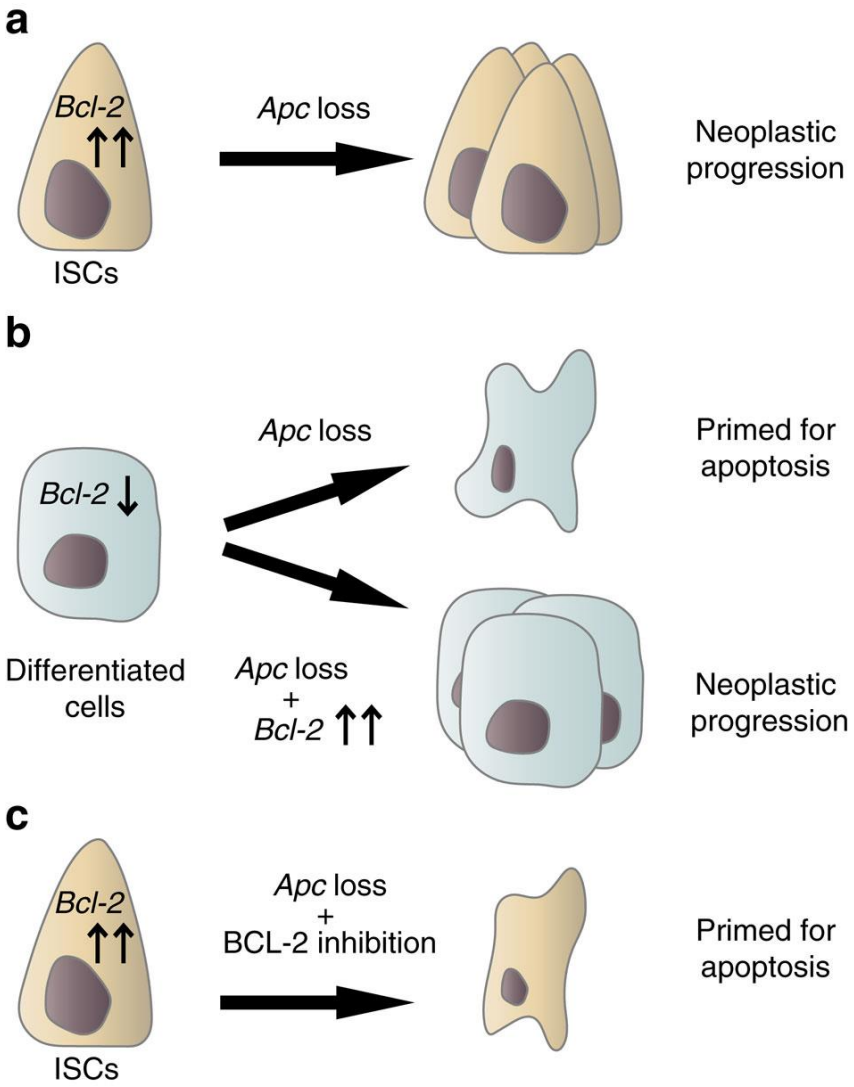

Fig 6.7. Intestinal tumorigenesis caused by *Apc* loss can be impaired by Bcl-2 inhibition. (**a**) *Apc* loss in intestinal stem cells (ISC) with increased Bcl-2 leads to neoplastic progression and subsequent intestinal tumorigenesis. (**b**) *Apc* loss in differentiated intestinal cells primes them for apoptosis due to cell stress. However, a subsequent increase in Bcl-2 allows the transformation of the differentiated cells. (**c**) In ISCs as in (a), when Bcl-2 is inhibited (by genetic of chemical methods), intestinal tumorigenesis is impaired and the cells are primed for apoptosis. Image taken from van den Heijden *et al.,* (2016).

intermediary phenotype between filamentous and swollen structures. As both *Apc* loss and ABT-737 increased Bcl-2 levels it is plausible that elevated Bcl-2 protein levels are in part due to the shift away from filamentous mitochondria.

Cells with mutant *Apc* (N-*Apc*) showed higher P-IRE levels when treated with Taxol®, although Taxol® treatment in cells with WT *Apc* had little effect. This suggests that the mutant *Apc* is synergizing with Taxol® to produce a higher UPR response. If *Apc* depletion is, as I have shown, an activator or the UPR (a stressor) then it is plausible that mutant *Apc*, lacking the middle and C-terminal portion of APC is also a stressor; as these cells contain short, mutant *Apc* fragments that produce dominant effects over the WT allele (Marshall *et al.,* 2011; Nelson *et al.,* 2012), and result in polyp formation (Kinzler and Vogelstein, 1996; Rowan *et al.,* 2000; Radulescu *et al.,* 2010). This means that *Apc* mutant cells would be inherently stressed (fig 6.8) and any subsequent stress to the cell such as ABT-737 or Taxol® treatment, would cause a higher increase that if carried out in cells with WT *Apc*.

6.5 Summary

To summarise my data, I propose a model, which suggests that combining specific cellular insults, such as losing *Apc*, treatment with Bcl-2 inhibitors or Taxol® can produce cumulative ER stress levels (fig 6.9). In this model, cells can cope with a certain amount of ER stress-induced UPR activation. However, a high a level of ER stress leads to UPR-induced cell death. This could explain why in cell culture, *Apc* deficient cells are more sensitive to the combination of Taxol® and ABT-737 than *Apc* WT cells. The *Apc* deficiency is a stressor in itself. Thus, the combination of Taxol®, ABT-737 and *Apc* depletion compound the ER stress effect causing cell death. Elevated Bcl-2 in both *Apc* depleted and ABT-737 treated cells may be the one reason for UPR activation. Activation of the UPR leads to a mitochondrial phenotype, causing them to cluster asymmetrically in peri-nuclear regions. However, no measurable change in mitochondrial function is associated with this translocation. Importantly, the combination of ABT-737 and Taxol® was successful in killing

Apc mutant organoids, much more effectively than *Apc* WT organoids. Combining these agents may constitute a possible chemotherapeutic approach for treating CRC.

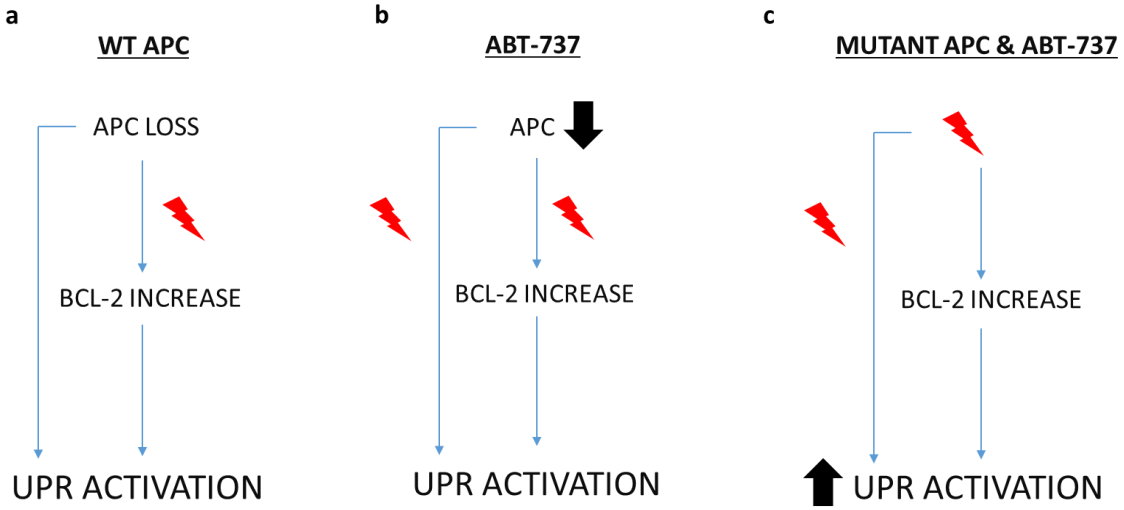

Fig 6.8. The relationship between APC, Bcl-2, ABT-737 and the UPR. (**a**) If APC is lost (RNAi) in cells expressing WT *Apc*, there is a stress response in activation of the UPR. In addition there is an increase in the Bcl-2 protein, which may also activate the UPR. (**b**) In cells expressing WT *Apc* that are treated with ABT-737 there is a decrease in APC, which mimics the stress effect of hypoxia. These cells show activation of the UPR. There is also an increase in Bcl-2, which may also activate the UPR. (**c**) In cells with mutant *Apc*, which are treated with ABT-737 there is activation of the UPR (probably due to stress caused by the *Apc* mutation) – at a higher level when compared to UPR activation in WT *Apc* cells. These cells also show an increase in Bcl-2, which may also activate the UPR.

6.6 Graphical summary

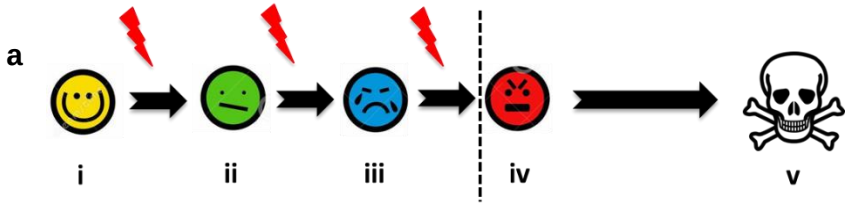

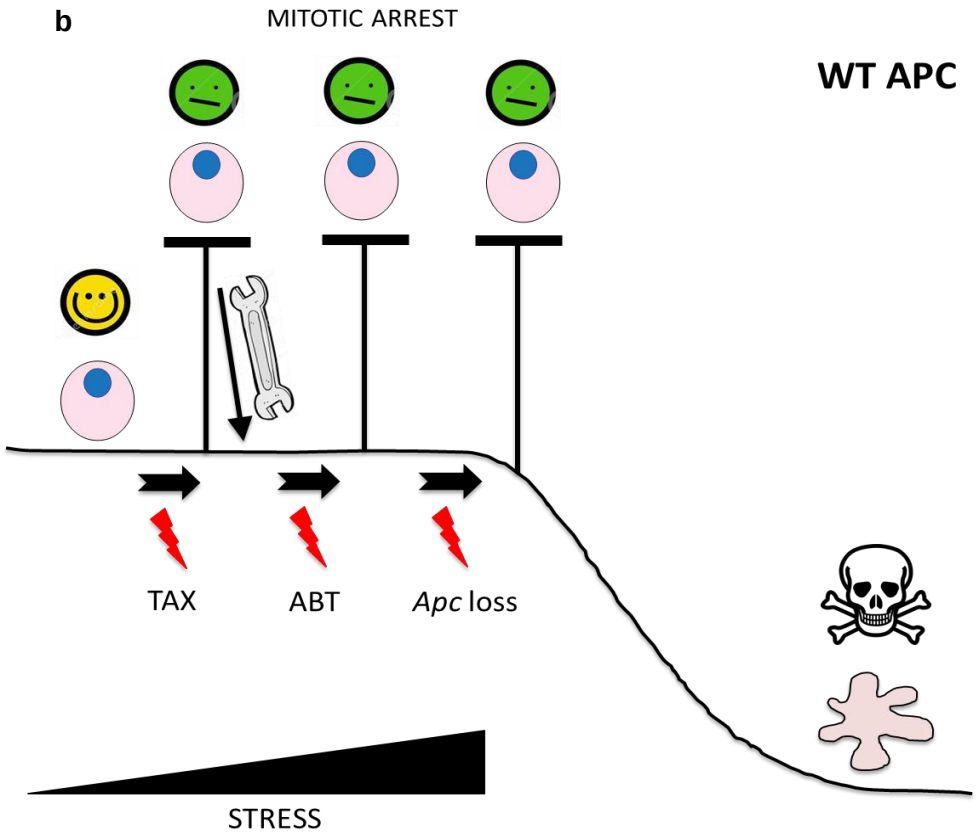

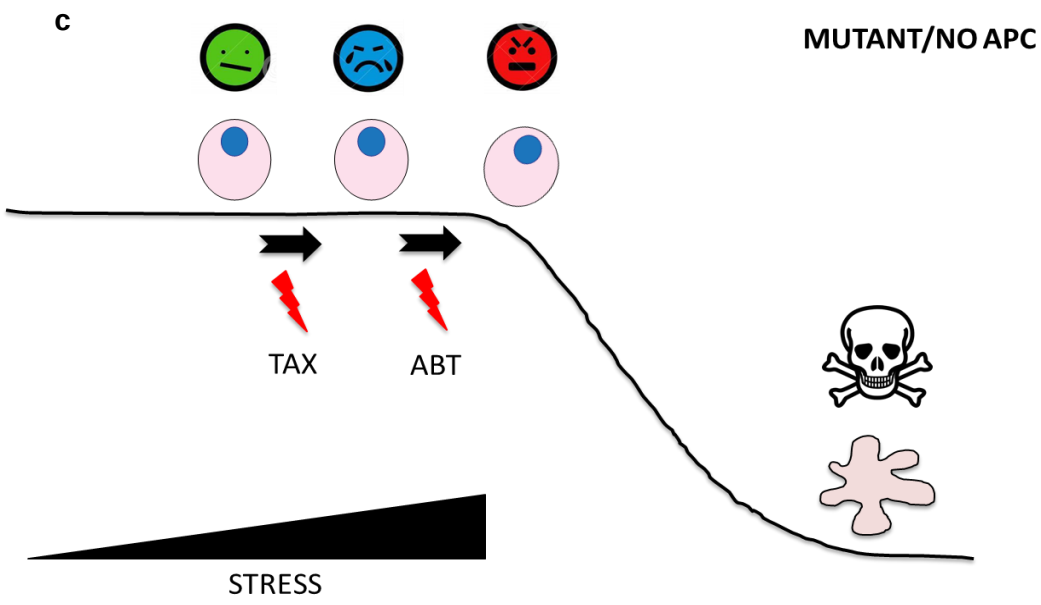

Fig 6.9. Graphical summary. Three-step model for stress-induced cell death. (**a**) In this model, it takes 3 independent stressors on the cell, to 'tip' the cell over the edge of what it can cope with and the cell dies. A normal, unstressed happy cell (i) encounters a stressor (represented by the lightning bolt) and becomes stressed. One more independent stressor a cell can survive (ii-iii). However, a third stressor is too much for the cell and it initiates apoptosis (iv) and dies (v). (**b**) When cells with WT *Apc* are treated with Taxol® they arrest in mitosis. The cell must then fix any damage before continuing on with the cell cycle. If the cell remains mitotically arrested, treatment with other drugs such as ABT-737 have less of an effect because the arrested cell is effectively on a pedestal out of reach because it has arrested. (**c**) As my experiments identified *Apc* depletion or mutant *Apc* as a stressor, cells with either no *Apc* or mutant *Apc* are likely to be inherently stressed, therefore they are already one step closer to death on the model, they lack step (i) in (a). The addition of 2 more stressors, Taxol® and ABT-737 are too much stress for the cell and it dies.

Supplementary Figures

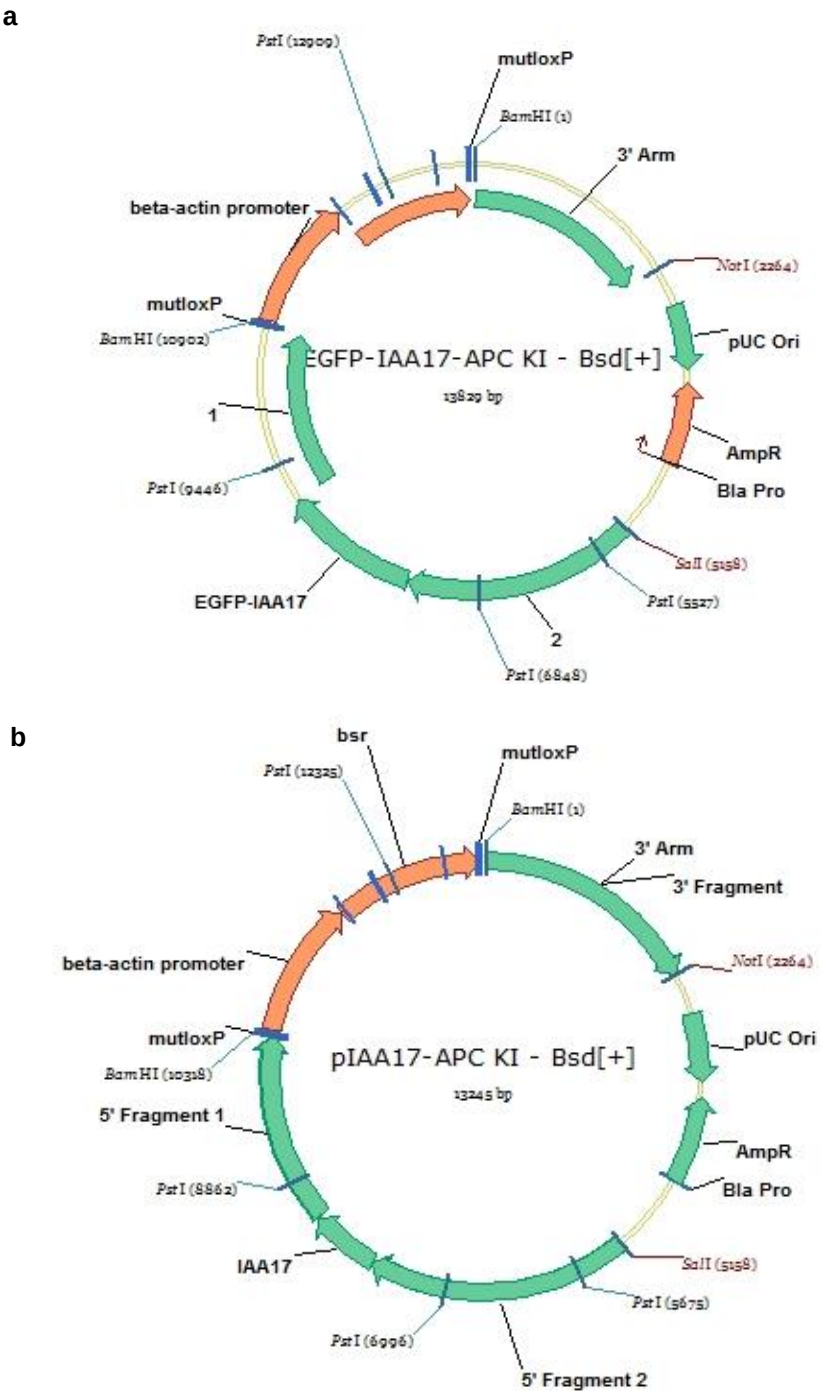

Supplemental figure 1. Targeting vectors used to create (EGFP-)degron-*Apc*. (**a**) pEGFP-IAA17-APC. The resistance cassette Blasticidin S is inserted so as to be in the same transcriptional orientation as *Apc* after homologous recombination. (**b**) pIAA17-APC. The resistance cassette Blasticidin S is inserted so as to be in the same transcriptional orientation as *Apc* after homologous recombination.

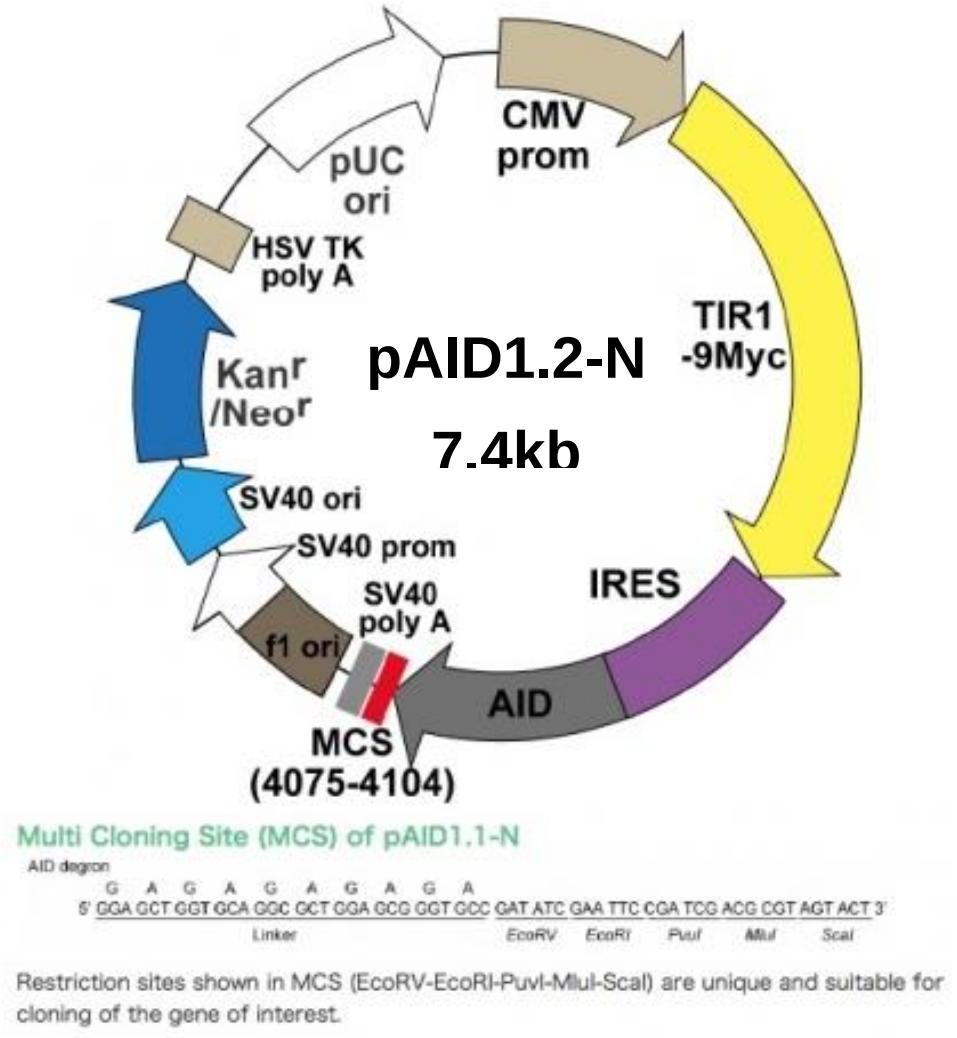

Supplemental figure 2. Expression vector. TIR-9Myc cDNA and degron (AID) cDNA to allow for expression of separate TIR and degron proteins.

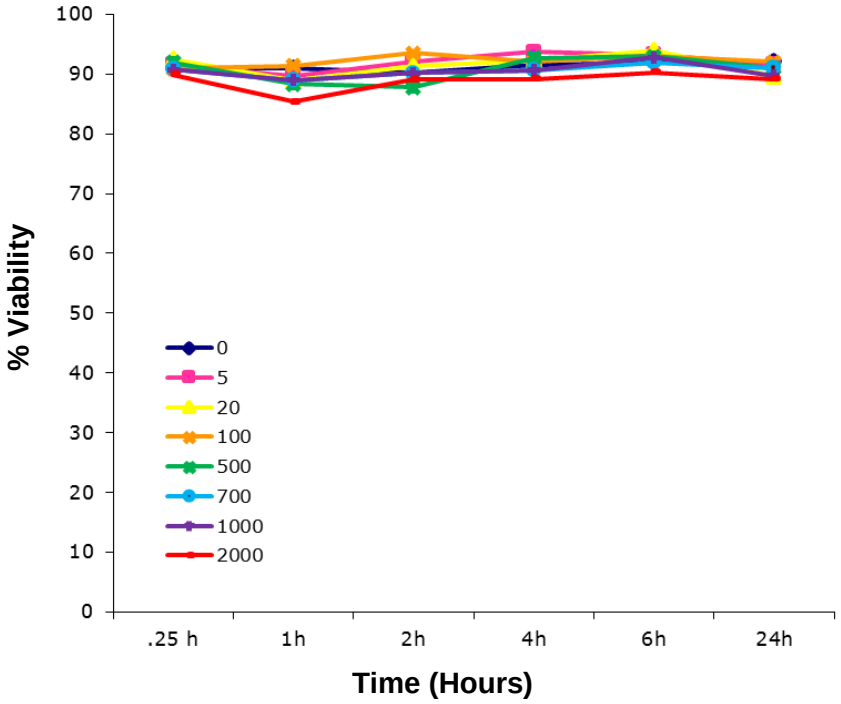

Supplemental figure 3. Auxin does not affect DT40 viability. WT DT40 cells were treated with varying concentrations of auxin (0-2000nM) over 24 hours and the percentage of viable cells was counted.

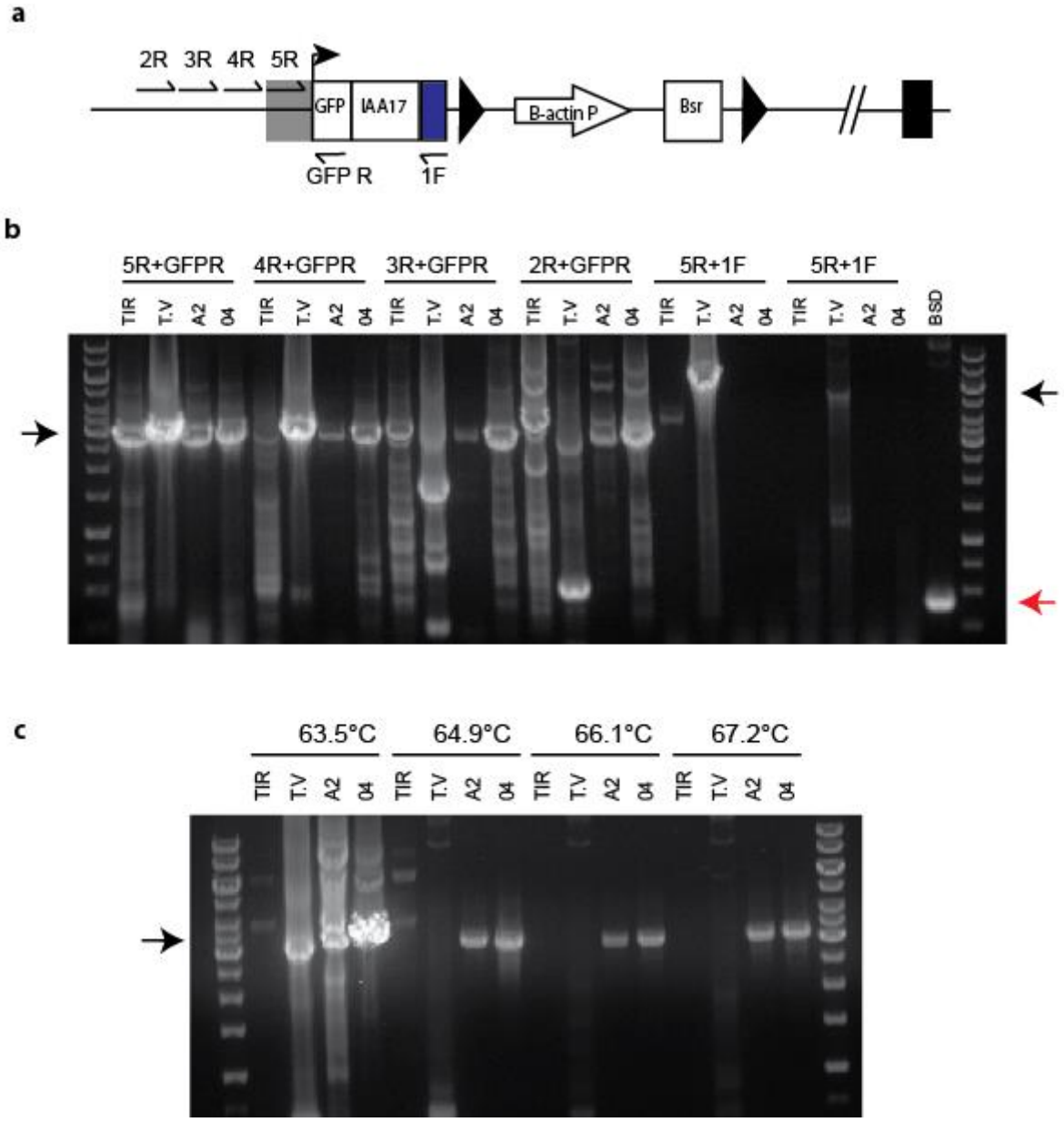

Supplemental figure 4. Optimising the PCR screen to identify cells transfected with EGFP-IAA17-APC. (**a**) Schematic showing the recombined allele after HR and the different primers used to amplify an area representative of a targeted insertion (i.e. primers 2R-4R are upstream of the insertion and GFP R is within the targeting vector). (**b**) Primer combinations 5R + GFP R, 4R + GFP R, 3R + GFPR, 2R + GFP R, 5R + 1F were tested on DT40^{TIR} cells, the targeting vector (T.V) and 2 test clones (A2 and O4). 5R + GFP R is a control PCR as it amplifies up the targeting vector. The black arrow shows the band expected for a targeted insertion. The red arrows shows the band representing Blasticidin, another control PCR. (**c**) Primer combination 2R + GFP R was chosen (b) and then a gradient PCR was performed to identify the optimum annealing temperature. DT40^{TIR} cells and the targeting vector are shown as negative controls. The arrow shows the expected band for a targeted insertion.

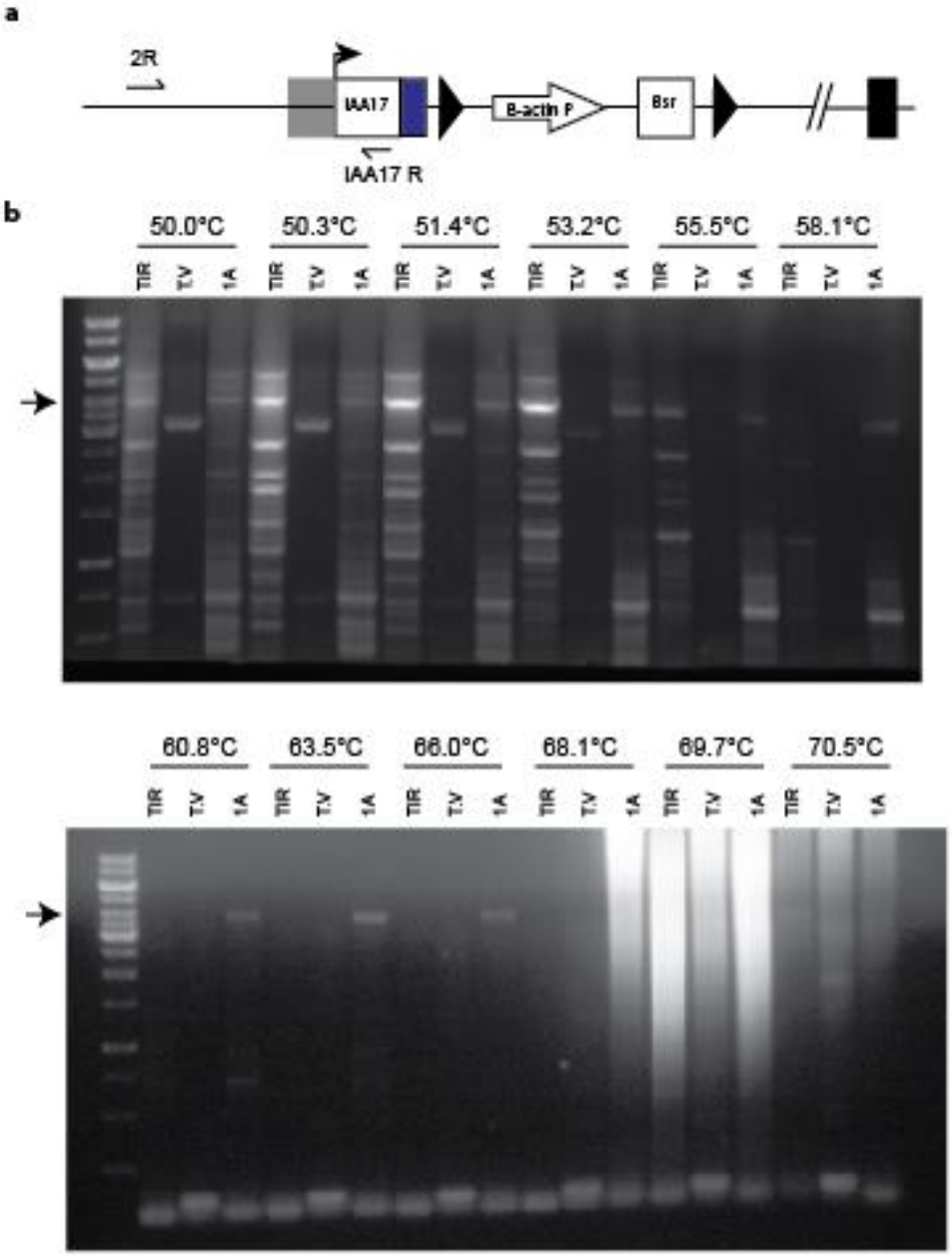

Supplemental figure 5. Optimising the PCR screen to identify cells transfected with IAA17-APC. (**a**) Schematic showing the recombined allele after HR and the different primers used to amplify up and area representative of a targeted insertion (i.e. using primer 2R upstream of the insertion and primer IAA17 R within the targeting vector). (**b**) Gradient PCRs using 2R and IAA17 primers. DT40^{TIR} cells and the targeting vector (T.V) were used as negative controls. Clone 1A, known to be positive for a targeted insertion from the previous transfection, was used as a positive control. The arrow shows the expected bands.

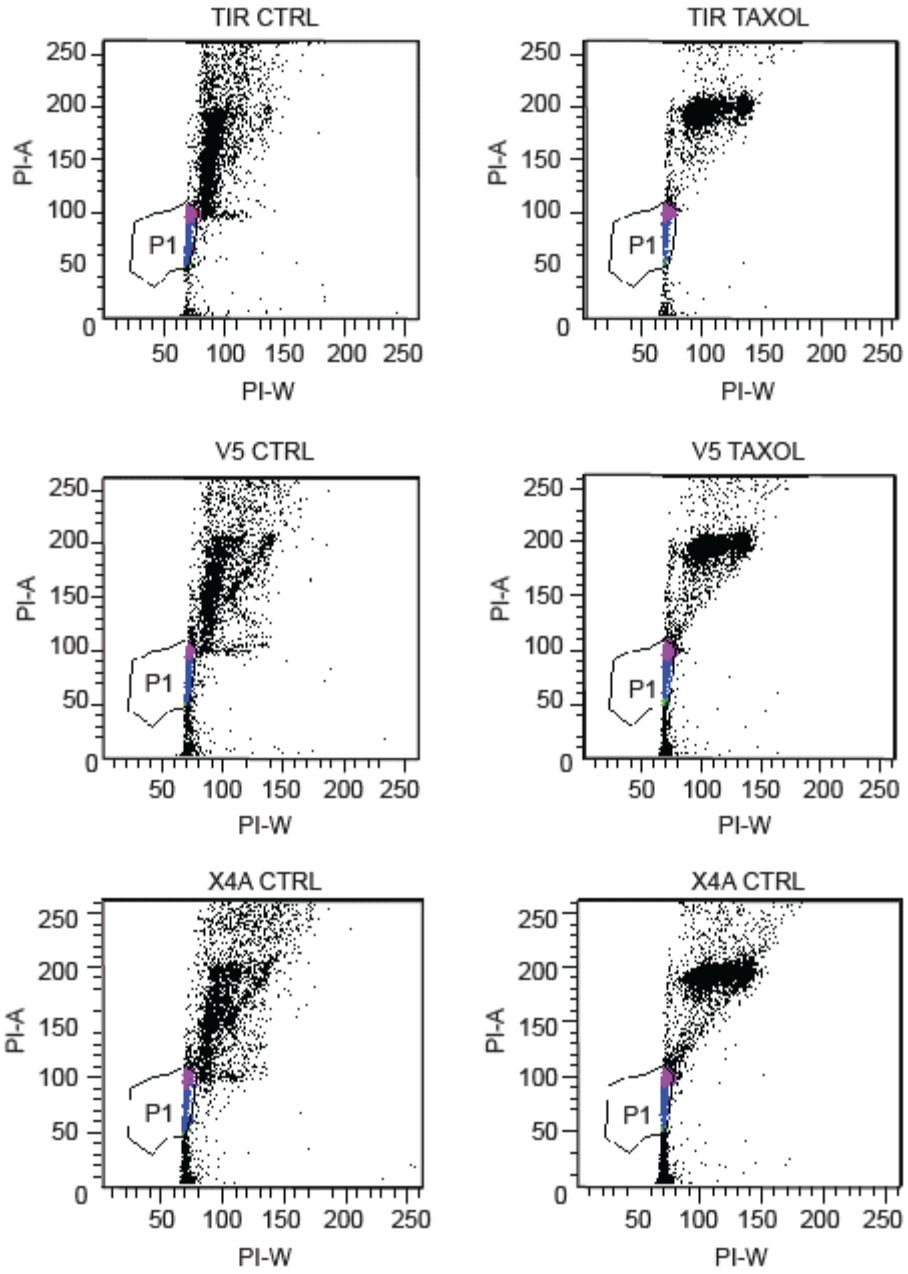

Supplementary figure 6. Selection of live, single cells for FACS analysis. Cells with varying APC expression were treated with 500µM Taxol® for 6 hours and then incubated with 20µM BrdU for 20 mins. Cells were then fixed and stained with an anti-BrdU antibody and PI. Using FACSDiva software the live cells (P1) were selected for, when PI-stained cells were visible, excluding dead cells and aggregates. This was performed for untreated (control) and Taxol® treated DT40^{TIR}, V5 and X4A cells.

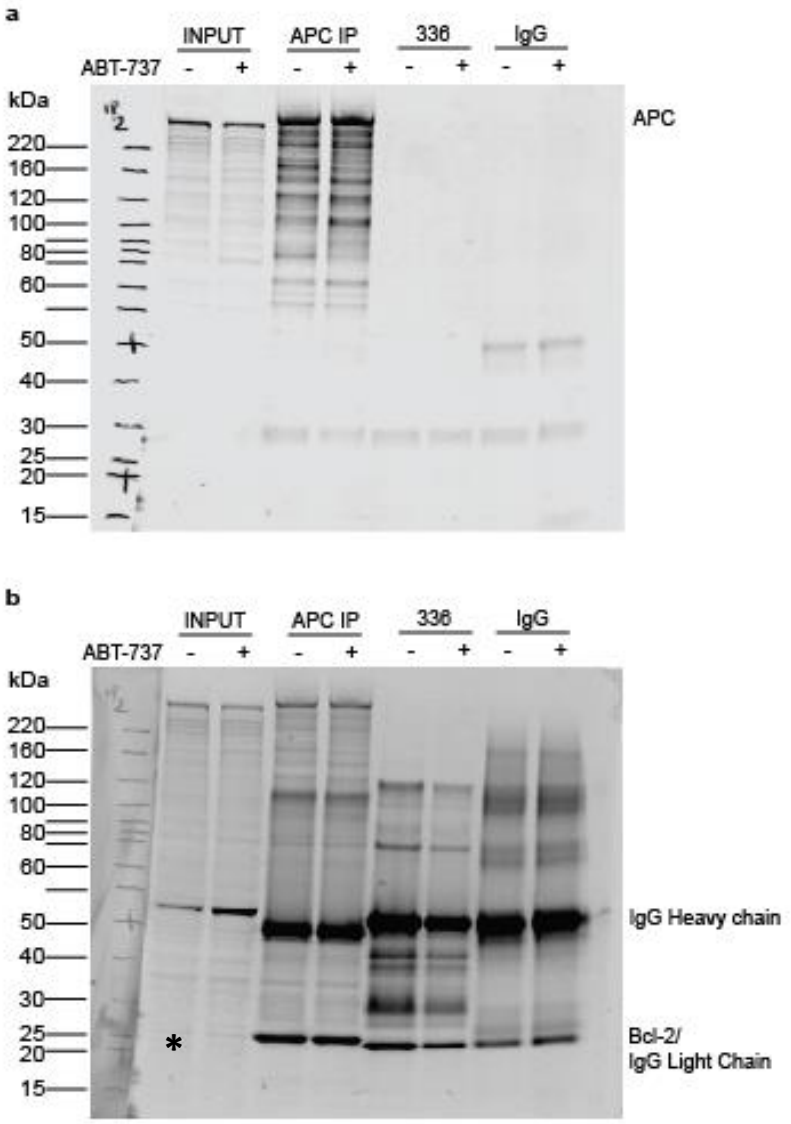

Supplementary figure 7. CoIP attempt of APC-Bcl-2. APC IP using 2mg lysate from U2OS cells treated plus or minus 7µM ABT-737. (**a**) Western blot against APC. (**b**) Western blot of APC IP (a) against Bcl-2. The faint band representing Bcl-2 in the input is marked with an asterisk immediately below it. Molecular weights in kDa are shown on the left-hand side. 336 is a negative control for the APC IP.

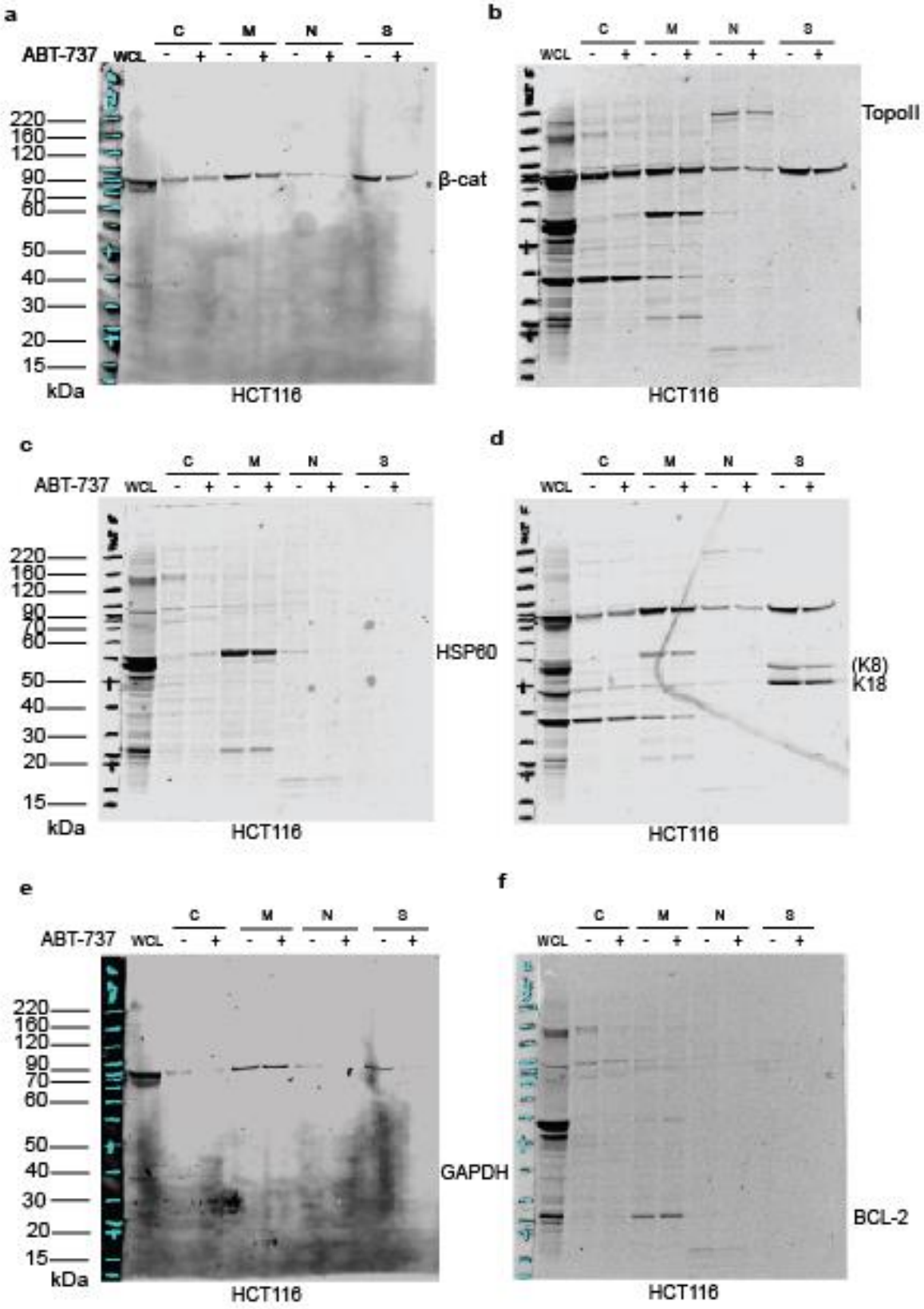
a
ABT-737
WCL
C
M
N
S
220
160
120
90
70
60
50
40
30
20
15
kDa
β-cat
HCT116
b
Topoll
HCT116
c
HSP60
HCT116
d
(K8)
K18
HCT116
e
GAPDH
HCT116
f
BCL-2
HCT116

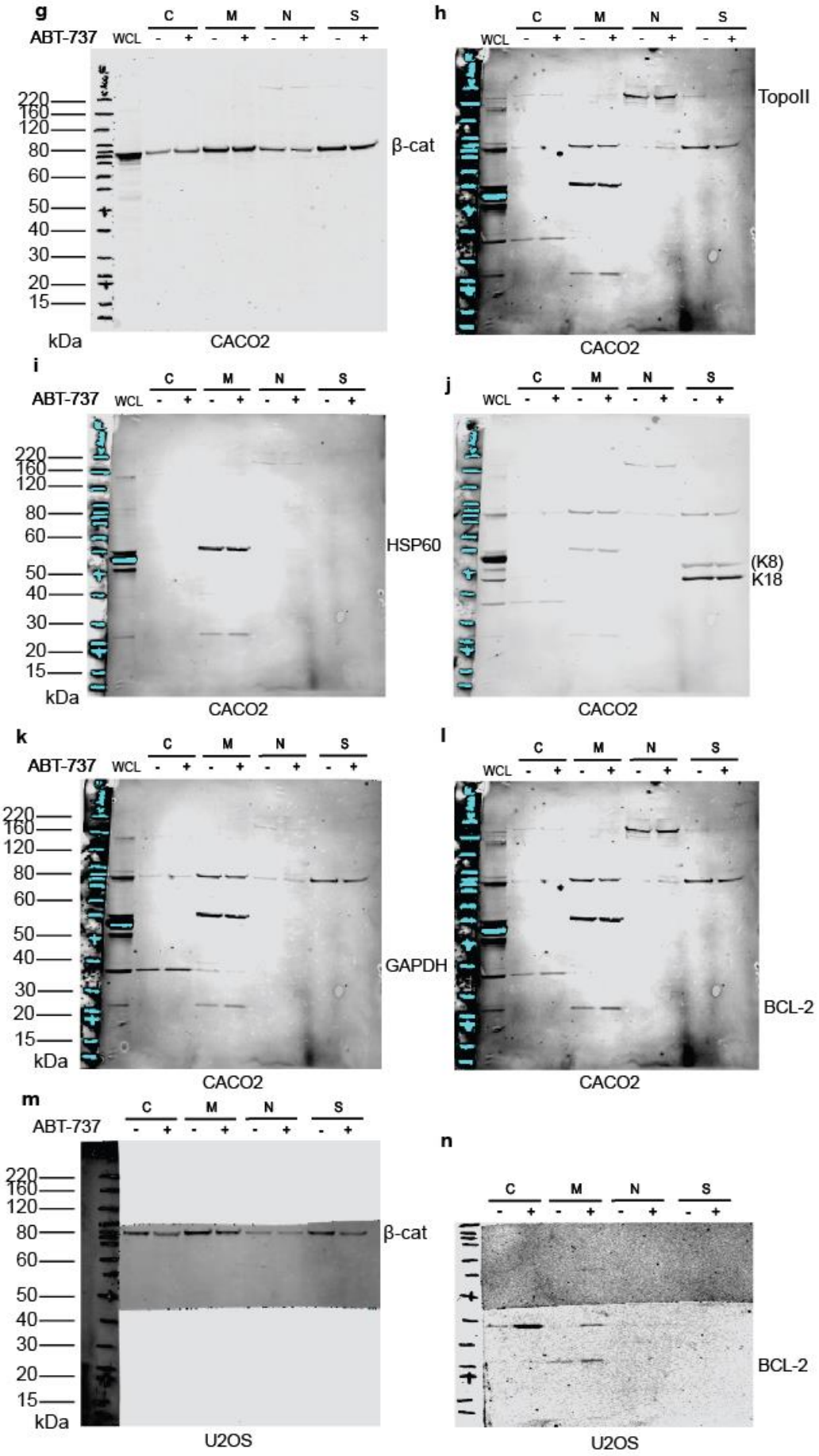
g
ABT-737
WCL
C
M
N
S
220
160
120
80
60
50
40
30
20
15
kDa
β-cat
CACO2
h
TopoII
CACO2
i
HSP60
CACO2
j
(K8)
K18
CACO2
k
GAPDH
CACO2
l
BCL-2
CACO2
m
β-cat
U2OS
n
BCL-2
U2OS

Supplemental figure 8. Fractionations show Bcl-2 increase in the membrane fraction. Cells were treated plus/or minus 7μM ABT-737 for 24 hours. The proteins were then separated into cytosol (C), membrane (M), nucleus (N) and cytoskeletal (S) fraction. Western blots show the increase in Bcl-2 in the membrane fraction as well as proteins used as markers for each fraction. Beta-catenin is a representative of a good fractionation as it is present in all fractions. (**a**) β-catenin in HCT116 cells. (**b**) Topoisomerase II in HCT116 cells. (**c**) HSP60 in HCT116 cells. (**d**) Keratin18 in HCT116 cells. The antibody also picks up keratin 8. (**e**) GAPDH in HCT116 cells. (**f**) Bcl-2 in HCT116 cells. (**g**) β-catenin in CaCo2 cells. (**h**) Topoisomerase II in CaCo2 cells. (**i**) HSP60 in CaCo2 cells. (**j**) Keratin 18 in CaCo2 cells. (**k**) GAPDH in CaCo2 cells. (**l**) Bcl-2 in CaCo2 cells. (**m**) β-catenin in U2OS cells. (**n**) Bcl-2 in U2OS cells.

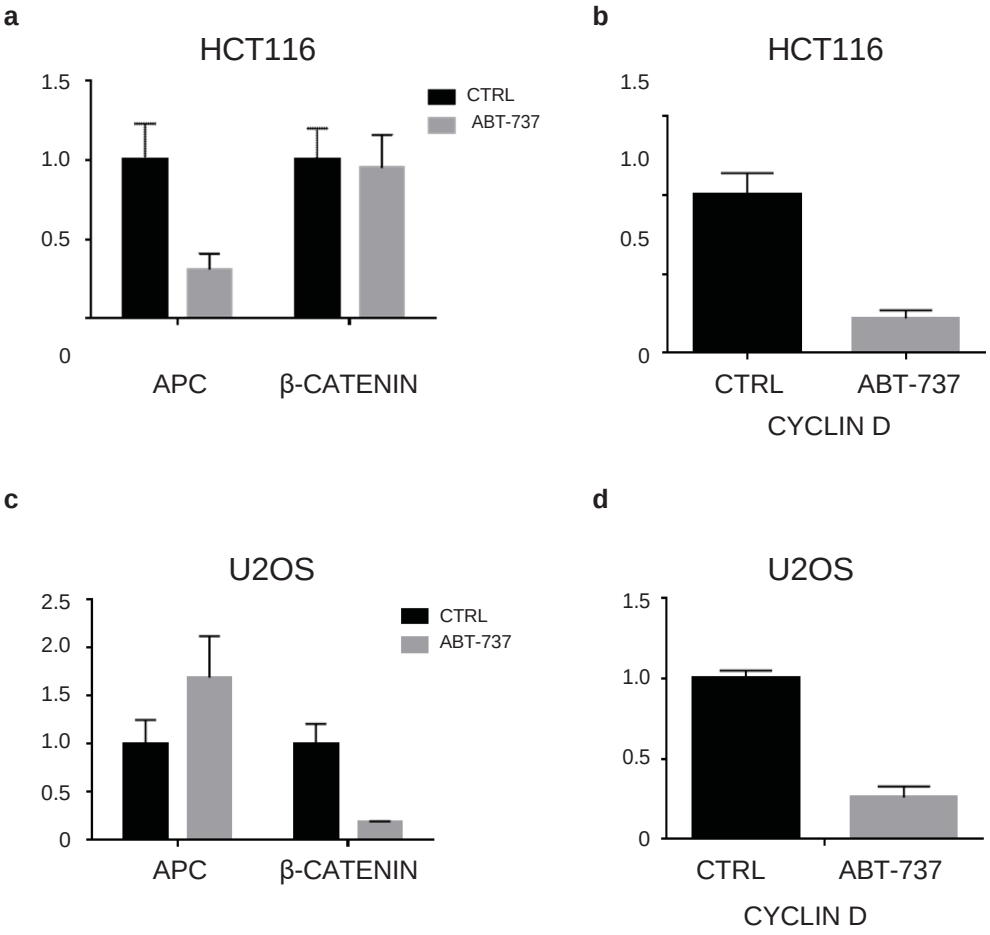

Supplemental figure 9. qRT-PCR of Wnt target gene *Cyclin D* in ABT-737 treated cells. Gene expression was normalised to *Actin* (**a**) qRT-PCR of *Apc* and *β-catenin* from HCT116 cells treated plus/minus 7μM ABT-737 for 24 hours.. (**b**) qRT-PCR of HCT116 cells treated as in (a). Beta-catenin target gene *Cyclin D*. (**c**) qRT-PCR of U2OS cells as in (a). (**d**) qRT-PCR of U2OS cells as in (b).

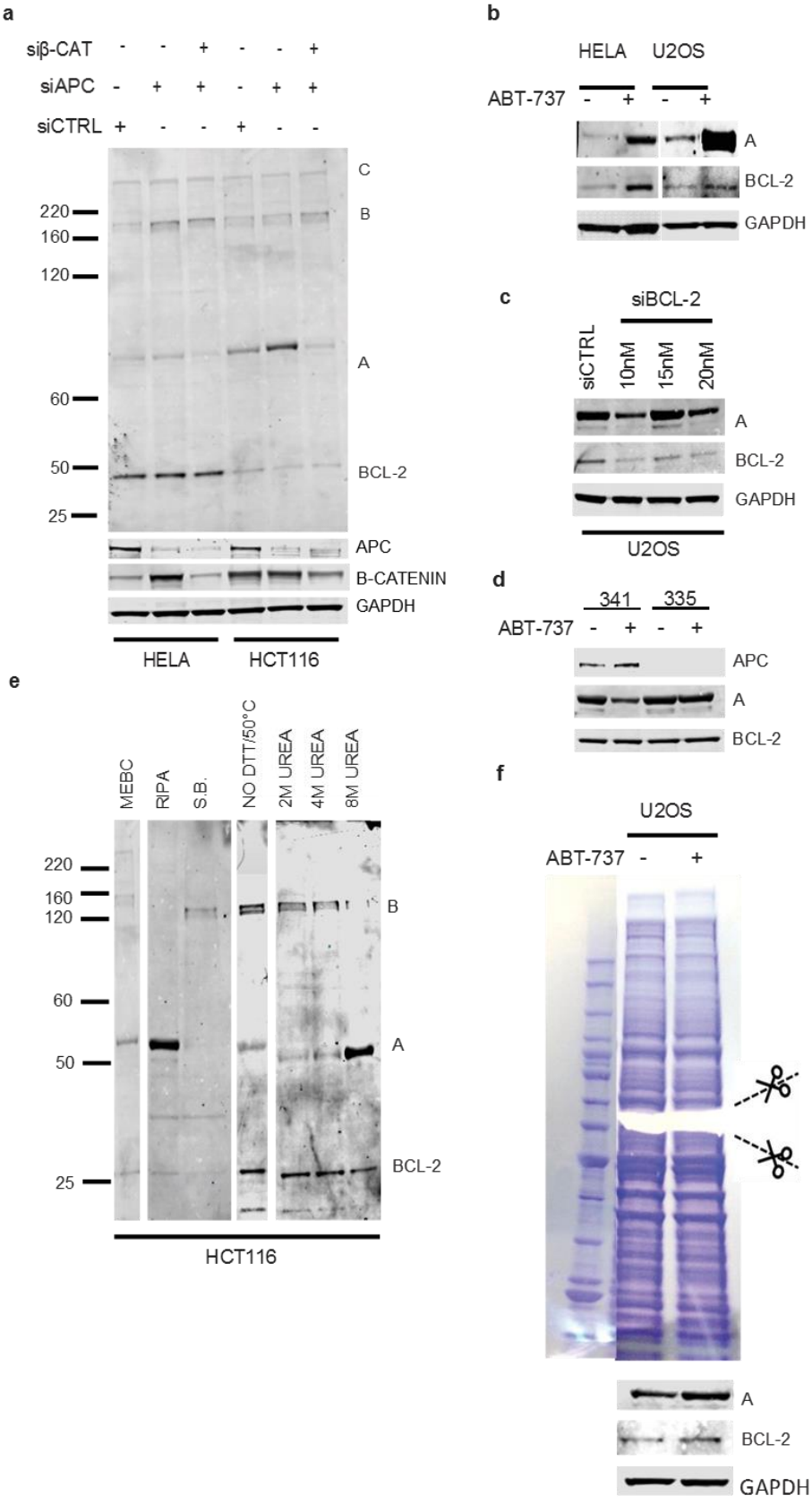
a
siβ-CAT - - + - - +
siAPC - + + - + +
siCTRL + - - + - -
220
160
120
60
50
25
C
B
A
BCL-2
APC
B-CATENIN
GAPDH
HELA
HCT116
b
HELA U2OS
ABT-737 - + - +
A
BCL-2
GAPDH
c
siBCL-2
siCTRL 10nM 15nM 20nM
A
BCL-2
GAPDH
U2OS
d
341 335
ABT-737 - + - +
APC
A
BCL-2
e
MEBC RIPA S.B. NO DTT/50°C 2M UREA 4M UREA 8M UREA
220
160
120
60
50
25
B
A
BCL-2
HCT116
f
U2OS
ABT-737 - +
A
BCL-2
GAPDH

g

SAMPLE	PROTEIN SCORE	EMPAI		
		EMPAI	EMPAI #	MOLAR %
CTRL	1. Hsp60	1. Pyruvate kinase	83.5	45.5
	2. Pyruvate kinase	2. Hsp60 *	50.8	27.6
	3. T complex	3. c14orf80	12.4	6.7
	4. Keratin 1	4. T complex *	10.1	5.5
	5. Ras GAP Binding protein 1	5. Tyrosine tRNA ligase	2.4	1.3
	6. Keratin 6A	6. Keratin 1	2.3	1.2
	7. Ribonuclear protein	7. PUF60	2.2	1.2
	8. PUF60	8. PURH	2.1	1.1
	9. DK 2	9. EH domain containing proteins	2.1	1.1
	10. eIF2A	10. HNRPL	2.0	1.1
	11. Chaperonin	11. Chaperonin containing TCP1 *	2.0	1.1
	12. PURH	12. DNAJ *	1.6	0.9
	13. Arf-GAP domain	13. Ser/thr kinase *	1.4	0.8
	14. Synembryin-A	14. Ras GTPase-activating protein-binding protein 1	1.4	0.8
	15. EH domain containing proteins	15. Highly similar to Dihydropyrimidinase -related protein 1a	1.3	0.7
	16. Tyrosine tRNA ligase	16. DK 2	1.3	0.7
	17. DNAJ	17. Synembryin-A	1.3	0.7
	18. UDP-N-c-P	18. Archain 1, isoform CRA	1.2	0.7
	19. PDI	19. Cytoplasmic dynein 1 light intermediate chain 1	1.1	0.6
	20. Ser/the kinase	20. Proteasome non-ATPase regulatory subunit 3	1.0	0.6

h

SAMPLE	PROTEIN SCORE	EMPAI		
		EMPAI	EMPAI #	MOLAR %
ABT-737	1. Hsp60	1. Pyruvate kinase	88.1	47.9
	2. Pyruvate kinase	2. Hsp60 *	48.2	26.3
	3. T complex	3. T complex *	10.6	5.8
	4. Ribonuclear protein	4. Ser/the kinase *	3.3	1.8
	5. Chaperonin	5. Keratin 1	3.2	1.7
	6. Ser/the kinase	6. Tyrosine tRNA ligase	3.0	1.6
	7. Keratin 6A	7. c14orf80	3.0	1.6
	8. Ras GAP Binding protein 1	8. DPP	2.9	1.6
	9. Synembryin-A	9. Chaperonin *	2.9	1.6
	10. DK 2	10. Heterogeneous nuclear ribonucleoprotein	2.3	1.3
	11. Tyrosine tRNA ligase	11. Asparagine synthetase	2.1	1.1
	12. Keratin 1	12. PUF60	1.8	1.0
	13. EH domain containing proteins	13. EH domain containing proteins	1.8	0.9
	14. PDI	14. UAP1	1.7	0.9
	15. eIF2A	15. Synembryin-A	1.6	0.9
	16. DNA J	16. DNAJ	1.6	0.9
	17. PUF60	17. Ras GTPase-activating protein-binding protein 1 *	1.4	0.8
	18. UDP-N-c-P	18. Adenosylhomocysteinase	1.4	0.8
	19. Apoptosis inhibitor 5	19. DK 2	1.4	0.8
	20. Regulator or chromosome condensation 2	20. NudC containing protein 1	1.4	0.7

Supplementary Figure 10. **Identifying the mystery band detected by anti-Bcl-2 (32124**). Experiments were carried out to identify the band detected by the anti-Bcl-2 antibody. (**a**) U2OS and HCT116 cells were treated with either ctrl, *Apc* or *β-catenin* siRNAs. A Western blot of the whole (uncut) membrane with anti-Bcl-2 reveals the expected band for Bcl-2 at 27kDa, but also unexpected bands A, B and C. A appears to be inversely correlated with Bcl-2 and increases upon *Apc* depletion. A is running at double the size of Bcl-2 and raised the possibility that it is a homodimer or a heterodimer of Bcl-2 family proteins. (**b**) HeLa and U2OS cells were grown plus/or minus 7μM ABT-737 for 24 hours. Western blots shows an increase in Bcl-2, but also in the unknown protein 'A'. (**c**) U2OS cells were treated with ctrl siRNA or varying concentrations of *Bcl-2* siRNA. Band 'A' decreases upon *Bcl-2* knock-down. (**d**) To determine if band 'A' was specific to epithelial cells, MEFs were cultured (see table 7) plus/or minus 7μM ABT-737 for 24 hours. Western blots reveal that band 'A' is present in fibroblasts as well, but in these cells it responds to ABT-737 differently and decreases with ABT-737. (**e**) To determine if bands A, B or C represent a complex of proteins, various protein lysing methods were used to denature any non-covalently associated complexes. A Western blot shows that boiling lysates in sample buffer (S.B.) causes band A to disappear, but there is no increase in monomeric Bcl-2, suggesting that Bcl-2 is not present in band 'A'. (**f**) Data from panels a-e suggest that band 'A' is not related to Bcl-2. Therefore mass-spectrometry was used to identify it. U2OS cells were cultured with/or without 7μM ABT-737 for 24 hours, lysed and 100μg of lysate was run on a gel and stained with Coomassie. Proteins in the molecular weight region of interest were cut out and sent for LC-MS-MS analysis. (**g, h**) Mass-spec analysis was applied to identify proteins in the control (g) and ABT-737 treated samples (h) with the aim of identifying proteins elevated in the latter that could represent band 'A' using MASCOT software. Specifically, protein scores (sum total of the number of peptides counted per protein) were compared by their emPAI scores, which represents proteins enriched in the sample based on abundance. As larger proteins can give to rise to more peptides by tryptic digestions, this can skew results in favour of larger proteins. PAI accounts for this by calculating the number of observed peptides divided by the theoretically observable peptides per protein. emPAI (10^{PAI}-1) allows the calculation of the molar fraction percentage of particular proteins, therefore a protein enriched in ABT-737 treated cells compared to untreated cells can be identified. Proteins highlighted in yellow are unique to each list. Red asterisks represent proteins involved in stress responses. It is likely that band A is a stress-related protein.

a

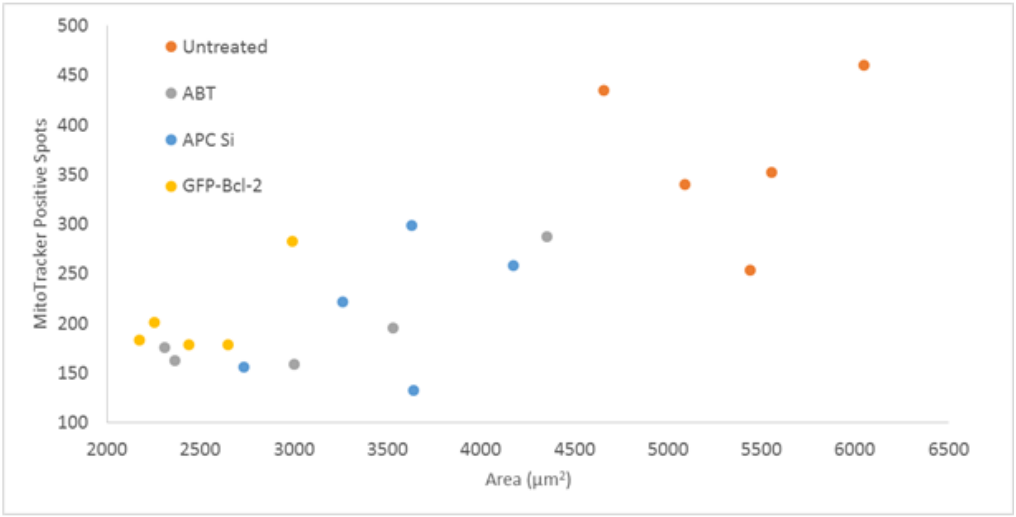

b

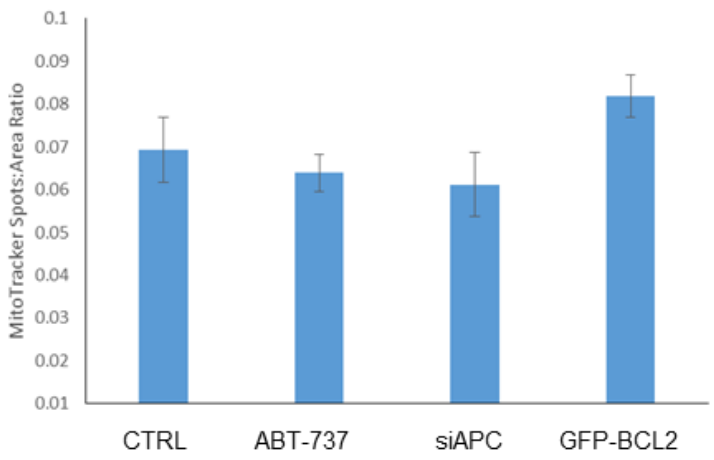

Supplemental figure 11. The effect of GFP-Bcl-2 on cell size and mitochondria. (**a**) U2OS cells were transfected with GFP-BCL-2. The cells were then cultured with MitoTracker® for 45 minutes. Mitochondria were visualised using fluorescent microscopy. Images were then imported into the microscopy software Imaris. Using fluorescence detection the number of MitoTracker®-positive spots were counted and the area of the cells were measured. 5 cells were analysed per treatment. There is a positive correlation between cell size and mitochondrial number. GFP-BCL-2 cells (yellow) are the smallest and so have the fewest mitochondria. (**b**) The number of mitochondria were divided by the area of the cell to give a ratio of MitoTracker® positive spots: area. The bar graph shows that there is no difference in mitochondrial size between treatments. Error bars represent the standard error.

References

Adams, J. M. and Cory, S. (2007). The Bcl-2 apoptotic switch in cancer development and therapy. *Oncogene.* **26**. Pp. 1324–1337.

Akao, Y., Orsuki, Y., Kataoka, S., Ito, Y. and Tsujimoto, Y. (1994). Multiple Subcellular Localization of bcl-2: Detection in Nuclear Outer Membrane, Endoplasmic Reticulum Membrane, and Mitochondrial Membranes. *Cancer Res.* **5**. Pp. 2468-2471.

Ali-Osman, F., Berger, M. S., Rajagopal, S., Spence, A. and Livingston, R. B. (1993). Topoisomerase II Inhibition and Altered Kinetics of Formation and Repair of Nitrosourea and Cisplatin-induced DNA Interstrand Cross-Links and Cytotoxicity in Human Glioblastoma Cells. *Cancer Res*. **53**. Pp. 5663-5668.

Al-Mehdi, A-B., Pastukh, V. M., Sewiger, B. M., Reed, D. J., Patel, M. R., Bardwell, G C., Pastukh, V. V., Alexeyev, M. F. and Gillespie, M. N. (2012). Perinuclear Mitochondrial Clustering Creates an Oxidant-Rich Nuclear Domain Required for Hypoxia-Induced Transcription. *Sci. Signal.* **5:231**. Doi: 10.1126/scisignal.2002712.

Baca, A. M. and Hol, W. G. J. (2000). Overcoming codon bias: A method for high-level overexpression of *Plasmodium* and other AT-rich parasite genes in *Escherichia coli. Int J Parisit.* **30:2**. Pp. 113–118.

Baeg, G. H., Matsumine, A., Kuroda, T., Bhattacharjee, R. N., Miyashiro, I., Toyoshima, K. and Akiyama, T. (1995). The tumour suppressor gene product APC blocks cell cycle

progression from G0/G1 to S phase. *EMBO*. **14:22**. Pp. 5618-25.

Balusu, R., Jaiswal, A. S., Armas, M. L., Kundu, C. N., Bloom, L. B. and Narayan, S. (2007). Structure/function analysis of the interaction of adenomatous polyposis coli with DNA polymerase beta and its implications for base excision repair. *Biochemistry.* **46:49**. Pp. 13961-74.

Barker, N. (2014). Adult intestinal stem cells: critical drivers of epithelial homeostasis and regeneration. *Nat Rev Mol Cell Biol.* **15**. *Pp.* 19–33.

Barker, N., Ridgway, R. A., van Es, J. H., van de Wetering, M., Begthel, H., van den Born, M., Danenberg, E., Clarke, A. R., Sansom, O. J. and Clevers, H. (2009). Crypt stem cells as the cells-of-origin of intestinal cancer. *Nature*. **457**. Pp. 608-611.

Behrens, J., Jerchow, B. A., Wurtele, M., Grimm, J., Asbrand, C., Wirtz, R., Kuhl, M., Wedlich, M. and Birchmeier, W. (1998). Functional interaction of an axin homolog, conductin, with beta-catenin, APC, and GSK3beta. *Science*. **280:5363**. Pp. 596-9.

Behrens, J., Von Kries, J. P., Kuhl, M., Bruhn, L., Wedlich, D., Grosschedl, R. and Birchmeier, W. (1996). Functional interaction of β-catenin with the transcription factor LEF-1. *Nature.* **382**. Pp. 638-642.

Bennett, R. A. O., Wilson III, D. M., Wond, D. and Demple, B. (1997). Interaction of human apurinic endonuclease and DNA polymerase β in the base excision repair pathway. *Proc Natl Acad Sci U S A*. **94:14**. Pp. 7166–7169.

Berrueta, L., Kraeft, S. K., Tirnauer, J. S., Schuyler, S. C., Chen, L. B., Hill, D. E., Pellman, D. and Bierer, B. E. (1998). The adenomatous polyposis coli-binding protein EB1 is associated with cytoplasmic and spindle microtubules. *Proc Natl Acad Sci U S A*. **95:18**. Pp. 10596-601.

Bertolotti, A., Zhang, Y., Hendershot, L. M., Harding, H. P. and Ron, D. (2000). Dynamic interaction of BiP and ER stress transducers in the unfolded-protein response. *Nat Cell Biol*. **2:6**. Pp. 326-32.

Bi, M., Naczki, C., Koritzinksy, M., Dels, D., Blais, J., Hu, N., Harding, H., Novoa, I., Varia, M., Raleigh, J., Scheuner, D., Kaufman, R. J., Bell, J., Ron, D., Wouters, B. G. and Koumenis, C. (2005). ER stress-regulated translation increases tolerance to extreme hypoxia and promotes tumor growth. *EMBO*. **24**. Pp. 3470-3481.

Bjerknes, M. and Cheng, H. (1981). The stem-cell zone of the small intestinal epithelium. I. Evidence from Paneth cells in the adult mouse. *Am J Anat.* **160:1***. Pp. 51-63.*

Bonnington, K. E. and Kuehn, M. J. (2014). Protein selection and export via outer membrane vesicles. *Biochim Biophys Acta.*. **1843:8**. Pp. 1612–1619.

Brocardo, M., Lei, Y., Tighe, A., Taylor, S. S., Mok, M. T. S. and Henderson, B. R. (2007). Mitochondrial Targeting of Adenomatous Polyposis Coli Protein Is Stimulated by Truncating Cancer Mutations: REGULATION OF Bcl-2 AND IMPLICATIONS FOR CELL SURVIVAL. *J Bio Chem*. **283**. Pp. 5950-5959.

Browne, S.J., Williams, A. C., Hague, A., Butt, A. J. and Paraskeva, C. (1994). Loss of APC protein expressed by human colonic epithelial cells and the appearance of a specific low-molecular-weight form is associated with apoptosis in vitro. *Int J Cancer*: **59:1**. Pp. 56-64.

Calarco, P.G. (1995). Polarization of mitochondria in the unfertilized mouse oocyte. *Dev Genet.* **16:1**. Pp. 36-43

Cheema, S. K., Mishra, S. K., Rangnekar, V. M., Tari, A. M., Kumar, R. and Lopez-Berestein, G. (2003). Par-4 Transcriptionally Regulates Bcl-2 through a WT1-binding Site on the *bcl-2*Promoter. *J Biol Chem*. **278**. Pp. 19995-20005.

Chen, B. B., Glasser, J. R., Coon, T. A., Zou, C., Miller, H. L., Fenton, M., McDyer, J. F., Boyiadzis, M. and Mallampalli, R. K. (2012). F-box protein FBXL2 targets cyclin D2 for ubiquitination and degradation to inhibit leukemic cell proliferation. *Blood*. **119:13**. Pp. 3132 – 3141.

Chen J., Young, F., Bottaro, A., Stewart, V., Smith, R. K. and Alt, F. W. (1993). Mutations of the intronic IgH enhancer and its flanking sequences differentially affect accessibility of the JH locus. *EMBO*. **12:12**. Pp. 4635-4645.

Chen, L., Willis, S. N., Wei, A., Smith, B. J., Fletcher, J. I., Hinds, M. G., Colman, P. N., Day, C. L., Adams, J. M. and Huang, D. C. S. (2005). Differential Targeting of Prosurvival Bcl-2 Proteins by Their BH3-Only Ligands Allows Complementary Apoptotic Function. *Mol Cell*. **17:3**. Pp. 393–403.

Cheng, H. and Leblond, C.P. (1974). Origin, differentiation and renewal of the four main epithelial cell types in the mouse small intestine. V. Unitarian theory of the origin of the four epithelial cell types. *Am J Anat*. **141**. Pp. 537–561.

Chonghaile, T. N., Gupta, S., John, M., Szegezdi, E., Logue, S. E. and Samali, A., (2015). BCL-2 modulates the unfolded protein response by enhancing splicing of X-box binding protein-1. *Biochim Biophys Res Commun*. **466:1**. Pp. 40-45.

Ciccia, A. and Elledge, S. J. (2009). The DNA Damage Response: Making It Safe to Play with Knives. *Mol Cell*. **40:2**. Pp. 179-204.

Clevers, H. (2013). The Intestinal Crypt, A Prototype Stem Cell Compartment. *Cell.* **154:2**. Pp. 274-284.

Cox, J. S. and Walter, P. (1996). A Novel Mechanism for Regulating Activity of a Transcription Factor That Controls the Unfolded Protein Response. *Cell*. **87:3**. Pp. 391–404.

Cox, J. S., Shamu, C. E and Walter, P. (1993). Transcriptional induction of genes encoding endoplasmic reticulum resident proteins requires a transmembrane protein kinase. *Cell*. **73**. Pp. 1197-1206.

Cristofaro, M., Contursi, A., D'Amore, S., Martelli, N., Spaziante, A. F., Moschetta, A. and Villani G. Adenomatous polyposis coli (APC-) induced apoptosis of HT29 colorectal cancer

cells depends on mitochondrial oxidative metabolism. *Biochim Biophys Acta*. **1852:9**. Pp. 1719-1728.

Czabotar, P. E., Lessene, G., Strasser, A. and Adams, J. M. (2014). Control of apoptosis by the BCL-2 protein family: implications for physiology and therapy. *Nature Rev Mol Cell Biol.* **15**. Pp. 49–63.

Czabotar, P.E., Westphal, D., Dewson, G., Ma, S., Hockings, C., Fairlie, W. D., Lee, E. F., Yao, S., Robin, A. Y., Smith, B. J., Huang, D. C. S., Kluck, R. M., Adams, J. A. and Colman, P. M. (2013). Bax Crystal Structures Reveal How BH3 Domains Activate Bax and Nucleate Its Oligomerization to Induce Apoptosis. *Cell*. **152:3**. Pp. 519–531.

D'Angiodella, V., Donata, V., Vijayakumar, S., Saraf, A., Florens, L., Washburn, M. P., Dynlacht, B. and Pagano, M. (2010). $SCF^{Cyclin\ F}$ controls centrosome homeostasis and mitotic fidelity through CP110 degradation. *Nature.* **466**. Pp. 138–142.

Damia, G., Filiberti, L., Vikhanskaya, F., Carrassa, L., Taya, Y., D'incalci, M. and Broggini, M. (2001). Cisplatinum and taxol induce different patterns of p53 phosphorylation. *Neoplasia.* **3:1** Pp. 10-6.

De Jong D., Prins, F. A., Mason, D. Y., Reed, J. C., van Ommen, G. B. and Kluin, P. M. (1994). Subcellular Localization of the bcl-2 Protein in Malignant and Normal Lymphoid Cells. *Cancer Res.* **54:1**. Pp. 256-260.

Deka, J., Kuhlmann, J. and Muller, O. (1998). A domain within the tumor suppressor protein APC shows very similar biochemical properties as the microtubule-associated protein tau. *Eur J Biochem*. **253:3**. Pp. 591-7.

Dewson, G., Kratina, T., Sim, H. W., Puthalakalth, H., Adams, J. M., Colman, P. M. and Kluck, R. M. (2008). To Trigger Apoptosis, Bak Exposes Its BH3 Domain and Homodimerizes via BH3:Groove Interactions. *Mol Cell*. **30:3**. Pp. 369–380.

Diaz, F., Menendez, M. and Andreu, J. M. (1993). Thermodynamics of ligand-induced assembly of tubulin. *Biochemistry*. **32:38**. Pp. 10067-10077.

Dikovskaya, D., Newton, I. P. and Näthke, I. S. (2004). The adenomatous polyposis coli protein is required for the formation of robust spindles formed in CSF Xenopus extracts. *Mol Biol Cell.* **15**. Pp. 2978–2991.

Dikovskaya, D., Schiffmann, D., Newton, I. P., Oakley, A., Kroboth, K., Sansom, O., Jamieson, T. J., Meniel, V., Clarke, A. and Näthke, I. S. (2007). Loss of APC induces polyploidy as a result of a combination of defects in mitosis and apoptosis. *J Cell Biol*. **176:2**. Pp. 183-195.

Draviam, V. M., Shapiro, I., Aldridge, B. and Sorger, P. K. (2006). Misorientation and reduced stretching of aligned sister kinetochores promote chromosome missegregation in EB1- or APC-depleted cells. *EMBO.* **25**. Pp. 2814-2827.

Du, C., Fang, M., Li, Y., L, L. and Wang, X. (2000). Smac, a mitochondrial protein that promotes cytochrome c-dependent caspase activation by eliminating IAP inhibition. *Cell*. **102:1**. Pp. 33-42.

Elford, H. L. (1968). Effect of hydroxyurea on ribonucleotide reductase. *Biochem Biophys Res Commun*. **33:1.** Pp. 129-35.

Ellis, G. K., Gralow, J. R., Pierce, H. I., Williams, M. A. and Livingston, R. B. (1999). Infusional paclitaxel and weekly vinorelbine chemotherapy with concurrent filgrastim for metastatic breast cancer: high complete response rate in a phase I-II study of doxorubicin-treated patients. *J Clin Oncol.* **17:5**. Pp. 1407-12.

Fodde, R., Edelmann, W., Yang, K., van Leeuwen, C., Carlson, C., Renault, B., Breukel, C., Alt, E., Lipkin, M. and Khan, P. M. (1994). A targeted chain-termination mutation in the mouse Apc gene results in multiple intestinal tumors. *Proc Natl Acad Sci U S A*. **91:19**. Pp. 8969–8973.

Fodde, R., Kuipers, J., Rosenberg, C., Smits, R., Kielman, M., Gaspar, C., van Es, J. H., Breukel, C., Wiegant, J., Giles, R. H. and Clevers, H. (2001). Mutations in the APC tumour suppressor gene cause chromosomal instability. *Nat Cell Biol.* **3**. Pp. 433–438.

Fodde, R., Smits, R. and Clevers, H. (2001). APC, signal transduction and genetic instability in colorectal cancer. *Nat. Rev. Cancer*. *1:1*. Pp. 55-67.

Franke, W. and Kartenbeck, J. (1971). Outer mitochondrial membrane continuous with endoplasmic reticulum. *Protoplasma*. **73.** Pp. 35–41.

Freeman, B. A. and Crapo, J. D. (1982). Biology of disease: free radicals and tissue injury. *Lab Invest*. **47:5**. Pp. 412-26.

Frieden, M., Dominic, J., Castelbou, C., Danckaert, A., Martinou, J-C. and Demaurex, N. (2004). Ca^{2+} Homeostasis during Mitochondrial Fragmentation and Perinuclear Clustering Induced by hFis1. *J Biol Chem*. **279**. Pp. 22704-22714.

Galluzzi, L., Blomgren, K. and Kromer, G. (2009). Mitochondrial membrane permeabilization in neuronal injury. *Nat Rev Neurosci.* **10**. Pp. 481-494.

Gerstel, L. D. U., and PHILLIPS, L.L. (1958). Segregation of synthetic amphiploids in Gossypium and Nicotiana. *Cold Spring Harbor Symposia Quant. Biol*. **23**. Pp. 225-237.

Gilkerson, R.W., De Vries, R. L. A., Lebot, P., Wikstrom, J. D., Torgyekes, E., Shirihai, O. S., Przedborski, S. and Schon, E. A. (2012). Mitochondrial autophagy in cells with mtDNA mutations results from synergistic loss of transmembrane potential and mTORC1 inhibition. *Hum Mol Genet*. **21:5**. Pp. 978-990.

Green, R. A. and Kaplan, R. B. (2003). Chromosome instability in colorectal tumor cells is associated with defects in microtubule plus-end attachments caused by a dominant mutation in APC. *J. Cell Biol.* **163**. Pp .949–961.

Griffiths, G. J., Dubrez, L., Morgan, C. P., Jones, N. A., Whitehouse, J., Corfe, B. M., Dive, C. and Hickman, J. A. (1999). Cell Damage-induced Conformational Changes of the Pro-Apoptotic Protein Bak In Vivo Precede the Onset of Apoptosis. *J Biol Chem*. **144:5**. Pp. 903-914.

Grossman, L., Riazuddin, S., Haseltine, W. A. and Lindan, C. (1979). Nucleotide excision repair of damaged DNA. *Cold Spring Harb Symp Quant Biol*. **43:2**. Pp. 947-955.

Hallmann, A., Milczarek, R., Lipinski, M., Kossowska, E., Spodnik, J. H., Wozniak, M., Wakabayashi, T. and Klimek, J. (2004). Fast perinuclear clustering of mitochondria in oxidatively stressed human choriocarcinom a cells. Folia Morphol. 63:4. Pp. 407-412.

Hans, F. and Dimitrov, S. (2001) Histone H3 Phosphorylation and cell division. *Oncogene*. **20:24**. Pp. 3021-3027.

Hao, B., Oehlmann, S., Sowa, M. E., Harper, J. W. and Pavletich, N. P. (2007). Structure of a Fbw7-Skp1-Cyclin E Complex: Multisite-Phosphorylated Substrate Recognition by SCF Ubiquitin Ligases*. Mol Cell*. **26:1**. Pp. 131–143.

Hardcastle, J. D., Balfour, T. W. and Amar, S. S. (1980). Screening for symptomless colorectal cancer by testing for occult blood in general practice. *Lancet*. **315:8172**. Pp. 791-3.

Harding, H. P., Novoa, I., Zhang, Y., Zeng, H., Wek, R., Schapira, M. and Ron, D. (2000). Regulated translation initiation controls stress-induced gene expression in mammalian cells. *Mol Cell.* **6:5**. Pp. 1099-108.

Harding, H. P. Zhang, Y, Ron, D. (1999). Protein translation and folding are coupled by an endoplasmic-reticulum-resident kinase. *Nature*. **397:6716**. Pp. 271-4.

Hart, M., Concordet, J-P., Lassot, I., Albert, I., del los Santos, R., Durand, H., Perret, C., Rubinfeld, B., Margottin F., Benarous, R. and Polakis, P. (1999). The F-box protein β-TrCP associates with phosphorylated β-catenin and regulates its activity in the cell. *Curr Biol*. **9:4**. Pp. 207–211.

Haze, K., Yoshida, H., Yanagi, H., Yura, T. and Mori, K. (1999). Mammalian transcription factor ATF6 is synthesized as a transmembrane protein and activated by proteolysis in response to endoplasmic reticulum stress. *Mol Biol Cell*. **10:11**. Pp. 3787-99.

He, T. C., Sparks, A. B., Rago, C., Hermeking, H., Zawel, L., da Costa, L. T., Morin, P. J., Vogelstein, B. and Kinzler, K. W. (1998). Identification of c-MYC as a target of the APC pathway. *Science*. **281:5382**. Pp. 1509-1512.

Henderson, B. R. (2000). Nuclear-cytoplasmic shuttling of APC regulates β-catenin subcellular localization and turnover. *Nat Cell Biol.* **2**. Pp. 653 – 660.

Hengstler, J. G., Lange, J., Kett, A., Dornhöfer, N., Meinert, R., Arand, M., Knapstein, P. G., Becker, R., Oesch, F. and Tanner, B. (1999). Contribution of c-erbB-2 and

topoisomerase IIalpha to chemoresistance in ovarian cancer. *Cancer Res*. **59:13**. Pp. 3206-14.

Hetz, C. (2012). The unfolded protein response: controlling cell fate decisions under ER stress and beyond. *Nat Rev Mol Cell Biol.* **13**. Pp. 89-102.

Hetz, C., Chevet E. and Oakes S. A. (2015). Proteostasis control by the unfolded protein response. *Nat Cell Biol*. **17**. Pp. 829–838.

Hinck, L., Nelson, W. J. and Papkoff, J. (1994). Wnt-1 modulates cell-cell adhesion in mammalian cells by stabilizing beta-catenin binding to the cell adhesion protein cadherin. *J Cell Biol*. **124:5**. Pp. 729-741.

Hirschl, D., Bayer, P. and Muller, O. (1996). Secondary structure of and armadillo repeat from the APC protein. *FEBS Lett*. **383**. Pp. 21-36.

Hockenbery, D., Nunez, G., Milliman, C., Schreiber, R. D. and Korsmeyer, S. D. (1990). Bcl-2 is an inner mitochondrial membrane protein that blocks programmed cell death. *Nature.* **348:6299**. Pp. 334-6.

Hollien, J. (2013). Evolution of the unfolded protein response. *Biochim Biophys Acta.* **1833:11**. Pp. 2458–2463.

Hollien, J., Lin, J. H., Li, H., Stevens, N., Walter, P. and Weissman, J. S. (2009). Regulated

Ire1-dependent decay of messenger RNAs in mammalian cells. *J Cell Biol*. **186:3**. Pp. 323–331.

Horvitz, H. R. (1999). Genetic control of programmed cell death in the nematode Caenorhabditis elegans. *Cancer Res*. **59:7** Suppl. Pp. 1701s-1706s.

Hoyt, M. A., Totis, A. and Roberts, T. (1991). S. cerevisiae Genes Required for Cell Cycle Arrest in Response to Loss of Microtubule Function. *Cell*. **66**. Pp. 507-517.

Hsu, J. Y., Sun, Z. W., Lix, X., Reuben, M., Tatchell, K., Bishop, D. K., Grushcow, J. M., Brame, C. J., Caldwell, J. A., Hunt, D. F., Lin, R., Smith, M. M. and Allis, C. D. (2000). Mitotic phosphorylation of histone H3 is governed by Ipl1/aurora kinase and Glc7/PP1 phosphatase in budding yeast and nematodes. *Cell*. **102:3**. Pp. 279-291.

Hu, P., Han, Z., Couvillon, A. D., Kaufman, R. J. and Exton, J. H. (2006). Autocrine Tumor Necrosis Factor Alpha Links Endoplasmic Reticulum Stress to the Membrane Death Receptor Pathway through IRE1α-Mediated NF-κB Activation and Down-Regulation of TRAF2 Expression. *Mol Cell Biol*. **26:8**. Pp. 3071–3084.

Ideka, S., Kishida, S., Yamamoto, H., Murai, H., Koyama, S. and Kikuchi, A. (1998). Axin, a negative regulator of the Wnt signaling pathway, forms a complex with GSK-3beta and beta-catenin and promotes GSK-3beta-dependent phosphorylation of beta-catenin. *EMBO*. **17:5**. Pp. 1371-84.

Jaiswal, A. S., Balusu, R., Armas, M. L., Kundu, C. N. and Narayan, S. (2006). Mechanism of adenomatous polyposis coli (APC)-mediated blockage of long-patch base excision repair. Biochemistry. **45:51**. Pp. 15903-14.

Jaiswal, A. S., Panda, H., Pampo, C. A., Siemann, D. W., Gairola, C. G., Hromas, R. and Narayan, S. (2013). Adenomatous polyposis coli-mediated accumulation of abasic DNA lesions lead to cigarette smoke condensate-induced neoplastic transformation of normal breast epithelial cells. *Neoplasia*. **15:4**. Pp. 454-60.

Johnson, L.V., Walsh, M. L. and Chen, L.B. (1980). Localization of mitochondria in living cells with rhodamine 123. *Proc. Natl. Acad. Sc. USA*. **77:2**. Pp. 990-994.

Jürgensmeier, J. M., Xie, Z., Deveraux, Q., Ellerby, L., Bredesen, D. and Reed, J. C. (1998). Bax directly induces release of cytochrome *c* from isolated mitochondria. *Proc. Natl. Acad. Sc. USA.* **95:9**. Pp. 4997–5002.

Kaplan, K. B., Burds, A. A., Swedlow, J. R., Bekir, S. S., Sorger, P. K. and Näthke, I. S. (2001). A role for the Adenomatous Polyposis Coli protein in chromosome segregation. *Nat Cell Biol.* **3**. Pp. 429–432.

Karagianni, N., Ly, M-C., Psarras, S., Chilichlia, K., Schirrmacher, V., Gounari, F. and Khazaie, K. (2005). Novel adenomatous polyposis coli gene promoter is located 40 kb upstream of the initiating methionine. *Genomics*. **85:2**. Pp. 231–2.

Kastan, M. B., Zhan, Q., El-Deiry, W. S., Carrier, F., Jacks, T., Walsh, W. V., Plunkett, B. S., Vogelstein, B. and Fornace Jr, A. J. (1992). A mammalian cell cycle checkpoint pathway utilizing p53 and GADD45 is defective in ataxia-telangiectasia. *Cell*. **71**. Pp. 587–597.

Kaufman, R. J. (2002). Orchestrating the unfolded protein response in health and disease. *J Clin Invest*. **110**. Pp. 1389–1398.

Kerr, J. F., Wyllie, A. H. and Currie, A. R. (1972). Apoptosis: a basic biological phenomenon with wide-ranging implications in tissue kinetics. *Br J Cancer*. **26:4**. Pp. 239-257.

Kim, I., Rodriquez-Enriquez, S. and Lemasters, J. J. (2007). Selective degradation of mitochondria by mitophagy. *Arch Biochem Biophys.* **462**. Pp. 245–253.

Kinzler, K. W. and Vogelstein, B. (1996). Lessons from Hereditary Colorectal Cancer. *Cell*. **87:2**. Pp. 159–170.

Kinzler, K. W., Nilbert, M C., Su, L. K., Vogelstein, B., Bryan, T. M., Levy, D. B., Smith, K. J., Preisinger, A. C., Hedge, P. and McKechnie, D. (1991). Identification of FAP locus genes from chromosome 5q21. Science. **253:5020**. Pp. 661-5.

Kita*,* K., Wittmann, T., Näthke, I. S. and Waterman-Storer, C. M. (2006). Adenomatous Polyposis Coli on Microtubule Plus Ends in Cell Extensions Can Promote Microtubule Net Growth with or without EB1. *Mol Biol Cell*. **17:5**. Pp. 2331-2345.

Kitagawa, M., Hatakeyama, S., Shirane, M., Matsumoto, M., Ishida, N. Hattori, K.,

Nakamichi, I., Kikuchi, A., Nakayama, K. and Nakayama, K. (1999). An F-box protein, FWD1, mediates ubiquitin-dependent proteolysis of beta-catenin. *EMBO*. **18:9**. Pp. 2401-10.

Klotz, D. M., Nelson, S. A., Kroboth, K., Newton, I. P., Radulescu, S., Ridgway, R. A., Sansom, O. J., Appleton, P. L. and Näthke, I. S. (2012). The microtubule poison vinorelbine kills cells independently of mitotic arrest and targets cells lacking the APC tumour suppressor more effectively. *J Cell Sci*. **125(Pt 4)**. Pp. 887-95.

Kluck, R. M., Bossy-Wetzel, E., Green, D. R. and Newmeyer, D. D. (1997). The Release of Cytochrome c from Mitochondria: A Primary Site for Bcl-2 Regulation of Apoptosis. *Science.* **275:5303**. Pp. 1132-1136.

Klungland, A. and Lindahl, T. (1997). Second pathway for completion of human DNA base excision-repair: reconstitution with purified proteins and requirement for DNase IV (FEN1). *EMBO*. **16:11**. Pp 3341-8.

Kobe, B. and Kajava, A. V. (2001). The leucine-rich repeat as a protein recognition motif. *Curr Opin Struct. Bio*. **11:6**. Pp 725–732.

Konopleva, M., Watt, J., Contractor, R., Tsao, T., Harris, D., Estrov, Z., Bornmann, W., Kantarjian, H., Viallet, J., Samudio, I. and Andreeff, M. (2008). Mechanisms of Antileukemic Activity of the Novel Bcl-2 Homology Domain-3 Mimetic GX15-070 (Obatoclax). *Can. Res.* **68:9**. Pp 3413-3420.

Korinek, V., Barker, N., Morin, P. J., van Wichen, D., de Weger, R., Kinzler, K. W., Vogelstein, B. and Clevers, H. (1997). Constitutive Transcriptional Activation by a β-Catenin-Tcf Complex in APC$^{-/-}$ Colon Carcinoma. *Science*. **275:5307**. Pp. 1784-1787.

Krajewski, S., Tanaka, S., Takayama, S., Schibler, M. J., Fenton, W. and Reed, J. C. (1993). Investigation of the subcellular distribution of the bcl-2 oncoprotein: residence in the nuclear envelope, endoplasmic reticulum, and outer mitochondrial membranes. *Cancer Res*. **53:19**. Pp. 4701-14.

Kroboth, K., Newton, I. P., Kita, K., Dikovskaya, D., Zumbrunn, J., Waterman-Storer, C. M. and Näthke, I. S. (2007). Lack of Adenomatous Polyposis Coli Protein Correlates with a Decrease in Cell Migration and Overall Changes in Microtubule Stability. *Mol Biol Cell*. **18:3**. Pp. 910-918.

Kroemer, G., El-Deiry, W. S., Golstein, P., Peter, M. E., Vaux, D., Vandenabeele, P., Zhivotovsky, B., Blagosklonny, M. V., Malorni, W., Knight, R. A., Piacentini, M., Nagata, S. and Melino, G. (2005). Classification of cell death: recommendations of the Nomenclature Committee on Cell Death. *Cell Death Differ*. **12**. Pp. 1463–1467.

Kroemer, G., Galluzzi, L., Vandenabeele, P., Abrams, J., Alnemri, E. S., Baehrecke, E. H., Blagosklonny, M. V., El-Deiry, W. S., Golstein, P., Green, D. R., Hengartner, M., Knight, R. A., Kumar, S., Lipton, S. A., Malorni, W., Nunez, G., Peter, M. E., Tschopp, J., Yuan, J., Piacentini, M., Zhivotovsky, B. and Melino, G. (2009). Classification of cell death: recommendations of the Nomenclature Committee on Cell Death 2009. *Cell Death Differ*. **16**. Pp. 3–11.

Kubota, Y., Nash, R. A., Klungland, A., Schar, P., Barnes, D. E. and Lindahl, T. (1996). Reconstitution of DNA base excision-repair with purified human proteins: interaction between DNA polymerase and the XRCC1 protein. *EMBO*. **15:23**. Pp 6662-6670.

Lallemand, Y., Luria, V., Haffner-Krausz, R. and Lonai, P. (1998). Maternally expressed PGK-Cre transgene as a tool for early and uniform activation of the Cre site-specific recombinase. *Transgenic Res*. **2**. Pp. 105-12.

Latres, E., Chjaur, D. S. and Pagano, M. (1999). The human F box protein beta-Trcp associates with the Cul1/Skp1 complex and regulates the stability of beta-catenin. *Oncogene*. **18:4**. Pp. 849-54.

Lee, E., Salic, A., Kruger, R., Heinrich, R. and Kirschner, M. W. (2003). The roles of APC and Axin derived from experimental and theoretical analysis of the Wnt pathway. *PLoS Biol.* **1**. DOI: 10.1371/journal.pbio.0000010.

Lee, H-C., Yin, P-H., Lu, C-Y., Chi, C-W. and Wei, W-H. (2000). Increase in mitochondria

and mitochondrial DNA in response to oxidative stress in human cells. *Biochem J.* **348:2.** Pp. 425-432.

Lee, J. M., Lee, J. S., Kim, H., Kim, K., Park, H., Kim, J-Y., Lee, S. H., Kim, I. S., Kim, J., Lee, M., Chung, C. H., Seo, S-B., Yoon, J-B., Ko, E., Noh, D-Y., Jim, K. I. and Baek, S. H. (2012). EZH2 Generates a Methyl Degron that Is Recognized by the DCAF1/DDB1/CUL4 E3 Ubiquitin Ligase Complex. *Mol Cell*. **48:4**. Pp. 572–586.

Lee, K., Tirasophon, W., Shen, X., Michalak, M., Prywes, R., Okada, T., Yoshida, H., Mori, K. and Kaufman, R. J. (2002). IRE1-mediated unconventional mRNA splicing and S2P-mediated ATF6 cleavage merge to regulate XBP1 in signaling the unfolded protein response. *Genes Dev*. **16**. Pp. 452-466.

Leibowitz, B., Qiu, W., Buchanan, M. E., Zou, F., Vernon, P., Moyer, M. P., Yin, Q. M., Schoen, R. E., Yu, J. and Zhang, L. (2014). BID mediates selective killing of APC-deficient cells in intestinal tumor suppression by nonsteroidal anti-inflammatory drugs. *Proc Natl Acad Sci U S A*. **111:46**. Pp. 16520-16525.

Letai, A., Bassik, M. C., Walensky, L. D., Sorcinelli, M. D., Weiler, S. and Korsmeyer, S. J. (2002). Distinct BH3 domains either sensitize or activate mitochondrial apoptosis, serving as prototype cancer therapeutics. *Cancer Cell*. **2:3**. Pp. 183–192.

Li, H., Zhu, H., Xu, C-J. and Yuan, J. (1998). Cleavage of BID by Caspase 8 Mediates the Mitochondrial Damage in the Fas Pathway of Apoptosis. *Cell*. **94**. Pp. 491–501.

Liao, P-C., Tan, S-K., Lieu, C-H. and Jung, H-K. (2008). Involvement of endoplasmic

reticulum in paclitaxel-induced apoptosis. *J Cell Biochem*. **104:4**. Pp. 1509–1523.

Lindahl, T. (1974). An N-Glycosidase from Escherichia coli That Releases Free Uracil from DNA Containing Deaminated Cytosine Residues. *Proc Natl Acad Sci U S A*. **71:9**. Pp 3649–365.

Lithgow, T., van Driel, R., Bertram, J. F. and Strasser, A. (1994). The protein product of the oncogene bcl-2 is a component of the nuclear envelope, the endoplasmic reticulum, and the outer mitochondrial membrane. *Cell Growth Differ*. **5:4**. Pp. 411-7.

Liu, C. Y., Schroder, M. and Kaufman, R. J. (2000). Ligand-independent dimerization activates the stress response kinases IRE1 and PERK in the lumen of the endoplasmic reticulum. *J Biol Chem.* **275:32**. Pp. 24881-5.

Liu, C., Li, Y., Semenov, M., Han, C., Baeg, C-H., Tan, Y., Zhang, Z., Lin, X. and He, X. (2002). Control of β-Catenin Phosphorylation/Degradation by a Dual-Kinase Mechanism. *Cell*. **108**. Pp. 837–847.

Liu, J., Xing, Y., Hinds, T. R., Zheng, J. and Xu, W. (2006). The third 20 amino acid repeat is the tightest binding site of APC for beta-catenin. *J Mol Biol*. **360**. Pp. 133-144.

Lobert, S., Vulevic, B. and Correia, J. J. (1996). Interaction of Vinca Alkaloids with Tubulin: A Comparison of Vinblastine, Vincristine, and Vinorelbine. *Biochemistry*. ***35*:21**. Pp. 6806–6814.

Longely, M. J., Pierce, A. J. and Modrich, P. (1997). DNA Polymerase d Is Required for

Human Mismatch Repair in Vitro. *J Biol Chem*. **272:16**. Pp 10917–10921.

Luo, X., Budihardjo, I., Zuo, H., Slaughter, C. and Wang, X. (1998). Bid, a Bcl2 Interacting Protein, Mediates Cytochrome c Release from Mitochondria in Response to Activation of Cell Surface Death Receptors. *Cell*. **94**. Pp. 481–490.

Lupardus, P.J., Shen, A., Bogyo, M. and Gargia, K. C. (2008). Small Molecule-Induced Allosteric Activation of the *Vibrio cholerae* RTX Cysteine Protease Domain. *Science*. **322: 5899**. Pp. 265-268.

Marciniak, S. J., Yun, C. Y., Oyadomari, S., Novoa, I., Zhang, Y., Jungreis, R., Nagata, K., Harding, H. P. and Ron, D. (2004). CHOP induces death by promoting protein synthesis and oxidation in the stressed endoplasmic reticulum. *Genes Dev*. **18**. Pp. 3066-3077.

Marshall, T. W., Lloyd, I. E., Delalande, J. M., Näthke, I. S. and Rosenblatt, J. (2011). The tumor suppressor adenomatous polyposis coli controls the direction in which a cell extrudes from an epithelium. *Mol Biol Cell*. **22:21**. Pp. 3962-70.

Matsumine, A., Ogai, A., Senda, T., Okumara, N., Satoh, K., Baeg, G-H., Kawahara, T., Kobayashi, S., Okada, M., Toyoshima, K. and Akiyama, T. (1996). Binding of APC to the Human Homolog of the *Drosophila* Discs Large Tumor Suppressor Protein. *Science*. **272:5624**. Pp. 1020-1023.

McDonnell, T. J., Deane, N., Platt, F. M., Nunez, G., Jaeger, U., McKearn, J. P. and Korsmeyer, S. J. (1989). *bcl*-2-Immunoglobulin transgenic mice demonstrate extended B

cell survival and follicular lymphoproliferation. *Cell*. **57:1**. P.p 79–88.

Mendez, A. S., Alfaro, J., Morales-Soto, M. A., Dar, A. C., McCullagh, E., Gotthardt, K., Li, H., Acosta-Alvear, D., Sidrauski, C., Korrenykh, A. V., Shokat, K. M and Water, P. (2015). Endoplasmic reticulum stress-independent activation of unfolded protein response kinases by a small molecule ATP-mimic. *eLife*. **4**:e05434.

Méniel, V., Megges, M., Young, M. A., Cole, A., Sansom, O. J. and Clarke, A. R. (2015). Apc and p53 interaction in DNA damage and genomic instability in hepatocytes. *Oncogene.* **34**. Pp. 4118–4129.

Merino, D., Khaw, S. L., Glaser, S. P., Anderson, D. J., Belmont, L. D., Wong, C., Yue, P., Robati, M., Phipson, B., Fairlie, W. D., Lee, E. F., Campbell, K. J., Vandenberg, C. J., Cory, S., Roberts, A. W., Ludlam, M. J. C., Huang, D. C. S., Bouillet, P. (2012). Bcl-2, Bcl-x_L, and Bcl-w are not equivalent targets of ABT-737 and navitoclax (ABT-263) in lymphoid and leukemic cells. *Blood*. **119:24**. Pp. 5807-5816.

Mimori-Kiyosue, Y., Shiina, N. and Tsukita, S. (2000). Adenomatous polyposis coli (APC) protein moves along microtubules and concentrates at their growing ends in epithelial cells. *J Cell Biol.* **148:3**. Pp. 505-18.

Mironov, S. L., Ivannikov, M. V. and Johansson, M. (2004). [Ca^{2+}]*i* Signaling between Mitochondria and Endoplasmic Reticulum in Neurons Is Regulated by Microtubules FROM MITOCHONDRIAL PERMEABILITY TRANSITION PORE TO Ca^{2+}-INDUCED Ca^{2+}RELEASE. *J Biol Chem*. **280**. Pp. 715-721.

Mogensen, M. M., Tucker, J. B., Mackie, J. B., Prescott, A. R. and Näthke, I. S. (2002). The adenomatous polyposis coli protein unambiguously localizes to microtubule plus ends and is involved in establishing parallel arrays of microtubule bundles in highly polarized epithelial cells. *J Cell Biol.* **157:6**. Pp. 1041-1048.

Mori, Y., Nagse, H., Ando, H., Horii, A., Ichii, S., Nakatsuru, S., Aoki, T., Miki, Y., Mori, T. and Nakamura, Y. (1992). Somatic mutations of the *APC* gene in colorectal tumors: mutation cluster region in the *APC* gene. *Hum Mol Genet*. **1:4**. Pp. 229-233.

Morin, P. J., Vogelstein, B. and Kinzler, K. W. (1996). Apoptosis and APC in colorectal tumorigenesis. *Proc Natl Acad Sci U S A*. **93:15**. Pp. 7950–7954.

Moseley, J. B., Bartolini, F., Okada, K., Wen, Y., Gundersen, G. G. and Goode, B. L. (2007). Regulated Binding of Adenomatous Polyposis Coli Protein to Actin. *J Biol Chem.* **282**. Pp. 12661-12668.

Muhua, L., Adames, N. R., Murphy, M. D., Shields, C. R. and Cooper, J. A. (1998). A cytokinesis checkpoint requiring the yeast homologue of an APC-binding protein. *Nature*. **393:6684**. Pp. 487-91.

Munemitsu, S., Souza, B., Muller, O., Albert, I., Rubinfeld, B. and Polakis, P. (1994). The APC gene product associates with microtubules in vivo and promotes their assembly in vitro. *Cancer Res*. **54:14**. Pp. 3676-81.

Muños, J. P., Ivanova, S., Sánchez-Wandelmer, J., Martinez-Cristóbal, P., Noguera, E.,

Sancho, A., Diaz-Ramos, A., Hernández-Alvarez, M. I., Sebastián, D., Mauvezin, C., Palacin, M. and Zorzano, A. (2013). Mfn2 modulates the UPR and mitochondrial function via repression of PERK. *EMBO*. **32**. Pp. 2348-2361.

Nagawa, T., Zhu, H., Morishima, N., Li, E., Xu, J., Yankner, B. A. and Yuan, J. (2000). Caspase-12 mediates endoplasmic-reticulum-specific apoptosis and cytotoxicity by amyloid-β. *Nature.* **403**. Pp. 98-103.

Nakamura, T., Hamada, F., Ishidate, T., Anai, K-I., Kawahara, K., Toyoshima, K. and Akiyama, T. (1998). Axin, an inhibitor of the Wnt signalling pathway, interacts with β-catenin, GSK-3β and APC and reduces the β-catenin level. *Genes Cells*. **3:6**. Pp. 395–403.

Narayan, S. and Jaiswal, A.S. (1997). Activation of adenomatous polyposis coli (APC) gene expression by the DNA-alkylating agent N-methyl-N'-nitro-N-nitrosoguanidine requires p53. *J Biol Chem*. **272:49**. Pp. 30619-22.

Narayan, S., Jaiswal, A. S. and Balusu, R. (2005). Tumor Suppressor APC Blocks DNA Polymerase-dependent Strand Displacement Synthesis during Long Patch but Not Short Patch Base Excision Repair and Increases Sensitivity to Methylmethane Sulfonate. *J Biol Chem*. **280:8**. Pp. 6942–6949.

Nash, P., Tang, X., Orlicky, S., Chen, Q., Gertler, F. B., Mendenhall, M. D., Sicheri, F., Pawson, T. and Myers, M. (2001). Multisite phosphorylation of a CDK inhibitor sets a threshold for the onset of DNA replication. *Nature*. **414:6863**. Pp. 514-21.

Nelson, S. A., Li, Z., Newton, I. P., Fraser, D., Milne, R. E., Martin, D. M., Schiffmann. D., Yang, X., Dormann, D., Weijer, C. J., Appleton, P. L. and Näthke, I. S. (2012). Tumorigenic fragments of APC cause dominant defects in directional cell migration in multiple model systems. *Dis Model Mech*. **5**. Pp. 940-947.

Nelson, S. and Näthke, I.S., (2013). Interactions and functions of the adenomatous polyposis coli (APC) protein at a glance. *J Cell Sci*. **126**. Pp. 873-877.

Neufeld, K. L. and White, R. L. (1997). Nuclear and cytoplasmic localizations of the adenomatous polyposis coli protein. *Proc Natl Acad Sci U S A*. **94:7**. Pp. 3034-9.

Neufeld, K. L., Nix, D. A., Bogerd, H., Kang, Y., Beckerle, M. C., Cullen, B. R. and White, R. L. (2000). Adenomatous polyposis coli protein contains two nuclear export signals and shuttles between the nucleus and cytoplasm. *Proc. Natl. Acad. Sc. USA.* **97:22**. Pp. 12085–12090.

Newton, I. P., Kenneth, N. S., Appleton, P. L., Näthke, I. S. and Rocha, S. (2010). Adenomatous polyposis coli and hypoxia-inducible factor-1{alpha} have an antagonistic connection. *Mol Biol Cell*. **21:21**. Pp. 3630-3638.

Nguyen, M., Millar, D. G., Yong, V. W., Korsmeyer, S. J. and Shore, G. C. (1993). Targeting of Bcl-2 to the mitochondrial outer membrane by a COOH-terminal signal anchor sequence. *J Biol Chem*. **268**. Pp. 25265-25268.

Nikawa, J. and Yamashita, S. (1992). IRE1 encodes a putative protein kinase containing a

membrane-spanning domain and is required for inositol phototrophy in *Saccharomyces cerevisiae. Mol Microbiol*. **6**. Pp. 1441-1446.

Nishimura, K., Fukagawa, T., Takisawa, H., Kakimoto, T. and Kanemaki, M. (2009). An auxin-based degron system for the rapid depletion of proteins in nonplant cells. *Nat Methods*. **6:12**. Pp. 917-923.

Oltersdorf, T., Elmore, S. W., Shoemaker, A. R., Armstrong, R. C., Augeri, D. J., Belli, B. A., Bruncko, M., Deckwerth, T. L., Dinges, J., Hajduk, P. J., Joseph, M. K., Kitada, S., Korsmeyer, S. J., Kunzer, A. R., Letai, A., Li, C., Mitten, M. J., Nettesheim, D. G., Ng, S., Nimmer, P. M., O'Connor, J. M., Oleksijew, A., Petros, A. M., Reed, J. C., Tahir, S. K., Thompson, C. B., Tomaselli, K. J., Wang, B., Wendt, M, D., Zhang, H., Fesik, S. W. and Rosenberg, S. H. (2005). An inhibitor of Bcl-2 family proteins induces regression of solid tumours. *Nature*. **435:7042**. Pp. 677-81.

Oltvai, Z. N., Milliman, C. L. and Korsmeyer, S. J. (1993). Bcl-2 Heterodimerizes In Vivo with a Conserved Homolog, Bax, That Accelerates Programed Cell Death. *Cell*. **74:4**. Pp. 609-619.

Oshima, M., Oshima, H., Kitagawa, K., Kobayashi, M., Itakura, C. and Taketo, M. (1995). Loss of Apc heterozygosity and abnormal tissue building in nascent intestinal polyps in mice carrying a truncated Apc gene. *Proc. Natl. Acad. Sci. USA*. **92**. Pp. 4482-4486.

Penman, G. A., Leung, L. and Näthke, I. S. (2005). The adenomatous polyposis coli protein (APC) exists in two distinct soluble complexes with different functions. *J Cell Sci*. **118:20.** Pp. 4741-50.

Perez-Galan, P., Roue, G., Lopez-Guerra, M., Nguyen, M., Villamor, N., Montserrat, E., Shore, G. C., Campo, E. and Colomer, D. (2008). BCL-2 phosphorylation modulates sensitivity to the BH3 mimetic GX15-070 (Obatoclax) and reduces its synergistic interaction with bortezomib in chronic lymphocytic leukemia cells. *Leukemia*. **22:9**. Pp 1712-20.

Petros, A. M., Medek, A., Nettesheim, D. G., Kim, D. H., Yoon, H. S., Swift, K., Matayoshi, E. D., Oltersdorf, T. and Fesik, S. W. (2001). Solution structure of the antiapoptotic protein bcl-2. *Proc Natl Acad Sci U S A*. **9:6**. Pp. 3012–3017.

Polakis, P. (2012). Wnt signaling in cancer. *Cold Spring Harb Perspect Biol*. **4:5**. Doi: 10.1101/cshperspect.a008052.

Porter, E.M., Bevins, C.L., Ghosh, D. and Ganz, T. (2002). The multifaceted Paneth cell. *Cell Mol Life Sci*. **59**. Pp. 156–170.

Potten, C. S. and Loeffler, M. (1990). Stem cells: attributes, cycles, spirals, pitfalls and uncertainties Lessons for and from the Crypt. *Development*. **110** .Pp. 1001-1020.

Quintana, A., Schwarz, E. C., Schwindling, C., Lipp, P., Kaestner, L. and Hoth, M. (2006). Sustained Activity of Calcium Release-activated Calcium Channels Requires Translocation of Mitochondria to the Plasma Membrane. *J Biol Chem*. **281**. Pp 40302-40309.

Radulescu, S., Ridgway, R. A., Appleton, A., Kroboth, K., Patel, S., Woodgett, J., Taylor, S., Nathke, I. S. and Sansom, O. J. (2010). Defining the role of APC in the mitotic spindle

checkpoint in vivo: APC-deficient cells are resistant to Taxol. *Oncogene*. **29:49**. Pp 6418-27.

Rafelski, S. M., Viana, M. P., Zhang, Y., Chan, Y-H. M., Thorn, K. S., Yam, P., Fung, J. C., Li, H., Costa, L da F. and Marshall, W. F. (2012). Mitochondrial Network Size Scaling in Budding Yeast. *Science*. **338:6108**. Pp. 822-824.

Rao, R. V., Hermel, E., Castro-Obregon, S., del Rio, G., Ellerby, L. M., Ellerby, H. M. and Bredesen, D. E. (2001). Coupling Endoplasmic Reticulum Stress to the Cell Death Program: MECHANISM OF CASPASE ACTIVATION. *J Biol Chem*. **276**. Pp. 33869-33874.

Rao, S., Krauss, N. E., Heerding, J. M., Swindell, C. S., Ringel, I., Orr, G. A. and Horwitz, S. B. (1994). 3'-(p-azidobenzamido)taxol photolabels the N-terminal 31 amino acids of beta-tubulin. *J Biol Chem*. **269:5**. Pp. 3132-3134.

Reed, E. (1998). Platinum-DNA adduct, nucleotide excision repair and platinum based anti-cancer chemotherapy. *Cancer Treat Rev*. **24:5**. Pp. 331-44.

Rohlin, A., Engwall, Y., Fritzell, K., Göransson, K., Bergsten, A., Einbeigi, Z., Nilbert, M., Karlsson, P., Björk, J. and Nordling, M. (2011). Inactivation of promoter 1B of APC causes partial gene silencing: evidence for a significant role of the promoter in regulation and causative of familial adenomatous polyposis. *Oncogene*. **30:50**. Pp. 4977-89.

Rouschop, K. M., van den Beucken, T., Dubois, L., Niessen, H., Bussink, J., Savelkouls, J., Keulers, T., Mujcic, H., Landuyt, W., Vonckem J. W., Lambin, P., van der Kogel, A. J.,

Koritzinsky, M. and Wouters, B. G. (2009). The unfolded protein response protects human tumor cells during hypoxia through regulat ion of the autophagy genes MAP1LC3B and ATG5. *J Clin Invest*. **120:1**. Pp. 127-141.

Rouse, J. and Jackson, S. P. (2002). Interfaces between the detection, signaling, and repair of DNA damage*. Science.* **297:5581**. Pp. 547-51.

Rowan, A. J., Lamlum, H., Ilyas, M., Wheeler, J., Straub, J., Papadopoulou, A., Bicknell, D., Bodmer, W. F. and Tomlinson, I. P. M. (2000). APC mutations in sporadic colorectal tumors: A mutational ‘‘hotspot’’ and interdependence of the ‘‘two hits’’*. Proc Natl Acad Sci U S A.* **97:7**. Pp. 3352-3357.

Rubinfeld, B., Albert, I., Porfiri, E., Fiol, C., Munemitsu, S. and Polakis, P. (1996). Binding of GSK3β to the APC-β-Catenin Complex and Regulation of Complex Assembly. *Science*. **272:5264**. Pp. 1023-1026.

Rubinfeld, B., Souza, B., Albert, I., Muller, O., Chamberlain, S.H., Masiarz, F.R., Munemitsu, S. and Polakis, P. (1993). Association of the APC gene product with beta-catenin. *Science.* **262:5140**. Pp. 1731–1734.

Rubinfeld, B., Tice, D. A. and Polakis, P. (2001). Axin-dependent phosphorylation of the Adenomatous Polyposis Coli protein mediated by casein kinase 1ϵ. *J Biol Chem*. **276**. Pp. 39037–39045.

Ryan, J. A., Brunelle, J. K. and Letai, A. (2010). Heightened mitochondrial priming is the basis for apoptotic hypersensitivity of CD4+ CD8+ thymocytes. *Proc. Natl Acad. Sci. USA.* **107**. Pp. 12895–12900.

Santoro, I. M. and Groden, J. (1997). Alternative splicing of the APC gene and its association with terminal differentiation. *Cancer Res*. **57:3**. Pp. 488-94.

Sato, T., Vries, R. G., Snippert, H. J., van de Wetering, M., Barker, N., Stange, D. E., van Es, J. H., Abo, A., Kujala, P., Peters, P.J. and Clevers, H. (2009). Single Lgr5 stem cells build crypt–villus structures in vitro without a mesenchymal niche. *Nature*. **459:7244**. Pp. 262-5

Schendel, S. L., Montal, M. and Reed, J. C. (1998). Bcl-2 family proteins as ion-channels. *Cell Death Differ*. **5**. Pp. 372-380.

Schendel, S. L., Xie, Z., Montal, M. O., Matsuyama, S., Montal, M. and Reed, J. C. (1997). Channel formation by antiapoptotic protein Bcl-2. *Proc. Natl. Acad. Sci. USA.* **94**. Pp. 5113–5118.

Schiff, P. B., Fant, J. and Horwitz, S. B. (1979). Promotion of microtubule assembly in vitro by taxol. *Nature.* **277:2598**. Pp. 665-667.

Schiff, P. B. and Horwitz, S. B. (1980). Taxol stabilizes microtubules in mouse fibroblast cells. *Proc Natl Acad Sci U S A*. 77. Pp. 1561–1565.

Schindelin, J., Arganda-Carreras, I., Frise, E., Kaynig, V., Longair, M., Pietzsch, T., Preibisch, S., Rueden, C., Saalfeld, S., Schmid, B., Tinevez, J. Y., White, D. J., Hartenstein, V., Eliceiri, K., Tomancak, P. and Cardona, A. (2012). Fiji: an open-source platform for biological-image analysis. *Nat Methods.* **9:7**. Pp. 676-82.

Schindler, A. J. and Schekman, R. (2009). In vitro reconstitution of ER-stress induced ATF6 transport in COPII vesicles. *Proc Natl Acad Sci U S A*. **106:42**. Pp. 17775-80.

Schlesinger, P. H., Gross, A., Yin, X. M., Yamamoto, K., Saito, M., Waksman, G. and Korsmeter, S. J. (1997). Comparison of the ion channel characteristics of proapoptotic BAX and antiapoptotic BCL-2. *Proc Natl Acad Sci USA.* **94**. Pp. 11357-11362.

Sena, P., Saviano, M., Monni, S., Losi, L., Roncucci, L., Marzona, L. and De Pol, A. (2006). Subcellular localization of beta-catenin and APC proteins in colorectal preneoplastic and neoplastic lesions. *Cancer Lett.* **241:2**. Pp. 203-12.

Senft, D. and Ronai, Z. A. (2015). UPR, autophagy, and mitochondria crosstalk underlies the ER stress response. *Trend. Biochem Sci*. **40:3**. Pp. 141–148.

Shamu, C. E. and Walter, P. (1996). Oligomerization and phosphorylation of the Ire1p kinase during intracellular signaling from the endoplasmic reticulum to the nucleus. *EMBO*. **15:12**. Pp. 3028–3039.

Sheridan, R. B. 3rd and Huang, P. C. (1977). Single strand breakage and repair in eukaryotic DNA as assayed by S1 nuclease. *Nucleic Acids Res*. **4:2**. Pp. 299-318.

Shtutman, M., Zhurinsky, J., Simcha, I., Albanese, C., D'Amico, M., Pestell, R. and Ben-Ze'Ev, A. (1999). The cyclin D1 gene is a target of the beta-catenin/LEF-1 pathway. *Proc Natl Acad Sci U S A*. **96:10**. Pp. 5522-5527.

Siddik, K. (2003). Cisplatin: mode of cytotoxic action and molecular basis of resistance. *Oncogene*. **22**. Pp. 7265–7279.

Sirbu, B. M., McDonald, W. H., Dungrawala, H., Badu-Nkansah, A., Kavanaugh, G. M., Chen, Y., Tabb, D. L. and Cortez, D. (2013). Identification of Proteins at Active, Stalled, and Collapsed Replication Forks Using Isolation of Proteins on Nascent DNA (iPOND) Coupled with Mass Spectrometry. *J Biol Chem*. **288:44**. Pp. 31458–31467.

Skaar, J.R., Pagan, J. K. and Pagano, M. (2013). Mechanisms and function of substrate recruitment by F-box proteins. *Nat Rev Mol Cell. Biol.* **14**. Pp. 369-381.

Smaili, S. S., Hsu, Y. T., Sanders, K. M., Russell, J. T. and Youle, R. J. (2001). Bax translocation to mitochondria subsequent to a rapid loss of mitochondrial membrane potential. Cell Death Differ. **8:9**. Pp. 909-20.

Smiley, S.T., Reers, M., Motolla-Hartshorn, C., Lin, M., Chen, A., Smith, T. W., Steele Jr, J. D., Chen, L. B. (1991). Intracellular heterogeneity in mitochondrial membrane potentials revealed by a J-aggregate-forming lipophilic cation JC-1. *Proc Natl Acad Sci U S A.* **88:9**. Pp. 3671-5.

Smith, K. J., Levy, D. B., Maupin, P., Pollard, T. D., Vogelstein, B. and Kinzler, K. W. (1994). Wild-type but not mutant APC associates with the microtubule cytoskeleton. *Cancer Res.* **54:14**. Pp. 3672-5.

Sofer, A., Lei, K., Johannessen, C. M. and Ellisen, L. W. (2005). Regulation of mTOR and Cell Growth in Response to Energy Stress by REDD1. *Mol Cell Biol*. **25:14**. Pp. 5834–5845.

Song, J. H., Kandasamy, K., Zemskova, M., Lin, Y-W. and Kraft, A. S. (2011). The BH3 Mimetic ABT-737 Induces Cancer Cell Senescence. *Cancer Re*s. **71:2**. Pp. 506–515.

Souers, A. J., Leverson, J. D., Boghaert, E. R., Ackler, S. L., Catron, N. D., Chen, J., Dayton, B. D., Ding, H., Enschede, S. H., Fairbrother, W. J., Huang, D. C., Hymowitz, S. G., Jin, S., Khaw, S. L., Kovar, P. J., Lam, L. T., Lee, J., Maecker, H. L., Marsh, K. C., Mason, K. D., Mitten, M. J., Nimmer, P. M., Oleksijew, A., Park, C. H., Park, C. M., Phillips, D. C., Roberts, A.W., Sampath, D., Seymour, J. F., Smith, M. L., Sullivan, G. M., Tahir, S. K., Tse, C., Wendt, M. D., Xiao, Y., Xue, J. C., Zhang, H., Humerickhouse, R.A., Rosenberg, S. H. and Elmore, S. W. (2013). *Nat Med*.**19:2**. Pp.202-208.

Srivastava, S. P., Davies, M. V. and Kaufman, R. J. (1995). Calcium Depletion from the Endoplasmic Reticulum Activates the Double-stranded RNA-dependent Protein Kinase (PKR) to Inhibit Protein Synthesis. *J Biol Chem*. **270**. Pp. 16619-16624.

Steffensen, I. L., Paulsen, J. E., Eide, T. J. and Alexander, J. (1997) 2-Amino-l-methyl-6-phenylimidazo[4,5-*b*]pyridine increases the numbers of tumors, cystic crypts and aberrant crypt foci in multiple intestinal neoplasia mice. *Carcinogenesis*. **18**. Pp. 1049–1054.

Stephens, S. G. (1961). Recombination between Supposedly Homologous Chromosomes of Gossypium Barbade nse L. and G.Hirsutum L. *Genetics*. **11**. Pp. 1483-1500.

Strasser, A., Harris, A. W. and Cory, S. (1991). *Bcl-2* transgene inhibits T cell death and perturbs thymic self-censorship. *Cell.* **67**. Pp. 889–899.

Su, L. K., Kinzler, K. W., Vogelstein, B., Preisinger, A. C., Moser, A. R., Luongo, C., Gould, K. A. and Dove, W. F. (1992). Multiple intestinal neoplasia caused by a mutation in the murine homolog of the APC gene. *Science*. **256:5057**. Pp. 668-670.

Su, L. K., Vogelstein, B and Kinzler, K. W. (1993). Association of the APC tumor suppressor protein with catenins. *Science* **262:5140**. Pp. 1734–1737.

Su, L-K., Johnson, K. A., Smith, K. J., Hill, D. E., Vogelstein, B., Kinzler, K. W. (1993). Association between Wild Type and Mutant APC Gene Products. *Cancer Res*. **53**. Pp. 2728-2731.

Sudhakar, A., Ramachandran, A., Ghosh, S., Hasnain, S. E., Kaufman, R. J. and Ramaiah, K. V. (2000). Phosphorylation of serine 51 in initiation factor 2 alpha (eIF2 alpha) promotes complex formation between eIF2 alpha(P) and eIF2B and causes inhibition in the guanine nucleotide exchange activity of eIF2B. *Biochemistry*. **39:42**. Pp. 12929-38.

Sun, F-C., Wei, S., Li, C-W., Chang, Y-S., Chao, C-C. and Lai, Y-K. (2006). Localization of

GRP78 to mitochondria under the unfolded protein response. *Biochem J*. **396**. Pp. 31–39.

Swiger, B., Patel, M., Pastukh, V., Gillespie, M. N. and Al-Mehdi, A. B. (2008). Hypoxia causes perinuclear mitochondrial clustering and nuclear oxidant stress in pulmonary artery endothelial cells (PAECS) via a dynein-dependent molecular motor. *FASEB J*. **22**. Pp. 1174-1176.

Tameire, F., Verginadis, I. I. and Koumenis, C. (2015). Cell intrinsic and extrinsic activators of the unfolded protein response in cancer: Mechanisms and targets for therapy. *Semin Cancer Biol*. **33**. Pp. 3–15.

Tan, X., Calderon-Villalobos, L. I. A., Sharon, M., Zheng, C., Robinson, C. V., Estelle, M. and Zheng, N. (2007). Mechanism of auxin perception by the TIR1 ubiquitin ligase. *Nature.* **446**. Pp. 640-645.

Tartaglia, L. A., Ayres, T. M., Wong, G. H. W. and Goeddel, D. V. (1993). A novel domain within the 55 kd TNF receptor signals cell death. *Cell*. **74:5**. Pp. 845–853.

Tetsu, O. and McCormick, F. (1999). Beta-catenin regulates expression of cyclin D1 in colon carcinoma cells. *Nature*. **398:6726**. Pp. 422-426.

Thliveris, A., Samowitz, W., Matsunami, N., Groden, J. and White, R. (1994). Demonstration of promoter activity and alternative splicing in the region 5' to exon 1 of the APC gene. *Cancer Res*. **54:11**. Pp. 2991-5.

Thode, S., Schafer, A., Pfeiffer, P. and Vielmetter, W. (1990). A novel pathway of DNA end-to-end joining. *Cell*. **60:6**. Pp. 921-928.

Tibbetts, R. S., Brumbaugh, G. M., Williams, J. M., Sarkaria, J. N., Cliby, W. A., Shieh, S. Y., Taya, Y., Prives, C. and Abraham, R. T. (1999). A role for ATR in the DNA damage-induced phosphorylation of p53. *Genes Dev.* **13:2**. Pp. 152-7.

Tickenbrock, L., Kossmeier, K., Rehmann, H., Herrmann, C. and Muller, O. (2003). Differences between the interaction of beta-catenin with non-phosphorylated and single-mimicked phosphorylated 20-amino acid residue repeats of the APC protein. *J Mol Biol.* **327**: 359–367.

Trudel, S., Li, Z. H., Rauw, J, Tiedemann, R. E., Wen, X. Y. and Stewart, A. K. (2007). Preclinical studies of the pan-Bcl inhibitor obatoclax (GX015-070) in multiple myeloma. *Blood.* **109:12**. Pp 5430-8.

Tse, C., Shoemaker, A. R., Adickes, J., Anderson, M. G., Chen, J., Jin, S., Johnson, E. F., Marsh, K. C., Mitten, M. J., Nimmer, P., Roberts, L., Tahir, S. K., Xiao, Y., Yang, X., Zhang, H., Fesik, S., Rosenberg, S. H. and Elmore, S. W. (2008). ABT-263: A Potent and Orally Bioavailable Bcl-2 Family Inhibitor. *Can. Res*. **68**. Pp 3421.

Vaillant, F., Merino, D., Lee, L., Breslin, K., Pal, B., Ritchie, M. E., Smyth. G. K., Christie, M., Phillipson, L. J., Burns, C. J., Mann, G. B., Visvader, J. E. and Lindeman, G. J. (2013).

Targeting BCL-2 with the BH3 Mimetic ABT-199 in Estrogen Receptor-Positive Breast Cancer. *Cancer Cell*. **24:1**. Pp 120–129.

Van de Wetering, M., Cavallo, R., Dooijes, D., van Beest, M., van Es, J., Loureiro, J., Ypma, A., Hursh, D., Jones, T., Bejsovec, A., Peifer, M., Mortin, M. and Clevers, H. (1997). Armadillo Coactivates Transcription Driven by the Product of the Drosophila Segment Polarity Gene dTCF. *Cell*. **88**. Pp. 789–799.

Van der Heijden, M., Zimberlin, C. D., Nicholson, A. M., Colak, S., Kemp. R., Meijer, S. L., Medema, J. P., Gretan, F. R., Jansen, M., Winton, D. J. and Vermeulen, L. (2016). *Bcl-2* is a critical mediator of intestinal transformation. *Nat Commun*. **7:10916**. DOI: 10.1038/ncomms10916.

Vander Heiden, M. G., Chandel, N. S., Li, X. X., Schumaker, P. T., Colombini, M. amd Thompson, C. B. (2000). Outer mitochondrial membrane permeability can regulate coupled respiration and cell survival. *Proc Natl Acad Sci U S A.* **97:9**. Pp. 4666–4671.

Vazquez, G., Wedel, B. J., Bird, G. J., Joseph, S. K. and Putney, J. W. (2002). An inositol 1,4,5-trisphosphate receptor-dependent cation entry pathway in DT40 B lymphocytes. *EMBO*. **21:17**. Pp. 4393 – 4748.

Verhagen, A. M., Ekert, P. G., Pakusch, M., Silke, J., Connolly, L. M., Reid, G. E., Moritz, R. L., Simpson, R. J. and Vaux, D.L. (2000) Identification of DIABLO, a mammalian protein that promotes apoptosis by binding to and antagonizing IAP proteins. *Cell*. **102**. Pp. 43–53.

Villunger, A., Michalak, E. M., Coultas, L., Mullauer, F., Bock, G., Ausserlechner, M. J., Adams, J. M. and Strasser, A. (2003). p53- and Drug-Induced Apoptotic Responses Mediated by BH3-Only Proteins Puma and Noxa. *Science*. **302:5647**. Pp. 1036-1038.

Walker, I. G. and Sridhar, R. (1976). The formation and repair of single-strand breaks in DNA of cultured mammalian cells treated with UV-light, methylating agents or 4-nitroquinoline-1-oxide. *Chem Biol Interact*. **12**. Pp. 229-39.

Wang, Y., Azuma, Y., Moore, D., Osheroff, N. and Neufeld, K. L. (2008). Interaction between tumor suppressor adenomatous polyposis coli and topoisomerase IIalpha: implication for the G2/M transition. *Mol Biol Cell*. **19:10**. Pp. 4076-4085.

Wang, Y., Coffey, R. J., Osheroff, N., Neufeld, K. L. (2010). Topoisomerase IIalpha binding domains of adenomatous polyposis coli influence cell cycle progression and aneuploidy. *PLoS One.* **5:4**. e9994.

Wildenberg, J. and Meselson, M. (1975). Mismatch repair in heteroduplex DNA. *Proc Natl Acad Sci U S A*. **72:6**. Pp. 2202-2206

Winston, J. T., Strack, P., Beer-Romero, P., Chu, C, Y., Elledge, S. J. and Harper, J. W. (1999). The SCFbeta-TRCP-ubiquitin ligase complex associates specifically with phosphorylated destruction motifs in IkappaBalpha and beta-catenin and stimulates IkappaBalpha ubiquitination in vitro. *Genes Dev.* **13:3**. Pp. 270-83.

Wolter, K. G., Hsu, Y. T., Smith, C. L., Nechushtan, A., Si, X. G. and Youle, R. J. (1997).

Movement of Bax from the cytosol to mitochondria during apoptosis. *J Cell Biol.* **139:5**. Pp. 1281-92.

Wroblewski, D., Jiang, C. C., Croft, A., Farrelly, M. L., Zhang, X. D. and Hersey, P. (2013). OBATOCLAX and ABT-737 induce ER stress responses in human melanoma cells that limit induction of apoptosis. *PLoS ONE*. **8:12**. e84073. doi:10.1371/journal.pone.0084073.

Xing, Y., Clements, W. K., Le Trong, I., Hinds, T. R., Stenkamp, R., Kimelman, D. and Xu, W. (2004). Crystal structure of a beta-catenin/APC complex reveals a critical role for APC phosphorylation in APC function. *Mol Cell*. **15:4**. Pp. 523-533.

Yamamoto, K., Sato, T., Matsui, T., Okada, T., Yoshida, H., Harada, A. and Mori, K. (2007). Transcriptional Induction of Mammalian ER Quality Control Proteins Is Mediated by Single or Combined Action of ATF6α and XBP1. *Dev Cell*. **13:3**. Pp. 365–376.

Yang, J., Liu, X., Bhalla, K., Kim, C. N., Ibrado, A. M., Cai, J., Peng, T. I., Jones, D. P. and Wang, X. (1997). Prevention of Apoptosis by Bcl-2: Release of Cytochrome c from Mitochondria Blocked. *Science.* **275:5303**. Pp .1129-1132.

Ye, J., Rawson, R. B., Komuro, R., Chen, X., Dave, U. P., Prywes, R., Brown, M. S. and Goldstein, J. L. (2000). ER stress induces cleavage of membrane-bound ATF6 by the same proteases that process SREBPs. *Mol Cell*. **6:6**. Pp. 1355-64.

Yen, H-C. S., Xu, G., Chou, D. M., Zhao, Z. and Elledge, S. J. (2008). Global Protein Stability Profiling in Mammalian Cells. *Science*. **322:5903**. Pp. 918-923.

Yilmaz, G. and Arslanyolu, M. (2015). Efficient expression of codon-adapted affinity tagged super folder green fluorescent protein for synchronous protein localization and affinity purification studies in *Tetrahymena thermophila. BMC Biotechnology*. **15:22**. doi: 10.1186/s12896-015-0137-9.

Yin, X-M., Oltvai, Z. N and Korsmeyer, S.J. (1994). BH1 and BH2 domains of Bcl-2 are required for inhibition of apoptosis and heterodimerization with Bax. *Nature.* **369**. Pp. 321 – 323.

Yoshida, H., Matsui, T., Yamamoto, A., Okada, T. and Mori, K. (2001). XBP1 mRNA Is Induced by ATF6 and Spliced by IRE1 in Response to ER Stress to Produce a Highly Active Transcription Factor. *Cell*. **107:7**. Pp. 881–891.

Yoshida, Y., Chiba, T., Tokunaga, F., Kawasaki, H., Iwai, K., Suzuki, T., Ito, Y., Matsuoka, K., Yoshida M., Tanaka K. and Tadaski, T. (2002). E3 ubiquitin ligase that recognizes sugar chains. *Nature*. **418**. Pp. 438-442.

Zha, H., Aimé-Sempé, C., Sato, T. and Reed, J, C. (1996). Proapoptotic Protein Bax Heterodimerizes with Bcl-2 and Homodimerizes with Bax via a Novel Domain (BH3) Distinct from BH1 and BH2. *J Biol Chem*. **271**. Pp. 7440-7444.

Zhang, J. H. and Xu, M. (2000). DNA fragmentation in apoptosis. *Cell Res*. **10**. Pp. 205–211.

Zinszner, H., Kuroda, M., Wang, X. Z., Batchvarova, N., Lightfoot, R. T., Remotti, H.,

Stevens, J. L. and Ron, D. (1998). CHOP is implicated in programmed cell death in response to impaired function of the endoplasmic reticulum. *Genes Dev*. **12**. Pp. 982-995.

Zumbrunn, J., Kinoshita, K., Hyman, A. A. and Näthke, I. S. (2001). Binding of the adenomatous polyposis coli protein to microtubules increases microtubule stability and is regulated by GSK3β phosphorylation. *Curr Biol*. **11:1**. Pp. 44–49.

Appendix

Appendix A

Wnt Target Genes – Nusse lab, Stanford (June 2015)				
Gene	**Organism/system**	**Direct?**	**Transcription**	**Reference(s)**
Axin-2	human colon cancer	yes	up	Yan, 2001 Lustig, 2002 Jho, 2002
betaTrCP		Independent of transcription	up	Spiegelman 2000
BMP4	human colon cancer	?	up	Kim, 2002
BMP4	Xenopus	?	down	Baker, 1999
Brachyury	Mouse (Wnt-3A)	yes	up	Yamaguchi, 1999 Arnold, 2000
c-jun	human colon cancer	yes	up	Mann B, 1999
c-myc	human colon cancer	yes	up	He, 1998
c-myc binding protein	human colon cancer	yes	up	Jung, 2005
Cacna1g	Neuron		up	Wisniewska, 2010
CCN1/Cyr61	Osteoblasts		up	Si, 2006
CD44	human colon cancer	?	up	Wielenga, 1999
Cdx1	Mouse embryo			Pilon, 2007
Cdx1	Mouse Wnt-3A	yes	up	Lickert, 2000
Cdx4	Mouse Wnt-3A			Pilon, 2006
Cdx4	Zebrafish HSC	?	up	Davidson, 2003
claudin-1	human colon cancer	yes	up	Miwa, 2002
connexin 30	Xenopus	?		McGrew, 1999
connexin43	Xenopus, Mouse	yes	up	van der Heyden, 1999

connexin43	rat cardiomyocytes	?	up	Ai, 2000
CTLA-4	Melanomas	yes	up	Shah, 2008
Cyclin D	human colon cancer	yes	up	Tetsu, 1999 Shtutman, 1999 Disputed by Sansom, 2005
cyclooxygenase-2	mouse (Wnt-1)	?	up	Howe, 1999 Haertel-Wiesmann, 2000
Delta-like 1	somites			Galceran, 2004 Hofmann, 2004
Dfrizzled2	Drosophila	?	down	Cadigan, 1998
dharma/bozozok	Zebrafish	yes	up	Ryu, 2001
Dickkopf	Various cells, tumours		up	Niida, 2004 Gonzalez-Sancho, 2004 Chamorro, 2004
Dpp	Drosophila	yes	down	Yang, 2000
E-cadherin	Mouse hair follicle	yes	down	Jamora, 2003
E-cadherin	ES/EB		down	Ten Berge, 2008
Eda (TNF-related)	Mouse hair follicle	?	up	Laurikkala, 2002 Durmowicz, 2002
EGF receptor	Liver		up	Tan, 2005
endothelin-1	human colon cancer		up	Kim, 2004
Engrailed	Drosophila	?	up	Hooper, 1994
engrailed-2	Xenopus	yes	up	McGrew, 1999
EphB/ephrin-B	human colon cancer	?	up/down	Batlle, 2002
FGF18	human colon cancer	yes	up	Shimokawa, 2003
FGF20	Various cells, tumours			Chamorro, 2004
FGF4	Mouse tooth bud	yes	up	Kratochwil, 2002
FGF9	ovarian endometrioid adenocarcinoma		up	Hendrix, 2006LB

Fibronectin	ES/EB		up	Ten Berge, 2008
Fibronectin	Mouse lung		up	De Langhe, 2005
fibronectin	Xenopus	yes	up	Gradl, 1999
Follistatin	EC cells, ovary	yes	up	Willert, 2002 Yao, 2004
FoxN1	thymus	?	yes	Balciunaite, 2002
fra-1	human colon cancer	yes	up	Mann B, 1999
Frizzled 7	EC cells	yes	up	Willert, 2002
Gastrin	human colon cancer	?	up	Koh, 2000
Gbx2	Neural Crest	yes	up	Li, 2009
Gremlin	fibroblasts		up	Klapholz-Brown, 2007
Hath1	human colon cancer	..	down	Leow, 2004
Id2	human colon cancer	yes	up	Rockman, 2001 Willert, 2002
Interleukin8	Endothelial cells			Masckauchan, 2005
Irx3 and Six3	Mouse brain			Braun, 2003
Islet1	Cardiac cells		up	Lin, 2007
ITF-2	human colon cancer	yes	up	Kolligs, 2002
Jagged	human colon cancer		up	Rodilla, 2009
Jagged1	Mouse hair follicle		up	Estrach, 2006
Keratin	Mouse hair follicle	yes	up	Dasgupta, 1999
L1 neural adhesion	human colon cancer		up	Gavert, 2005
LBH	breast cancer		up	Rieger, 2010
LEF1	human colon cancer	yes	up	Hovanes, 2001 Filali, 2002

LGR5/GPR49	Intestine	yes	up	Barker, 2007
matrix metalloproteinase MMP-7	human colon cancer	yes	up	Brabletz, 1999 Crawford, 1999
matrix metalloproteinase-26	Human			Marchenko, 2002
mBTEB2	Mouse	Independent β-catenin	up	Ziemer, 2001
Met	human colon cancer		up	Boon, 2002
MITF/nacre	Zebrafish	yes	up	Dorsky, 2000 Saito, 2002 Yasumoto, 2002
MMP2, MMP9	T cells			Wu, 2007
movo1	Mouse hair follicle	yes	up	Li, 2002
Msl1	human colon cancer		up	Spears, 2011
myogenic bHLH	Xenopus	?	up	Munsterberg, 1995
n-myc	mesenchyme limbs		up	Ten Berge, 2008
nanog	ES			Pereira, 2006 Cole, 2008
Nemo				
NeuroD1	Mouse Brain	yes	up	Kuwabara, 2009
neurogenin 1	Mouse brain	yes	up	Hirabayashi, 2004
Nitric Oxide Synthase 2	Hepg2 cells		up	Du, 2006
Nkx2.2	Neural tube	yes	down	Lei, 2006
Nr-CAM	human colon cancer	yes	up	Conacci-Sorrell, 2002
Oct 4	ES		up	Cole, 2008
Osteocalcin	Mouse	yes	down	Kahler, 2003
Osteoprotegerin	Osteoblasts		up	Glass, 2005

P16ink4A	Melanocytes	yes	down	Delmas, 2007
periostin	Mouse Wnt-3	not through β-catenin?	down	Haertel-Wiesmann, 2000
PTTG	oesophageal squamous cell carcinoma			Zhou, 2004
Pitx2	pituitary	yes	up	Kioussi, 2002
PPARdelta	human colon cancer	yes	up	He TC, 1999
Proglucagon	Mouse	?	up	Ni, 2003
RANK ligand	Osteoblasts		down	Spencer, 2006
ret	rat PC12	?	up	Zheng, 1996
retinoic acid receptor gamma	Xenopus	?		McGrew, 1999
Runx2	chondrocytes		up	Dong, 2006
SALL4				Bohm, 2006
sFRP-2	Mouse (Wnt-4)	?	up	Lescher, 1998
shavenbaby	Drosophila	?	down	Payre, 1999
Siamois	Xenopus	yes	up	Brannon, 1997
snail	ES/EB		up	Ten Berge, 2008
Sox17	gastrointestinal tumours		up	Du, 2009
Sox2	Xenopus retina		up	Van Raay, 2005
Sox9	Intestine		up	Blache, 2004
Sox9	mesenchyme		down	Hill, 2005 Day, 2005 Yano, 2005
SP5	Mouse brain	yes	up	Weidinger, 2005 Fujimura, 2007
Stra6	Wnt-1 transformed mouse cells	? co-induced by Wnt plus RA	up	Szeto, 2001
stripe	Drosophila	yes	down	Piepenburg, 2000

Stromelysin	Wnt-1 transformed mouse cells		up	Prieve, 2003
Survivin	human colon cancer		up	Zhang, 2001
Tcf-1	human colon cancer	yes	up	Roose, 1999
Telomerase	ES, other stem	yes	up	Hoffmyer, 2012
Tiam1	Colon tumours			Malliri, 2005
TNF family 41BB ligand, ephrinB1, Stra6, autotaxin and ISLR	Wnt-1 transformed mouse cells	By Wnt plus retinoic acid	up	Tice, 2002
Tnfrsf19	Somitic mesoderm	yes	up	Buttitta, 2003
twin	Xenopus	yes	up	Laurent, 1997
Twist	Wnt1 induced mammary cancer		up	Howe, 2003
Ubx	Drosophila	yes	up or down	Riese, 1997
uPAR	human colon cancer	?	up	Mann B, 1999
VEGF	human colon cancer	yes	up	Zhang, 2001
versican	vascular smooth muscle cells	yes	up	Rahmani, 2005
wingless	Drosophila	?	up or down	Yu, 1998
WISP	Wnt-1 transformed mouse cells	yes, but not through TCF (Xu, 2000)	up	Xu, 2000
WISP-1, WISP-2, IGF-II , Proliferin-2, Proliferin-3, Emp, IGF-I, VEGF-C, MDR1, COX-2, IL-6	3T3-L1 Preadipocytes	?	up	Longo, 2002
Wnt3a	EC cells			Zhang, 2009

Wrch-1	Wnt-1 transformed mouse cells	? Not through TCF	up	Tao, 2001
Xnr3	Xenopus	yes	up	McKendry, 1997

Appendix B

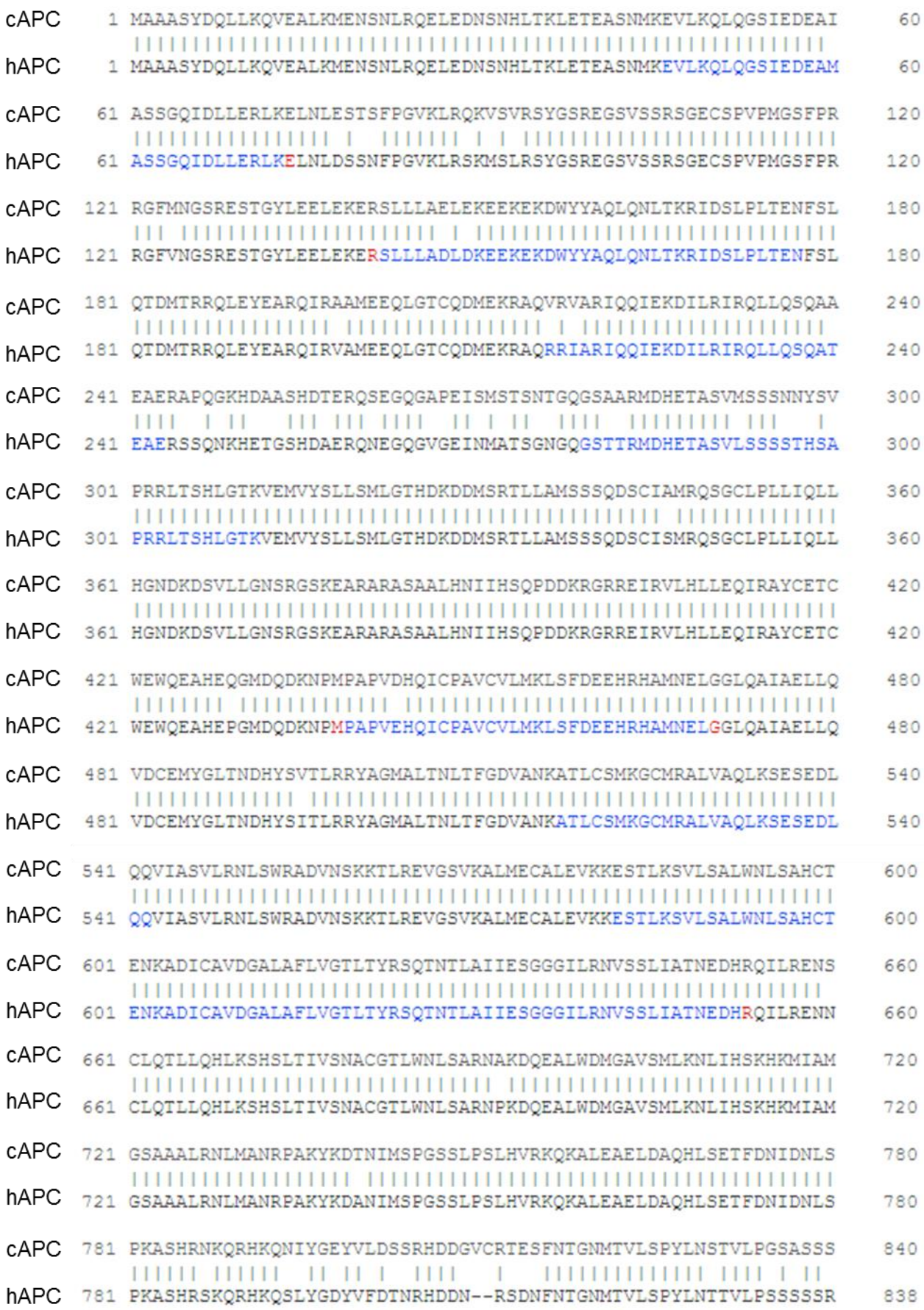
cAPC 1 MAAASYDQLLKQVEALKMENSNLRQELEDNSNHLTKLETEASNMKEVLKQLQGSIEDEAI 60
hAPC 1 MAAASYDQLLKQVEALKMENSNLRQELEDNSNHLTKLETEASNMKEVLKQLQGSIEDEAM 60
cAPC 61 ASSGQIDLLERLKELNLESTSFPGVKLRQKVSVRSYGSREGSVSSRSGECSPVPMGSFPR 120
hAPC 61 ASSGQIDLLERLKELNLDSSNFPGVKLRSKMSLRSYGSREGSVSSRSGECSPVPMGSFPR 120
cAPC 121 RGFMNGSRESTGYLEELEKERSLLLAELEKEEKEKDWYYAQLQNLTKRIDSLPLTENFSL 180
hAPC 121 RGFVNGSRESTGYLEELEKERSLLLADLDKEEKEKDWYYAQLQNLTKRIDSLPLTENFSL 180
cAPC 181 QTDMTRRQLEYEARQIRAAMEEQLGTCQDMEKRAQVRVARIQQIEKDILRIRQLLQSQAA 240
hAPC 181 QTDMTRRQLEYEARQIRVAMEEQLGTCQDMEKRAQRRIARIQQIEKDILRIRQLLQSQAT 240
cAPC 241 EAERAPQGKHDAASHDTERQSEGQGAPEISMSTSNTGQGSAARMDHETASVMSSSNNYSV 300
hAPC 241 EAERSSQNKHETGSHDAERQNEGQGVGEINMATSGNGQGSTTRMDHETASVLSSSSTHSA 300
cAPC 301 PRRLTSHLGTKVEMVYSLLSMLGTHDKDDMSRTLLAMSSSQDSCIAMRQSGCLPLLIQLL 360
hAPC 301 PRRLTSHLGTKVEMVYSLLSMLGTHDKDDMSRTLLAMSSSQDSCISMRQSGCLPLLIQLL 360
cAPC 361 HGNDKDSVLLGNSRGSKEARARASAALHNIIHSQPDDKRGRREIRVLHLLEQIRAYCETC 420
hAPC 361 HGNDKDSVLLGNSRGSKEARARASAALHNIIHSQPDDKRGRREIRVLHLLEQIRAYCETC 420
cAPC 421 WEWQEAHEQGMDQDKNPMPAPVDHQICPAVCVLMKLSFDEEHRHAMNELGGLQAIAELLQ 480
hAPC 421 WEWQEAHEPGMDQDKNPMPAPVEHQICPAVCVLMKLSFDEEHRHAMNELGGLQAIAELLQ 480
cAPC 481 VDCEMYGLTNDHYSVTLRRYAGMALTNLTFGDVANKATLCSMKGCMRALVAQLKSESEDL 540
hAPC 481 VDCEMYGLTNDHYSITLRRYAGMALTNLTFGDVANKATLCSMKGCMRALVAQLKSESEDL 540
cAPC 541 QQVIASVLRNLSWRADVNSKKTLREVGSVKALMECALEVKKESTLKSVLSALWNLSAHCT 600
hAPC 541 QQVIASVLRNLSWRADVNSKKTLREVGSVKALMECALEVKKESTLKSVLSALWNLSAHCT 600
cAPC 601 ENKADICAVDGALAFLVGTLTYRSQTNTLAIIESGGGILRNVSSLIATNEDHRQILRENS 660
hAPC 601 ENKADICAVDGALAFLVGTLTYRSQTNTLAIIESGGGILRNVSSLIATNEDHRQILRENN 660
cAPC 661 CLQTLLQHLKSHSLTIVSNACGTLWNLSARNAKDQEALWDMGAVSMLKNLIHSKHKMIAM 720
hAPC 661 CLQTLLQHLKSHSLTIVSNACGTLWNLSARNPKDQEALWDMGAVSMLKNLIHSKHKMIAM 720
cAPC 721 GSAAALRNLMANRPAKYKDTNIMSPGSSLPSLHVRKQKALEAELDAQHLSETFDNIDNLS 780
hAPC 721 GSAAALRNLMANRPAKYKDANIMSPGSSLPSLHVRKQKALEAELDAQHLSETFDNIDNLS 780
cAPC 781 PKASHRNKQRHKQNIYGEYVLDSSRHDDGVCRTESFNTGNMTVLSPYLNSTVLPGSASSS 840
hAPC 781 PKASHRSKQRHKQSLYGDYVFDTNRHDDN--RSDNFNTGNMTVLSPYLNTTVLPSSSSSR 838

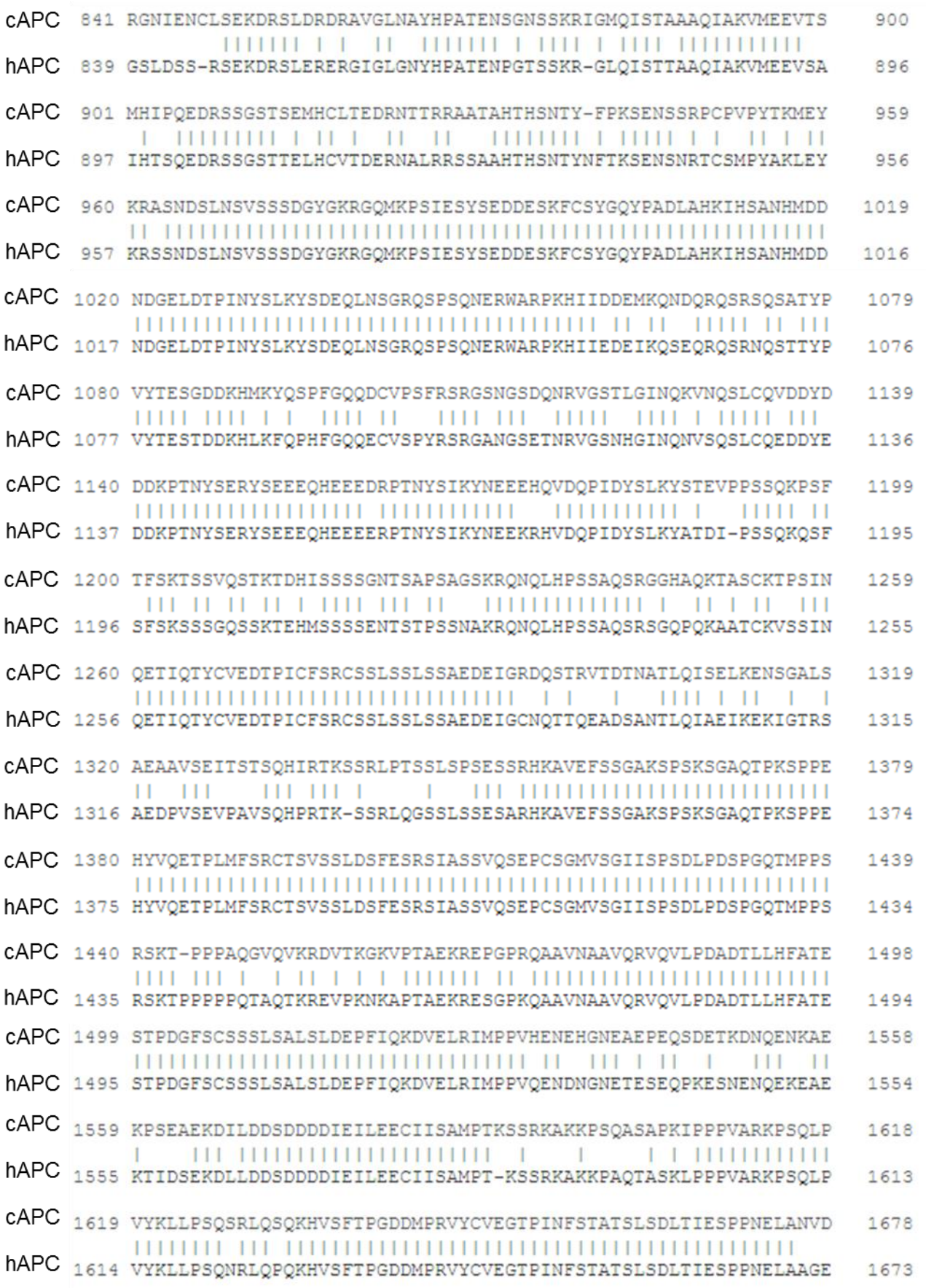
cAPC 841 RGNIENCLSEKDRSLDRDRAVGLNAYHPATENSGNSSKRIGMQISTAAAQIAKVMEEVTS 900
hAPC 839 GSLDSS-RSEKDRSLERERGIGLGNYHPATENPGTSSKR-GLQISTTAAQIAKVMEEVSA 896
cAPC 901 MHIPQEDRSSGSTSEMHCLTEDRNTTRRAATAHTHSNTY-FPKSENSSRPCPVPYTKMEY 959
hAPC 897 IHTSQEDRSSGSTTELHCVTDERNALRRSSAAHTHSNTYNFTKSENSNRTCSMPYAKLEY 956
cAPC 960 KRASNDSLNSVSSSDGYGKRGQMKPSIESYSEDDESKFCSYGQYPADLAHKIHSANHMDD 1019
hAPC 957 KRSSNDSLNSVSSSDGYGKRGQMKPSIESYSEDDESKFCSYGQYPADLAHKIHSANHMDD 1016
cAPC 1020 NDGELDTPINYSLKYSDEQLNSGRQSPSQNERWARPKHIIDDEMKQNDQRQSRSQSATYP 1079
hAPC 1017 NDGELDTPINYSLKYSDEQLNSGRQSPSQNERWARPKHIIEDEIKQSEQRQSRNQSTTYP 1076
cAPC 1080 VYTESGDDKHMKYQSPFGQQDCVPSFRSRGSNGSDQNRVGSTLGINQKVNQSLCQVDDYD 1139
hAPC 1077 VYTESTDDKHLKFQPHFGQQECVSPYRSRGANGSETNRVGSNHGINQNVSQSLCQEDDYE 1136
cAPC 1140 DDKPTNYSERYSEEEQHEEEDRPTNYSIKYNEEEHQVDQPIDYSLKYSTEVPPSSQKPSF 1199
hAPC 1137 DDKPTNYSERYSEEEQHEEEERPTNYSIKYNEEKRHVDQPIDYSLKYATDI-PSSQKQSF 1195
cAPC 1200 TFSKTSSVQSTKTDHISSSSGNTSAPSAGSKRQNQLHPSSAQSRGGHAQKTASCKTPSIN 1259
hAPC 1196 SFSKSSSGQSSKTEHMSSSSENTSTPSSNAKRQNQLHPSSAQSRSGQPQKAATCKVSSIN 1255
cAPC 1260 QETIQTYCVEDTPICFSRCSSLSSLSSAEDEIGRDQSTRVTDTNATLQISELKENSGALS 1319
hAPC 1256 QETIQTYCVEDTPICFSRCSSLSSLSSAEDEIGCNQTTQEADSANTLQIAEIKEKIGTRS 1315
cAPC 1320 AEAAVSEITSTSQHIRTKSSRLPTSSLSPSESSRHKAVEFSSGAKSPSKSGAQTPKSPPE 1379
hAPC 1316 AEDPVSEVPAVSQHPRTK-SSRLQGSSLSSESARHKAVEFSSGAKSPSKSGAQTPKSPPE 1374
cAPC 1380 HYVQETPLMFSRCTSVSSLDSFESRSIASSVQSEPCSGMVSGIISPSDLPDSPGQTMPPS 1439
hAPC 1375 HYVQETPLMFSRCTSVSSLDSFESRSIASSVQSEPCSGMVSGIISPSDLPDSPGQTMPPS 1434
cAPC 1440 RSKT-PPPAQGVQVKRDVTKGKVPTAEKREPGPRQAAVNAAVQRVQVLPDADTLLHFATE 1498
hAPC 1435 RSKTPPPPPQTAQTKREVPKNKAPTAEKRESGPKQAAVNAAVQRVQVLPDADTLLHFATE 1494
cAPC 1499 STPDGFSCSSSLSALSLDEPFIQKDVELRIMPPVHENEHGNEAEPEQSDETKDNQENKAE 1558
hAPC 1495 STPDGFSCSSSLSALSLDEPFIQKDVELRIMPPVQENDNGNETESEQPKESNENQEKEAE 1554
cAPC 1559 KPSEAEKDILDDSDDDDIEILEECIISAMPTKSSRKAKKPSQASAPKIPPPVARKPSQLP 1618
hAPC 1555 KTIDSEKDLLDDSDDDDIEILEECIISAMPT-KSSRKAKKPAQTASKLPPPVARKPSQLP 1613
cAPC 1619 VYKLLPSQSRLQSQKHVSFTPGDDMPRVYCVEGTPINFSTATSLSDLTIESPPNELANVD 1678
hAPC 1614 VYKLLPSQNRLQPQKHVSFTPGDDMPRVYCVEGTPINFSTATSLSDLTIESPPNELAAGE 1673

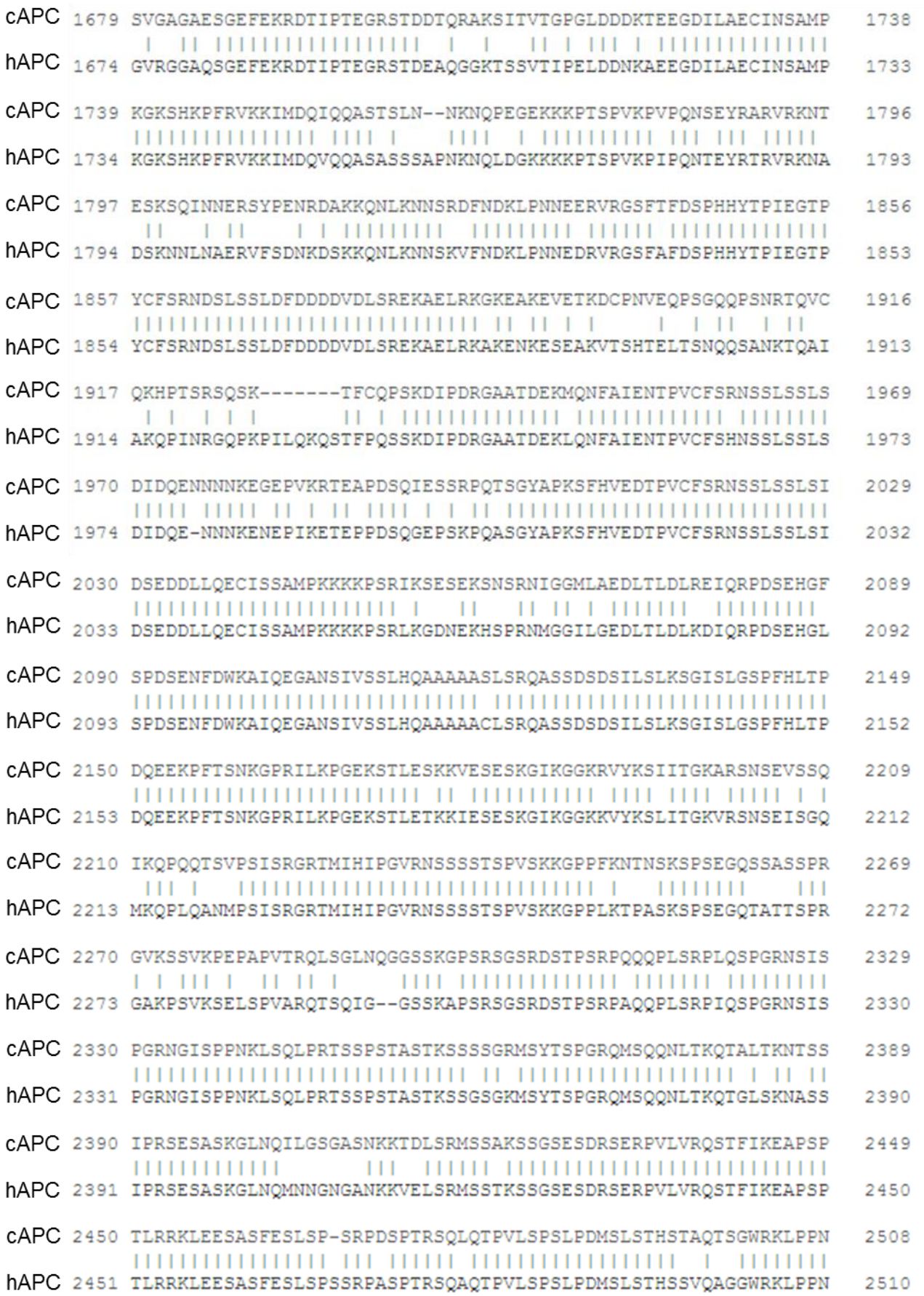
cAPC 1679 SVGAGAESGEFEKRDTIPTEGRSTDDTQRAKSITVTGPGLDDDKTEEGDILAECINSAMP 1738
hAPC 1674 GVRGGAQSGEFEKRDTIPTEGRSTDEAQGGKTSSVTIPELDDNKAEEGDILAECINSAMP 1733
cAPC 1739 KGKSHKPFRVKKIMDQIQQASTSLN--NKNQPEGEKKKPTSPVKPVPQNSEYRARVRKNT 1796
hAPC 1734 KGKSHKPFRVKKIMDQVQQASASSSAPNKNQLDGKKKKPTSPVKPIPQNTEYRTRVRKNA 1793
cAPC 1797 ESKSQINNERSYPENRDAKKQNLKNNSRDFNDKLPNNEERVRGSFTFDSPHHYTPIEGTP 1856
hAPC 1794 DSKNNLNAERVFSDNKDSKKQNLKNNSKVFNDKLPNNEDRVRGSFAFDSPHHYTPIEGTP 1853
cAPC 1857 YCFSRNDSLSSLDFDDDDVDLSREKAELRKGKEAKEVETKDCPNVEQPSGQQPSNRTQVC 1916
hAPC 1854 YCFSRNDSLSSLDFDDDDVDLSREKAELRKAKENKESEAKVTSHTELTSNQQSANKTQAI 1913
cAPC 1917 QKHPTSRSQSK-------TFCQPSKDIPDRGAATDEKMQNFAIENTPVCFSRNSSLSSLS 1969
hAPC 1914 AKQPINRGQPKPILQKQSTFPQSSKDIPDRGAATDEKLQNFAIENTPVCFSHNSSLSSLS 1973
cAPC 1970 DIDQENNNNKEGEPVKRTEAPDSQIESSRPQTSGYAPKSFHVEDTPVCFSRNSSLSSLSI 2029
hAPC 1974 DIDQE-NNNKENEPIKETEPPDSQGEPSKPQASGYAPKSFHVEDTPVCFSRNSSLSSLSI 2032
cAPC 2030 DSEDDLLQECISSAMPKKKKPSRIKSESEKSNSRNIGGMLAEDLTLDLREIQRPDSEHGF 2089
hAPC 2033 DSEDDLLQECISSAMPKKKKPSRLKGDNEKHSPRNMGGILGEDLTLDLKDIQRPDSEHGL 2092
cAPC 2090 SPDSENFDWKAIQEGANSIVSSLHQAAAAASLSRQASSDSDSILSLKSGISLGSPFHLTP 2149
hAPC 2093 SPDSENFDWKAIQEGANSIVSSLHQAAAAACLSRQASSDSDSILSLKSGISLGSPFHLTP 2152
cAPC 2150 DQEEKPFTSNKGPRILKPGEKSTLESKKVESESKGIKGGKRVYKSIITGKARSNSEVSSQ 2209
hAPC 2153 DQEEKPFTSNKGPRILKPGEKSTLETKKIESESKGIKGGKKVYKSLITGKVRSNSEISGQ 2212
cAPC 2210 IKQPQQTSVPSISRGRTMIHIPGVRNSSSSTSPVSKKGPPFKNTNSKSPSEGQSSASSPR 2269
hAPC 2213 MKQPLQANMPSISRGRTMIHIPGVRNSSSSTSPVSKKGPPLKTPASKSPSEGQTATTSPR 2272
cAPC 2270 GVKSSVKPEPAPVTRQLSGLNQGGSSKGPSRSGSRDSTPSRPQQQPLSRPLQSPGRNSIS 2329
hAPC 2273 GAKPSVKSELSPVARQTSQIG--GSSKAPSRSGSRDSTPSRPAQQPLSRPIQSPGRNSIS 2330
cAPC 2330 PGRNGISPPNKLSQLPRTSSPSTASTKSSSSGRMSYTSPGRQMSQQNLTKQTALTKNTSS 2389
hAPC 2331 PGRNGISPPNKLSQLPRTSSPSTASTKSSGSGKMSYTSPGRQMSQQNLTKQTGLSKNASS 2390
cAPC 2390 IPRSESASKGLNQILGSGASNKKTDLSRMSSAKSSGSESDRSERPVLVRQSTFIKEAPSP 2449
hAPC 2391 IPRSESASKGLNQMNNGNGANKKVELSRMSSTKSSGSESDRSERPVLVRQSTFIKEAPSP 2450
cAPC 2450 TLRRKLEESASFESLSP-SRPDSPTRSQLQTPVLSPSLPDMSLSTHSTAQTSGWRKLPPN 2508
hAPC 2451 TLRRKLEESASFESLSPSSRPASPTRSQAQTPVLSPSLPDMSLSTHSSVQAGGWRKLPPN 2510

Appendix B. APC amino acid sequence alignment. Chicken APC (cAPC) amino acid sequenced is aligned with human APC (hAPC) amino acid sequence and shows 84% sequence homology. Matched amino acids are shown with a line. Alternating exons are shown in black and red. Red represents a residue overlap splice site.